Syntheses of Novel Side-Arm Functionalized *N*-Heterocyclic Silylene Transition Metal Complexes

Dissertation

zur Erlangung des mathematisch-naturwissenschaftlichen Doktorgrades

„Doctor rerum naturalium“

der Georg-August-Universität Göttingen

im Promotionsprogramm Catalysis for Sustainable Synthesis (CaSuS)

der Georg-August University School of Science (GAUSS)

vorgelegt von

Alexander Noel Paesch

aus Celle

Göttingen

2019

Thesis Committee:

Prof. Dr. Dietmar Stalke	*Institute of Inorganic Chemistry, Georg-August-University, Göttingen*
Prof. Dr. Franc Meyer	*Institute of Inorganic Chemistry, Georg-August-University, Göttingen*

Members of the Examination Commission:

Reviewer:

Prof. Dr. Dietmar Stalke	*Institute of Inorganic Chemistry, Georg-August-University, Göttingen*

Co-Reviewer:

Prof. Dr. Franc Meyer	*Institute of Inorganic Chemistry, Georg-August-University, Göttingen*

Additional Members of the Examination Commission:

Prof. Dr. Manuel Alcarazo	*Institute of Organic and Biomolecular Chemistry, Georg-August-University, Göttingen*
Dr. Michael John	*Institute of Organic and Biomolecular Chemistry, Georg-August-University, Göttingen*
Jun.-Prof. Dr. Nathalie Kunkel	*Institute of Inorganic Chemistry, Georg-August-University, Göttingen*
Dr. Matthias Otte	*Institute of Inorganic Chemistry, Georg-August-University, Göttingen*

Day of the Oral Examination:

13.06.2019

The work described in this doctoral thesis has been carried out under the guidance and supervision of Prof. Dr. Dietmar Stalke at the Institute of Inorganic Chemistry of the Georg-August-University, Göttingen between April 2015 and April 2019.

Publications

- Alexander N. Paesch, Anne-Kathrin Kreyenschmidt, Regine Herbst-Irmer, and Dietmar Stalke, *Inorg. Chem.* **2019**, *online*, DOI: 10.1021/acs.inorgchem.9b00629.

- Soumen Sinhababu, Subrata Kundu, Mujahuddin M. Siddiqui, Alexander N. Paesch, Regine Herbst-Irmer, Brigitte Schwederski, Pinaki Saha, Lili Zhao, Gernot Frenking, Wolfgang Kaim, Dietmar Stalke, and Herbert W Roesky, *Chem. Commun*. **2019**, 1359–7345.

- Jennifer Hahn, Constanze Keck, Cäcilia Maichle-Mössmer, Paul Niklas Ruth, Alexander N. Paesch, Esther von Grotthuss, Dietmar Stalke, and Holger F. Bettinger, *Chem Eur. J.* **2018**, *24*, 18634–18637.

- Soumen Sinhababu, Subrata Kundu, Alexander N. Paesch, Regine Herbst-Irmer, Dietmar Stalke, and Herbert W. Roesky, *Eur. J. Inorg. Chem.* **2018**, *20*, 2237–2240.

- Soumen Sinhababu, Subrata Kundu, Alexander N. Paesch, Regine Herbst-Irmer, Dietmar Stalke, Israel Fernández, Gernot Frenking, A. Claudia Stückl, Brigitte Schwederski, Wolfgang Kaim, and Herbert W. Roesky, *Chem. Eur. J.* **2018**, *24*, 1264–1268.

- Jayasree Kumar, N. V. T. Sai Manoj Gorantla, Sudipta Roy, Alexander N. Paesch, Regine Herbst-Irmer, Dietmar Stalke, Chakkittakandiyil Anusha, Susmita De, Pattiyil Parameswaran, Herbert W. Roesky, and Kartik Chandra Mondal, *ChemistrySelect* **2018**, *3*, 8221–8228.

- Chandrajeet Mohapatra, Subrata Kundu, Alexander N. Paesch, Regine Herbst-Irmer, Dietmar Stalke, Diego M. Andrada, Gernot Frenking, and Herbert W. Roesky, *J. Am. Chem. Soc.* **2016**, *138*, 10429−10432.

- Dennis Rottschäfer, Christian J. Schürmann, Jan-Hendrik Lamm, Alexander N. Paesch, Beate Neumann, and Rajendra S. Ghadwal, *Organometallics* **2016**, *35*, 3421−3429.

Table of Contents

Abbreviations

Å	Ångstrom
Ac	acetyl
ADP	anisotropic displacement parameters
α-NP	α-aminophosphine
aNHC	abnormal *N*-heterocyclic carbene
amu	atomic mass unit
Ar	aryl; any aromatic substituent
β-NP	β-aminophosphine
BINAP	2,2'-bis(diphenylphosphino)-1,1'-binaphthyl
Bu	butyl
cat.	catalyst
CCDC	Cambridge Crystallographic Database
CO	carbonyl
COD	cyclooctadiene
COSY	Correlated Spectroscopy
Cp/Cp*	cyclopentadienyl / pentamethylcyclopentadienyl
CSD	Cambridge Structural Database
CuAAC	copper(I)-catalyzed azide-alkyne cycloaddition
Cy	cyclohexyl
d	days
DCM	dichloromethane
Dipp	(2,6-di-*iso*-propyl)phenyl
DMF	dimethylformamide
DMSO	dimethyl sulfoxide
DOSY	Diffusion Ordered NMR Spectroscopy
DMS	dimethylsulfide
ECC	External Calibration Curve (Method)
EI	Electron Ionization
EPR	Electron Paramagnetic Resonance
ESI	Electrospray Ionization
eq.	equivalent(s)
Et	ethyl
et al.	*et alii,* and others
Et_2O	diethyl ether
EtOH	ethanol
EWG	electron withdrawing group
h	hour(s)
HBPin	Pinacolborane
HMBC	Heteronuclear Multiple Bond Correlation
HMDS	bis(trimethylsilyl)amino
HMPA/HMPT	hexamethylphosphoric triamide
HOMO	Highest Occupied Molecular Orbital
HSQC	Heteronuclear Single Bond Correlation
IDipp	1,3-di-(2,6-di-*iso*-propyl)phenylimidazol-2-ylidene
IMes	1,3-di-mesitylimidazol-2-ylidene
*i*Pr	*iso*-propyl
I*i*Pr	1,3-di- *iso*-propylimidazol-2-ylidene
iso	bound to a secondary atom
IR	Infrared (Spectroscopy)
I*t*Bu	1,3-di-*tert*-butylimidazol-2-ylidene

K	Kelvin
LIFDI	Liquid Injection Field Desorption Ionization
LMCT	Ligand to Metal Charge Transfer
LUMO	Lowest Unoccupied Molecular Orbital
m	meta
Me	methyl
MeCN	acetonitrile
MeOH	methanol
Mes	mesityl; (2,4,6-trimethylphenyl)
MHz	Megahertz
Min	minute
MS	Mass Spectrometry
MW	Molecular Weight
m/z	mass/charge
n	normal
*n*BuLi	*n*-butyllithium
NHC	*N*-heterocyclic carbene
NHSi	*N*-heterocyclic silylene
NMR	Nuclear Magnetic Resonance
Nu	nucleophil
o	ortho
OAc	acetoxy
OLED	Organic Light Emitting Diode
p	para
Ph	phenyl
pKs	acid dissociation constant
ppm	parts per million
Py	pyridyl
R	any alkyl substituent if not defined otherwise
s	second
SPHOS	2-dicyclohexylphosphino-2',6'-dimethoxybiphenyl
rt	room temperature
*t*Bu	*tertiary* butyl
TEP	Tolman Electronic Parameter
tert	bound to a tertiary atom
TGA	Thermogravimetric Analysis
THF	tetrahydrofuran
TMEDA	tetramethylethylenediamine
TMS	tetramethylsilane / trimethylsilyl
tol	meta-/toluene
UV/Vis	Ultraviolet-Visible (Spectroscopy)
V_{bur}	buried volume
X-ray	X-ray radiation, a form of electromagnetic radiation
XRD	X-ray Diffraction Analysis
z	charge

List of Compounds

1

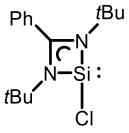

2

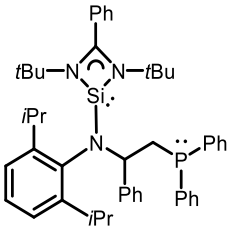

3

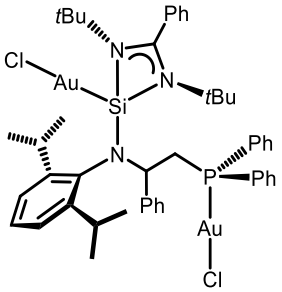

4

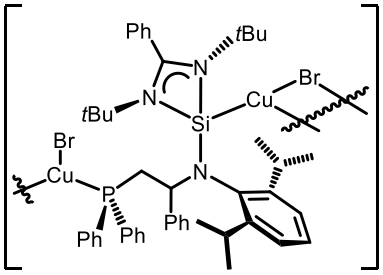

5

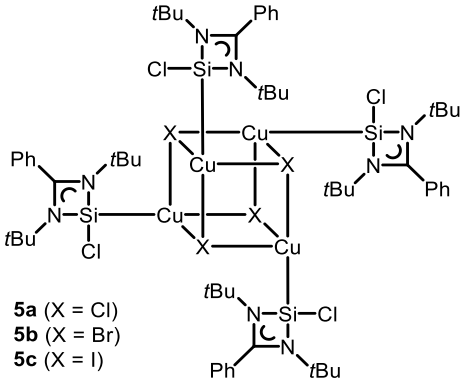

5a (X = Cl)
5b (X = Br)
5c (X = I)

6

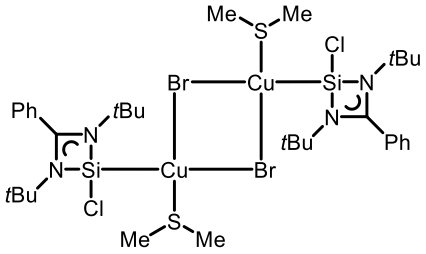

7

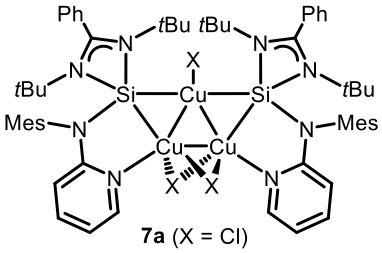

7a (X = Cl)
7b (X = Br)
7c (X = I)

8

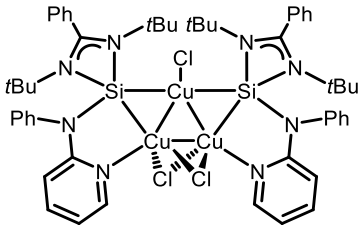

9

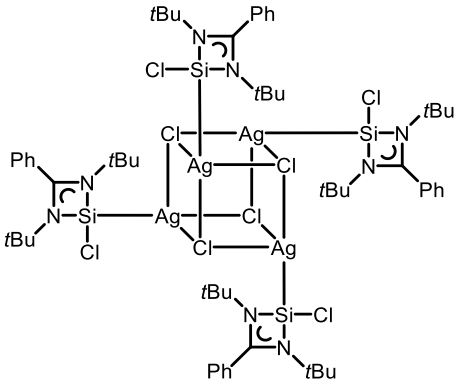

10

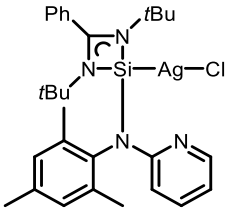

11

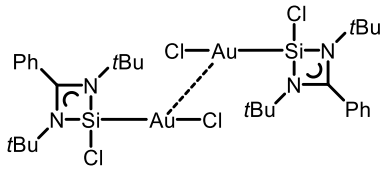

12

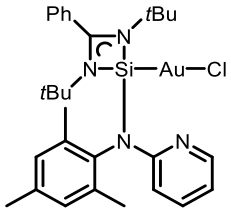

13

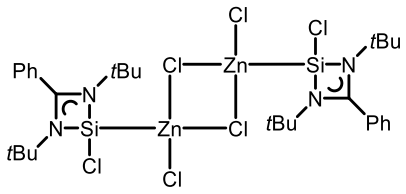

14

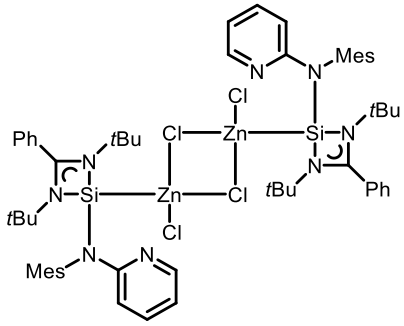

15

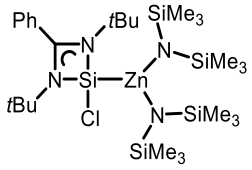

16

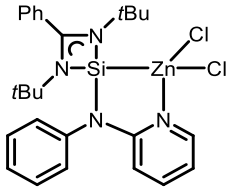

1. Introduction

1.1. Development of Silylenes

The recent decades of silicon chemistry are mainly based on silicon (IV) compounds, whereas that of silicon(II) is considerably less mature, but developing into an emerging field.[1,2] Until the mid-nineties, silylenes were generally considered to be highly reactive and unstable species that decompose or polymerize readily above temperatures of -196°C and therefore isolation seemed inconceivable. However, the first report of a silylene is dated back to 1977, when *Welz* & *Schmid* were able to synthesize and characterize the *N*-heterocyclic silylene $Fe(CO)_4$ complex **I**, which was still thermolabile and decomposed above temperatures of -20°C (see Scheme 1, **I**).[3] In addition, this early example of a donor-stabilized *N*-heterocyclic silylene (NHSi) was not isolated as the free silylene, but only in form of the transition metal complex **I**, which is quite apparent considering that the coordination to a metal center tames the high reactivity of the silylene.

Scheme 1. Synthesis of the first silylene employed in a transition metal complex (**I**) by *Welz* & *Schmid* in 1977[3].

Shortly after, *West*, *Fink* and *Michl* were able to characterize the formation of a silylene as an intermediate while investigating the synthesis of tetramesityldisilene (see Scheme 2).[4] Photolysis of 2,2-bis(2,4,6-trimethylphenyl)hexamethyltrisilane resulted in the stable compound **IIa** under the formation of dimesitylsilylene **II**, which could be trapped utilizing a suitable reagent, like triethylsilane (see Scheme 2, **IIb**). Hence, at temperatures above -170°C or due to the absence of trapping reagents, the silylene underwent the dimerization to **II**.

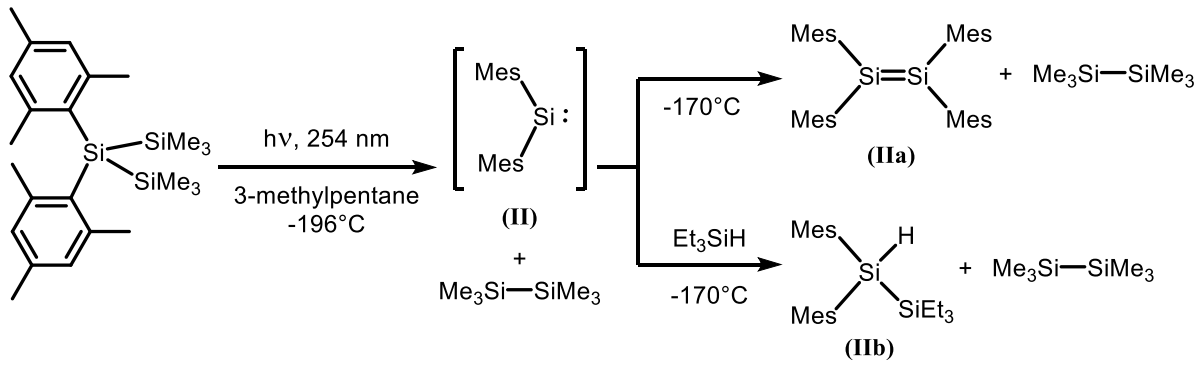

Scheme 2. Synthesis of 2,2-bis(2,4,6-trimethylphenyl)hexamethyltrisilane (**IIa**) under the formation of the free dimesitylsilylene (**II**) *via* photolysis by *West*, *Fink* and *Michl* in 1981[4]. The silylene could be trapped using, e.g., Et_3SiH, resulting in compound **IIb**.

Roughly ten years later *Jutzi et al.* were able to isolate the first free silylene which was also stable at room temperature, the decamethylsilicocen $SiCp^*_2$ (see Scheme 3, **III**).[5] With this breakthrough, they also managed to synthesize one of the few compounds counting to the rare subclass of silylenes bearing π-coordinated ligands.

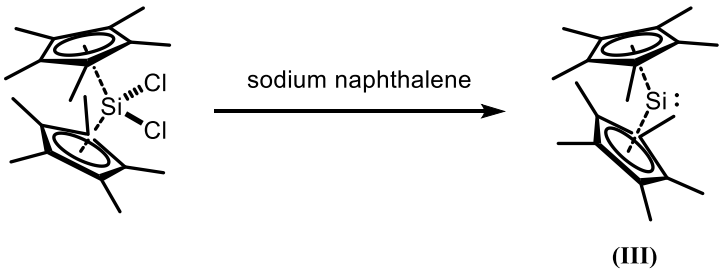

(III)

Scheme 3. Synthesis of the first free room temperature stable silylene *via* reduction using sodium naphthalene to generate the free π-coordinated silylene the decamethylsilicocen $SiCp^*_2$ (**III**) by *Jutzi et al.* in 1989[5].

In 1994, *Denk* & *West et al.* adapted the preceding work of *Arduengo et al.* in the field of *N*-heterocyclic carbenes[6] and reported the synthesis of a free five-membered *N*-heterocyclic silylene showing an *Arduengo*-type motif and therefore establishing the subclass of *N*-heterocyclic silylenes (see Scheme 5, **IV**).[7]

This pioneering work was the starting point for upcoming work in the area of silylenes, not only with motifs similar to the NHSi as mentioned above. In the following, the different types of low-valent silicon compounds referred to as silylenes, will be summarized in certain classes: (**A**) *N*-heterocyclic silylenes, (**B**) donor-stabilized *N*-heterocyclic silylenes, (**C**) cyclic donor-stabilized silylenes and (**D**) acyclic silylenes (see Scheme 4).[2,8] The strict definition of silylenes stipulates a silicon(II) atom bearing two substituents. However, additional donating groups are an important feature in the ligand design of silylenes and will be described in detail later on. For the purpose of simplification, the definition of *N*-heterocyclic silylenes will be generalized and include both cases, bearing additional donating-groups or not, and it will be referred to them as NHSis in general.

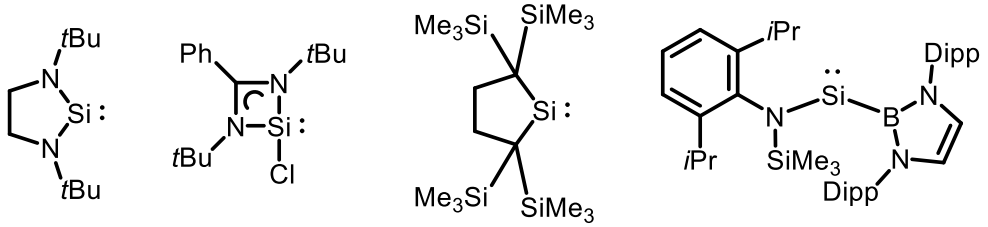

(**A**) (**B**) (**C**) (**D**)

Scheme 4. Overview of the four classes of low-valent silicon(II) compounds: (**A**) *N*-heterocyclic silylenes; (**B**) donor-stabilized *N*-heterocyclic silylenes; (**C**) cyclic donor-stabilized silylenes; (**D**) acyclic silylenes.

N-heterocyclic silylenes (**A**) and especially donor-stabilized NHSis (**B**) are by far the most investigated classes of silylenes. After the aforementioned achievements of *Denk* & *West et al.* (see Scheme 5, **IV**), various derivatives of the five-membered NHSi were published in the first decade of the 21th century. Besides the presence of an additional donating group these two subclasses of silylenes primarily differ in length and type of their backbone and can vary from a four-membered ring to a six-membered ring (see Scheme 5 and Scheme 5). Shortly after, *Lappert* & *Gehrhus et al.* published the synthesis and isolation of a five-membered NHSi bearing a benzyl-ring in the backbone (**V**).[9] In 1998 the group of *Veszprémi* modified this structure by introducing a pyridyl group to the backbone, thus illustrating the first possibilities of ligand design.[10]

Ten years later, *Driess et al.* elongated the list of *N*-heterocyclic silylenes by the synthesis of the β-diketiminate silylene (**VI**).[11] This motif, being the only representative of six-membered NHSis, led to many investigations of this structure and its derivatives, due to its unusual reactivity towards nucleophiles owing to its butadiene backbone. In 2009 *Cui et al.* published further isolable NHSis with varying residues adjacent to the nitrogen atoms further illustrating the versatility of NHSis and their ligand design (see Scheme 5, **VII**).[12]

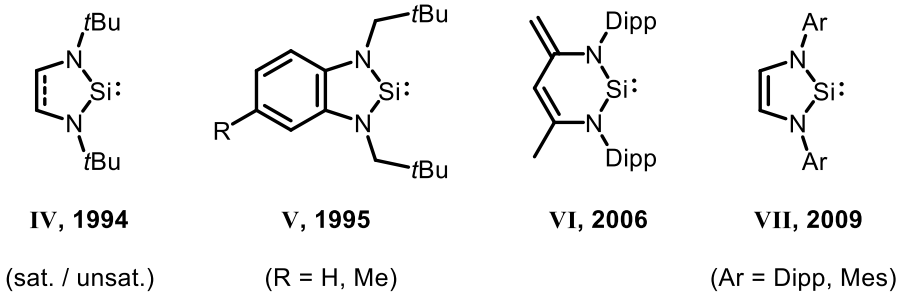

Scheme 5. Prominent examples of *N*-heterocyclic silylenes (**A**) (f.l.t.r.): *West* & *Denk et al.* (**IV**, 1994[7]); *Lappert* & *Gehrhus et al.* (**V**, 1995[9]); *Driess et al.* (**VI**, 2006[11]); *Cui et al.* (**VII**, 2009[12]).

In the case of donor-stabilized NHSis (**B**), the silicon atom exhibits three bonds of which one formally counts as the donor-group donating electron density into the vacant p-orbital for stabilization (structural details will be pointed out in Chapter 1.2). Among this class, one system has to be highlighted not only in the context of this work. In 2006 *Roesky et al.* reported the synthesis and isolation of the four-membered free benzamidinato chloro silylene (**VII**, see Scheme 6) and therefore the smallest representative of the subclass of silylenes (**B**).[13] Due to the very low yields of approximately 10% it did not raise a lot of awareness in the beginning, but only a few years later the same group was able to improve the yield up to 90% utilizing an alternative milder dehydrochlorination using LiHMDS.[14] This facile access in high yields raised a lot of attention, not only in the area of synthetic chemistry, and increased further investigation of this system to this day.[15]

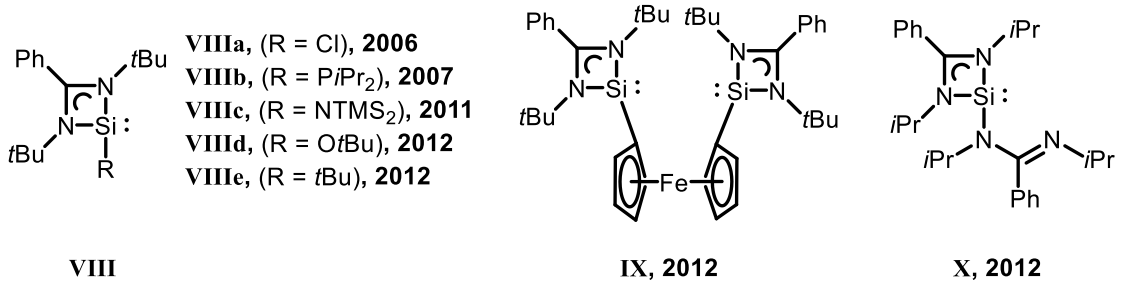

Scheme 6. Prominent examples of Lewis base donor-stabilized *N*-heterocyclic silylenes (**B**) (f.l.t.r.): *Roesky et al.* (**VIIIa**, 2006[13], **VIIIb**, 2007[16], **VIIIc**, 2011[17] & **VIIId-e**, 2012[18]); *Driess et al.* (**IX**, 2012[19]); *Tacke et al.* (**X**, 2012[20,21]).

The chloro group of the benzamidinato silylene **VIIIa** appeared to be easily substitutable, which paved the way for facile functionalization of this silylene (e.g. **VIIIb-e**, **IX** and **X**).[13,16–19] In the following years, the group of *Driess* for example characterized various functionalized benzamidinato silylenes and *inter alia* concentrated on the synthesis of chelate like ligands for the complexation of transition metal centers by connecting two benzamidinato silylenes, employing e.g. a ferrocyl group (**IX**).[19] Some of these transition metal complexes also proved to be active catalysts in certain reactions, like C–C cross-coupling, hydrogenation or cyclotrimerization reactions, just to name a few (see Chapter 1.3).[22] The group of *Tacke* also published a series of four-membered NHSis in 2012 (see Scheme 6, **X**). Due to their ligand design, the functional group can act as a side-arm with an additional donor-site, or coordinate to the silicon center leading to a double donation (see Chapter 1.4 ff for more details).[20,21]

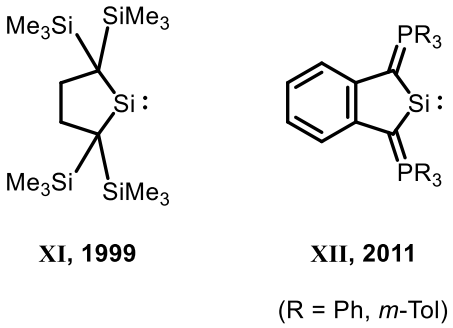

Scheme 7. Prominent examples of carbocyclic silylenes (**C**) (f.l.t.r.): *Kira et al.* (**XI**, 1999[23]); *Driess et al.* (**XII**, 2011[24]).

The classes of cyclic donor-stabilized silylenes (**C**) and acyclic silylenes (**D**) are comparatively less renowned, but not less interesting. The main difference of class (**C**) is the absence of adjacent nitrogen atoms, which is a fundamental factor in the stabilization of the silicon center and thus the primary reasons why these silylenes are challenging to isolate. By now, there are only five-membered carbocyclic silylenes known, which were initially investigated by *Kira et al*. (see Scheme 7, **XI**).[23] Through the introduction of sterically demanding trimethylsilyl residues, they gained a kinetic stabilization and hence inhibit dimerization. The group of *Driess* recently reported the synthesis of a

carbocyclic silylene bearing aromatic phosphorous ylide moieties adjacent to the silicon center therefore stabilizing the silylene (see Scheme 7, **XII**).[24]

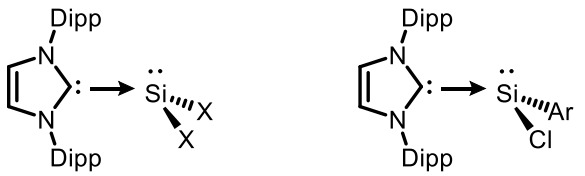

XIIIa/b, 2009 (X = Cl, Br) **XIV, 2010** (Ar = 2,6-Mes_2-C_6H_3)

Scheme 8. Examples of NHC donor-stabilized SiX_2 and SiXAr silylene adducts (f.l.t.r.): *Roesky et al.* (**XIIIa**, X = Cl, 2009[25]); *Filippou et al.* (**XIIIb**, X = Br, 2009[26]); *Filippou et al.* (**XIV**, 2010[27]).

Silylenes belonging to the acyclic class (**D**) are by far the rarest and most recent ones. For decades, they had only been observed as transient intermediates or on the basis of trapping experiments. There were attempts to isolate SiX_2 fragments via π-donor stabilization and thus after the strict definition not belonging to this class of compounds, but worth mentioning (see Scheme 8). In 2009 the group of *Roesky* published a donor-stabilized dichloro silylene bearing an NHC as the Lewis base (**XIIIa**).[25] Simultaneously *Filippou et al*. were also able to isolate the dibromo analogue in a similar manner (**XIIIb**).[26] Since the $SiCl_2$ fragment is an key intermediate, e.g., for the Siemens process of the synthesis of high-purity silicon by thermal decomposition of $HSiCl_3$, the isolation of the donor-stabilized $SiCl_2$ moiety was a milestone in silicon chemistry.

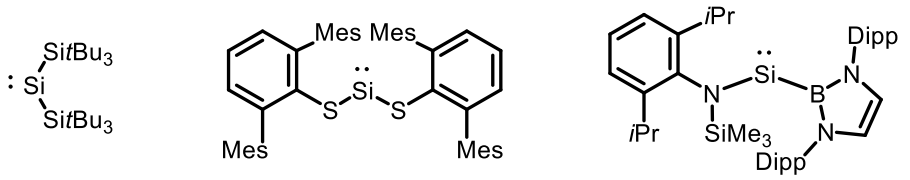

XV, 2003 **XVI, 2012** **XVII, 2012**

Scheme 9. Prominent examples of acyclic silylenes (**D**) (f.l.t.r.): *Sekiguchi* & *Akiyama et al.* (**XV**, 2003[28]); *Power et al.* (**XVI**, 2012[29]); *Jones, Mountford, Aldridge and Kaltsoyannis* (**XVII**, 2012[30]).

However, the isolation of a stable donor-free acyclic silylene was still outstanding. In 2003, *Sekiguchi* & *Akiyama et al*. synthesized the acyclic bis(tri-*tert*-butylsilyl)silylene **XV** at temperatures below -196°C and were able to confirm a triplet ground state of the silicon center *via* EPR spectroscopy.[28] Since silylenes generally exhibit singlet ground states (see Chapter 1.2), this seminal work suggests that acyclic silylenes could be the key to triplet state silylenes and therefore potentially increasing the reactivity in regard to, e.g. small molecule activation. But the synthesis of isolable acyclic silylenes remained elusive until very recently. In 2012, when *Power et al.* and separately *Jones*, *Mountford*, *Aldridge* and *Kaltsoyannis* were able to finally present the first isolable acyclic low-valent silicon(II)

compounds (see Scheme 9, **XVI** & **XVII**).[29,30] Unfortunately, both compounds exhibit singlet ground states, but through crystal structure analysis and computational studies, the assumption could be supported that the angle around the silicon center correlates to the HOMO-LUMO gap and therefore to the singlet-triplet energy gap, which suggests it is mainly influenced by electronical factors.[31]

This manifold types of silylenes were expanded by their utilization in catalytical transformations and producing even more isolable silylenes, which will be partially highlighted in Chapter 1.3.

1.2. Electronical and Structural Properties

As already mentioned, the applications of recent low-valent silicon(II) compounds appear to focus on organometallic ligands for transition metal complexes regarding new or improved catalytical properties as well as metal-free alternatives for usually metal-mediated transformations, e.g. small molecule activations.[2,32] Considering the properties and electronical structure of silylenes, as well as the similarities and more importantly the significant differences to the ubiquitous NHCs, this class of organometallic ligands is particularly interesting for modern synthesis. The fundamental differences can be best compared on the basis of the calculated molecule structures and electron configurations of the smallest corresponding systems, the methylene ($:CH_2$) and silylene ($:SiH_2$), and therefore the direct comparison to the well-investigated NHCs can be drawn.[33,34] Carbenes can occur in two geometrical structures: linear and angled. Linear carbenes show a sp-hybridization with two degenerate non-bonding orbitals $2p_x$ and $2p_z$. The more common bent structure shows a sp^2-hybridization with an energetically stabilized $2p_x$-orbital (σ-orbital) compared to the $2p_z$-orbital (p_π-orbital) (see Scheme 10).

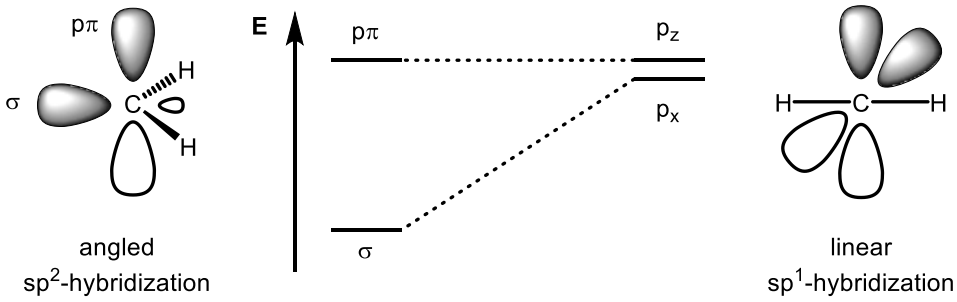

Scheme 10. Schematic relation between angled and linear geometry and their corresponding hybridization and respective electronical configuration.[33,34]

For the bent carbenes the spin multiplicities singlet ($\sigma^2p\pi^0$, $^1A_1$, spin paired) and triplet ($\sigma^1p_\pi^1$, $^3B_1$, spin unpaired) result from the size of the orbital splitting of the σ- and p_π-orbital, which is mainly influenced by the adjacent substituents. A large splitting leads to a singlet state while the triplet state is favored for smaller separation (see Scheme 11).[35]

Scheme 11. Schematic illustration of the two appropriate ground states for carbenes using the example of ($:CH_2$). **Left**: triplet ($o^1p_\pi^1$, $^3B_1$, spin unpaired); **right**: singlet (σ^2, $^1A_1$, spin paired).[33,34]

In general, carbenes and silylenes can occur in either states, depending on the electronical conditions mostly influenced by the adjacent substituents and their properties. The methylene ($:CH_2$) favors a

triplet ground state, whereas the silylene (:SiH_2) shows a singlet ground state, due to the higher s-p-orbital separation of the silicon atom, which makes the formation of hybrid orbitals energetically higher compared to the carbon atom.[36] Electron density investigations show the lone-pair to have predominantly s-character.[25] In addition, the inert-pair-effect causes an even larger HOMO-LUMO separation for higher homologues of group 14 elements, which usually results in a separation energy higher than the spin pairing energy, thus favoring the singlet ground state.[33] A triplet ground state for silylenes is very scarce (see Chapter 1.1).[28,37]

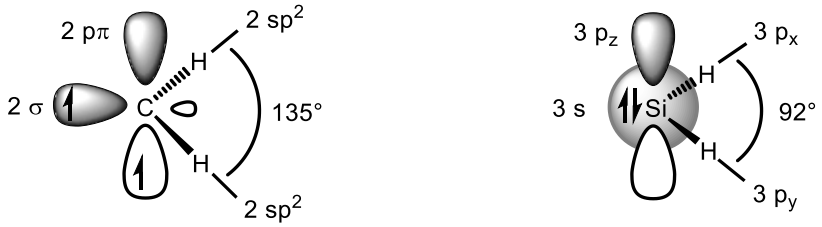

Scheme 12. Comparison of the schematic molecular structures and electron configurations of methylene (:CH_2) and silylene (:SiH_2) by means of hybridization and ground states.[33]

The singlet configuration of silylenes results in an unoccupied p_z-orbital which stabilization is mandatory for the isolation of the free species. It can either be stabilized through kinetic or thermodynamic effects. The latter is accomplished primarily by the introduction of π-donor substituents, which donate electron density *via* mesomeric effects (+M) into the empty p-orbital of the low-valent Si(II) atom, thus assuring the formal compliance of the octet rule (see Scheme 13, left).[38]

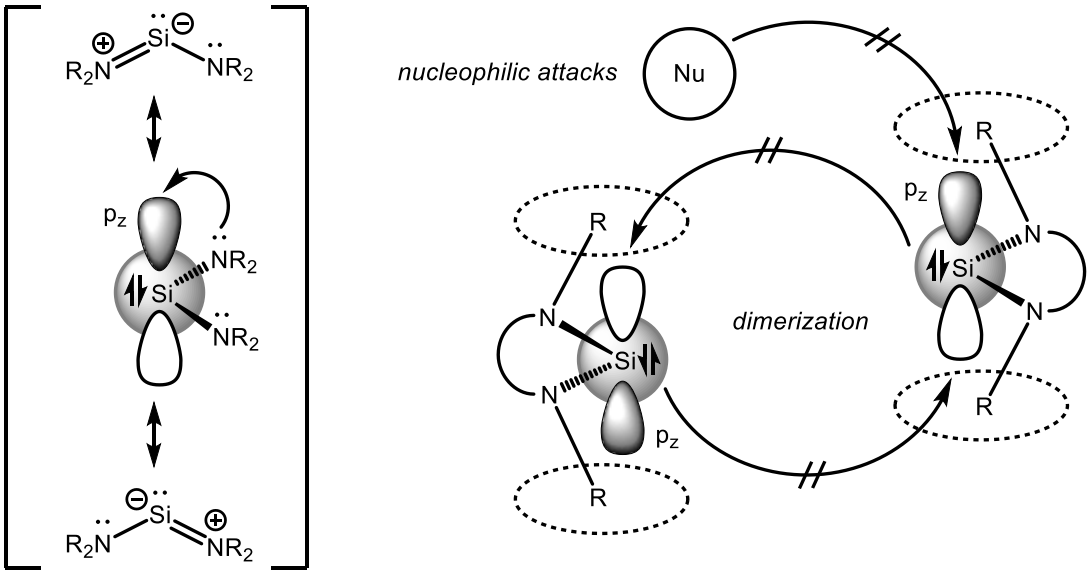

Scheme 13. Schematic illustration of thermodynamic stabilization elucidated at the example of diaminosilylene (left) and kinetic stabilization visualized at the example of sterically demanding residues "R" (right).[33,38]

This approach of stabilization is widely spread and usually achieved by employing nitrogen atoms bearing electron donating alkyl-groups, thus establishing the class of *N*-heterocyclic silylenes (see Chapter 1.1). A further thermodynamic effect occurs in cyclic systems through chelating effects, which

N-heterocyclic systems are entailing as well. Kinetic stabilization is mostly achieved by the introduction of sterically demanding groups adjacent to the reactive center to protect the empty p-orbital of nucleophilic attacks as well as prevent dimerization (see Scheme 13, right).

With the synthesis of the first isolable silylenes and accompanied with the progressive investigation of their reactive behavior, they became an interesting topic for computational studies. An early attempt was published by *Frenking* and *Boehme* in 1998, where they were discussing calculated coinage metal silylene complexes and came to the conclusion that silylenes show a trend of σ-donation equally strong to NHCs.[39] Fortunately, over the past years, not only numerous reports on experimental achievements and applications, but also recent comprehensive theoretical studies were able to show that silylenes can compete and even exceed the potential of common carbenes of modern chemistry.[2,8,15,22,40]

One example are the comprehensive studies of *Benedek* and *Szilváski* from 2015 which, *inter alia*, gave a detailed understanding of the properties of different classes.[8] To compare the utilization of silylenes as organometallic ligands in transition metal complexes, they analyzed the σ-donor and π-acceptor ability, the ligand to metal charge transfer (LMCT) and sterical factors of commonly used NHCs, phosphines and novel silylenes of the different classes (see Chapter 1.1), **A**-**D**). Throughout these studies they emphasized the importance of additional donor-groups regarding the ligand design against strong σ-donor ligands.

As discussed above, the electron deficient silicon atom bears a vacant p_z-orbital which stabilization is compulsory and primarily managed by introducing adjacent nitrogen atoms donating electron density (see Scheme 14 **[I]**). Furthermore, the σ-donor strength of the low-valent silicon(II) atom is mainly determined by the localized electron density. Certainly, functional groups adjacent to the vacant orbital of the silicon atom have direct influence on the stabilization of the silylene through electron donating or withdrawing effects and thus on the σ-donor strength. *N*-heterocyclic silylenes flanked by two electronegative nitrogen atoms significantly withdraw electron density and only weakly donate to the π-system, hence damping its total σ-donor strength. On the other hand, this weak π-donation provides the option for additional donor groups to coordinate the silicon atom by donating lone-pairs into the vacant p-orbital, thus significantly increasing the σ-donor ability (see Scheme 14, **[II]**). As a result, donor-free *N*-heterocyclic silylenes also show to have the highest π-acceptor ability.

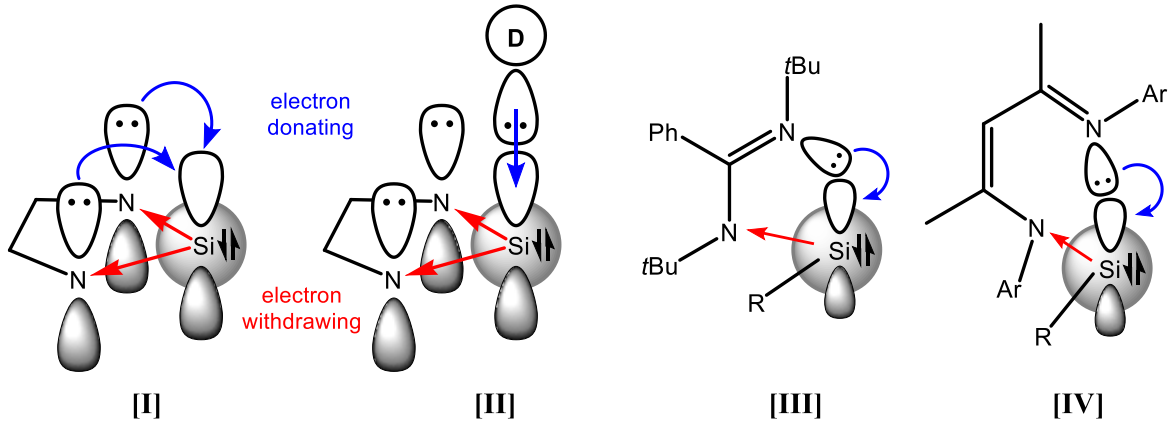

Scheme 14. Illustration of electron donating (**blue**) and withdrawing (**red**) effects of adjacent functional groups within the molecular structures of NHSis (**I**), donor-stabilized NHSis (**II**) and at the concrete example of donor-stabilized benzamidinato (**III**) and β-diketiminato silylenes (**IV**) according to *Benedek* and *Szilváski*.[8] (This graphic is only intended to illustrate electronical influences, not actual bonds.)

Besides, *Benedek* and *Szilváski* compared the influence of different ring sizes regarding to their σ-donor ability. The N–Si–N angles of the donor-free four-membered ring is 67.9° (**[III]**, for R = H), whereas the corresponding six-membered ring is 88.2° (**[IV]**, for R = H, Ar = Dipp), which is more favored for the overlapping of the involved orbitals, thus showing a stronger σ-donor ability. Nevertheless, the introduction of an electron-rich donating group to the silicon center seems to boost the σ-donor-ability significantly in both cases, again emphasizing the positive effect of extra donor groups and its potential for ligand design. These properties could also be confirmed computationally, e.g. towards the reactivity of small molecule activation reactions, as well as by evaluating experimental achievements, which will be highlighted later on.[41]

Due to the additional electron donation into the vacant orbital, donor-stabilized NHSis appeared to be superior regarding their σ-donor abilities. However, this is not the only benefit of donating groups. The introduction adjacent to the low-valent silicon center enables the possibility to implement other functionalities right next to the reactive site, like extra sterically demanding residues, additional donor-sites or linking functions. This feature can be instrumentalized, turning donor-stabilized NHSis into an almost freely customizable all-rounder with excellent σ-donor and π-acceptor abilities for the synthesis of transition metal complexes and thus a promising tool for future metal-mediated catalysis.

Depending on the choice of functional group silylenes can be turned into monodentate, bidentate and tridentate ligands. Monodentate silylenes are the simplest kind of ligands, whether historical NHSis (see Chapter 1.1), the facile access to β-diketiminato silylenes or the famous benzamidinato silylenes, they are widely spread in this field of chemistry. Bidentate ligands, also known as chelate-ligands, can be achieved by the introduction of donating groups which simultaneously act as linking moieties of two silylenes, or by groups bearing an additional donor-site on a, e.g., nitrogenous basis.

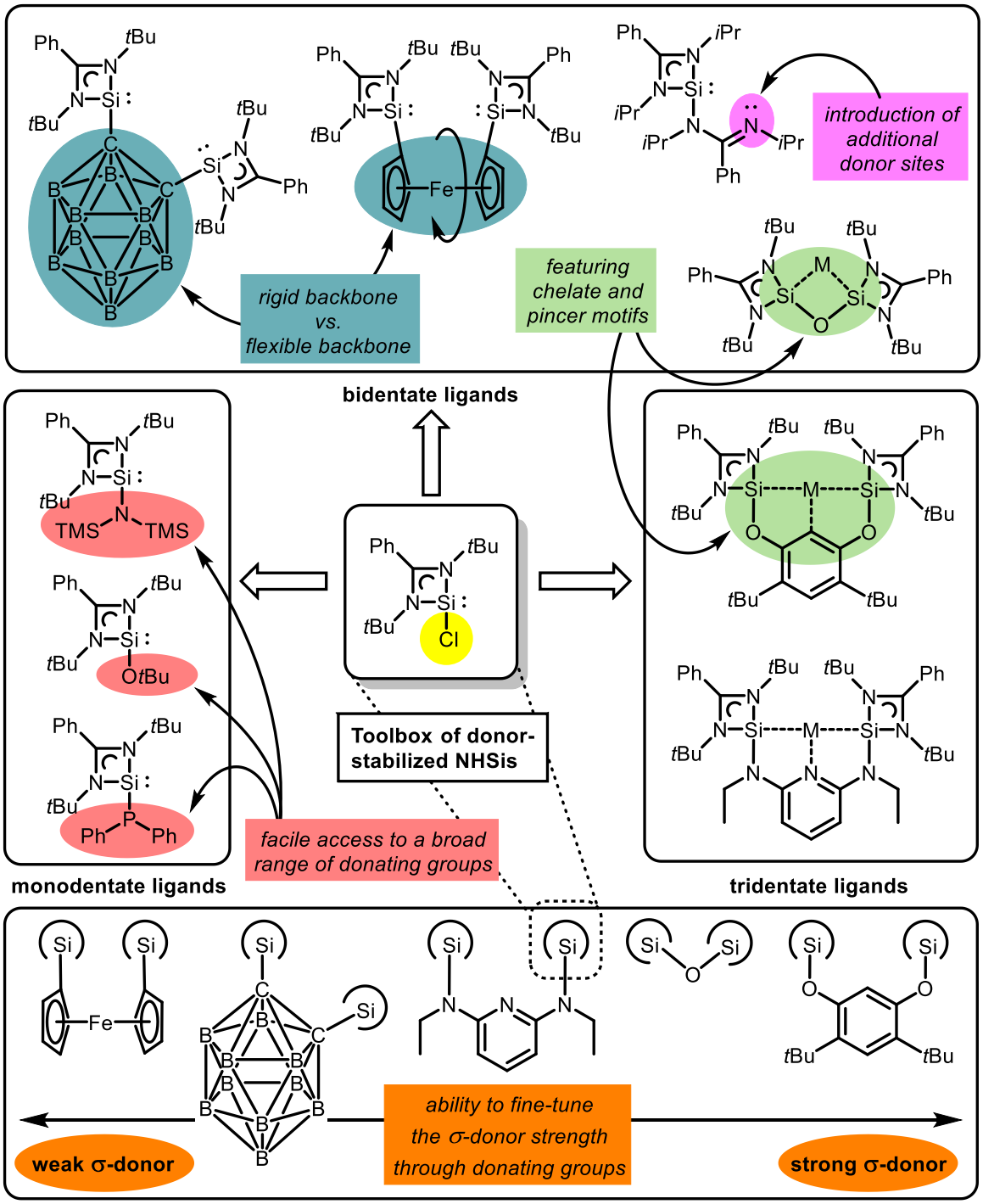

Scheme 15. Overview of the possible ways of utilizing donor-stabilized NHSis at the example of the chloro benzamidinato silylene. Further details to the shown structures are described in Chapter 1.1 to 1.3.

In the case of linking moieties, a further feature has to be taken into account, whether the linker shows a flexibility, or not. The introduction of ferrocene as a donating group, published by *Driess et al.*, acts as a very flexible backbone, due to the possible free rotation of the η^5-bound cyclopentadienyl ligands (see Scheme 15).[19][42] The application of a carborane backbone on the contrary provides a rigid linker.[43] The primarily method to introduce such linkers is done *via* salt metathesis of the, e.g., chloro benzamidinato silylene and the metalated spacing group. On the same way it is possible to introduce

linking moieties which provide an additional donor-site, thus creating multidentate scaffolds known as pincer ligands, or in this context, tridentate ligands. The group of *Driess* was one of the first, who reported the synthesis of an early isolable example of pincer ligands, by employing a 4,6-di-*tert*-butylresorcinol moiety and successively coordinating transition metal centers in a Si–C–Si fashion, by insertion into the C–H bond of the backbone.[44]

As previously mentioned, sterically demanding residues are used to gain a kinetic stabilization on low-valent centers of carbenes or silylenes. But this effect can be transferred and extended to affect the ligand-metal coordination, too. The so-called buried volume (%V_{bur}) is a common concept in ligand design and describes the amount of space occupied by the ligand compared to the theoretical sphere around the metal center (with a radius of 3 Å) in percent.[45] Comparing the topology of commonly used ligands, traditional phosphines usually show a tapered cone angle and therefore a low value of buried volume (see Scheme 16, left),[46] whereas NHCs often form a hemisphere around the metal center, thus a higher %V_{bur} (see Scheme 16, middle).[47] This concept was traditionally designed to interpret phosphines and NHCs, but since donor-free five-membered *N*-heterocyclic silylenes most likely show a similar geometry compared to most of the prominent NHCs, it could be transferred to compare them to NHCs, hence correspondingly a comparable %V_{bur} (see Scheme 16, middle/right). The possible introduction of additional Lewis-base donor-groups could enable the opportunity to introduce supplementary sterically demanding residues to generate bulkier geometries. Following this concept, ligands can be designed to form a "coordination pocket" around the metal center to modulate the reactivity on a kinetically basis.

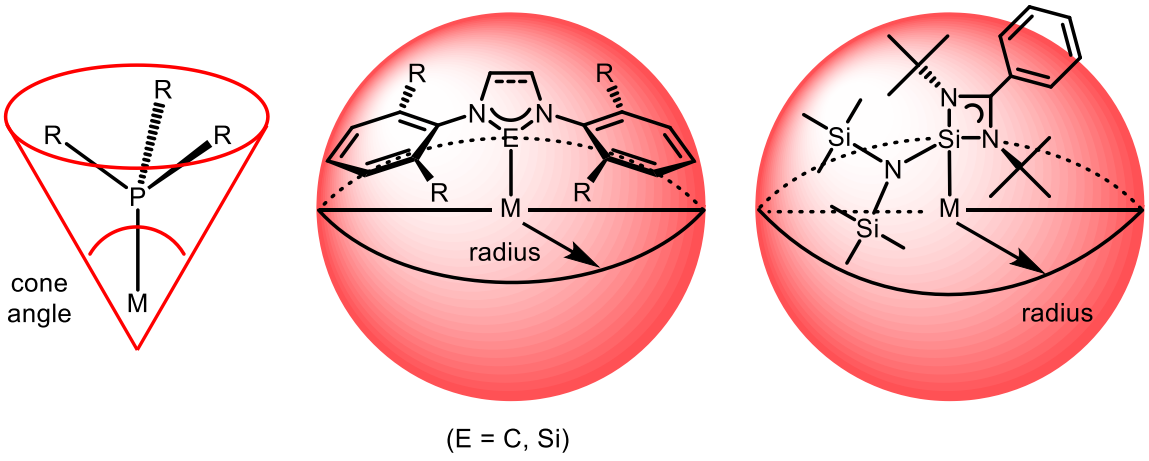

Scheme 16. Graphical illustration of different methods for the determination of buried volume in organometallic complexes (**left**: cone angle; middle: buried volume %V_{bur}) and the possible transformation of the concept to NHSis (**middle**/**right**: buried volume %V_{bur}).

After presenting the electronical features and general structure of NHSis, as well as a first look at the possibilities to modify them and exert sterical influence on metal coordination, it is also important to highlight concepts for determining the σ-donor strength. The σ-donor ability plays a vital role in the

design of organometallic ligands, since its electronical features have direct influence on the electronical structure of metal centers and thus on the corresponding metal-mediated catalysis. Such correlations could be investigated using methods like the *Tolman electronic parameter* (TEP). The TEP is widely used to compare the overall σ-donor strength of usually low-valent carbon and phosphorous ligands. Primarily $LNi(CO)_x$ complexes, derived from the corresponding free ligand and the nickel carbonyl precursor, are used and analyzed via IR spectroscopy to determine the CO stretching vibration modes. The elementary principle works as followed: the stronger the σ-donor ability of the ligand, the higher is the electron density at the metal center. The electron richer the metal center, the stronger is the π-backdonation to the CO ligand in *trans*-position to the σ-donor ligand (*trans-effect*), which has a destabilizing effect on the CO-bond. This lowers the wavenumbers of the CO stretching frequencies of the in comparison to the 'free' CO ligand. In conclusion: the higher the σ-donor strength, the lower the CO stretching frequency and *vice versa*.[46]

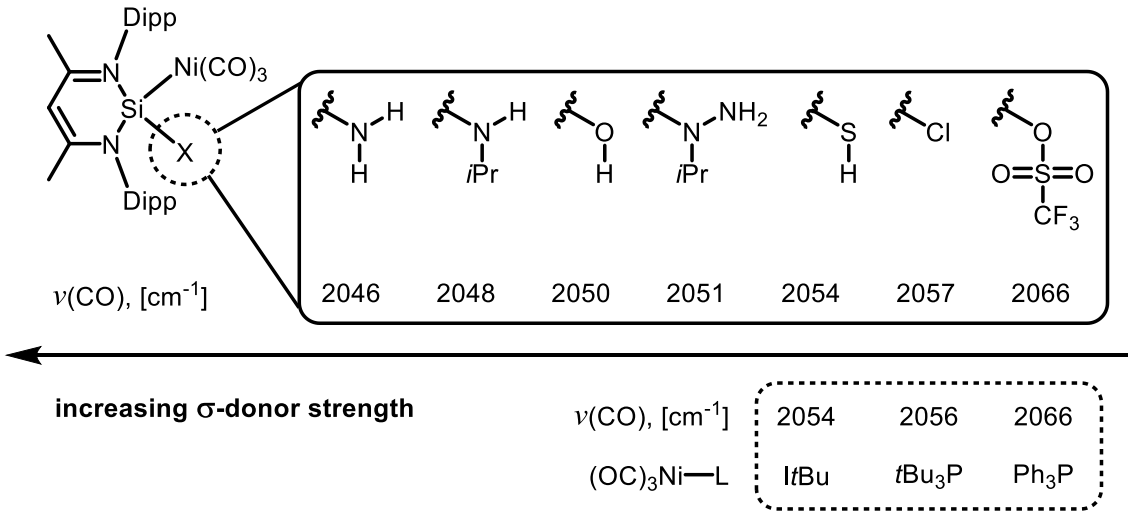

Scheme 17. Graphical illustration of the tuning ability of the donor functionality "X" of the β-diketiminato silylene derived from their CO frequencies of the corresponding $LNi(CO)_3$ complex (in wavenumbers ν in [cm^{-1}]), sorted by their increasing σ-donor strength. The wavenumbers of 1,3-di-*tert*-butylimidazolium (I*t*Bu), tri-*tert*-butylphosphine (tBu$_3$P) and triphenylphosphine (Ph_3P) are listed in the dashed box for comparison purposes.[48]

In 2010 *Driess et al.* investigated the influence of certain additional donating groups on the basis of their previously reported *N*-heterocyclic β-diketiminato silylene (see Scheme 17).[48] Following the concept described above, they analyzed the CO frequencies of the respective $NHSi\text{-}Ni(CO)_x$ complex bearing different donor groups and were able to determine the order of their σ-donor ability: $-NH_2$ (2046 cm^{-1}), –NH*i*Pr (2048 cm^{-1}), –OH (2050 cm^{-1}), $-N(NH_2)(iPr)$ (2051 cm^{-1}), –SH (2054 cm^{-1}), –Cl (2057 cm^{-1}), $-O_3SCF_3$ (2066 cm^{-1}). On the one hand, this illustrates the potential of the tuning functionality of donor groups and on the other hand, drawing the comparison to common NHCs and phosphines shows that several compounds are able to outperform their performances: I*t*Bu (2054 cm^{-1}), tBu$_3$P (2056 cm^{-1}), Ph_3P (2058 cm^{-1}).

In the previous chapter, the different types of silylenes were categorized into four classes, sorted by their general type of structural and electronical features: (**A**) *N*-heterocyclic silylenes, (**B**) donor-stabilized *N*-heterocyclic silylenes, (**C**) cyclic donor-stabilized silylenes and (**D**) acyclic silylenes. When it comes to the utilization of silylenes as steering ligands in transition metal complexes, these classes can be redefined according to their σ-donor abilities.

Driess and *Zhou* recently characterized the different classes of silylenes by the comparison of their ^{29}Si NMR signals, suggesting, that the σ-donor strength shows a direct relation to the respective chemical shifts (see Scheme 18).[49] Concluding, that deshielded ^{29}Si nuclei belong to electronically depleted silicon(II) centers (e.g. dialkylsilylenes, **[1]**) and *vice versa* shielded nuclei to electron rich centers (e.g. donor-stabilized *N*-heterocyclic silylenes, **[5]**), based on concrete experimental observations derived by ^{29}Si NMR spectroscopy by *Iwamoto et al.*, *Kato et al., Denk et al.* and *Baceiredo et al*.[7,23,50,51] According to these studies and as visualized in Scheme 18 (top), dialkylsilylenes (**[1]**) prove to exhibit the weakest σ-donor strengths, while donor-stabilized NHSis (**[5]**) show the strongest σ-donor strengths.

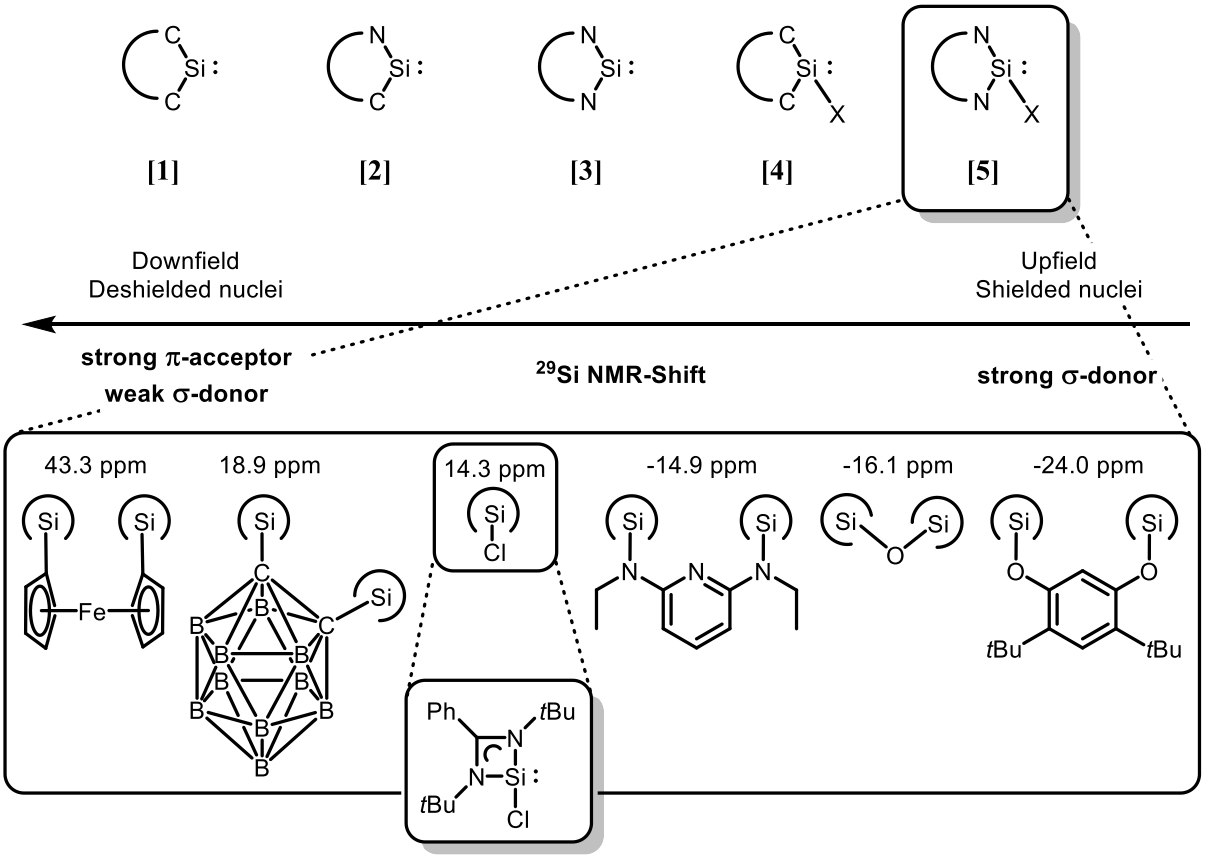

Scheme 18. Top: Redefined classes of silylenes, sorted by their fixed σ-donor strength derived by their respective ^{29}Si NMR signals. **Bottom**: Classification of σ-donor strengths of functionalized benzamidinato silylenes derived by their ^{29}Si NMR signals.[49]

The π-acceptor ability of the Si(II) center decreases by the stepwise introduction of adjacent nitrogen atoms, due to the aforementioned π-donor bonding interactions (dialkysilylenes **[1]** < cyclic alkyl-(amino)silylenes **[2]** < two-coordinate NHSi systems **[3]**). By introducing additional donating groups, the electron density gets pushed to the silicon center, due to reasons described above (donor-stabilized dialkysilylenes **[4]** < donor-stabilized NHSi systems **[5]**). Within class **[5]** *Zhou* and *Driess* went even more into detail and compared different types of linked bidentate and tridentate NHSi ligands *via* the same method (see Scheme 18, bottom). The highest upfield shift, hence the strongest σ-donor ability is shown by oxo-based linkers (-24.0 to -16.1 ppm), followed by amino- and carbo-substituted silylenes (-14.9 to 17.3 ppm) and the lowest downfield shifts are observed at the ferrocyl and carborane linked moieties (18.9 to 43.3 ppm).

Hence, in the ligand design of silylenes one can affect the basis of σ-donor and π-acceptor abilities by choosing the right class of silylene and in case of donor-stabilized silylenes, fine-tune its properties by introducing certain functional groups with electron-donating or withdrawing effects. Moreover, the combination with a linking ability offers the opportunity to manufacture chelate or pincer type ligands.

1.3. Silylenes in Homogeneous Catalysis

As outlined in the previous chapters, the investigation of silylenes was always captivating, since this class of compounds are key intermediates in various thermal, photochemical and redox reactions of organosilicon compounds. Nevertheless, the primary role of silylenes are, *inter alia*, applications as ligands in transition metal chemistry due to their interesting electronical properties and superior σ-donor strength, described in the previous chapter (see chapter 1.2).

Transition metal catalysts are used in almost every field of chemistry, hence there is still a lot of potential undiscovered and a great demand for more specific catalysts. To gain new adapted catalytical properties, one of the best options is still to modify the ligation of the metal center.[52] Traditionally, phosphines were used as ligands for transition metal catalysts with various applications, because of their strong σ-donor character. The groundbreaking work of the groups of *Bertrand*[53] and *Arduengo*[6] in the late eighties and early nineties paved the way for a new class of ligands, the so-called carbenes. Especially the *N*-heterocyclic carbenes appeared to be very successful due to their versatility and facile access and thus replacing the phosphines in many applications of homogeneous catalysis. The most famous applications of phosphines and NHCs are undoubtedly combined in the transition metal catalysts by *Grubbs* and *Nolan* in the field of ruthenium catalyzed metathesis reactions,[54,55] which led to the awarding of the Nobel Prize in 2006.[56] Through the substitution of one out of two tricyclohexylphosphines (*Grubbs I cat.*) with a NHC ligand (*Grubbs II cat.*) the ruthenium complex gained stability and activity in its olefin metathesis (see Scheme 19, **XVIII**). The NHC causes a stronger *trans-effect*, which results in an easier dissociation of the phosphine.[57] In addition, the catalytically active π-complex gets stabilized through the more electron rich ruthenium center caused by the stronger σ-donor ability of the NHC ligand.[58] But also far away from the field of classical catalytical chemistry NHCs found their entrance into the everyday life through, e.g., organic light emitting diodes (OLEDs) in the self-aggregating *Janus* type like NHC metal complexes (see Scheme 19, **XIX**).[59,60]

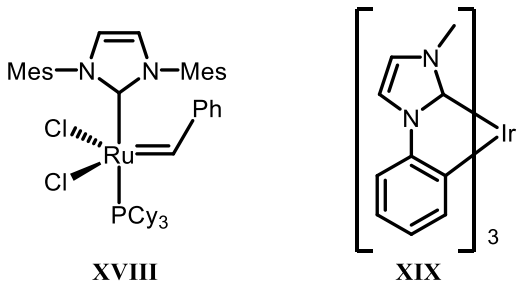

XVIII **XIX**

Scheme 19. (**Left**) Precursor of the active catalyst for the olefin metathesis reaction (**XVIII**) by *Grubbs* and *Nolan* in 1999[54,55] (better known as the *Grubbs II* catalyst); (**right**) NHC-Ir-complex (**XIX**) as application in OLEDs by *Thompson et al*. (2005/2006[59,60]).

Considering the fact that NHCs have become one of the most famous sort of ligands in organometallic chemistry over the past decades, it raises the question whether other low-valent compounds of the heavier homologues like silylenes can be used for the same purpose.

As previously mentioned, the first report of a transition metal complex employing a silylene as coordinating ligand was already published in 1977 by *Welz* and *Schmid* (see Scheme 20, **XX**).[3] Even though, this particular complex never found any applications in catalysis, it is still noteworthy and so are the seminal work of *Zybill et al.* and *Tilley et al.*, who reported their following work on silylene transition metal complexes one decade later. In 1987 the group of *Zybill* was able to isolate the first donor-stabilized acyclic silylene iron complex [$(CO)_4$Fe={Si(O*t*Bu)$_2$←donor}] (see Scheme 20, **XXI**). The stabilization *via* additional π-donor group took place by employing hexamethylphosphoramide (HMPA/HMPT) or THF.[61] A few years later in 1993 and 1994, *Tilley* and his co-workers published important work on analogues *Fischer* and *Schrock* type carbene complexes employing different types of silylenes, like in [$(CO)_4$Os=Si{S-p-Tol}{Ru(η^5-C_5Me_5)}] (**XXII**) or [PtH(PCy_3)$_2$=Si-(SEt)$_2$]BPh_4 (**XXIII**).[62–64] These achievements not only contributed to the understanding of silylene transition metal chemistry in general, certain compounds like complex **XXIV** also found application in catalytical transformations (e.g., hydrosilation or cycloaddition reactions).[65]

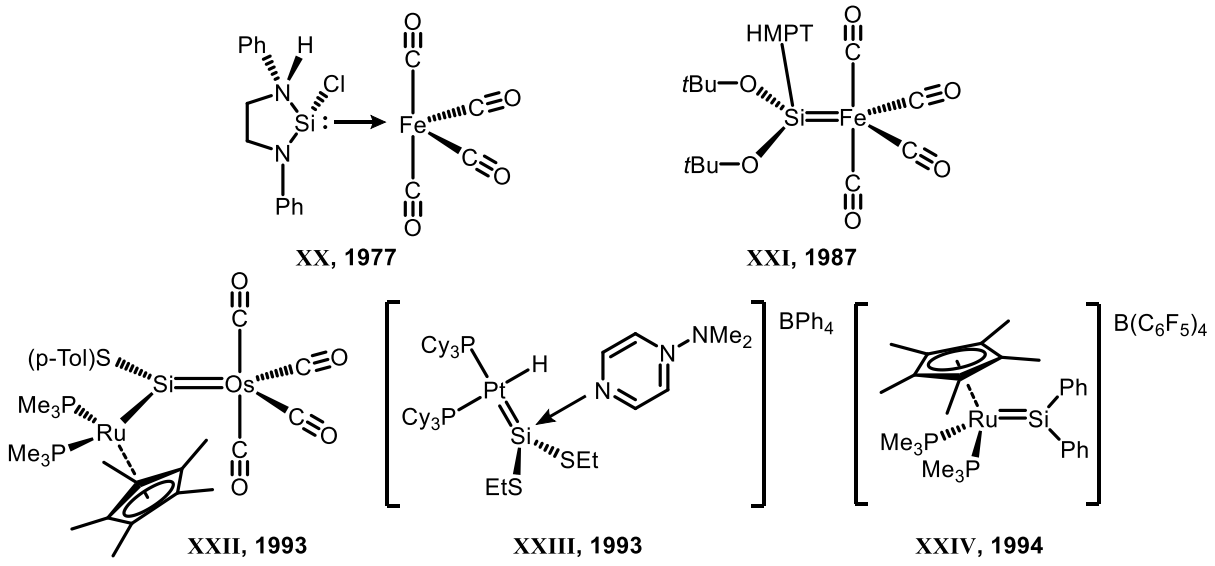

Scheme 20. Seminal work in the area of silylene transition metal complexes (**f.l.t.r.**): chloro stabilized NHSi iron tetracarbonyl complex (**XX**) by *Welz* and *Schmid* in 1977[3]; HMPT stabilized di-*tert*-butylsilylene iron tetracarbonyl complex (**XXI**) by *Zybill et al.* in 1987[61]; donor-free silylene osmium tetracarbonyl complex (**XXII**) and *Fischer*-type silylene platinum complex (**XXIII**) by *Tilley et al.* in 1993[62,63]; donor free silylene ruthenium complex (**XXIV**) by *Tilley et al.* in 1994[64].

Despite these early achievements in this field of chemistry, it took some time until the first applications of silylenes in homogenous catalysis were reported. Nowadays, there is a significant number of reports, publications and reviews about various transformations utilizing silylenes as the supporting ligand in metal-mediated homogenous catalysis, *inter alia*, C–C cross-coupling, hydrogenation,

cyclotrimerization, borylation, amination, hydrosilylation, hydroformylation or deuteration.[49] In the following, some important examples of silylenes in homogeneous catalysis will be highlighted to give a short overview of recent accomplishments thus giving a glance on its superior properties.

Fürstner et al. described the earliest application of a *N*-heterocyclic silylene in catalysis in 2001.[66] By employing a five-membered *N*-heterocyclic silylene as a bridging ligand to a dinuclear Pd(0) complex, they were able to perform *Suzuki* cross-coupling reactions with aryl boronic acids and bromo arenes in good yields (see Scheme 21). However, the recognition of the role and potential of silylenes as organometallic ligands was quite late, considering the fact that further examples remained rare until the recent work of *Hartwig* and *Driess*, more than a decade later.[19,22,44,67,68]

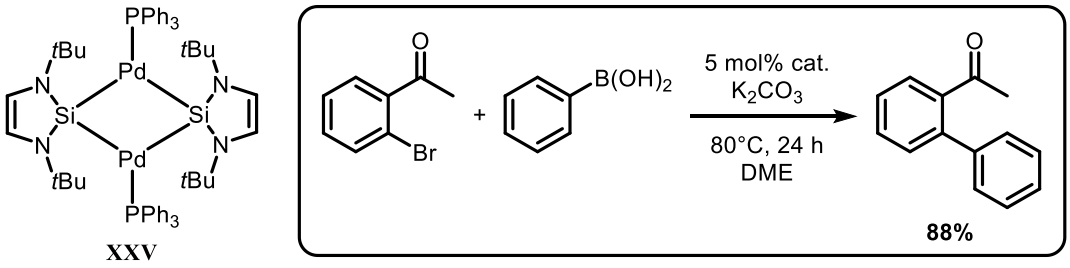

Scheme 21. *Suzuki* cross-coupling reaction catalyzed via Pd(0)-NHSi complex (**XXV**) by *Fürstner et al*. in 2001[66].

Roesky et al. investigated the catalytical properties of a similar NHSi palladium complex (η^3-C_3H_5)Pd{Si[N*t*Bu]-CH]$_2$}Cl (**XXVI**) in 2008 (see Scheme 22).[69] It not only proved to be active in *Heck* coupling reactions of styrene and bromo acetophenone, moreover they reported a first screening by investigating the effects of electron withdrawing and electron donating substituents by systematically varying the aromatic compounds coupled with styrene and improving the yield by performing the reaction under different reaction conditions. Thus, they were able to gain almost quantitative yields at 140°C within 24 h.

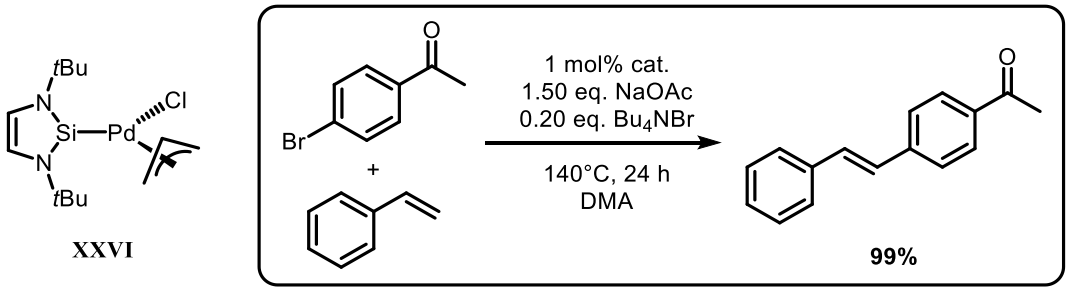

Scheme 22. Palladium catalyzed Heck coupling of styrene and *p*-bromo acetophenone showing almost quantitative yields by *Roesky et al.* in 2008[69].

Another example of the utilization in C–C bond formation reactions was given by Driess *et al.* Their bidentate NHSi ligand featuring a ferrocyl linker was used to form a cobalt complex in a [(η^5-C_5H_5)Co(η^2-NHSi)] fashion (see Scheme 23, **XXVII**). This system proved to be catalytically active in

[2+2+2] cyclotrimerization reactions of phenylacetylene in good to moderate yields.[19] In addition, performing the reaction in the presence of acetonitrile led to the formation of pyridine derivatives.

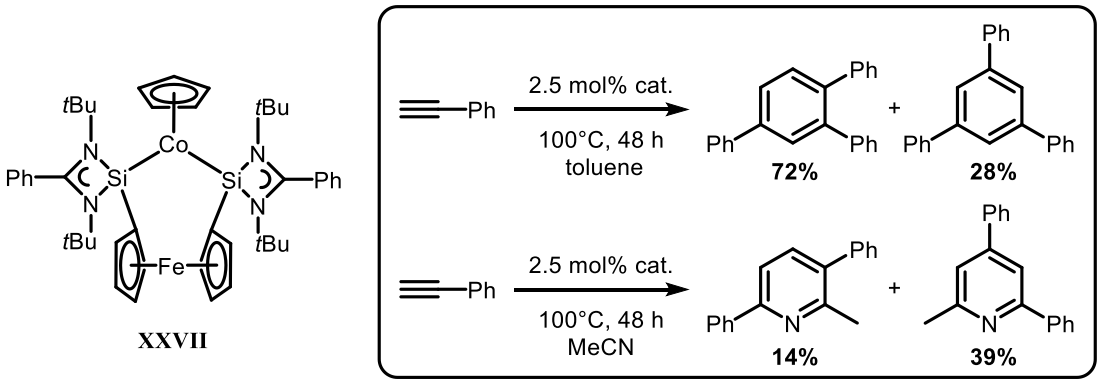

Scheme 23. Catalytical cyclotrimerisation using the bis-NHSi Co complex (**XXVII**) as a pre-catalyst under certain conditions by *Driess et al.* 2012[19].

The same group also published the first pincer ligand bearing two benzamidinato moieties (see Chapter 1.2), derived from the coordination of the free ligand and accompanied by a C-H insertion of the iridium precursor $[IrCl(coe)_2]_2$ into the ligands backbone, which proved to be an active catalyst for C-H borylation of arenes using pinacolborane (see Scheme 24, **XXVIII**). Within this article, they also compared the catalytical performances of this bis-NHSi iridium complex to structurally analogues complexes bearing phosphorous and low-valent germanium featured ligands, proving that the silicon(II) based ligand outperforms its competitors. With a conversion of 90–91% "SiCSi" showed the best performance, followed by the "GeCGe" analogue with 39–80% and the phosphine version "PCP" 40–64%. On the basis of the *Dewar-Chatt-Duncanson* model they suggested that the catalytical performances of these corresponding complexes are in line with their σ-donor strength (Si > Ge > P).[44,70]

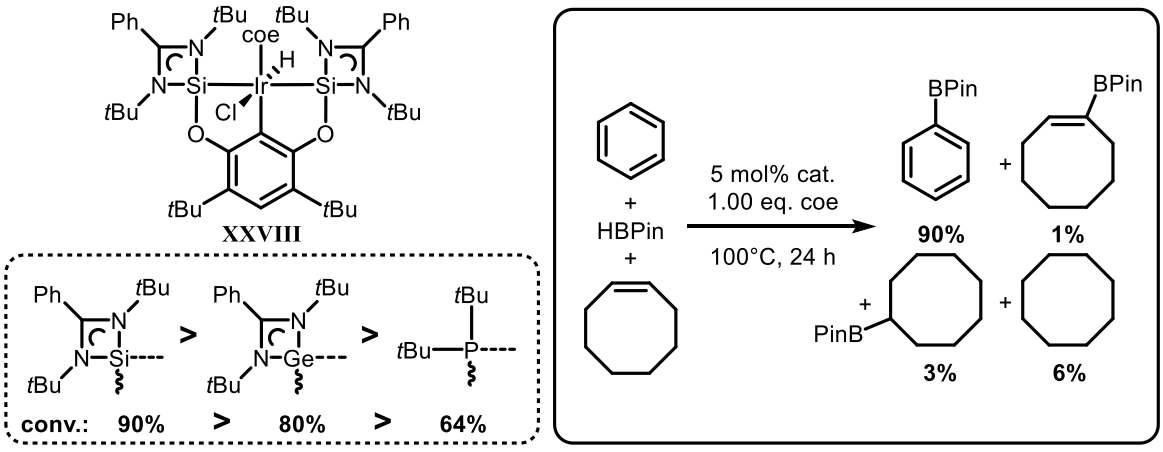

Scheme 24. Borylation of arenes using the iridium pincer complex (**XXVIII**) as a pre-catalyst (the given yield is exemplary for benzene as the substrate and the presence of cyclooctene (coe)). Germylene and phosphine ligands to indicate the structures of the corresponding pincer-complexes in order of reactivity (dashed box).[44]

In the field of C–N bond formations, the group of *Driess* recently investigated a nickel complex which showed to be a highly reactive catalyst for Buchwald-Hartwig amination reactions of aryl halides and secondary amines (see Scheme 25, **XXIX**).[43] Remarkably, a screening and optimization of the catalytical experiments revealed that very low catalyst loadings of only 0.5 mol% are necessary and with a conversion rate of 79–93% the bis-NHSi *ortho*-carborane ligand showed the highest performance, followed by its phosphorous analogue with 63–66%. This observation was supported by IR spectroscopic analysis, showing lower wavenumbers of the CO stretching vibrations of the silicon(II) based ligand compared to the phosphorous analogue, thus indicating a significantly higher σ-donor strength.

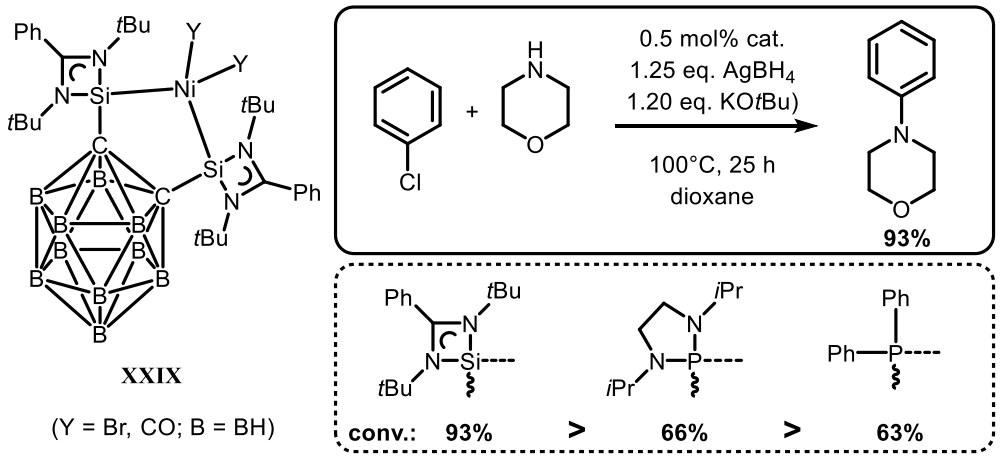

Scheme 25. Buchwald-Hartwig amination of aryl halides (e.g. chlorobenzene) and secondary amines (e.g. morpholine) utilizing Ni complexes (**XXIX**) bearing bis-NHSi (and bis-phosphinyl *ortho*-carborane) at minimal catalyst loadings. Phosphine ligands to indicate the structures of the corresponding pincer-complexes in order of reactivity (dashed box).[43]

Low-valent silicon complexes also demonstrated their efficiency in catalytical reduction reactions. In 2016, an uncommon representative of silylenes was investigated by *Kato et al.* which was successfully applied in hydrosilylation of bulky ketones (see Scheme 26).[50,51] The complex **XXX** was derived from the facile reaction of the isolable base-stabilized silacyclopropylidene with the metal halide precursor. The catalytical activity was compared to phosphorous analogues, showing an excellent conversion rate for the silylene complex with 90% far in front of 53% and 23% of the phosphine-featured complexes.[50]

This type of ligand proved as such effective, that the group of *Kato* also tested other transition metal centers, like platinum, in order to test their potential in olefin hydrosilylation reactions (see Scheme 27).[51] To date, the so-called *Karstedt*-catalyst is widely used for this kind of reaction. Using the aforementioned silylene ligand with the same platinum(0) precursor, *Kato et al.* received a catalyst (**XXXI**) as reactive as the *Karstedt*-catalyst (conv.: 91% *vs.* 78%) and significantly faster as the corresponding NHC analogue (conv.: 91% in 20 min *vs.* 96% in 3 h). However, reducing the catalyst

loadings from 30 ppm to 0.3 ppm, the silylene Pt complex **XXXI** is way faster than the *Karstedt*-catalyst (conv.: 86% in 24 h *vs.* 50% in 24 h), thus demonstrating its superior activity.

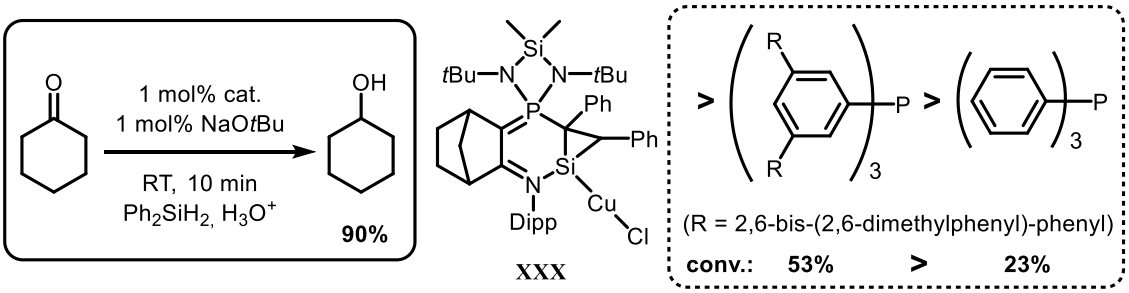

Scheme 26. Hydrosilylation of ketones (e.g. cyclohexanone) followed by an aqueous workup utilizing a base-stabilized silacyclopropylidene ligand. Comparison of the conversion rates to some phosphine analogues in order of activity (dashed box).[50]

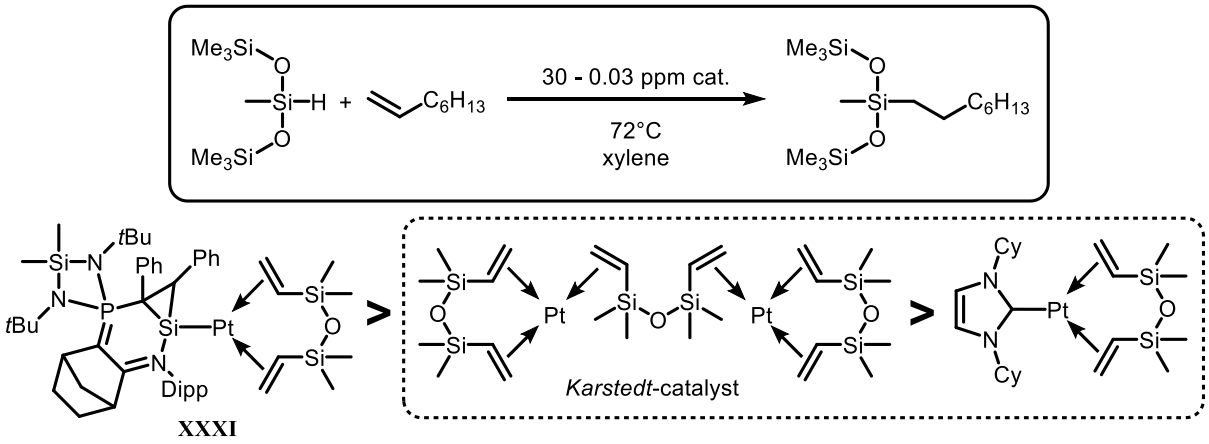

Scheme 27. Catalytical hydrosilylation of olefins using NHSi, olefin and NHC Pt catalysts (see text for details).[51]

In conclusion, the recent accomplishments in the field of homogenous catalysis illustrates the high potential of certain classes of low-valent silicon(II) ligands. It was shown, that silylenes in the role as supporting ligands in metal-mediated catalysis are able to exceed the steering properties of common *N*-heterocyclic carbenes and phosphines, yet providing high performances, chemo-, regio- and stereoselectivities.

1.4. Conventional Route of Functionalizing NHSis

The first part of this thesis shall focus on the conventional synthetic route to the preparation and functionalization of benzamidinato silylenes, for which the basic methods and processes as well as important developments will be highlighted in this chapter.

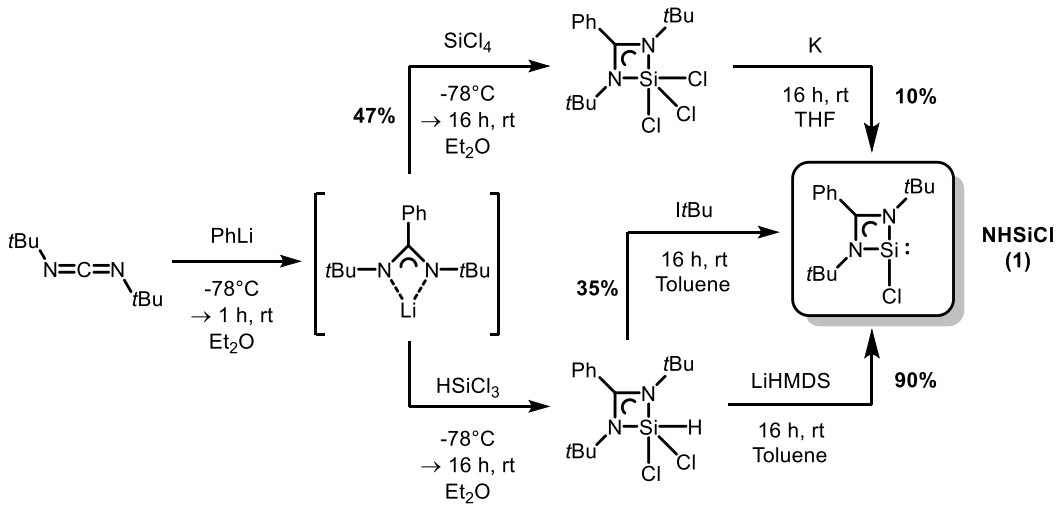

Scheme 28. Overview of the different synthetic approaches to the isolation of [PhC(N*t*Bu)$_2$]SiCl ("NHSiCl", **1**) by *Roesky et al.* (2006[13], 2010[14]).

In 2006, the group of *Roesky* published the initial synthesis of this type of ligand with a promising future.[13] The reaction starts with the lithiation of *tert*-butylcarbodiimide using one eq. of phenyl lithium in diethyl ether at -78°C leading to a nucleophilic attack of the phenyl-group at the carbodiimide backbone.[71] Successive addition of $SiCl_4$ results in the isolable intermediate [PhC(N*t*Bu)$_2$]$SiCl_3$ *via* salt metathesis in moderate yields of 47%. The highly hydrolysis-sensitive crystalline solid was treated with two eq. of potassium metal in THF in order to reduce the silicon center and gain the monomeric chloro benzamidinato silylene **1** in 10% yield (see Scheme 28, top). The isolated NHSiCl was stable in solution and solid state at ambient temperatures under an inert gas atmosphere, however, due to the low yield, it was somewhat unattractive for synthetic chemistry and further investigations remained limited. But the group around *Roesky* was able to develop an improved synthetic route in the coming years, by following the work of *Benkeser et al.*, who were investigating the treatment of trichlorosilane with amines,[72] and the former achievements of *Cui et al.* about the employment of NHCs for dehydrochlorination reactions.[73] Lithiation of the carbodiimide remained the same, but in the following step the $SiCl_4$ was exchanged with $HSiCl_3$, resulting in the new intermediate [PhC(N*t*Bu)$_2$]$SiHCl_2$. This allowed the employment of a reductive dehydrochlorination, which can be carried out under milder conditions than utilizing neat potassium metal, which is often accompanied by side reactions. The group reported two methods, dehydrochlorination *via* the carbene 1,3-di-*tert*-butylimidazol-2-ylidene (I*t*Bu) under the subsequently formation of the hydrochloride I*t*BuHCl

resulting in a slightly improved yield of 35% and the application of the lithium-bis(trimethylsilyl)amide (LiHMDS), which significantly improved the yield up to 90% (see Scheme 28, bottom).[14]

This high yield access to the chloro benzamidinato silylene paved the way for further investigation of its reactivity towards various kinds of classes of compounds. However, according to its recent main application, one of the most interesting reactivities, should remain the facile possibility to exchange the chloro group at the silicon(II) center without changing its oxidation state.

These simple substitution reactions, also known as salt metathesis reactions, are primarily done with alkali-metal salts of secondary amines and phosphines or alkoxy groups, but also transformations with, e.g., lithiated alkyl- and aryl-groups were reported.[18,74,75] One of the first attempts of "functionalizing" this donor-group of the benzamidinato silylene was also done by the group of *Roesky* in 2007, shortly after their first report on the chloro derivative, but before their improved synthesis.[16] Therefore their first strategy was presumably based on the salt metathesis reaction employing the at the time higher yielding [PhC(N*t*Bu)$_2$]SiCl$_3$ (47% vs. 10%), followed by the reduction step *via* potassium metal at room temperature, to achieve the corresponding free silylene (see Scheme 29, right dashed box). Yet, the reported yields remained only moderate (41 to 52%), due to the obviously harsh reduction conditions.

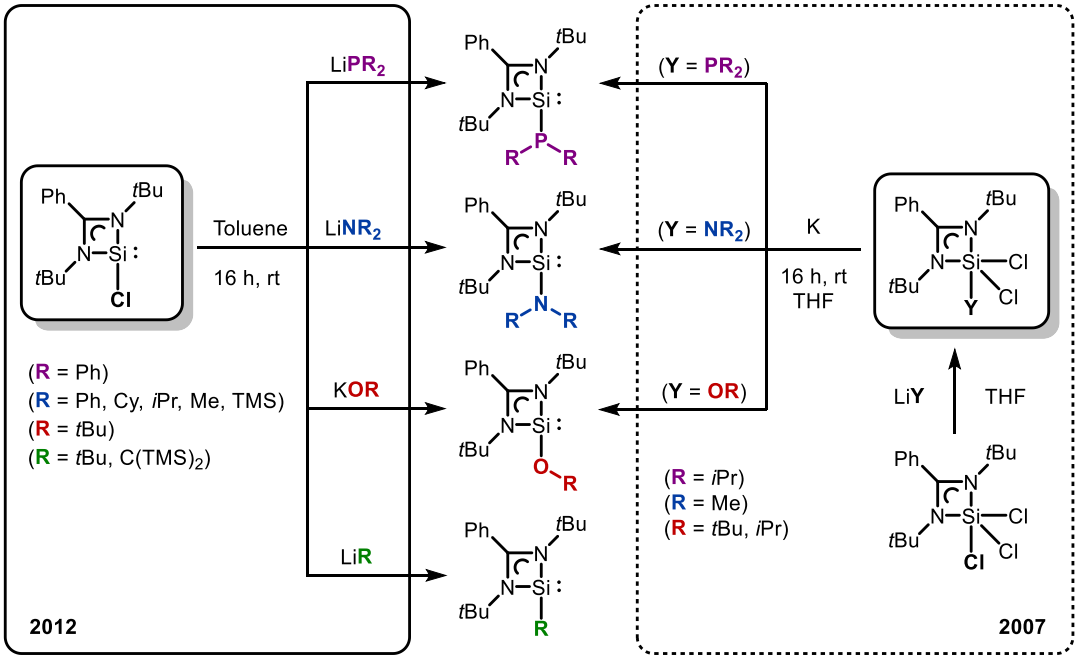

Scheme 29. Direct comparison of different attempts of functionalizing the chloro group of the benzamidinato silylene. **Left**: direct salt metathesis of the chloro benzamidinato complex and the corresponding alkali metal amide, phosphide, alkoxide or alkyle, by *Roesky et al.* in 2012[18]. **Right**: salt metathesis of the trichloro benzamidinato silane and subsequent reduction *via* potassium metal, by *Roesky et al.* in 2007[16].

Over the next years, several working groups adopted this promising *N*-heterocyclic silylene and joined the investigation of its properties, *inter alia*, pushed by the aforementioned novel high-yielded access. In 2012, solely the group around *Roesky* published seven new isolable structures featuring an improved

salt metathesis by preponing the recently introduced reductive dehydrochlorination step (see above) and postponing the metathesis with alkali metal salts. All compounds, including $NHSiPPh_2$, $-NCy_2$, $-N(TMS)_2$ and -O*t*Bu, were synthesized in high yields (82 to 93%) in form of simple one-pot reactions at ambient temperatures using toluene as solvent (see Scheme 29, left box).

In conclusion, a facile synthetic route to the basic module, aka. chloro benzamidinato silylene **1**, in high yields was achieved, as well as a facile access to introduce various donor-groups, thus, the foundation for what should be known as a modular kit for silylenes was laid.

Driess et al. further illustrated how NHSis could be seen as a modular system, to which it should develop from now on, by isolating the first chelate ligand. Hence, they combined the previously mentioned methods of synthesis and substitution and gained an interesting silylene in moderate to good yields. By employing 1,1,3,3-tetrachlorodisiloxane instead of trichlorosilane, they isolated the oxo-linked $((PhC(NtBu)_2)SiHCl)_2O$ species (see Scheme 30, **XXXII**). This way they introduced the silicon(IV) center into the benzamidinato scaffold and the linking moiety at the same time. Also, they ensured the presence of the hydrochloride, located at the silicon center, which could easily undergo the reductive dehydrochlorination *via* LiHMDS, leading to the low-valent bis-NHSi **XXXII**.[76]

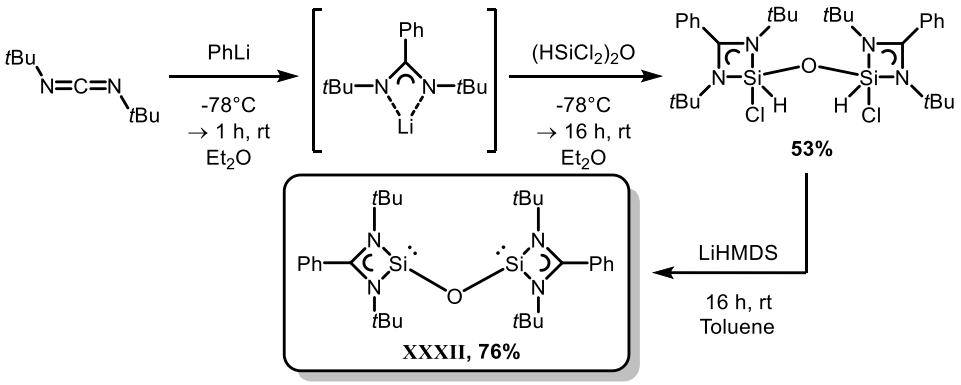

Scheme 30. Synthesis of the first chelate-ligand (**XXXII**) featuring the benzamidinato silylene moiety by *Driess et al.* in 2010[76].

One of the first compounds, which was substituted in the meanings of a legit "functionalization", was presumably also reported by the working group of *Driess*, since the introduced donor-group, or more like the introduced backbone, had an active part in ensuing transformations. Until then, most of the substitution reactions were more of a proof of principle to investigate the general behavior of silylenes. This isolable pincer-ligand bearing two benzamidinato silylene moieties and an alkoxy-based linking backbone was published in 2012.[77] They were also employing the facile method of lithiating the functional group (4,6-di-*tert*-butylresorcinol) and subsequently adding the NHSiCl **1** to achieve the free silylene **XXXIII** (see Scheme 31). This precursor was coordinated to metal precursors by undergoing a

C-H insertion with the phenyl-backbone moiety, thus generating the "Si-C-Si" pincer-type bonding motif (also see Chapter 1.3 for application in catalysis).[44]

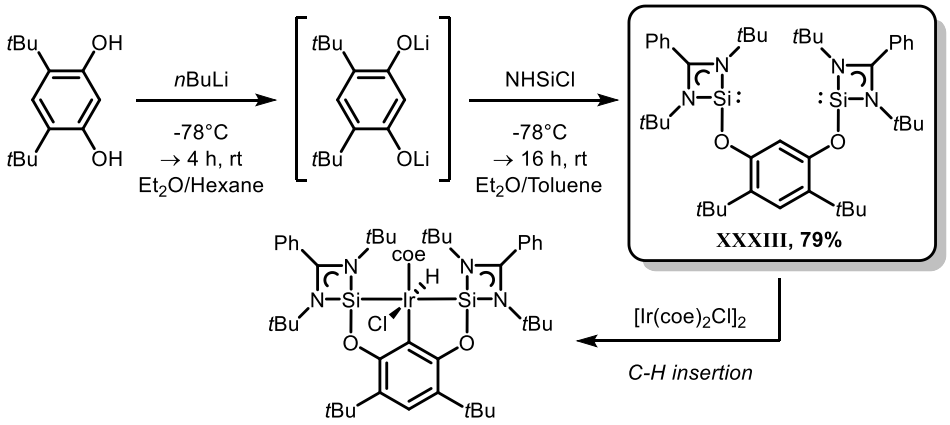

Scheme 31. Synthesis of the pincer-ligand precursor **XXXIII** *via* salt metathesis of the lithiated 4,6-di-*tert*-butylresorcinol and NHSiCl and further coordination of an iridium precursor performing an C-H insertion to result the "Si-C-Si" pincer motif, by *Driess et al*. in 2012[77].

In conclusion, due to the easily substituted chloro group, the benzamidinato silylene NHSiCl **1** is a versatile building block. As described in Chapter 1.2, fine tuning of the electronical and sterical environment around silicon(II) is possible, which has a great influence on the reactivity of the molecule and also to coordinated metals. As indicated above, there are many ways to gain various types of benzamidinato-based silylene ligands, but in ways of versatility and efficiency, the optimal method still seemed to be the salt metathesis of the chloro benzamidinato silylene using alkali-metal salts. As already described in the previous chapters, the past years created a large variety of different classes of silylenes with many applications, leading to the perception, that the "new" low-valent group 14 compounds are holding a huge potential for certain applications, especially metal-mediated homogenous catalysis.

1.5. Investigation of NHSiN(C)$_x$P Silylenes

Referring to the last chapter, the investigation of novel bidentate *N*-heterocyclic silylene ligands will be focused, based on the NHSiCl **1** to exploit its versatile access of functionalization by the meaning of tuning the structural and electronical environment of the silicon(II) atom in new ways. The majority of reports of bidentate silylenes are referring to chelate-like structures containing two NHSi moieties and a linking backbone. In contrast, donor-stabilized silylenes solitary bearing a "side-arm" with an additional donor-site in order to coordinate transition metal centers had not been the focus of recent research of silylene-chemistry, hence there are only a few examples known in literature relating to this scenario. In fact, there is only one working group, which intensively studied corresponding NHSis, owing a side-arm and thus can feature additional metal coordination.

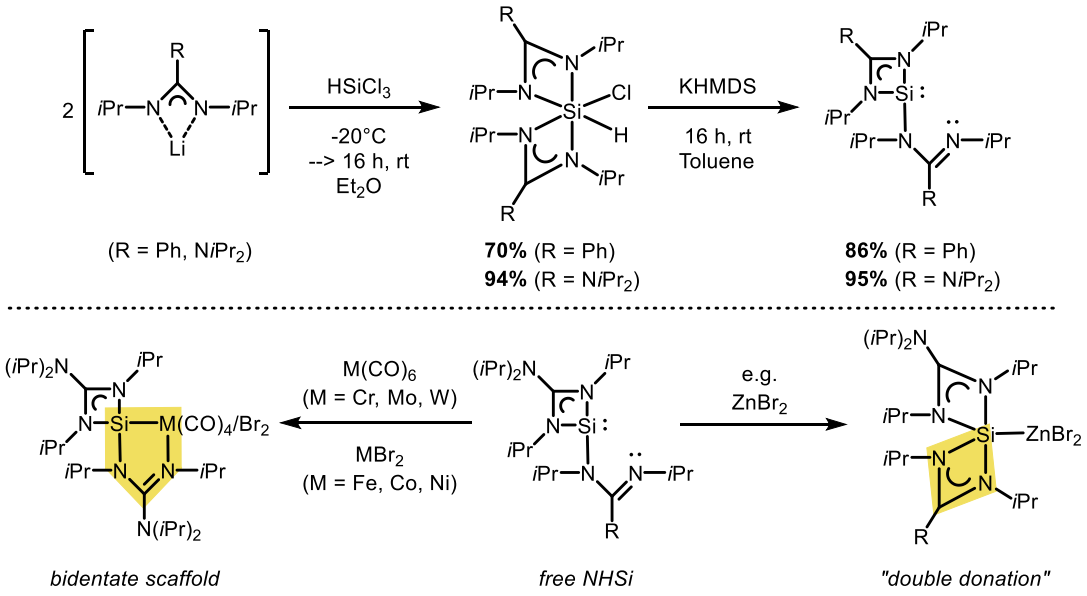

Scheme 32. Synthesis of amidinato and guanidinato based *N*-heterocyclic silylenes (**top**, 2013[78]) and examples of the different modes of complexation in a bidentate fashion or a double donation (**bottom**, 2017[79]), by *Tacke et al.*

The group of *Tacke* is investigating several four-membered *N*-heterocyclic silylenes based on benzamidinato and guanidinato derivatives. As illustrated in Scheme 32 (top) they employed the same synthetic method previously discussed (see Chapter 3.1) with the pivotal difference of using two equivalents of lithiated benzamidinato substrate, resulting in the octahedrally coordinated silane $[PhC(N\textit{i}Pr)_2]_2SiHCl$, which can be analogously dehydrochlorinated using KHMDS.[20,78] The resulting free NHSis show a nitrogen donor atom bearing a lone-pair available for potential metal coordination. Interestingly, throughout their studies of its reactivity, the side-arm did not interact with most substrates; it "re-bounded" to the silicon atom instead, leading to a symmetrical double donation of both benzamidinato scaffolds most likely for reasons of stabilization (see Scheme 32, bottom).[79]

The only case in which the NHSi acted as a bidentate ligand was observed by the complexation of the bis-guanidinato NHSi and carbonyl precursors $M(CO)_6$ (with M = Cr, Mo, W)[80] or halide precursors MBr_2 (with M = Fe, Co, Ni)[81], noteworthy that the coordination of ZnX_2 resulted in the double donation again. This was the first time such complexation and generation of a five-membered M-Si-N_2C ring was observed. Furthermore, it has to be noted, that the corresponding benzamidinato analogue did not show the same behavior towards these metal precursors, instead it also led to double donation.

Although *Tacke et al*. did not further investigated this symmetrical substituted ligand by means of exploiting it as a side-arm for a targeted bidentate complexation, these examples illustrate the potential. Alternatively to these attempts, an unsymmetrical ligand design leading to bidentate hemilabile complexes could also draw significant benefits. Hemilabile complexes have at least one bidentate ligand, with at least two electronically different donating groups (e.g. in relation to the HSAB

concept; see below). It can influence the coordination sphere and electronical properties of metal centers in a unique way or show reversible ligation and dissociation of one coordinating group, which could be beneficial for catalytical transformations.[82]

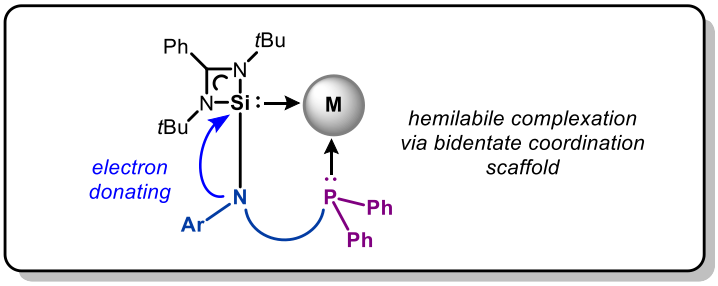

Scheme 33. Graphical illustration of a possible structure motif of novel donor-functionalized NHSis based on the benzamidinato silylene.

Additional donor-groups based on secondary amines not only proved to be very versatile (high abundancy, stable, easy to modify), but also showed a good electron donating influence on the silicon(II) center (see Chapter 1.2), thus, providing the ideal basis for the functionalization of the NHSiCl. Furthermore, the investigation of the advantages of a softer donor-atom, which will be fulfilled through a phosphorous(III) species, will be in the focus of this work. Referring to the *Pearson* concept aka. the '*hard and soft acids and bases*' (HSAB) concept, the introduction of a, e.g., phosphorous donor atom favors the coordination of softer metal cations, like silver(I) or gold(I).[33,83] This way, a novel NHSi containing a secondary amine as an electron rich donor group bearing a softer P(III) donor-site in contrast to the strong σ-donor ability of the harder Si(II) atom for a bidentate complexation in metal complexes would be isolated (see Scheme 33).

Until now, there is only one example of a NHSi functionalized with a side-arm bearing a phosphor(III) atom. *Khan et al.* characterized the luminescence properties of gold(I) complexes with PNP- and PNB-based ligands systems, in their recent studies (see Scheme 34). The specially designed ligands facilitate Au(I)-Au(I) dimers in a bidentate fashion and thus featuring aurophilic interactions with very short Au–Au-bonds (2.7944(19) Å).[84]

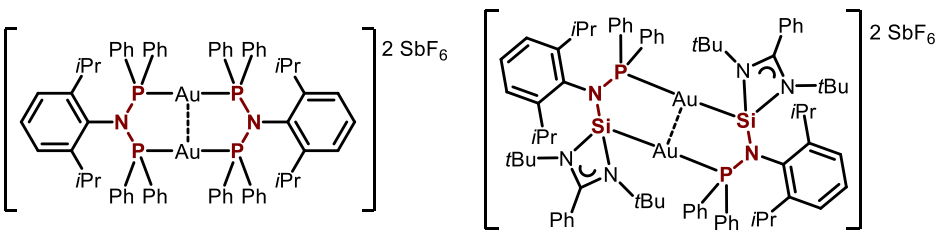

Scheme 34. Schematically illustration of the PNP- and NHSi-ligand systems *Khan et al*. utilized to study the luminescence properties of their gold(I) complexes.

The term "aurophilicity" was introduced in 1989 and primarily coined by the seminal work of *Schmidbaur*[85] and refers to the tendency of Au complexes to form aggregates *via* weak metallophilic

interactions.[86–89] These non-covalent interactions between the two closed-shell atoms usually occur in the range of 2.5 to 3.5 Å and therefore below the sum of their van der Waals radii (3.80 Å) and the distance between atoms in the cubic close-packed gold metal (2.89 Å)[87] and show a bond strength of about 7-12 kcal/mol, which is comparable to a hydrogen bond.[89,90] Purely from their electronical configuration (closed-shell, [5d^{10}]) gold(I) atoms should experience only weak vdW forces and should hence be unexpected, but occur in various compounds. The lighter homologues copper(I) and silver(I) can exhibit the same phenomenon analogously referring to as cuprophilicity and argentophilicity, yet, the effect is greatest for gold, which is traced back to increased relativistic effects, which were primarily examined and confirmed through theoretical studies by *Pyykkö* and *Schwerdtfeger* shortly after these effects were observed.[91,92,93]

These interactions can lead to outstanding photophysical properties in solution and solid state,[94] which is the reason such compounds had become subject of current research in that area of chemistry (e.g. for organic light-emitting diodes[95]).[96] Their luminescent properties are supposed to be in direct relation to the distance of the Au(I) centers. To exploit these Au-Au dimers, ligand systems with soft donor-atoms are required. To explore possible new complexes with improved properties, the group of *Khan* enhanced their ligand concept from the PNP- to an SiNP-motif in order to investigate the influence of silylenes on such gold-dimers (see Scheme 34).[97]

For the synthesis to these functionalized silylenes *Khan et al.* utilized the conventional method as well (see Scheme 35). Following their previous achievements in that area, after stepwise lithiation of 2,6-di-*iso*-propyl-aniline and addition of an equimolar amount of chloro diphenylphosphine, the isolated lithium salt was employed in the salt metathesis step with NHSiCl **1**, resulting in the **NHSiNP** ligand.

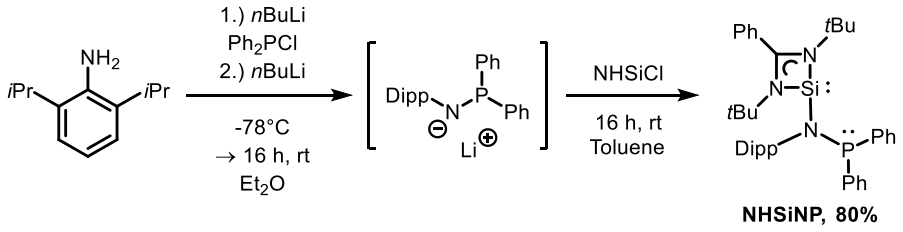

Scheme 35. Synthesis of the **NHSiNP** motif *via* salt metathesis, derived by the previous formation of the lithiated NP-precursor, by *Khan et al.* in 2016[97].

2. Research Scope

Reviewing the achievements that have been made in the area of silylene chemistry over the last decades, the main field of application is emerging towards the utilization as strong σ-donating ligands for transition metal complexes. Despite all efforts, this area of chemistry can still be described as relatively premature. Up to now, the focus was set primarily on the recreation of previous successes of known ligand systems, comparing their reactivities, whereas the fundamental concept of exploring ligands in new ways is often neglected. To this effect, the work presented here contributes to the essential exploration of new ways of accessing *N*-heterocyclic silylenes providing new features.

The first part of this thesis concentrates on the investigation and introduction of phosphorous-based side-arms adapting the conventional method of substituting chloro benzamidinato silylene **1**, which was presented during the introduction. The possibility of modifying **1** in this way holds an enormous potential for ligand design and tuning, but has not yet been pushed to its limits. Utilizing secondary amines as basis for functionalized donating groups proved to be the most versatile ones regarding the intention of this work. Thus, the focus will be set on researching bidentate ligands with a combination of softer (P(III)) and harder (Si(II)) donor atoms, regarding the *Pearson* concept, to engage possible hemilabile complexation or encounter later transition metal atoms. The synthesis of the required amines, which were to serve as side-arms, should not be reinvented, but oriented on already known motifs and modified for these purposes. The general motif of these groups should concentrate on a "N(C)$_x$P"-backbone, which, after functionalization with the NHSiCl, should form a "SiN(C)$_x$P"-scaffold (with x = 1, 2) (see Scheme 36). Within the framework of this project, simple phenyl-/aryl-groups should be chosen as residues.

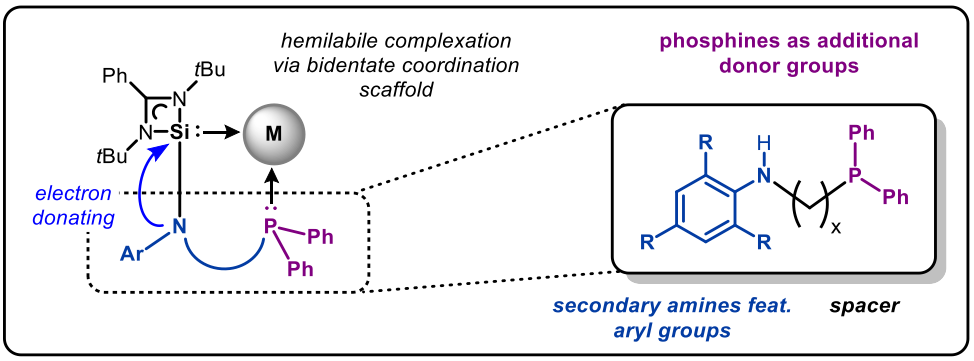

Scheme 36. Graphically illustration of the general concept to the synthesis of NHSiN(C)$_x$P ligands employing α-/β-aminophosphines (x = 1: α-NP; x = 2: β-NP).

The second and main part also focuses on the introduction of side-arms, but under the aspect of developing novel synthetic routes to TM complexes. Considering the purpose of isolating, characterizing and utilizing NHSi transition metal complexes, the prior isolation of the free

functionalized silylene ligand can mostly be dispensed. The basic idea is built on the concept of "occupying" the free silylene **1** with the desired transition metal and thus simultaneously protecting the highly sensitive lone-pair of following operation conditions. The chloro group would remain unaffected and accessible for subsequent functionalization reactions (see Scheme 37). Such reactivity has not been investigated yet, but would open wide awareness to new synthetic approaches, which is why this chapter should examine such alternative routes. For these purposes, a more stringent side-arm motif also based on the utilization of secondary amines, but employing pyridyl groups as the source for additional donor sites, will be targeted. Readily available TM halide precursors of d^{10}-transition metals of group 11 (Cu(I), Ag(I), Au(I)) and group 12 (Zn(II)) should be utilized, whose investigation of NHSi complexes are still comparatively scarce, hence adding a vital contribution to silylene chemistry by means of investigating the reactive behavior towards TM coordination. As a result, not only the functionalization itself is to be investigated, but also the influence of the introduction of the side-arm on the previously isolated NHSiCl TM complexes.

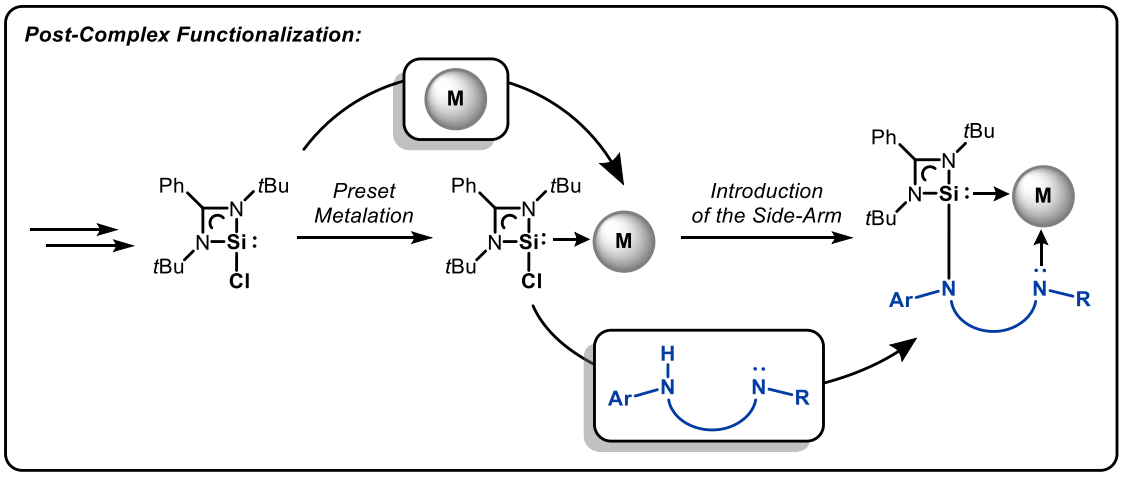

Scheme 37. Schematic illustration of a possible alternative route *via* preset complexation of transition metal precursors followed by the functionalization of the chloro group of **1**.

Furthermore, a second method should be developed within the framework of this thesis, in regard to recent publications that revealed a certain behavior of the chloro group of **1** towards zinc organyl precursors, which will be investigated in order to exploit this reactivity. Under concomitant complexation to the metal atom, the negatively charged residues of the precursor underwent a shift with the adjacent chloro group. The behavior behind this observation should be transferred to the selective application in easily accessable organo transition metal salts (see Scheme 38). The synthesis of more complex ligands bearing one or more highly sensitive coordination sites is often as elaborate as the additional synthesis of a suitable metal precursor to gain very specific complexes, by means of reaction steps, workups, purifications and yields. On the contrary, the synthesis of TM precursors already holding the desired functionalities is often more versatile and readily accessible. This way, due to economizing reaction steps, this method will be investigated towards the application of Cu(I) and

Zn(II) atoms by employing them in organo salts bearing the same pyridyl substituted amine motifs and examine their behavior towards **1**.

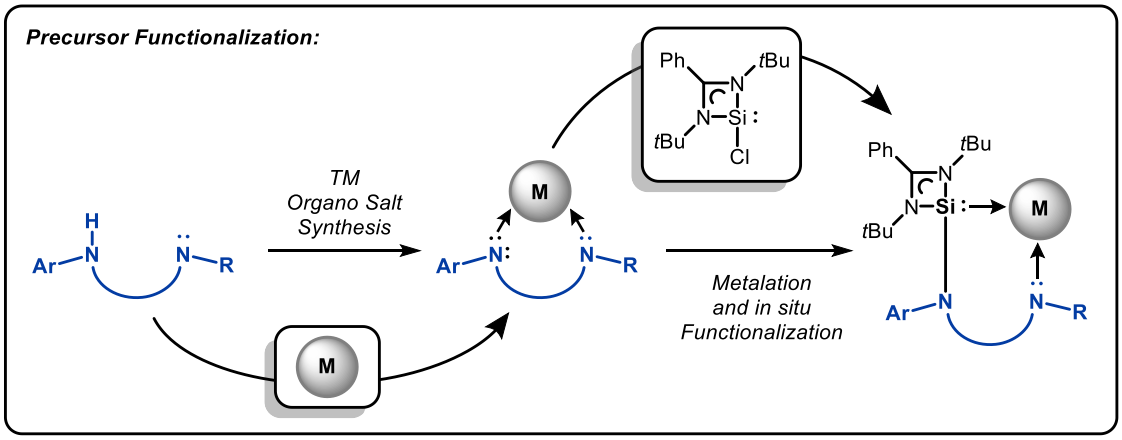

Scheme 38. Schematic illustration of utilizing pre-coordinated transition metal atoms by functional donor groups and following addition of **1**.

Under the prerequisite of the successful isolation of novel NHSi TM complexes, the focus should be set on examining if the side-arm functionalization shows an influence on its reactivity. Thereby, the NHSiCl TM complexes, as well as their functionalized congeners, should be investigated towards their catalytical behavior by subjecting them to renowned transformations, like the copper(I)-catalyzed azide-alkyne cycloaddition (CuAAC).

3. Results and Discussion

Within this thesis, the directed functionalization of the *N*-heterocyclic chloro benzamidinato silylene [PhC(N*t*Bu)$_2$]SiCl for metal coordination was in the focus. Although the term "NHSi" is rather biased by the general definition of "*N*-heterocyclic silylenes" introduced in the first chapters, throughout this work this structure is referred to as "NHSiCl" and following products as "NHSiX" (with X as the regarding donor-group), for reasons of simplification (see Scheme 39). In the first part, the general methods and opportunities of synthesizing and functionalizing NHSiCl will be described and detailed insights to the introduction of novel functional donor-groups will be given. Thereby, already established methods (see Chapter 3.1ff) will be illustrated and the investigation of novel ways of functionalizing the NHSiCl (see Chapter 3.2ff) will be introduced.

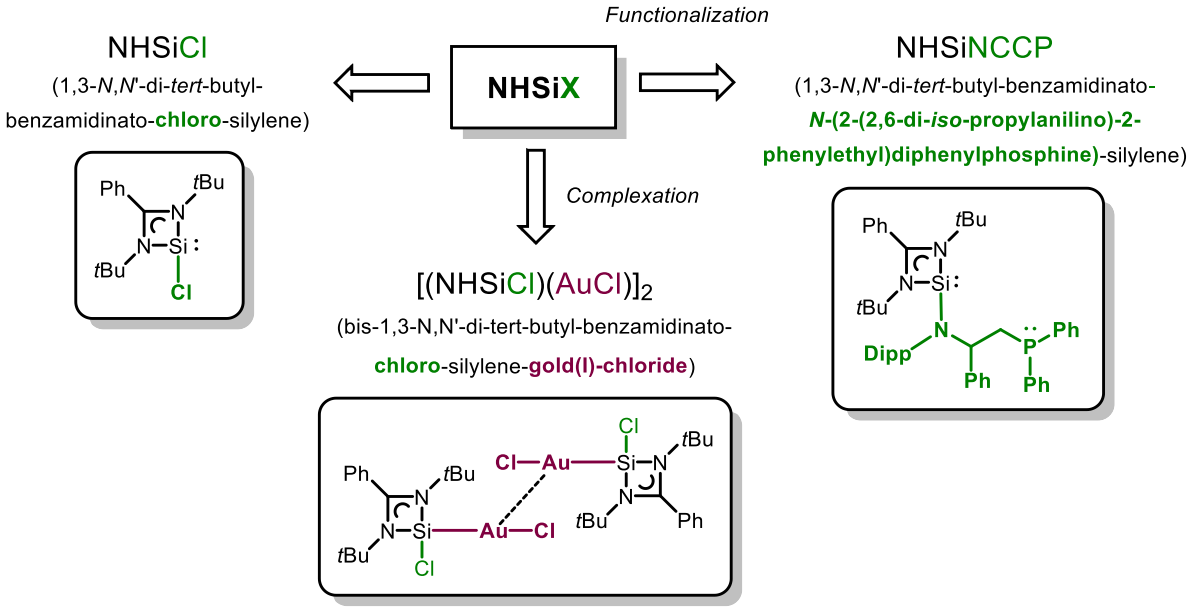

Scheme 39. Schematic guideline to the nomenclature of *N*-heterocyclic silylenes and their complexes used throughout this thesis.

3.1. Conventional Route to Novel Functionalized NHSis

3.1.1. Salt Metathesis Reactions of Silylenes with α-Aminophosphines – NHSiNCP

The aim of this work was to introduce new side-arms based on secondary amines bearing phosphor(III) donor sites for an enhanced bidentate metalation. Therefore, most attention was paid to the design and synthesis of a similar binding motif to the above mentioned (**NHSiNP**), adding the vital point of inserting methylene moieties between the nitrogen and phosphor atoms, in order to achieve a chelate like coordination and gain control over the bite angle at the metal center (see Scheme 40).

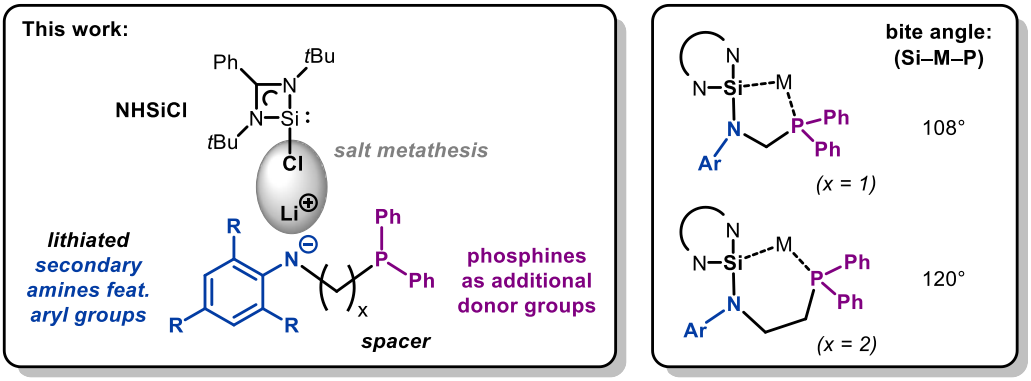

Scheme 40. (**Left**) Graphically illustration of the general concept to the synthesis of NHSiN(C)$_x$P ligands employing α-/β-aminophosphines (x = 1: α-NP; x = 2: β-NP); (**right**) the influence of the methylene units (x = 1, 2) on the bite angle for bidentate complexation.

One decisive criterion for potential new functional groups is an isolable secondary amine and its successful lithiation to introduce it to the NHSiCl **1**. To get a silylene following the general type "**NHSiNCP**" the former isolation of HNCP is mandatory. The so-called α-aminophosphines (α-NP) have interesting properties, which investigation occupied certain working groups (including ours[98]) over the past decades.[99,100] However, the crux of this class of compounds is their stability in solution. Whilst species bearing a tertiary amino-group are stable in solid state and in solution,[101] α-NPs with a secondary amine tend to show a P–C bond cleavage in solution,[102,103] yet, for the introduction of the α-aminophosphine into the silylene, a secondary amine is mandatory, as mentioned above (see Scheme 40).

The synthesis of NCPs can be performed through certain synthetic methods. Tertiary amine substituted α-aminophosphines, for example, can be achieved by the *Mannich* reaction of the corresponding phosphine Ph_2PH, ketone CH_2O and amine Me_2NH, which results in the formation of $Ph_2PCH_2NMe_2$.[104] α-Aminophosphines bearing secondary amines can be prepared *via* facile hydrophosphination reactions of the corresponding imines and diphenylphosphines.[103] Moreover, undergoing a nucleophilic addition of the lithiated Ph_2P^- Li^+ at the imine leads to an anionic α-aminophosphine ligand, which can be transformed to the amine by an aqueous workup (see Scheme 41).[105]

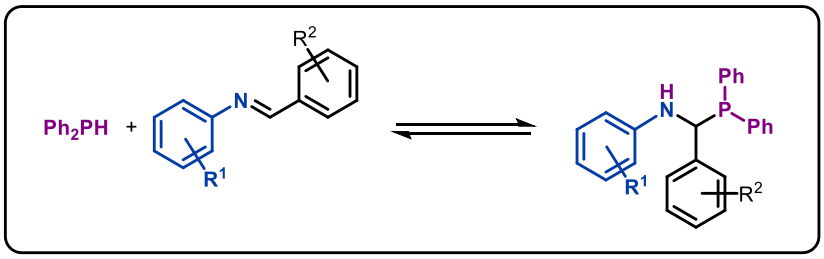

Scheme 41. Exemplary hydrophosphination reaction of Ph_2PH and $R^1CH{=}NR^2$ to $Ph_2PCH(R^1)NHR^2$ in solution described by *Andrieu* and *Poli* in 1999. The position of the equilibrium reaction is dependent of the introduction of electron withdrawing or donating substituents (R^1/R^2).

Within this work, the method of choice to start with, was the hydrophosphination reaction under proton migration. As previously mentioned, this formation is an equilibrium reaction (see Scheme 41), which position is dependent on the substituents of the aryl-rings adjacent to the nitrogen or carbon atom. *Andrieu* and *Poli* investigated these equilibrium reactions of Ph_2PH and $R^1CH{=}NR^2$ to $Ph_2PCH(R^1)NHR^2$ in solution and came to the conclusion, that electron-withdrawing substituents at R^1 or R^2 favor the formation of the α-aminophosphine as well as the coordination of the phosphorous donor to transition metal atoms (e.g. Cu(I)).[103] Furthermore, they observed an enhanced stereoselective P–C bond formation by utilizing an bulky η^6-$Cr(CO)^3$- and *ortho* Cl-substituted R^1-aryl group as the starting material.[102] Considering these methods, the question was whether to take moderate yields into account or substituted α-aminophosphines. To prevent side-reactions, the application of metal-substituted HNCPs was out of question and since the investigation of the neat ligand system should be focused at the beginning, the isolation of the unsubstituted HNCP was chosen.

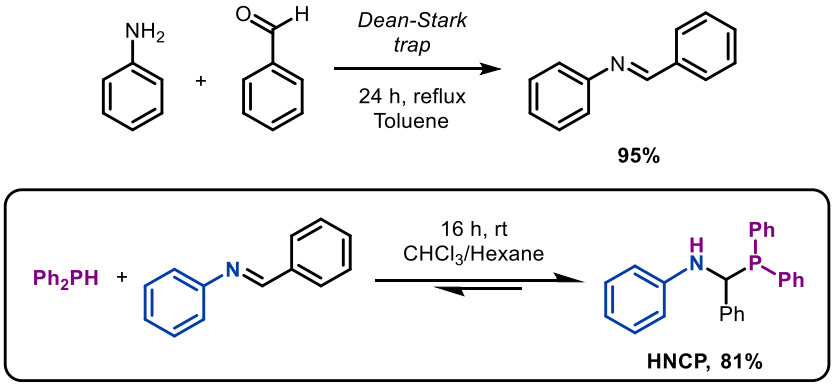

Scheme 42. Synthesis of (*E*)-*N*,1-diphenylmethanimine *via* condensation reaction (top) and subsequent synthesis of (1-anilino-1-phenyl-methyl)diphenylphosphine (**HNCP**) performing an hydrophosphination reaction with diphenylphosphine according to *Andrieu* and *Poli*, in 1999[102,103] (bottom).

At first, the corresponding *Schiff* base had to be synthesized *via* condensation reaction of aniline and benzaldehyde. The utilization of a *Dean-Stark* apparatus and toluene as a solvent proved as the most reliable and simplest way to gain (*E*)-*N*,1-diphenylmethanimine in high yields (see Scheme 42, top). It soon became apparent, that modifying the synthesis postulated by *Andrieu et al.* towards performing the reaction in small amounts of a solvent-mixture of CH_3Cl and hexane (1:5) resulted in the precipitation of the pure product overnight at room temperature and was simply filtrated and washed with further hexane. This way, the product **HNCP** was easily isolated in yields of 81% in high purity (see Scheme 42, bottom) and confirmed *via* multinuclear NMR spectroscopy and high-resolution mass spectrometry analyses.

Thus, the isolation of the **HNCP** was rather unproblematic, since the position of the equilibrium reaction was moved towards the formation of the product by choosing a solvent-mixture in which the product showed a very low solubility. In the following step, the secondary amine had to be lithiated

and subsequently the NHSiCl **1** was added in order to undergo the salt metathesis reaction. As mentioned above, *Andrieu et al.* described the reversibility of the P–C bond formation, which is reflected in the equilibrium reaction. By deprotonating the secondary amine, the equilibrium changes to an ionic analogue, featuring the lithiated phosphine ($Li^+ {}^-PPh_2$) and the neutral imine (Ph-N=C-Ph) on the one side and the lithiated α-NP ($Li^+ {}^-NCP$) on the other side, of which the position is unknown.

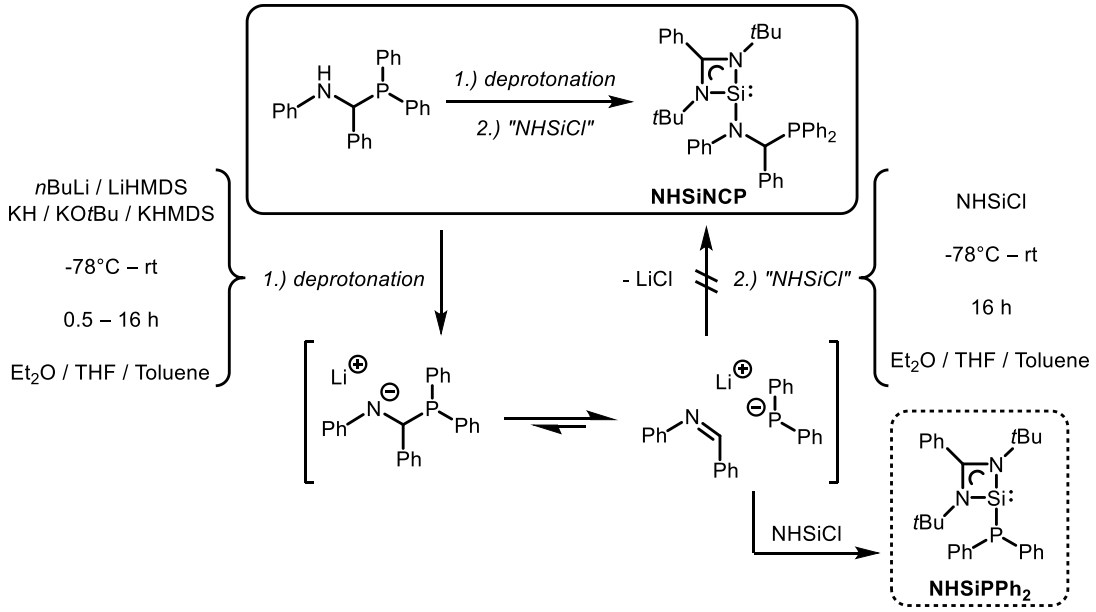

Scheme 43. Schematic illustration of the original salt metathesis reaction to **NHSiNCP** *via* preset lithiation of **HNCP** (top) undergoing an equilibrium reaction employing the ionic species (middle) and side reaction to **$NHSiPPh_2$** (bottom).

As shown in Scheme 43 several deprotonating agents were used in different solvents under different conditions, orders and reaction times, to facilitate the formation of the P–C bond and hence the formation of the product. Unfortunately, the free intermediate could not been isolated. *Andrieu et al.* described the process to the equilibrium position of the α-aminophosphine in solution as a slow "decomposition", sometimes taking hours or days. This statement is in agreement with the observations made during this work. The freshly prepared substrate solutions stayed colorless to slightly yellowish and turned dark red to brown by the time the deprotonating agent was added, nearly independent of the reaction temperature. Such bright or deep red to brown solutions can be often observed when working with lithiated phosphines (e.g. $LiPPh_2$). All common attempts of isolating reaction products under inert conditions led to highly air- and moisture-sensitive brownish oils. ^{31}P NMR spectroscopy showed various signals which could not been unambiguously identified to any meaningful species. Mass spectrometric analysis of the reaction mixture also showed no corresponding signals of the desired product or meaningful side products, which led to the conclusion, that the equilibrium reaction of "Ph-N=C-Ph + $Li^+ {}^-PPh_2$ / $Li^+ {}^-NCP$" hinders the successful transformation. In some cases, after several days, a minor crystal growth was observed, which could

be identified as the already known structure **NHSiPPh$_2$**, indicating, that the formation of the "decomposed" anionic species Li$^+$ $^-$PPh$_2$ seems to be favored.

As previously mentioned, aryl-groups substituted with electron withdrawing residues adjacent to the nitrogen or carbon backbone atom are supposed to favor the P–C bond formation of α-aminophosphines, but were initially excluded in the first syntheses. After all attempts of isolating the **NHSiNCP** ligand failed, the idea grew to introduce pyridyl-groups at the imine substrate (R^1-N=C-R^2), alternating at the R^1- or R^2-positions (**H^{Py}NCP**, **HNC^{Py}P**), as well as the combination of R^1 and R^2 (**H^{Py}NC^{Py}P**). Although their electron withdrawing character is comparatively weak, their introduction is very simple and should be investigated (see Scheme 44).

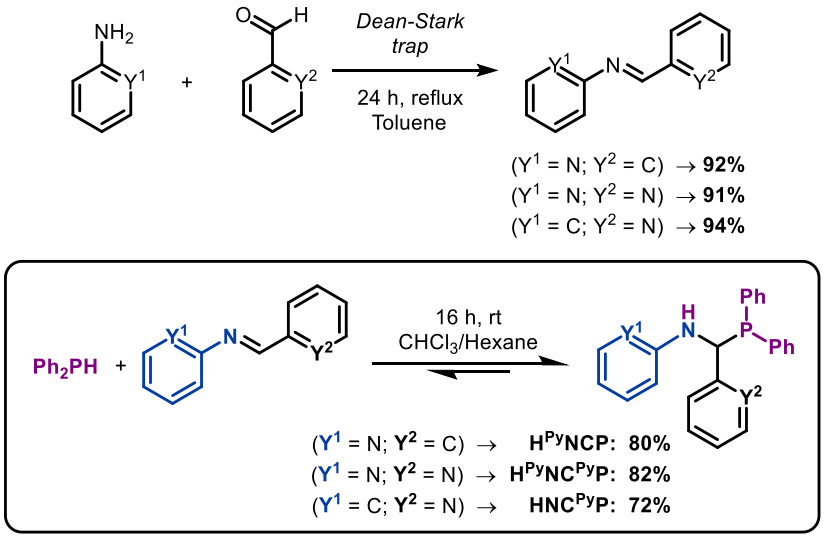

Scheme 44. Modified syntheses of the pyridyl-functionalized *Schiff* bases *via* condensation reactions (top) and subsequent syntheses of the corresponding functionalized α-aminophosphines by undergoing the analogues hydrophosphination reactions with diphenylphosphine (bottom).

The synthesis is easily modified towards the introduction of the pyridyl-groups. By interchanging the according substrates for the *Schiff* base to the pyridyl-analogue the corresponding imine was synthesized in the same manner described above in very good yields (see Scheme 44, top). Analogously, the hydrophosphination reactions of the pyridyl-functionalized imines with diphenylphosphine led to the corresponding HNCPs in good yields and purity. Despite all efforts and the facile access to the pyridyl-functionalized HNCPs, they did not improve the syntheses and therefore the attempts to isolate the novel **NHSiNCP** species.

In conclusion, deprotonated unsubstituted and pyridyl-functionalized α-aminophosphines bearing a secondary amine are too unstable in solution. The position of the equilibrium reaction seems to lay on the side of the P–C cleaved species. Apart from the facile access *via* simple hydrophosphination reactions, for the purpose of following transformations in solution, this class of ligand proved to be unsuitable.

If revisited, the obvious course of action in the future would be the introduction of strongly electron withdrawing substituents adjacent to the nitrogen or carbon backbone atom, in order to force the equilibrium position towards the P–C bond formation. Consequently, the influence of these modified aryl-groups should be analyzed regarding the aspect of transition metal complexation. Moreover, the method of improving the formation of the α-NPs introducing Cu(I) metal precursors could prove as versatile, under the point of a later complexation of the low-valent Si(II) center accompanied by the introduction of **NHSiCl** (**1**) (compare *"precursor functionalization",* Chapter 3.2.1.3).

In addition, an alternative ligand motif of the type "HNCP", which could be suitable for the generation of a potential NHSiNCP silylenes, could be found in the synthesis of the HN-C=P ligand, as shown in Scheme 45. The tedious synthesis undergoes a proton migration in the last step, leading from a phosphaneyl-imine motif (N=C-PH) to the phosphaneylidene-aniline motif (HN-C=P).[106–109] This secondary amine, as well as the lithiated subsequent stage, proved to be stable in solid state and solution,[108] hence seemingly very promising for further investigations of this type of ligands.

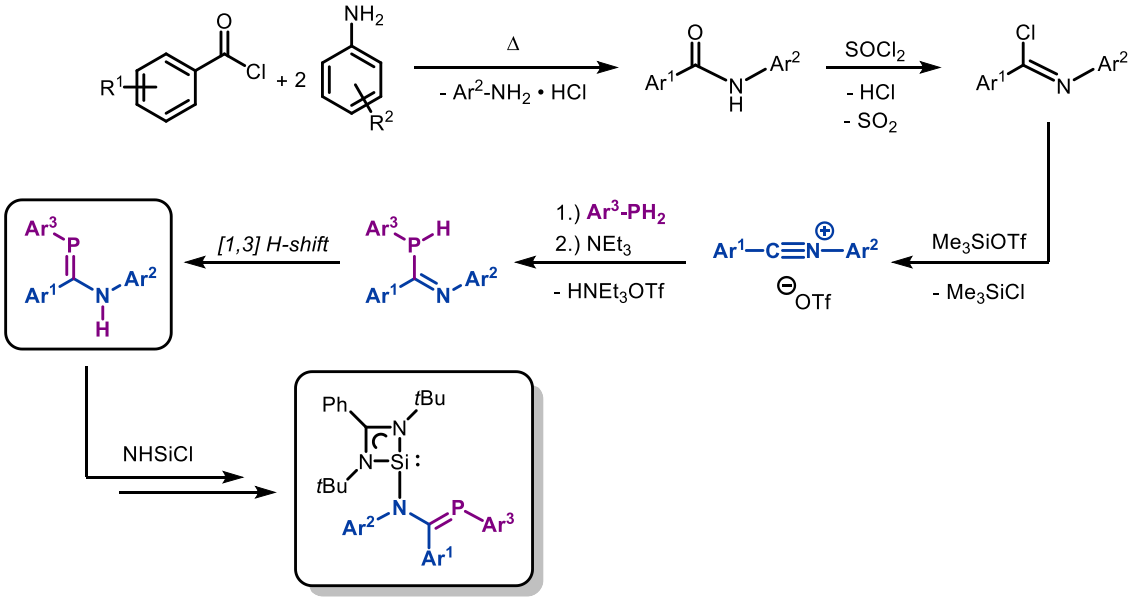

Scheme 45. Outlook on the synthesis of an alternative HNCP ligand, proving to be more stable towards deprotonation reactions, hence to utilize it in order to form novel NHSiNCP silylenes.[106–109]

3.1.2. Salt Metathesis Reactions of Silylenes with β-Aminophosphines – NHSiNCCP

The previous challenging attempts of the functionalization via α-aminophosphines led to changing the focus to the β-aminophosphines. As with the α-NPs, so shows the β-analogue **"HNCCP"** interesting properties, but offer the crucial advantage that these compounds are not so severely affected by the P–C bond cleavage, which is one reason that their investigation occupied certain working groups over the past decades. The synthesis of **HNCCP** aka. (2-(2,6-di-*iso*-propylanilino)-2-phenylethyl)diphenyl-phosphine was already reported by *Andrieu et al.*[110] who presented an improved synthesis in comparison to its elaborate predecessor by *Palacios et al.*[111] They were investigating the reactive behavior of aminophosphines towards certain organic electrophiles and the bidentate coordination of palladium metal precursors, since similar ligands could be successfully utilized in catalytical applications in form of corresponding Ru, Ni and Rh-complexes.[100,112]

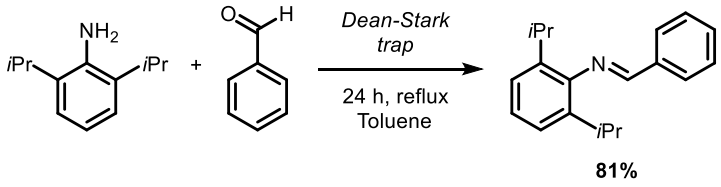

Scheme 46. Synthesis of (*E*)-*N*-(2,6-di-*iso*-propylphenyl)-1-phenylmethanimine via condensation reaction.

The synthesis of **HNCCP** was achieved in two consecutive reaction steps. At first, the corresponding *Schiff* base had to be synthesized *via* a condensation reaction of 2,6-di-*iso*-propylaniline and benzaldehyde. The utilization of a *Dean-Stark* apparatus and toluene as a solvent once again proved as the most reliable and simplest way to gain imines, which are also bulkier, like (*E*)-*N*-(2,6-di-*iso*-propylphenyl)-1-phenylmethanimine in high yields (see Scheme 46).

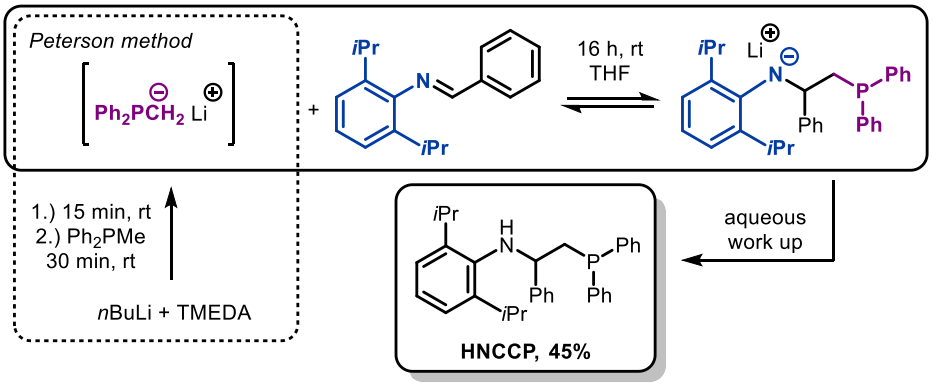

Scheme 47. Synthesis of (2-(2,6-di-*iso*-propylanilino)-2-phenylethyl)diphenylphosphine (**HNCCP**) according to *Andrieu et al.* in 2001[110].

The lithiation of methyldiphenylphosphine was done *via Peterson's* method (see Scheme 47).[113] A highly reactive lithium-complex is generated by adding *n*-butyllithium in hexane to an equimolar amount of TMEDA, which selectively deprotonates the methyl group after the subsequent addition.

The resulting lithium salt is dissolved in THF and added to a solution of the imine, which undergoes a nucleophilic attack at the imine moiety, whereby the solution turned dark red overnight. To generate the secondary amine, the reaction mixture had to be quenched with degassed water and afterwards extracted with THF and dried. The resulting solution is concentrated and degassed methanol is added, whereupon the product precipitates as a white solid overnight.

The compound was unequivocally identified by multinuclear NMR spectroscopy, mass spectrometry and X-ray diffraction analysis (see *Kyba*[110] for XRD-details). One single ^{31}P NMR signal at -23.76 ppm and a corresponding unsoiled ^{1}H NMR under the presence of an amine proton confirmed the purity of the product. The comparatively low yield of only 45% can be attributed to certain drawbacks of the synthetic route. On the one hand, the lithiation through *Peterson's* method will not go beyond 85%, due to a second lithiation reaction described in the corresponding literature (see *Kyba*[114]). On the other hand, the equilibrium position of the reaction shown in Scheme 47 is depending upon the utilized amine (compare equilibrium reaction Scheme 42, p.34).[103] Hence, the amount of side reactions is considerably high, but can be accepted regarding the otherwise reliable synthesis and workup, which can be easily upscaled to a 5-10 g scale. In addition, this ligand could be isolated, albeit in low yields, and did not show decomposition *via* P–C bond cleavage upon recrystallization as its α-analogue (compare Chapter 3.1.1).

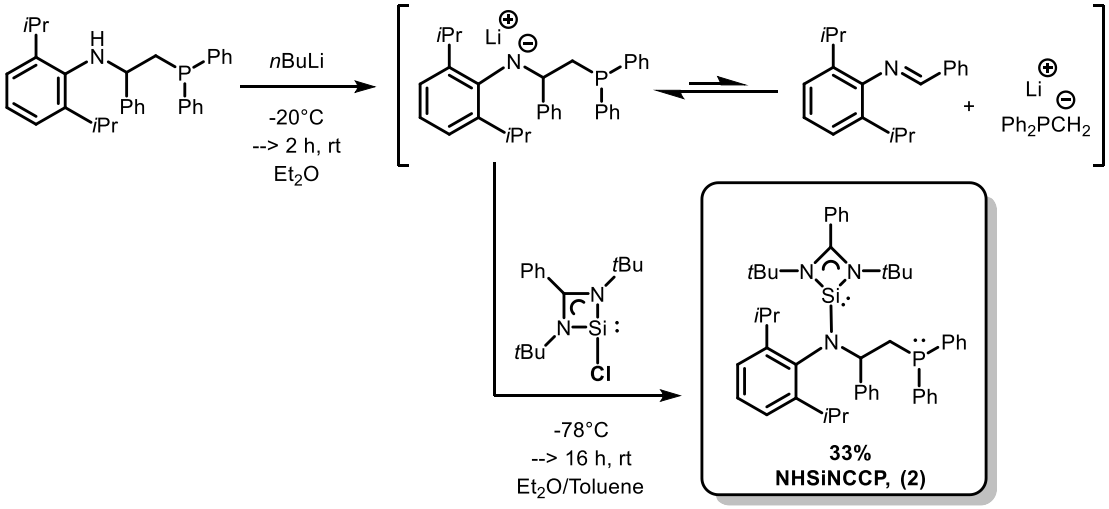

Scheme 48. Synthesis of 1,3-*N*,*N*'-di-*tert*-butyl-benzamidinato-*N*-(2-(2,6-di-*iso*-propylanilino)-2-phenylethyl)diphenylphosphine)-silylene (**NHSiNCCP, 2**) *via* salt metathesis reaction of the previously lithiated amine **HNCCP** and the chloro benzamidinato silylene **NHSiCl, 1**.

For the synthesis of the corresponding silylene the following salt metathesis was initiated by the lithiation of **HNCCP** via *n*BuLi in diethyl ether at -20°C (see Scheme 48). Performing the reaction utilizing alkali metal amides as bases, like LiHMDS, led to the isolation of **HNCCP** and **NHSiHMDS**. The reaction mixture was allowed to warm up to ambient temperatures and stirred for another 2 h. After that, it was cooled down to -78°C and a separate solution of NHSiCl in toluene was slowly added. The resulting

mixture was allowed to warm up to room temperature again and stirred overnight. After removal of all volatiles, the brown sluggish was extracted with hexane in order to remove the LiCl. Concentration of the solution and storing it at -26°C for several days resulted in the crystalline product (see Scheme 48).

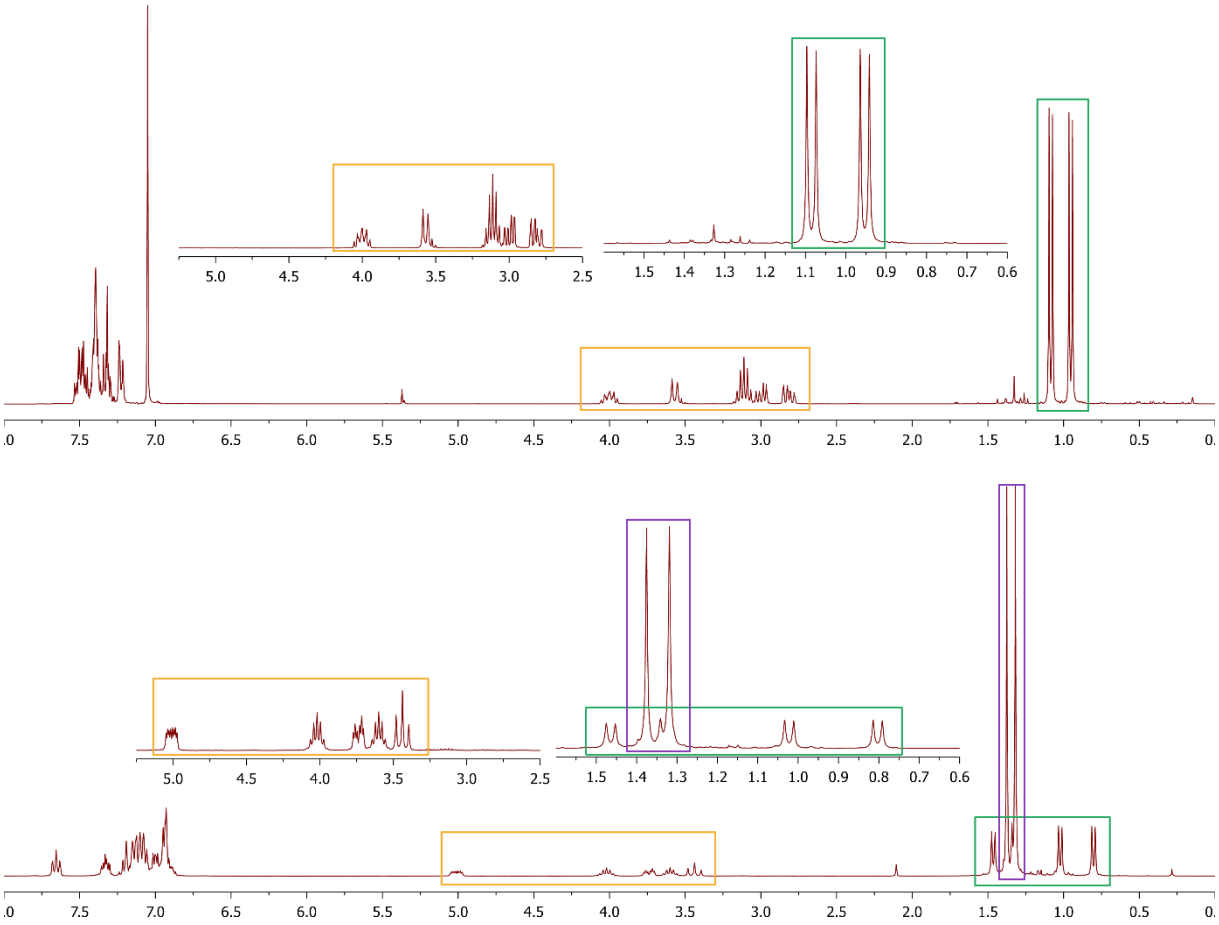

Figure 1. Comparison of the ^{1}H NMR spectrum of the ligand **HNCCP** (**top**) and novel silylene **2** (**bottom**); chemical shift *δ* in [ppm]. The framed display details show examples of the signals derived by the backbone and di-*iso*-propyl groups (**orange** & **green**), as well as the *tert*-butyl groups (**purple**).

The isolated product was fully analyzed by multinuclear NMR spectroscopy, mass spectrometry, elemental analysis and XRD solid state analysis. The single ^{31}P signal is only slightly shifted downfield with -20.05 ppm, compared to the neat amine, whereas the ^{29}Si NMR shows one signal with a significant upfield shift from 14.26 ppm (**1**) to -11.96 ppm (**2**) indicating an increase of its σ-donor ability referring to the recent studies of *Driess et al.*[49] (see chapter 1.2) and therefore laying in range of other amino-functionalized benzamidinato silylenes. Interestingly, the ^{1}H NMR data of the free substrate **HNCCP** shows two doublets and one septet for their characteristic *iso*-propyl groups (see Figure 1, top, orange), whereby the spectrum of **2** shows a splitting into four doublets and two septets, corresponding to their integrals, representing four chemically inequivalent CH_3-groups (see Figure 1, bottom, green). This indicates a hindered rotation of the NCCP- and NHSi-moiety around their linking N–Si bond plus a hindered rotation of the *iso*-propyl groups, most likely derived by the very bulky

substituents. This assumption is underlined by the fact, that the singlet corresponding to the *tert*-butyl groups is also split into two singlets showing consistent integrals (see Figure 1, bottom, purple). Since the similar **NHSiNP** by *Khan et al.* does not show a similar splitting, it can be speculated that the elongated ethylene backbone participates in the hindered rotation.

The novel silylene **2** crystallizes in the monoclinic space group $P2_1/c$ (see Figure 2, left). The bond length Si1–N3 of the newly introduced donor-group (1.7701(13) Å) lies in the area of other amino-substituted benzamidinato silylenes (1.644 to 2.048 Å). The direct comparison to the **NHSiNP** ligand by *Khan et al.* shows a slightly elongated Si–N bond of 1.796(2) Å, as well as the amidinato silylene of *Tacke et al.* with 1.7885(12) Å and quite similar to the guanidinato analogue with 1.7633(18) Å (see Scheme 32, p.26). Obviously, the P(III) donor lone-pair is pointing in the opposite direction of the Si(II) lone-pair, which is surrounded by the *tert*-butyl groups of the benzamidinato moiety and the *iso*-propyl groups of the donor group. The orientation seems reasonable, since this is the best positioning for the bulky substituents. Drawing the comparison to the similar **NHSiNP** by *Kahn et al.*, which shows a very similar orientation (see Figure 2, right).

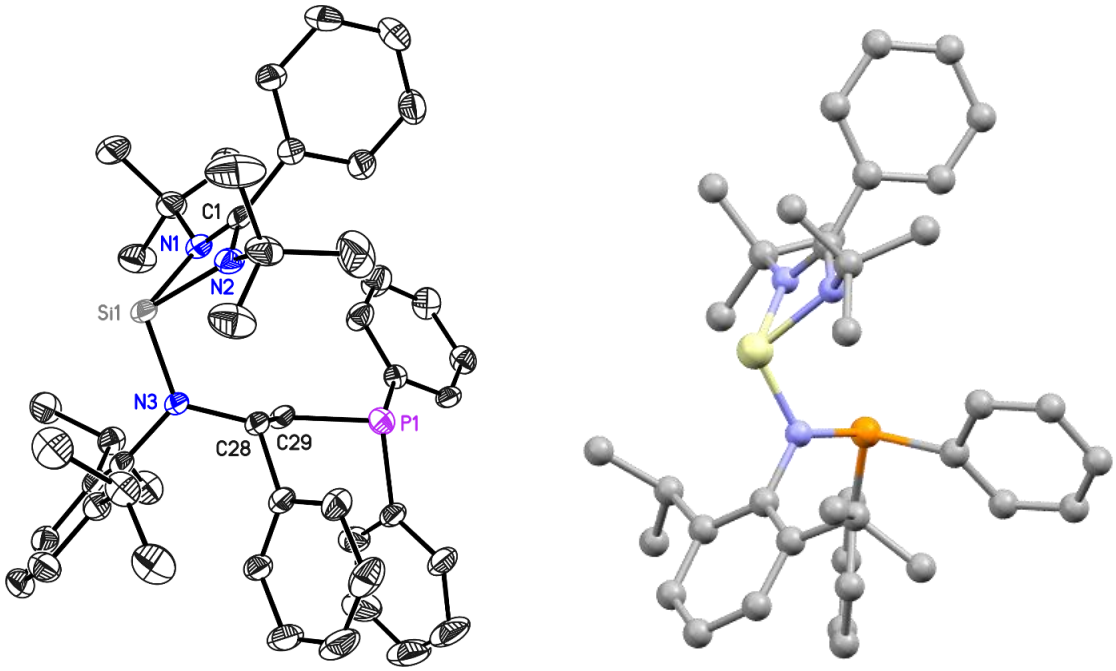

Figure 2. (**Left**) Crystal structure of **2**. The structure crystallizes in the space group $P2_1/c$ in a monoclinic crystal system with a = 20.289(3) Å, b = 10.643(2) Å, c = 21.683(2) Å and β = 99.78(10)°. The hydrogen atoms, disorder and solvent molecules has been omitted for clarity. The anisotropic displacement parameters are depicted at the 50% probability level. (**Right**) Crystal structure of **NHSiNP** by *Khan et al.*,[97] for visual comparison purposes.

The rather low yield of 33% can be primarily traced back to the previously mentioned side products and decomposition reactions. The lithiation of the isolated amine compulsorily leads to the equilibrium between lithiated amine and the P–C bond cleaved species, which has a direct influence on the formation of the target compound. Various efforts have been made to improve this reaction, e.g. slower or stepwise addition of the **NHSiCl** (**1**) solution under varying reaction conditions, unfortunately

without success. To gain further insights of **2**, the formation of certain reactions were tracked via ^{31}P NMR spectroscopy, supporting the assumption that only a partial amount of **HNCCP** reacts. Nevertheless, prior isolation of **HNCCP** is inevitable, to get rid of the previously indicated side products. A direct application of the lithiated species, as seen in Scheme 48, ended up in a mixture of numerous ^{31}P NMR signals that could not been assigned to meaningful species, yet isolated.

3.1.3. Reactivity of NHSiNCCP towards Coinage Metals

Organometallic complexes employing coinage metal atoms as the reactive center have proven to form highly reactive catalysts bearing, e.g. *N*-heterocyclic carbenes, as steering ligands,[115] thus enabling several captivating catalytical transformations, for example:

- Copper(I)-catalysts:[116] C–H bond activations (e.g. CO_2 insertions or arylation reactions)
- Silver(I)-catalysts:[117] C–C bond activations (e.g. synthesis of oxazolines) or selective oxidation reactions (e.g. alcohols to aldehydes)
- Gold(I)-catalysts:[118] nucleophilic addition reactions (of e.g. alkenes or alkynes), carboxylative cyclization reactions or [4+2]-cycloadditions.

Since the investigation of silylene group 11 transition metal complexes is quite rare, the focus was laid on isolable coinage metal complexes utilizing the novel ligand system **NHSiNCCP** (**2**), hence, the behavior and potential benefits of the softer phosphorous(III) donor-atom shall be investigated as well.

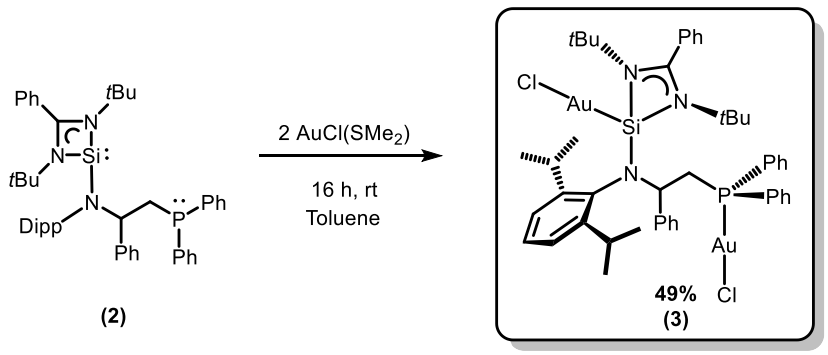

Scheme 49. Synthesis of 1,3-*N*,*N'*-di-*tert*-butyl-benzamidinato-*N*-(2-(2,6-di-*iso*-propylanilino)-2-phenylethyl)diphenylphosphine-silylene-*Si*,*P*-di-gold(I)-chloride aka. **[(ClAu)(NHSiNCCP)(AuCl)]** (**3**).

Following established methods of the complexation of gold(I) chloride complexes, the convenient precursor Au(I)Cl(SMe_2) was added to a solution of the novel silylene **2** at ambient temperature and stirred overnight. Traces of a black precipitate were filtered, the colorless solution was concentrated and stored at -35°C, whereupon a crystal growth was observed. The target compound could be isolated and analyzed by multinuclear NMR spectroscopy, mass spectrometry and XRD analyses (see Scheme 49).

The ^{31}P NMR spectrum shows a single downfield shifted signal at 25.82 ppm, which is evidently traced back to the coordination of the gold(I) atom, hence laying in a similar area as complexes bearing comparable motifs, such as the complex [((Et)PPh$_2$)(AuCl)], which exhibits a ^{31}P signal at 33.72 ppm.[119] Unfortunately, a ^{29}Si NMR signal could not be detected under no circumstances. It is believed that the already low abundance of the ^{29}Si-isotope in combination with the moderate solubility of this compound would lead to a vanishingly low intensity. Even NMR experiments with acquisition times ten times longer than the standard experiment, could not locate the corresponding signal. In addition, the coordination to a metal center could influence the relaxation times of a coordinating nucleus, thus leading to a broadened signal, further impeding the signal detection. Indeed, the ^{1}H NMR spectrum shows partially broadened signals. It indicates the presence of the silicon atom, since the complex splitting patterns of the *iso*-propyl dublets and septets, as well as the *tert*-butyl singlets, already described in the previous chapter, would not have been resolved if the NHSi- and NCCP-moieties were not linked by the Si–N bond. Furthermore, *Liquid Injection Field Desorption Ionization* (LIFDI) mass spectrometric analysis confirmed the successful synthesis and also the solid-state structure was determined by single crystal X-ray analysis, unambiguously identifying the presence of the low-valent silicon atom (see Figure 3).

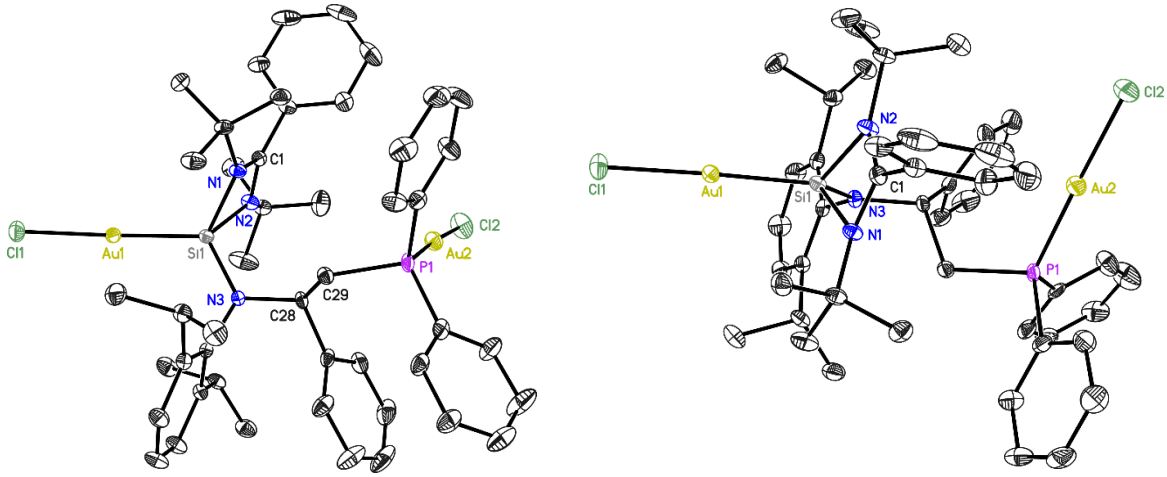

Figure 3. Crystal structure of **3** (**left**: side view; **right**: top view). The structure crystallizes in the space group $P2_1/c$ in a monoclinic crystal system with a = 19.201(4) Å, b = 13.865(3) Å, c = 24.736(5) Å and β = 100.62(2)°. The hydrogen atoms, disorder and solvent molecules has been omitted for clarity. The anisotropic displacement parameters are depicted at the 50% probability level.

The novel multinuclear gold(I) complex crystallizes in the same monoclinic space group $P2_1/c$ as the free **NHSiNCCP** ligand **2**. In comparison, the conformation of the structure did not change through the metal complexation. Supposing the Si(II)-site is the "head" and the P(III)-site is the "tail", head and tail are pointing to opposite directions, whereby the Au-Cl-moieties are roughly orientated perpendicular to each other. The bond length of Si1–Au1 (2.2447(7) Å) can be assigned to the shorter bonds, when comparing with the range of the few gold(I) silylene complexes known to date (2.246(2) to 2.317(3) Å), which also show primarily amino-substituted silylenes.[97,120] The P1–Au2 bond length of 2.210(18) Å

matches the range of typical of alkyl(diphenylphosphine) ligands of the type "R(Ph)$_2$P(III)–Au(I)" (2.319 to 2.195 Å). The angles around both gold(I) atoms confirm the estimated linear coordination sphere with Si1–Au1–Cl1 = 177.845(19)° and P1–Au2–Cl2 = 177.9(3)°. Furthermore, the newly formed Si–N bond length to the side-arm is slightly shortened from 1.7701(13) Å (**2**) to 1.7245(17) Å as a consequence of the metal coordination (see Table 1).

Table 1. Selected bond lengths [Å] and angles [°] of **3** and **[(NHSiNP)(AuCl)]** and **[(NHSiNP)(Au)]$_2$(SbF$_6$)$_2$** by *Khan et al*.

	3	**[(NHSiNP)(AuCl)]**	**[(NHSiNP)(Au)]$_2$(SbF$_6$)$_2$**	**[(NHSiHMDS)(AuCl)]**
Si–Au1	2.2447(7)	2.246(2)	2.317(3)	2.265(1)
Au1–Cl1	2.3290(7)	2.341(3)		2.341(1)
P1–Au2	2.210(18)			
Au2–Cl2	2.2810(7)			
Si–N3	1.7245(17)	1.735(7)	1.764(8)	1.716(3)
Si1–Au1–Cl1	177.845(19)	177.39(9)		179.47(3)
P1–Au2–Cl2	177.9(3)			

Worth to mention is how the group of *Khan* described their gold(I) complexation. They observed the solitary coordination of the low-valent silicon atom to the gold cation, while the adjacent P-donor atoms stay uncoordinated. In contrast, in **NHSiNCCP** (**2**) both donor-sites are addressed equally, even when performing the reaction at a 2:1 ratio. The main difference between those two silylenes is the presence or absence, respectively, of two methylene units between the P(III) and Si(II) atom ("Si–N–P" vs. "Si–N–C–C–P"). Thus, in the case of **NHSiNP**, it is conceivable, that due to the metal coordination at the silicon(II) atom, the electronical properties of the P(III) donor site would slightly change towards a disfavored second metal coordination. Moreover, the pure spatial proximity to the bulky substituents (*t*Bu-, Dipp-groups) could sterically hinder a second complexation, as well.

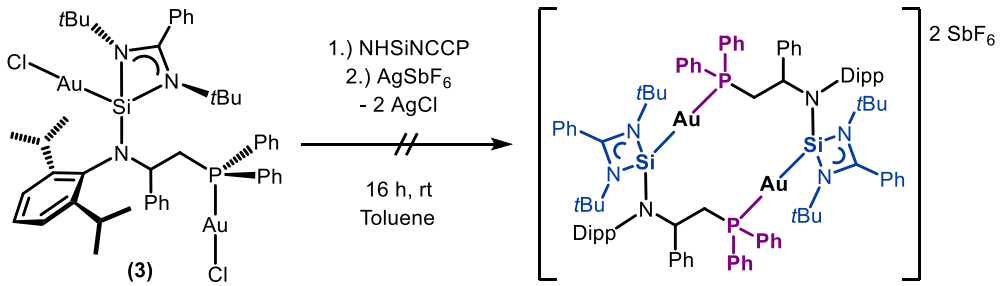

Scheme 50. Synthetic attempt to the isolation of an Au(I)-Au(I) dimer featuring a hemilabile complexation of two **NHSiNCCP** ligands (color-coded: purple [P(III)] vs. blue [Si(II)]).

To investigate whether the ligand is able to adopt a hemilabile complexation or not, further experiments concentrated on the formation of Au(I) dimers in relation to preceding attempts.[97] To a solution of the previously isolated complex **3** in toluene one equivalent of silylene **2** was added and stirred at ambient temperature. Subsequently two equivalents of commonly utilized $AgSbF_6$ were added in order to abstract the halide and generate the dimer by undergoing a salt elimination to

remove the chloro groups to form a dimeric structure in a head-tail/tail-head fashion (see Scheme 50). Unfortunately, despite all efforts the desired formation of a dimer remained elusive. With the addition of the silver salt the reaction mixture formed a black suspension. Additionally, a gold mirror within the reaction vessel indicated the decomposition of the complex. Varying the conditions (e.g. temperature, exclusion from light) or the reagent for the halide abstraction (e.g. $NaSbF_6$) also did not lead to the desired complexation. In general, the attempts to isolate a pure Ag(I) complex of **2** also ended in the aforementioned formation of a black precipitate and decomposition of the ligand, monitored *via* ^{1}H NMR spectroscopic measurements.

To further investigate the behavior of the novel NHSi ligand **2** towards coinage metals and possible bidentate complexation, the metal source was changed to Cu(I)Br(SMe_2). To a solution of **2** in DCM two equivalents of the copper precursor were added and stirred overnight at ambient temperature, which led to a very fine crystalline precipitation that proved to be nearly insoluble in all common solvents. Analysis *via* NMR-spectroscopy or mass spectrometry failed, nevertheless through slow vapor diffusion over several days at -35°C it was possible to gain colorless crystals big enough to perform XRD analysis. Although still too small to gain sufficiently good data for a suitable structure analysis, yet sufficient to get reliable insights into the bonding nature of this crystalline powder (see Scheme 51 and Figure 4).

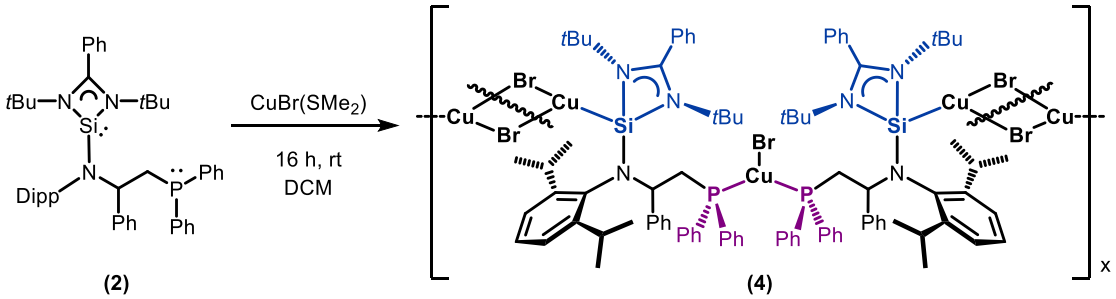

(2) (4)

Scheme 51. Supposed synthesis of the barely soluble polymer-like complex 1,3-*N*,*N*'-di-*tert*-butyl-benzamidinato-*N*-(2-(2,6-di-*iso*-propylanilino)-2-phenylethyl)diphenylphosphine-silylene-*Si*,*P*-di-copper(I)-bromide **4** aka. **[(BrCu)(NHSiNCCP)(CuBr)$_{0.5}$]$_x$**.

The multinuclear copper(I) complex **4** crystallizes in the monoclinic space group $P2_1/c$. It shows a polymer coordination structure of repeating [Cu–μ-Br]$_2$- and [μ-Cu–Br]-moieties in a [head-tail-tail-head] manner (see Figure 4), which could be an explanation for the rather poor solubility. As mentioned above, a conclusive discussion of the bond lengths and angles is prevented, though, the crystal structure displays the same orientation of head and tail, as with the silylene **NHSiNCCP** (**2**) and the Au(I) complex **3**. These observations led to the assumption that the ligand and his backbone is not as flexible as anticipated. The rather bulky *iso*-propyl and *tert*-butyl groups seem to form a sterical barrier inhibiting free rotation around the Si–N_{Subst} bond, thus strongly impairing the formation of a bidentate complexation leading to a 6-membered metallacycle. Oddly enough, drawing the

comparison to the work of *Khan et al.*, who were able to observe exactly such a rotation (see Scheme 52),[97] suggests that the backbone, elongated by two methylene units, contributes to this disfavored rotation, probably due to the increased amount of degrees of freedom offered by the backbone.

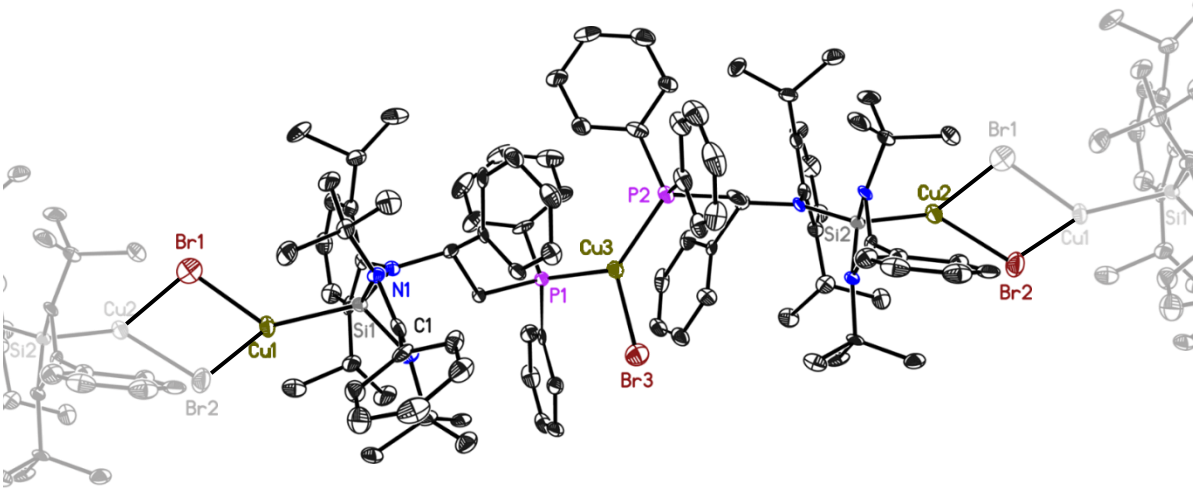

Figure 4. Crystal structure of **4**. The structure crystallizes in the space group $P\bar{1}$ in a triclinic crystal system with a = 13.171(2) Å, b = 15.396(2) Å, c = 23.231(3) Å and α = 92.20(2)°, β = 93.61(3)°, γ = 92.28(2). The hydrogen atoms, disorder and solvent molecules has been omitted for clarity. The anisotropic displacement parameters are depicted at the 50% probability level.

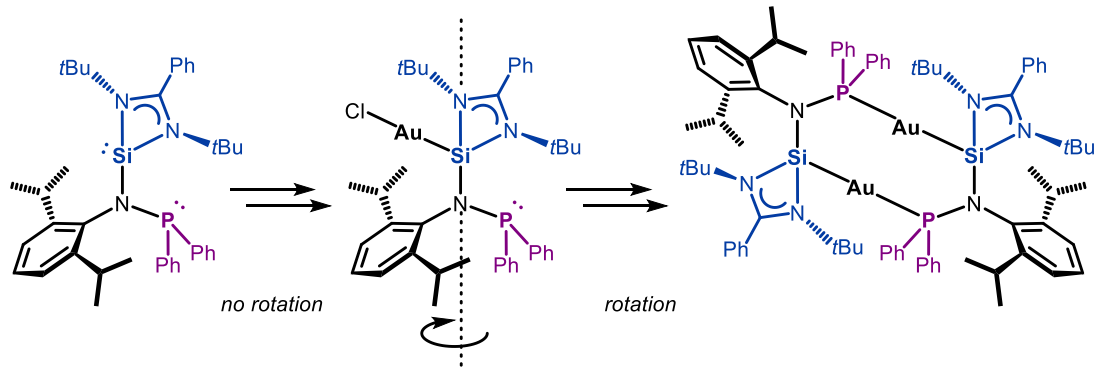

Scheme 52. Schematic illustration of the possible rotation of the bulky Dipp- and benzamidinato moieties around the Si–N_{Subst} bond at the example of the preceding work of *Khan et al.* in 2016.

Although, such a chain-like complexation is quite interesting, due to the obstacles accorded analyses and the non-bidentate coordination of **3** and **4** gained by the solid state structure, the ligand **2** proved to be unsuitable for chelation and hemilabile complexation. Besides the assumption that the adjacent residues of the silicon atom and the functional group are sterically too demanding, the length of the backbone seems to have a great influence on the favoritism of a bidentate coordination of a single metal atom and rather favors the formation of multinuclear complexes.

In order to exclude the possibility that the ligand shows such behavior only through the sterically demanding residues, future work should concentrate on the synthesis and analyses of the introduction of sterically less demanding substituents, like phenyl-groups. However, during this work other systems

have proved to be more versatile and promising, which is why no further attempts were undertaken at this point.

3.2. Development of Alternative Routes to Novel NHSis

One of the main goals of this thesis was to develop of novel methods to gain transition metal complexes featuring NHSis on the basis of the benzamidinato silylene **1**. The primary focus was to change the process of the conventional synthetic route, to achieve alternative methods and investigate a possibly more efficient and controllable way of complexation (see Scheme 53).

As the very early attempts of investigating silylenes have shown, isolation is easier by taming the high reactivity of the lone-pair by transition metal coordination (e.g., see Chapter 1.3, Scheme 20, p.17).[3][61–64] Over the past decades there were plenty reports on transition metal complexes employing the **NHSiCl** (**1**) (e.g., Co,[121,122] V,[122] Cr,[123] Mo,[123] W,[123] Re,[124] Mn,[124] Ti,[125] Fe,[67] Rh,[126] Cu,[127] Ni[128]), but never under the aspect to perform follow-up functionalization reactions. Once these TM NHSiCl complexes will be isolated, the substitution of the chloro group with donating groups bearing even more complex features can be undertaken.

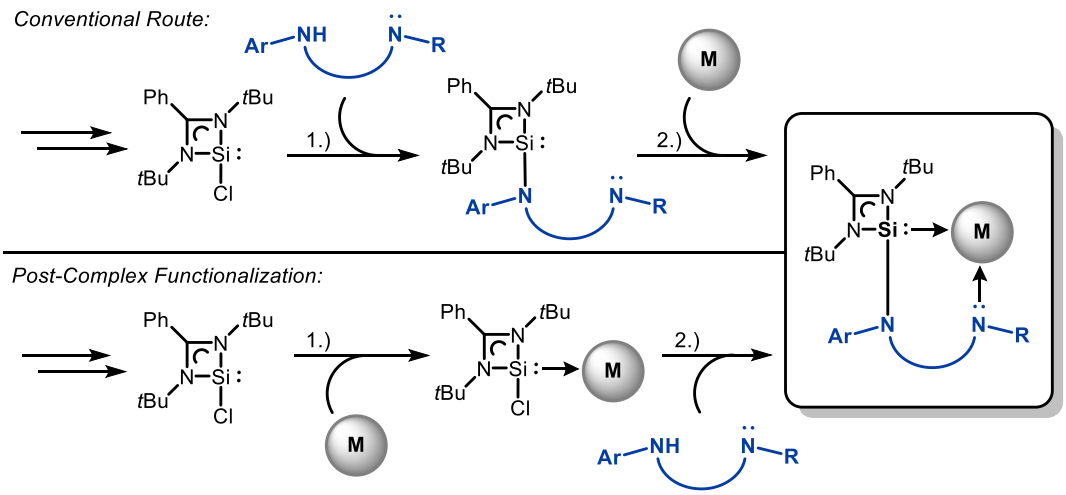

Scheme 53. Schematic illustration of changing the conventional route of functionalization followed by metalation (**top**), to the post-complex functionalization *via* preset complexation of transition metal precursors followed by the functionalization step (**bottom**).

In Chapter 3.1 and following, the recent conventional strategy of the functionalization of chloro benzamidinato silylenes was presented and applied (see Scheme 53, top). Among other things, the work of *Tacke et al.* was presented and thereby also the first examples of NHSis showing side-arm donating complexes. After the investigation of the phosphorous based NCP-ligands and the concomitant challenges of the synthesis and the subsequent functionalization, the focus was realigned on nitrogenous based side-arms, more precisely on the utilization of pyridyl-groups.

In the following chapters, methods to synthesize and characterize novel group 11 and group 12 transition metal NHSiCl complexes as well as their subsequent functionalization with side-arm donating pyridyl-groups will be presented.

As already mentioned at the beginning of Chapter 3.1.3, the lighter homologues, the *N*-heterocyclic carbenes, proved to form highly reactive coinage metal catalysts as steering ligands,[115] thus enabling several captivating catalytical transformations. Since the investigation of silylene group 11 transition metal complexes is quite rare and limited to a small number of compounds, with no catalytical applications yet, there is still a lot of potential undiscovered in that field of chemistry. For these reasons, the following chapters will examine the alternative methods on the basis of coinage metal atoms.

3.2.1. Presentation of NHSi Copper(I) Complexes

3.2.1.1. Synthesis of Pseudocubane NHSiCl Cu(I) Halide Complexes – [(NHSiCl)(CuX)]$_4$

In order to investigate the synthesis of NHSi TM complexes, the reaction protocol was inspired by preceding methods, featuring the straightforward one-pot synthesis of the free ligand **1** and common TM halide precursors at partially lowered temperatures.[67,121–128]

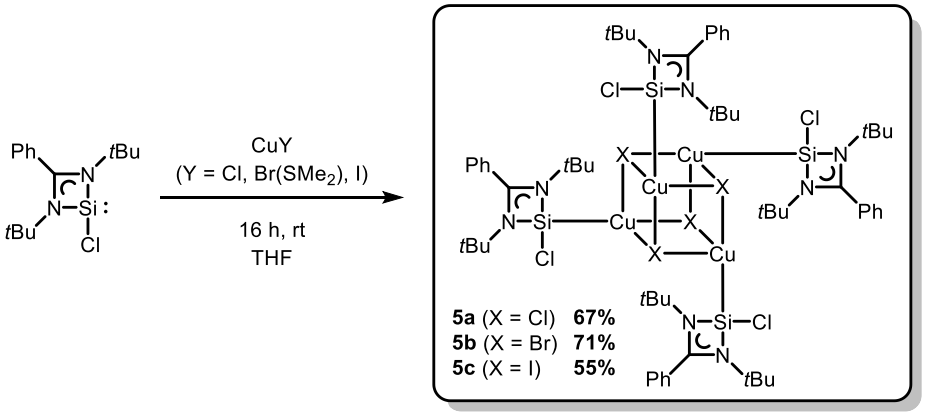

Scheme 54. Synthesis of the pseudocubane tetramer complexes **[(NHSiCl)(CuX)]$_4$** (with X = Cl, Br, I) aka. tetrakis-1,3-*N*,*N*'-di-*tert*-butyl-benzamidinato-chloro-silylene-copper(I)-chloride/bromide/iodide (**5a-c**).

The chloro benzamidinato silylene PhC(N*t*Bu)$_2$SiCl (**1**) was dissolved in THF and an equimolar amount of the corresponding copper(I) halide precursor (CuCl, CuBr(SMe$_2$), CuI) was added in small portions to the stirring solution at ambient temperatures. The white suspension turned into a yellowish clear solution after approximately one hour, but kept stirring overnight (see Scheme 54). The color intensity thereby depended on the utilized halide (Cl<Br<I). The resulting reaction mixture was filtered to remove suspended particles and concentrated right afterwards. Subsequent addition of a similar volume of *n*-hexane to the concentrate resulted in an immediate (5-30 min) crystal growth at room

temperature. It is worth mentioning, that the same crystals were isolated without using hexane, but crystal growth prolonged up to days. The target compounds were easily isolated up to a scale of one gram as slightly yellow to yellowish crystals in moderate to good yields.

All compounds were analyzed *via* multinuclear NMR spectroscopy, elemental analysis and XRD analysis. Latter shows the pseudocubane nature of **5a-c** in a $Cu_4(\mu_3\text{-}X)_4$ manner. The tetramer consists of alternating copper(I) atoms each coordinated by a **NHSiCl** ligand **1** and linked by μ_3-bridging halide atoms. The formation of such pseudocubanes is not uncommon for $[MX]_4L_n$ complexes featuring M = Cu, Ag; X = Cl, Br, I; and L = neutral donor ligands.[129,130] The molecular structures of **5a-c**, shown Figure 5, crystallize in the monoclinic space group *C*2/c. The metal-halide bond lengths and angles (M–X and M–X–M, respectively) correlate to the corresponding halides and therefore lay in a typical range of such pseudocubanes (see Table 2). The Si–M bond lengths of **5a-c** (2.1889(8)-2.2306(13) Å) are comparable to $[MX]_4L_n$ cubane systems bearing common phosphine ligands (e.g., $[CuX]_4L_n$; L = PPh_3, X = Br; Cu–P = 2.209 Å).[130,131] The few related silylene Cu(I) complexes known to date by *Khan et al.*[132,133] and *Driess et al*.[127] display a narrow range of Si–Cu bond lengths (2.199–2.231 Å) to which the corresponding bond lengths of **5a-c** fit perfectly.

Table 2. Selected bond lengths [Å] and angles [°] for complexes **5a-c**.

	5a	**5b**	**5c**
Si–Cu	2.1889(8)-2.1930(9)	2.2068(7)-2.2085(7)	2.2285(13)-2.2306(13)
Cu–X	2.3097(8)-2.7844(10)	2.4632(8)-2.7860(10)	2.5993(9)-2.9641(9)
Cu–X–Cu	69.96(2)-90.07(3)	68.02(2)-85.16(2)	65.48(3)-78.57(4)
X–Cu–X	84.81(3)-111.93(3)	88.59(2)-114.22(2)	93.21(4)-116.56(3)

Hitherto, there are no reports on tetramers of the type $[MX]_4L_n$ bearing silylenes and especially the well-known chloro benzamidinato silylene ligand **1**. However, looking at recent achievements of the higher homologue germanium there are certain reports on the synthesis and characterization of similar pseudocubane complexes utilizing the analogues germylene benzamidinato ligands (*Polo et al.*) or six-membered germylenes (*Mak et al.*) (see Scheme 55).[134,135]

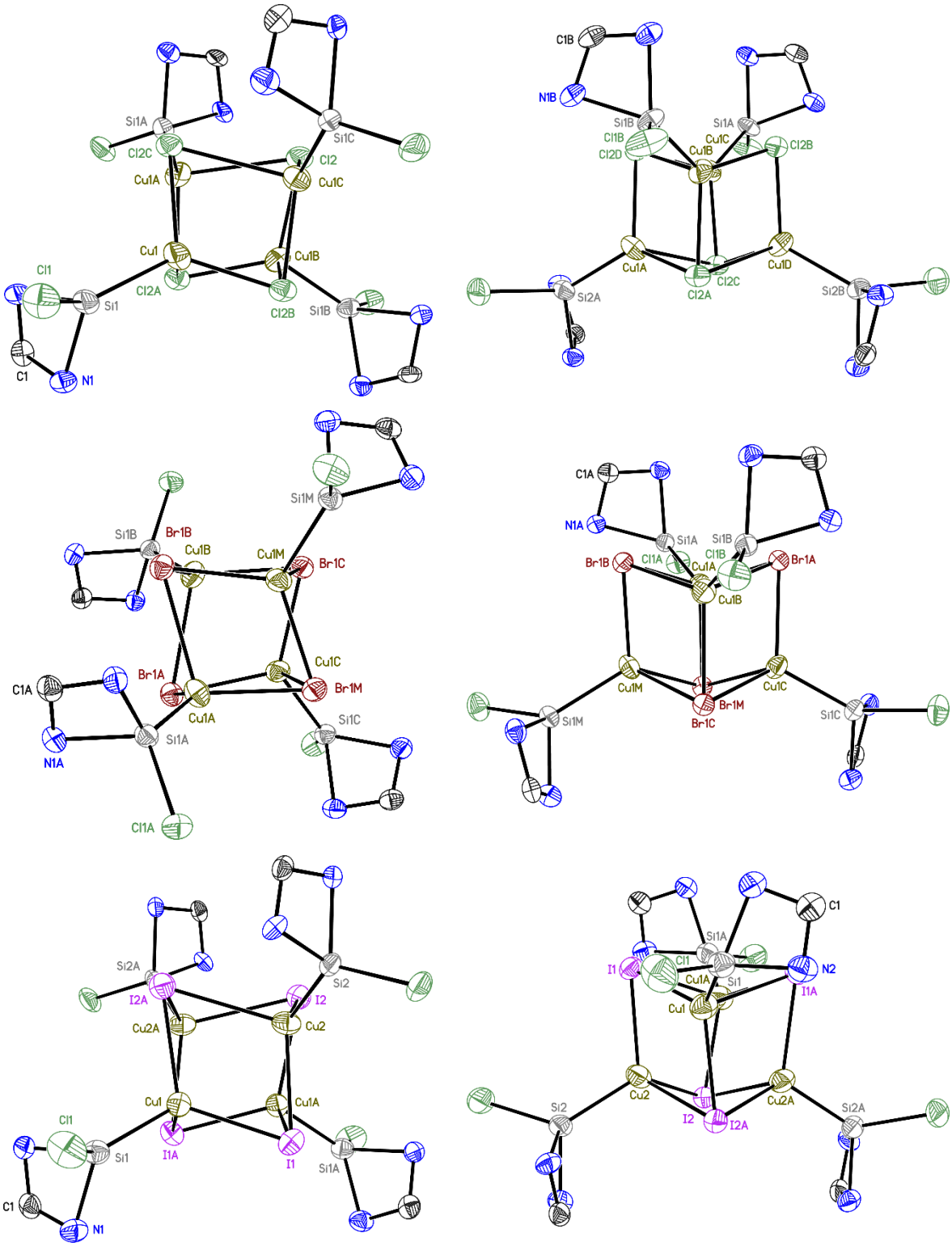

Figure 5. Crystal structures of **5a-c** (**left**: top view; **right**: side view)**.** The isostructural compounds crystallize in the space group *C*2/c, in monoclinic crystal systems with a = 19.064(2) Å, b = 18.785(2) Å, c = 25.746(3) Å and β = 103.96(2)° for **5a** (**top**), with a = 20.130(3) Å, b = 18.444(2) Å, c = 26.594(3) Å and β = 109.17(3)° for **5b** (**middle**) and with a = 19.751(2) Å, b = 18.807(2) Å, c = 25.572(3) Å and β = 103.53(2)° for **5c** (**bottom**). The *tert*-butyl-/phenyl-groups, hydrogen atoms, disorder and solvent molecules has been omitted for clarity. The anisotropic displacement parameters are depicted at the 50% probability level.

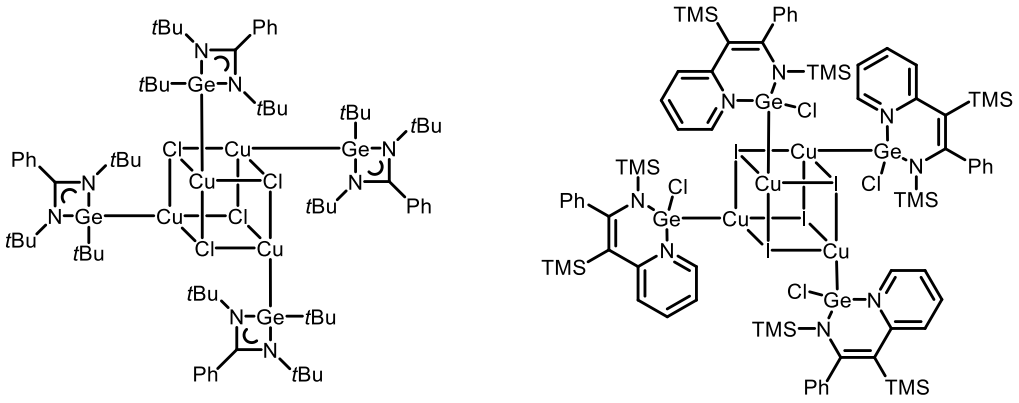

Scheme 55. Similar pseudocubane tetramer complexes of the type $[MX]_4L_n$; with L = benzamidinato germylene, by *Polo et al*.[134]; and L = six-membered germylenes, by *Mak et al*.[135]

It has to be stated, that the crystal structures of **5b** and **5c** revealed that the halide positions of the alleged precursors are partially occupied by chloro atoms. Since the only source of chloro atoms could be the **NHSiCl** (**1**), a halide-interchange is most likely, nevertheless, the occupation only lies at < 5% and is therefore negligible.

The ^{1}H NMR spectra of complexes **5a-c** show a slightly shifted solitary singlet characteristic for the *tert*-butyl groups of the benzamidinato scaffold, as well as the corresponding aromatic multiplets derived by the phenyl backbone. Accordingly, the ^{13}C NMR spectra are in line with the expected signals. But more importantly the ^{29}Si NMR show solitary fairly broadened singlets at 27.73 (**5a**), 26.09 (**5b**) and 22.62 ppm (**5c**), respectively. To gain these signals, unusual high concentrated solutions and prolonged measuring times were necessary. Possible reasons for the weak and broad signals could be relaxation effects induced by the transition metal coordination, or fluctuating complexation and decomplexation processes of the tetramer to a dimer structure appearing in solution (*vide infra*). This could be verified by performing temperature dependent NMR measurements of the corresponding compounds, to possibly decelerate such processes, hence determining the nature of the signal as a function of temperature. Unfortunately, such experiments could not be performed within this project, but definitely should be considered for future work.

In 2014 *Driess et al*. published the first heteroleptic silylene copper(I) complexes employing the NHSiCl ligand **1** [(NHSiCl)(Cu(TMEDA))]OTf (see Scheme 56 for comparison), thereby reporting a similar ^{29}Si NMR shift of 32.9 ppm.[127] Other comparable compounds where reported by *Khan et al.* in 2015, who investigated early coinage metal complexes bearing the uneventful **NHSiHMDS** ligand, which copper(I) complex shows an upfield shifted ^{29}Si signal of 16.85 ppm, most likely due to the presence of the electron donating $N(SiMe_3)_2$ (HMDS) group.[120]

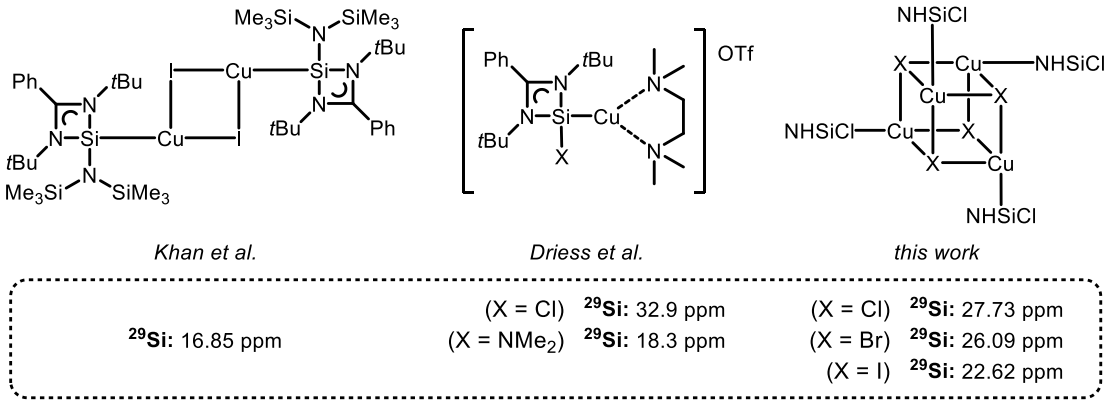

Scheme 56. Comparison of certain ^{29}Si NMR Shifts by *Khan et al*.[120] and *Driess et al*.[127] towards the complexes **5a-c**.

In order to further investigate the structure of **5a-c** various mass spectrometric techniques were performed (LIFDI, ESI, MALDI and EI), yet, it was not possible to detect any meaningful signals related to any relevant structures or fragments of the compounds **5a-c**. The compounds are probably too sensitive towards any traces of air or moisture or towards the ionization methods, thus decomposing during the process. However, while searching for ways to identify the pseudocubane *via* ESI-HRMS experiments, it was possible to identify a side product containing the characteristic $[CuX]_4$ core unit. In order to exchange a halide and possibly generate a structure which is easier to ionize, **5b** was treated with a slight excess of $NaSbF_6$, which led to the oxidized species $[(NHSiCl)_4(Cu^{+I}_2Cu^{+II}_2)Br_3(SbF_6)_2]^+$. Even though this structure contains oxidized copper(II) atoms the matching isotope pattern of m/z = 2144.78 compared to the simulated spectrum confirms the presence of the core moiety known by XRD experiments. To support this observation, the corresponding complexes **5a** and **5c** were treated the same way, but only led to a black suspension without meaningful signal interpretation.

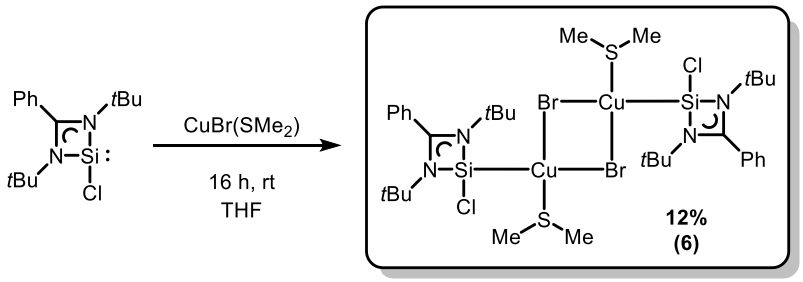

Scheme 57. Isolation of the intermediate/byproduct **[(NHSiCl)(CuBrSMe$_2$)]$_2$** (**6**) by performing the reaction in low volumes of solvent at low temperatures.

While optimizing the reaction conditions of $[(NHSiCl)(CuBr)]_4$ (**5b**) using the precursor $CuBr(SMe_2)$, it was noticeable, that performing the reaction in very small amounts of solvent at -30°C, led to a partially formation of a pale green precipitate overnight. The filtrate proved to contain the desired complex **5b**, whereas recrystallization of the isolated solid from DCM showed to be the subspecies/intermediate $[(NHSiCl)(CuBrSMe_2)]_2$ **6** (see Scheme 57).

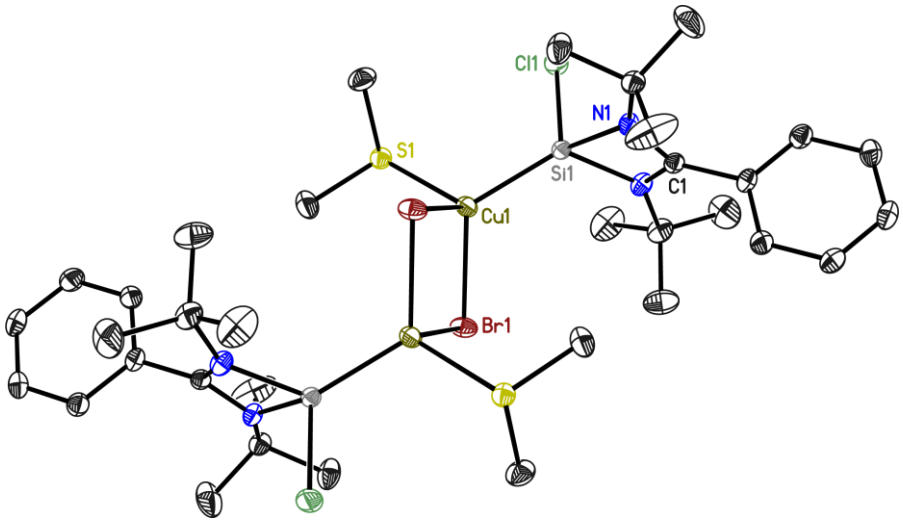

Figure 6. Crystal structure of **6**. The structure crystallizes in the space group $P2_1/c$ in a monoclinic crystal system with a = 9.265(2) Å, b = 28.831(3) Å, c = 8.806(2) Å and β =107.60(2). The hydrogen atoms, disorder and solvent molecules has been omitted for clarity. The anisotropic displacement parameters are depicted at the 50% probability level.

Compound **6** was analyzed by ^{1}H and ^{13}C NMR spectroscopy and XRD analysis. In addition to the common characteristic singlets derived by the *tert*-butyl-groups (1.27 ppm) of the benzamidinato scaffold, the new singlets belonging to the SMe_2 ligands (2.25 ppm) were unambiguously identified *via* ^{1}H and ^{13}C NMR spectra. Unfortunately, due to high sensitivity towards air and moisture and volatility of the SMe_2 ligands, the compound decomposed during elemental and LIFDI mass spectrometric analyses. The Si–Cu bond length of **6** (2.2082(5) Å) is very similar to its tetrameric congener **5b**, which shows a wider range of bond lengths and angles, due to its distorted geometry (see Table 3). Accordingly, the remaining Cu–Br bond length and angles fit into this range as well, hence showing good consistency to each other and suggesting, that the formation of dimer or tetramer seemingly has no great influence on the silicon(II) metal bonds.

Table 3. Selected bond lengths [Å] and angles [°] for complexes **6** and **5a-c**.

	6	**5b**
Si–Cu	2.2082(5)	2.2068(7)-2.2085(7)
Cu–Br	2.4828(5)/2.5046(3)	2.4632(8)-2.7860(10)
Cu–S	2.3787(8)	
Cu–Br–Cu	78.423(13)	68.02(2)-85.16(2)
Br–Cu–Br	101.577(13)	88.59(2)-114.22(2)

Keeping in mind that the fourth coordination site at the copper(I) atom, here occupied by the dimethyl sulfide ligand, could be replaced by a donating solvent molecule (e.g. THF), this could be interpreted as the possibility of the tetramer to be also present as a dimer in solution. In fact, diffusion ordered spectroscopy (DOSY) analysis of a solution of $[(NHSiCl)(CuBr)]_4$ **5b** in THF indicates the presence of a dimeric structure in solution. *Via* the *external calibration curve* (ECC) method, established in our group by *Neufeld*, molecular weights of compounds and intermediates in solution can be determined utilizing

DOSY experiments.[136,137] The hypothetical aggregates are adjusted in relation to the ECCs and the corresponding diffusion coefficient. Thus, the determined molecular weights vary according to the physical composition of the aggregates. Accordingly, the deviation derives from the difference between the determined MW and the calculated one. This way, a molecular weight in the area of a dimeric structure, attended by THF molecules, was determined (see Scheme 58).

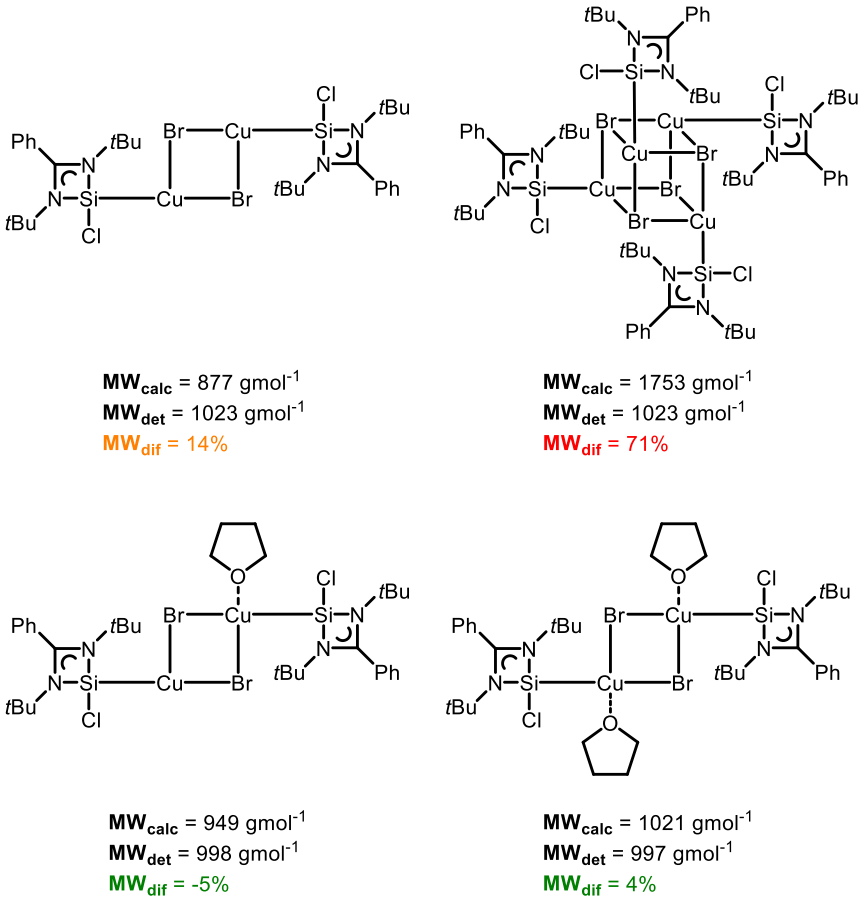

Scheme 58. Most likely hypothetical aggregates of **5b** in THF, determined by the ECC method *via* DOSY experiments. The data indicates a dimeric species with possible free coordination sites that might be occupied by THF molecules.

3.2.1.2. Functionalization with Pyridyl-Substituted Amino Groups – $[(NHSiMes)_2(CuX)_3]$

With the tetrameric copper(I) complexes **5a-c** in hand, the following investigations concentrate on the functionalization of the chloro group on the benzamidinato silylene **1**. As comprehensively described in Chapter 1.4 and 3.1, the substitution is commonly performed *via* a salt metathesis reaction primarily employing lithiated amines. Once the lone-pair of the low-valent silicon atom was occupied by the transition metal atom (in this case copper(I)), the subsequent substitution procedure was inspired by the above mentioned preceding methods, featuring the utilization of frequently used lithium based deprotonating agents, like LiHMDS.

To gain the amine *N*-mesityl-*N*-(2-pyridyl)amine (**MesNHPy**) various synthetic routes can be considered. A rather elegant way is the palladium-catalyzed *Buchwald-Hartwig*-amination of aryl halides and amines. This method allows a wide range of substrates and shows a broad tolerance towards functional groups.[138–141] *Via* application of a Pd-catalyst (e.g. $Pd_2(dba)_3$, $Pd(OAc)_2$), a base (e.g. NaOtBu, Cs_2CO_3) and an additional ligand (e.g. BINAP, SPHOS), the C–N bond formation takes place in common solvents (e.g. toluene, dioxane) at temperatures around 100°C resulting in good yields (see Scheme 59, **(A)**).

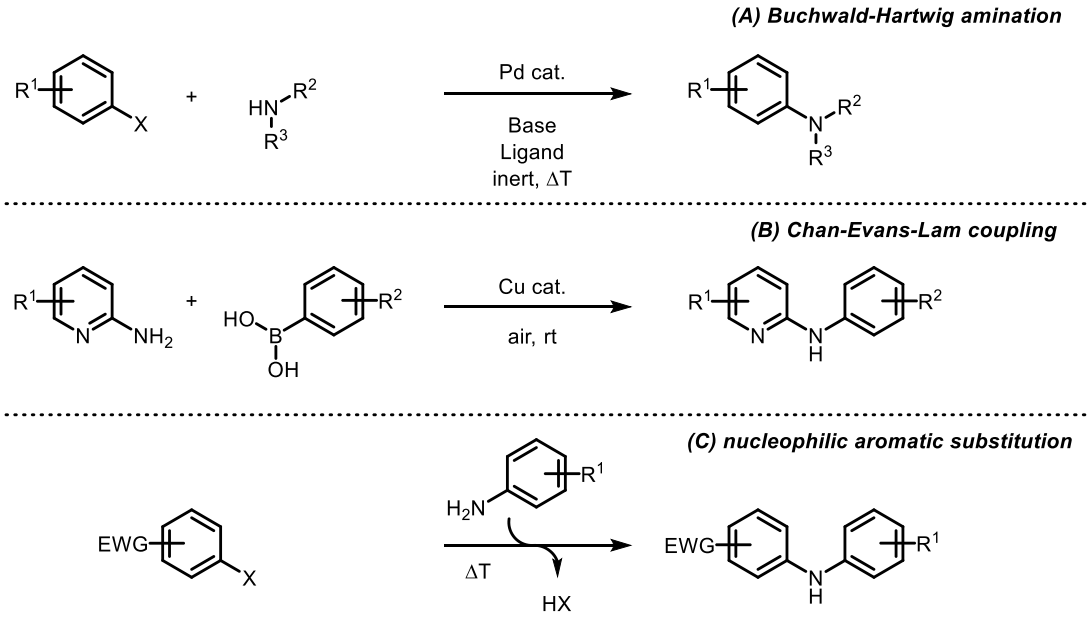

Scheme 59. Schematic overview of common methods for C–N-bond formation reactions. (A) *Buchwald-Hartwig*-amination (Pd cat. = e.g. $Pd_2(dba)_3$, $Pd(OAc)_2$; Base = e.g. NaO*t*Bu, Cs_2CO_3; Ligand = e.g. BINAP, SPHOS),[138–141] (B) *Chan-Evans-Lam*-coupling (Cu cat. = e.g. $Cu(OAc)_2$),[142–144] (C) nucleophilic aromatic substitution (EWG = electron withdrawing group); with X = Cl, Br, I; R^1/R^2 = alkyl, aryl, H; R^3 = alkyl, aryl.[145–148]

Another catalytical attempt to form the carbon-nitrogen bond is the copper-catalyzed *N*-arylation of 2-amino-*N*-heterocycles by cross-coupling boronic acids and amines. This reaction, also known as the *Chan-Evans-Lam* coupling, promotes a functional group tolerance and mild reaction conditions by employing weak or no bases at ambient atmosphere and temperatures - so-called open-flask chemistry

(see Scheme 59, **(B)**).[142–144] A more direct method is the nucleophilic aromatic substitution reaction between, e.g., 2-amino-pyridines (nucleophiles) and aryl halides (electrophiles). While this reaction is limited to a narrower scope and a lower tolerance towards functional groups, for the synthesis of more straightforward substrates like *N*-aryl-*N*-(2-pyridyl)amines, this technique proves to be more suitable, due to the dispensability of an expensive noble metal catalyst and additive ligands as well as an complex experimental setup (see Scheme 59, **(C)**) and was therefore used in the following.

The reaction was performed based on modification of previous reports,[145–148] and can be easily upscaled to at least 10 g. 2,4,6-trimethylaniline and 2-bromopyridine were stirred overnight in a high-pressure flask at 170°C. The reaction mixture was subsequently allowed to cool down to 90°C and immediately quenched with a saturated aqueous solution of $NaHCO_3$. During this process, the products partially precipitated and had to be extracted with diethyl ether. The dried organic phase was concentrated, whereby the crude product readily precipitated in form of colorless crystals, which were eventually washed with hexane. For further purification steps, the crude product was recrystallized from hot toluene, or *via* distillation using a *Kugelrohr* apparatus to gain the product **MesNHPy** as a pure colorless crystalline solid. The successful synthesis and purity was determined *via* evaluation of the ^{1}H and ^{13}C NMR spectra and mass spectrometric analysis.

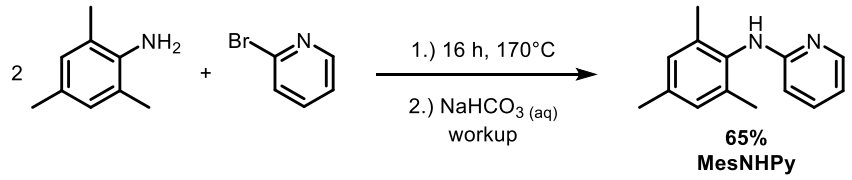

Scheme 60. Synthesis of *N*-mesityl-*N*-(2-pyridyl)amine (**MesNHPy**) via S_NAr reaction (yield after purification steps).

The complexes **7a-c** were synthesized in the same manner in an inert atmosphere inside a glovebox. Four equivalents of the amine **MesNHPy** were added to a solution of the corresponding precursor $[(NHSiCl)(CuX)]_4$ (**5a-c**) in a mixture of toluene and THF, in a ratio of 1:1, and subsequently cooled down to -30°C. A separately prepared solution of LiHMDS in THF was added dropwise and afterwards allowed to warm up to ambient temperature under constant stirring overnight. The resulting suspension was concentrated until a yellowish solid precipitated, which was filtered off and redissolved in DCM in order to remove the LiCl salt in another filtration step. The new concentrated solution was stored at -35°C for one day to gain the desired compounds **7a-c** in form of bright yellow crystals with high purity (see Scheme 61, Method **A**).

Alternatively, the amine **MesNHPy** can be lithiated and isolated in a separate preset step to undergo the same salt metathesis reaction (see Scheme 61, Method **B**). Both methods worked equally reliable, whereas the yields of method B were slightly higher (e.g. **7b**, 49% *vs.* 42%). However, the advantage of

the presented method **A** was its simplicity, since the workup of the lithiated species MesNLiPy is expendable.

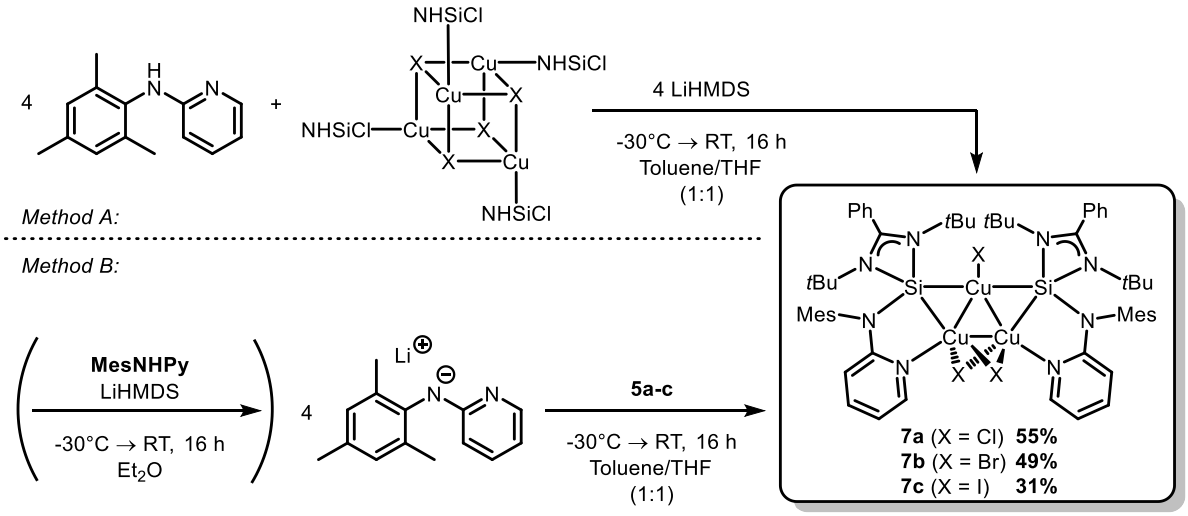

Scheme 61. Synthesis of bis-1,3-*N*,*N*'-di-*tert*-butyl-benzamidinato-*N*-mesityl-*N*-(2-pyridyl)amino-silylene-tris-copper(I)-chloride/bromide/iodide **[(NHSiMes)$_2$(CuCl)$_3$]** (**7a-c**), by (**A**) *in situ* deprotonation using LiHMDS; or (**B**) preset lithiation of the amine **MesNHPy** and subsequent utilization in the salt metathesis step.

Similar to **5a-c**, compounds**7a-c** have been characterized by elemental analysis, ^{1}H, ^{13}C and ^{29}Si NMR spectroscopy, mass spectrometry and single crystal XRD analysis. The most prominent characteristic of the resulting structures is the triangular copper(I) core moiety, which is accompanied by two newly functionalized benzamidinato silylenes. The dimeric structure was initially elucidated by solid state structure analysis (see Figure 7) and confirmed the intentional binding motif of the functionalized **NHSiMes** silylene. The five-membered metallacycle ("Si–N–C–N–Cu"), with in each case one copper-atom of the "base" of the triangle is supported by the coordination of the corresponding pyridine group of the newly introduced functional group. Additionally, the silicon(II) atoms of both ligands coordinate a further copper(I) atom (the "tip" of the Cu_3-triangle) in a shared "Si–Cu–Si" fashion, leading to a five-coordinated silicon-atom. The tip of the triangle bears a terminal halide, which points out of the Cu_3-plane, whereas the base-Cu(I) atoms showing two bridging halide atoms in a $Cu_2(\mu\text{-}X)_2$ fashion. As one can see in Figure 7, in the Cu_3-plane the **NHSiMes** ligands form a butterfly-like shape along the triangle.

The reasons for the transformation of the pseudocubane into a trinuclear core can only be conjectured. One possible explanation would be that after the successful introduction of the side-arm, the bidentate coordination initiated the transformation of the cubane. To the best of our knowledge, there are no previous reports on such exact copper-triangles bearing terminal and bridging halide atoms following $[X\text{-}\{Cu\text{-}Cu_2\}(\mu\text{-}X)_2]$. The formation of copper triangles itself however, is not new in organometallic chemistry, yet rarely observed, especially in compounds bearing low-valent group 14 elements.

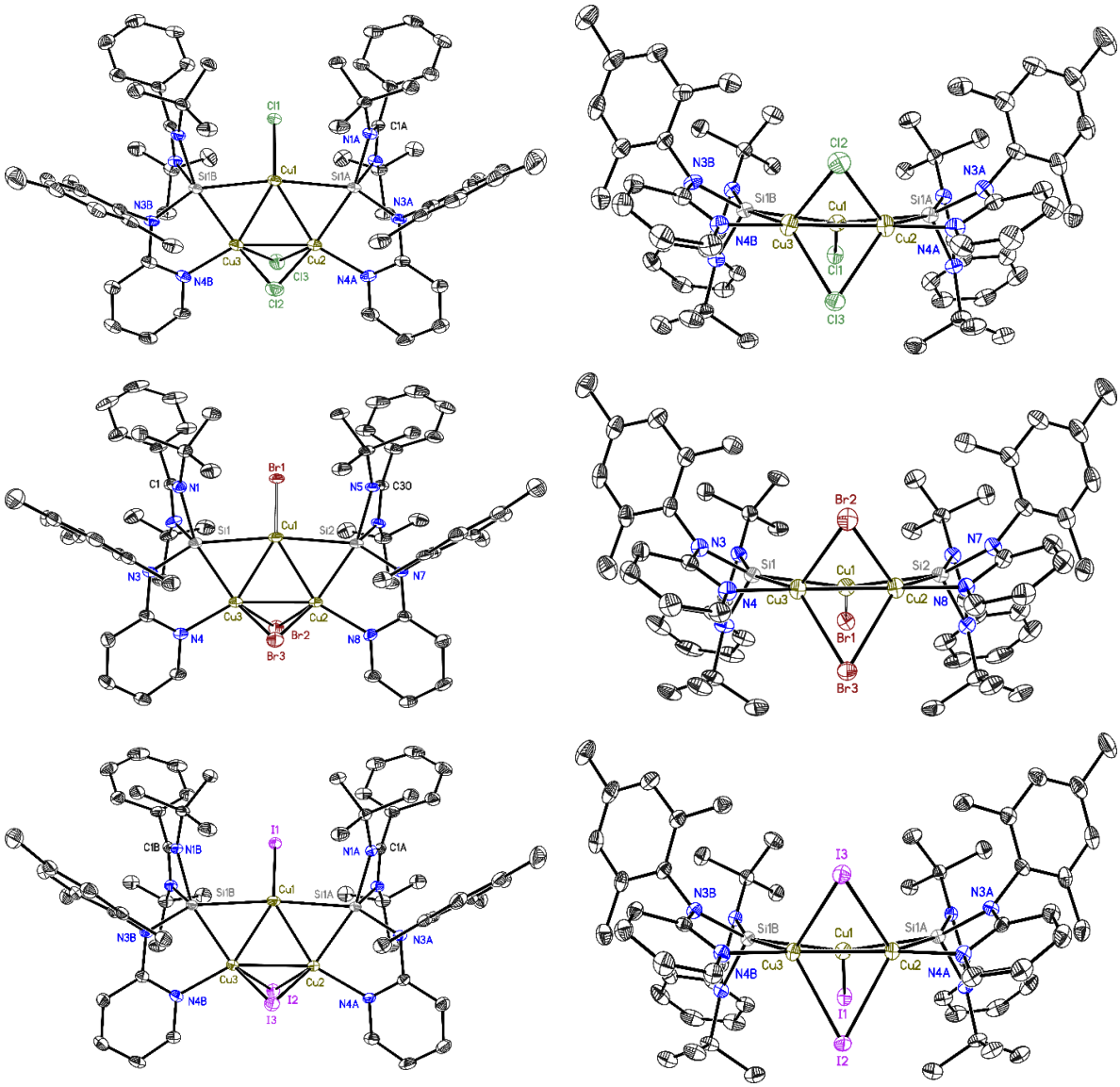

Figure 7. Crystal structures of **7a-c**. All structures crystallize in the space group $P\bar{1}$ in a triclinic crystal system with *a* = 10.376(2) Å, *b* = 18.154(2) Å, *c* = 20.423(3) Å and α = 89.56(2)°, β = 77.14(2)°, γ = 89.75(3)° for **7a**, with *a* = 10.460(2) Å, *b* = 18.205(4) Å, *c* = 20.522(4) Å and α = 88.29(3)°, β = 77.36(2)°, γ = 89.01(3)° for **7b** and with *a* = 10.498(3) Å, *b* = 18.205(2) Å, *c* = 20.437(2) Å and α = 87.32(2)° and β = 77.16(2)°, γ = 88.91(3)° for **7c**. The hydrogen atoms, disorder and solvent molecules has been omitted for clarity. The anisotropic displacement parameters are depicted at the 50% probability level.

Table 4. Selected bond lengths [Å] and angles [°] for complexes **7a-c**.

	7a	**7b**	**7c**
Si–Cu1	2.5427(13)/2.5569(14)	2.5806(14)/2.5812(14)	2.5985(8)/2.6063(8)
Si–Cu2/3	2.2564(14)/2.2647(15)	2.2678(15)/2.2689(15)	2.2819(11)/2.2838(11)
Cu1–Cu2/3	2.4305(10)/2.4399(10)	2.4289(11)/2.4323(11)	2.4227(9)/2.4333(9)
Cu2–Cu3	2.5078(7)	2.5350(9)	2.5458(5)
N4–Cu2/3	1.995(4)/1.998(4)	2.005(4)/2.014(4)	2.009(2)/2.014(2)
N3–Si	1.813(4)/1.828(4)	1.814(4)/1.823(4)	1.815(2)/1.821(2)
Cu–X	2.2240(11)	2.307(5)	2.550(5)
Cu–(μ-X)	2.3699(13)-2.4333(13)	2.5043(10)-2.5308(9)	2.6629(6)-2.6698(8)
Cu2–Cu1–Cu3	61.98(2)	62.86(3)	63.24(2)
Cu1–Cu2/3–Cu3/2	58.82(3)/ 59.19(3)	58.50(3)/58.63(3)	58.18(3)/58.59(3)
Cu1–Si–Cu2/3	60.41(4)/60.53(4)	59.71(4)/59.78(4)	59.08(3)/59.26(3)
Si–Cu2/3–N4	85.82(12)/85.94(12)	85.39(11)/85.59(12)	84.83(7)/84.92(7)
Cu–(μ-X)–Cu	62.64(3)/63.31(3)	60.25(2)/60.69(2)	56.986(16)/57.039(12)

In the late 1970s *Kubiak* and *Eisenberg* coined the term of "*A-frame complexes*" by investigating binuclear rhodium(I) complexes bearing two bidentate phosphine ligands (PCP) that forced the metal atoms in close proximity to each other.[149] This specific conformation led to further studies of various groups in the following years *inter alia* our own (see Scheme 62, left).[150,151] Such PCP and NCN ligands were also utilized to synthesize non-A-frame copper(I) complexes and investigate possible d^{10}-d^{10} interactions between the metal atoms (see Scheme 62, middle).[152,153] As briefly described in Chapter 1.5, so count cuprophilic interactions to the class of metallophilicities. These even weaker interactions usually occur at Cu(I)–Cu(I) distances from roughly 2.4 to 3.5 Å.[152,154] In fact, it is assumed that chelating ligands and bridging atoms as shown in Scheme 62 favor the formation of d^{10}-d^{10} interactions.

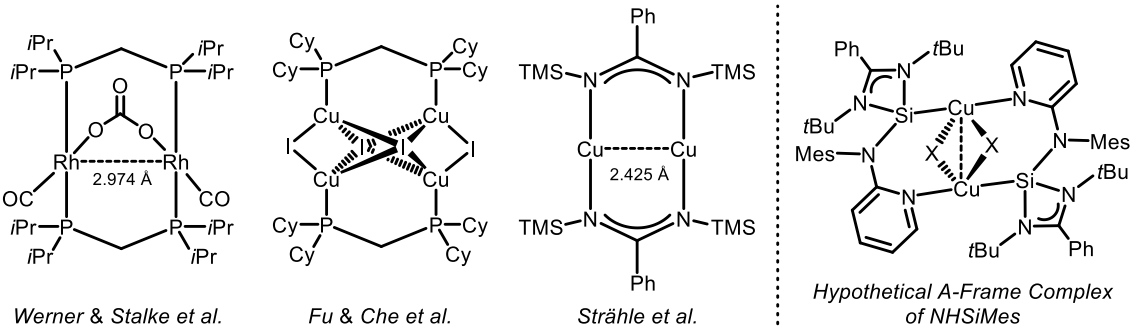

Scheme 62. Examples of A-frame complexes by *Werner* & *Stalke et al*. in 1998[150] (**left**), PCP Cu(I)I complexes by *Fu* & *Che et al.* in 2004[152] and NCN Cu(I) complexes by Strähle et al. in 1998[153] (**middle**). Hypothetical dimeric A-frame complex of NHSiMes (**right**).

Due to the chelate-like structure of the **NHSiMes** silylene the formation of a similar complexation could conceivably have occurred. The side-arm functionality could arrange Cu(I) atoms in a dimeric conformation as seen in Scheme 62 (right), similar to analogues NHC complexes as published by *Danopoulos et al*. in 2001.[155] However, the copper(I) halides of **7a-c** formed the aforementioned triangular core moiety. The tendency of copper(I) to center to clusters is long known and the existence of d^{10}–d^{10} interactions between Cu(I) metal atoms widely investigated and can be presumed here regarding the Cu–Cu bond lengths of **7a-c** (2.4305(10) to 2.5458(5) Å).[92,93,156]

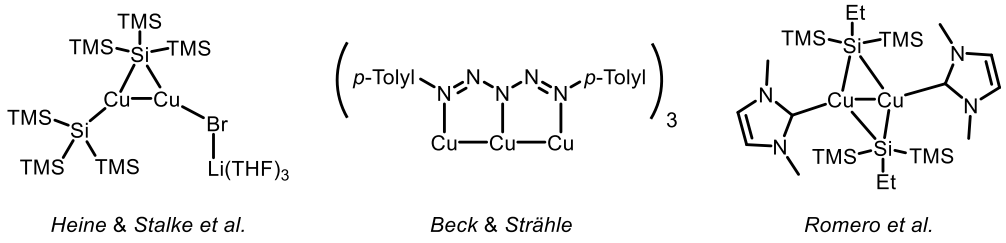

Scheme 63. Examples of silyl-bridged binuclear copper(I) complex by *Heine* & *Stalke et al.* in 1993[157] (**left**) and *Romero et al.* in 2015[158] (**right**); as well as the trinuclear Cu(I) complex by Beck & Strähle in 1985[159] (**middle**).

The fact that the low-valent Si(II) atoms are bridging two Cu(I) atoms could contribute to the formation of the triangle. This bridging behavior by silicon-centered ligands is quite common and can be observed

in various TM complexes, yet, this is one of the rare examples of involving low-valent silicon atoms. In 1993 our group investigated very short Cu(I)–Cu(I) distances (2.369(1) Å) by utilizing μ-bridging $Si(TMS)_3$ groups on multinuclear copper(I) halide complexes (see Scheme 63, left).[157,160] One of the shortest Cu–Cu distances ever reported (2.348(2) Å, which is far shorter than r(Cu–Cu) = 2.56 Å) was already published in 1985 by *Strähle* and *Beck* by enforcing three Cu(I) atoms into a line utilizing 1,5-di(*p*-tolyl)-1,4-pentaazadien-3-ide (see Scheme 63, middle).[159] The asymmetric bonding nature of silyl groups is often observed in $M_2(\mu\text{-}SiR_3)$ moieties and is pursued in **7a-c**. The shorter Si–Cu2/3 bond of **7a-c** (2.2564(14 to 2.2838(11) Å) is in good agreement with the corresponding ones presented by *Heine* & *Stalke et al.* (2.406(2)/2.283(2) Å). The elongated Si–Cu1 bonds (2.5427(13) to 2.6063(8) Å) are rather comparable to bridging silyl-groups, as in dimeric NHC copper(I) complexes published by *Romero et al*. or *Kleeberg et al*. (2.385 to 2.618 Å; see Scheme 63, right).[158,161]

Apparently, the design of this novel NHSi leads to a hybrid structure of the previously described ones. Each ligand taken for itself coordinates two Cu(I) atoms which corresponds to a bidentate fashion as in chelating ligands or A-frame complexes. Yet, the tendency of silicon to bridge M–M bonds seems to further support the formation of the Cu1–Cu2/3 and hence the d^{10}-d^{10} interactions. This in combination with the propensity of copper(I) to form clusters and the bridging halide atoms along Cu2–Cu3 could be reasons for the special architecture of this novel complex.

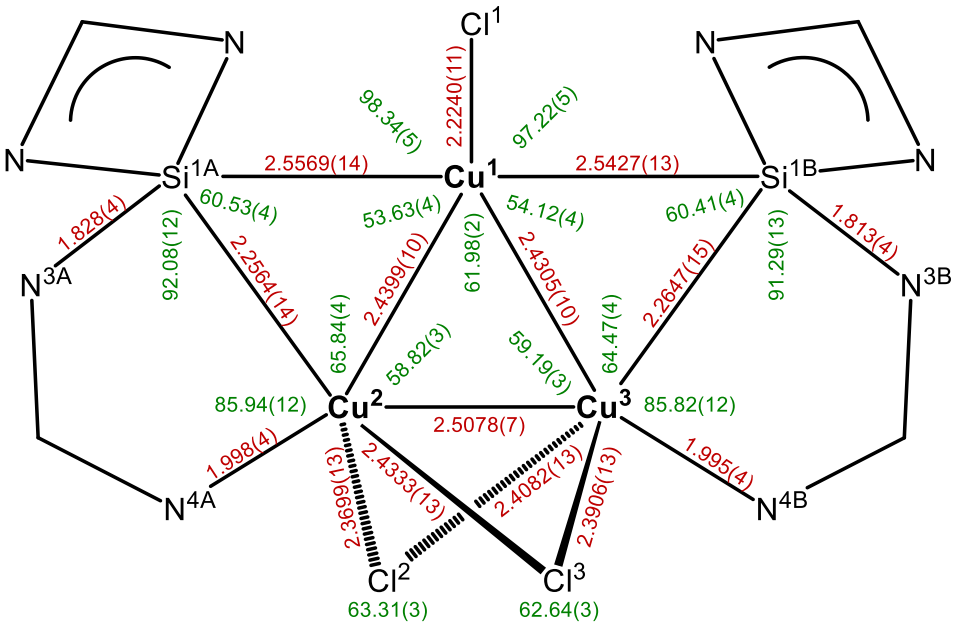

Scheme 64. Illustration of the bonding situation by visualizing the bond lengths (red, in [Å]) and angles (green, in [°]) of the trinuclear complexes **[(NHSiMes)$_2$(CuX)$_3$]** (**7a-c**), by the example of **7a** (X = Cl).

Comparable trinuclear copper clusters were recently published by *Lu et al.* and *Chen et al.* featuring functionalized NHCs similarly employing pyridyl- and triazolyl-groups as additional donor-sites (see Scheme 65).[162,163] In all cases the copper triangles are entirely enclosed by the NHC ligands in a ratio

of 1:1 (ligand *vs*. copper atom) and complexated by the low-valent carbene carbon atoms and pyridine or triazole nitrogen atoms. It is to emphasize that the carbene atoms present a similar binding situation by coordinating two copper atoms at a time, but showing nearly equal bond lengths to both metal atoms, whereas the Si–Cu1 bond lengths of **7a-c** are significantly longer in comparison to the Si–Cu2/Cu3 bond lengths (e.g. **7a**, 2.543(2)/2.557(2) Å *vs*. 2.256(2)/2.265(2) Å).

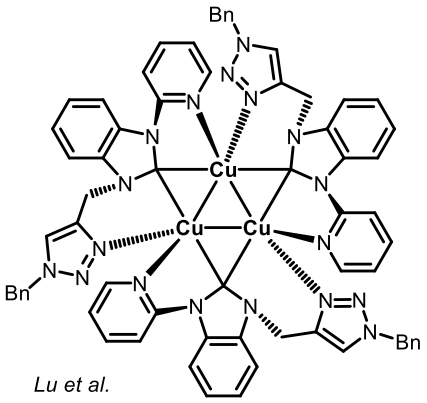

Scheme 65. Illustration of exemplary compounds: triangular copper(I) pyridyl-functionalized NHC complex by *Lu et al.* (2016[162]).

Due to the C3 like symmetry of, e.g., *Lu*'s reported complex (see Scheme 65), the triangles are nearly isosceles (e.g., 60±0.25°, 2.490±0.007 Å).[162] The isolated complexes **7a-c** however, exhibit a C2 like symmetry, which results in a slightly distorted triangle. With shortened distances to the tip (e.g. **7a**, Cu2/3–Cu1, 2.431(10)–2.440(10) Å) and an elongated distance of the base (e.g. **7a**, Cu2–Cu3, 2.508(7) Å) which also results in diverging angles (e.g. **7a**, 62.0(2)° (tip), 59.2(3)°/58.8(3)° (base)).

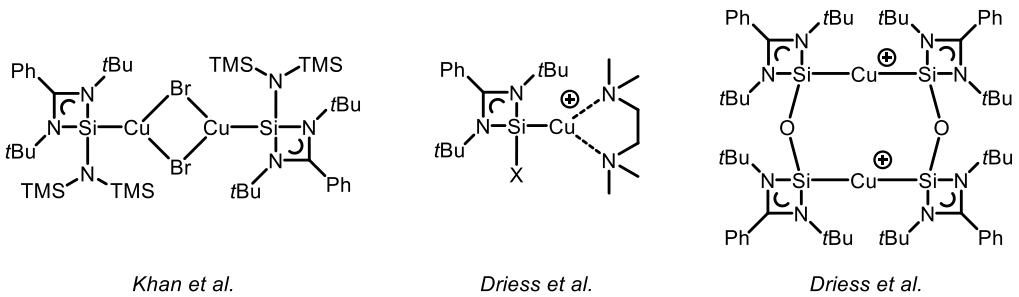

Scheme 66. Illustration of recent copper(I) complexes by *Khan et al.* (2015[120]) and *Driess et al.* (with X = NMe_2, O*t*Bu; 2014[127]).

In the field of NHSi transition metal complexes, there are certain complexes, which are closely related to this structure, by means of the utilization of the benzamidinato silylene and the coordination to copper(I) metal centers (see Scheme 66). The structures by *Khan et al.*[132,133] and *Driess et al*.[127] display a narrow range of Si–Cu bond lengths (2.199–2.231 Å) and N^{Subst}–Si bond lengths (1.710–1.737 Å) for that the shorter Si–Cu2/3 bond of complexes **7a-c** show to be marginally elongated (2.257–2.283 Å), which could be attributed to the formation of the copper-cluster. The newly formed Si–N^{Subst} bond,

originating from the functionalization step, is noticeable elongated in the case of **7a-c** (1.812–1.828 Å), probably due to the same effect.

The trinuclear copper(I) complexes **7a-c** were also identified by LIFDI mass spectrometry by assigning the ion peaks to the corresponding cationic moieties of $[M\text{-}X]^+$ (X = Cl, Br, I) with m/z = 1117.2 (**7a**), 1291.2 (**7b**) and 1385.3 (**7c**), respectively. The NMR spectroscopic analyses of **7a-c** show the expected additional aromatic signals of the pyridyl- and mesityl-groups. Even though the absolute structures known from XRD analyses illustrate a butterfly-like shape, the NMR spectra show one set of signals only, which can be fulfilled only when the nuclei of both **NHSiMes** ligands are chemically equivalent to each other, thus indicating that the complexes **7a-c** must be flattened under the NMR timescale in solution. The usually sharp multiplets seen in ^{1}H NMR spectra of pyridyl-groups, as well as the commonly sharp singlet derived by the *tert*-butyl groups, are frequently seriously broadened, supporting the assumption of a fluctuating structure in solution (see Figure 8, top & bottom). Furthermore, the ^{1}H NMR spectra exhibit noticeable upfield shifted pyridyl-signals due to the functionalization and metal coordination (e.g. 8.09 → 8.72 ppm or 6.26 → 6.80 ppm) (see Figure 8, top & bottom). The respective ^{13}C NMR spectra of **7a-c** exhibit one set of corresponding signals that are consistent with their ^{1}H NMR resonances.

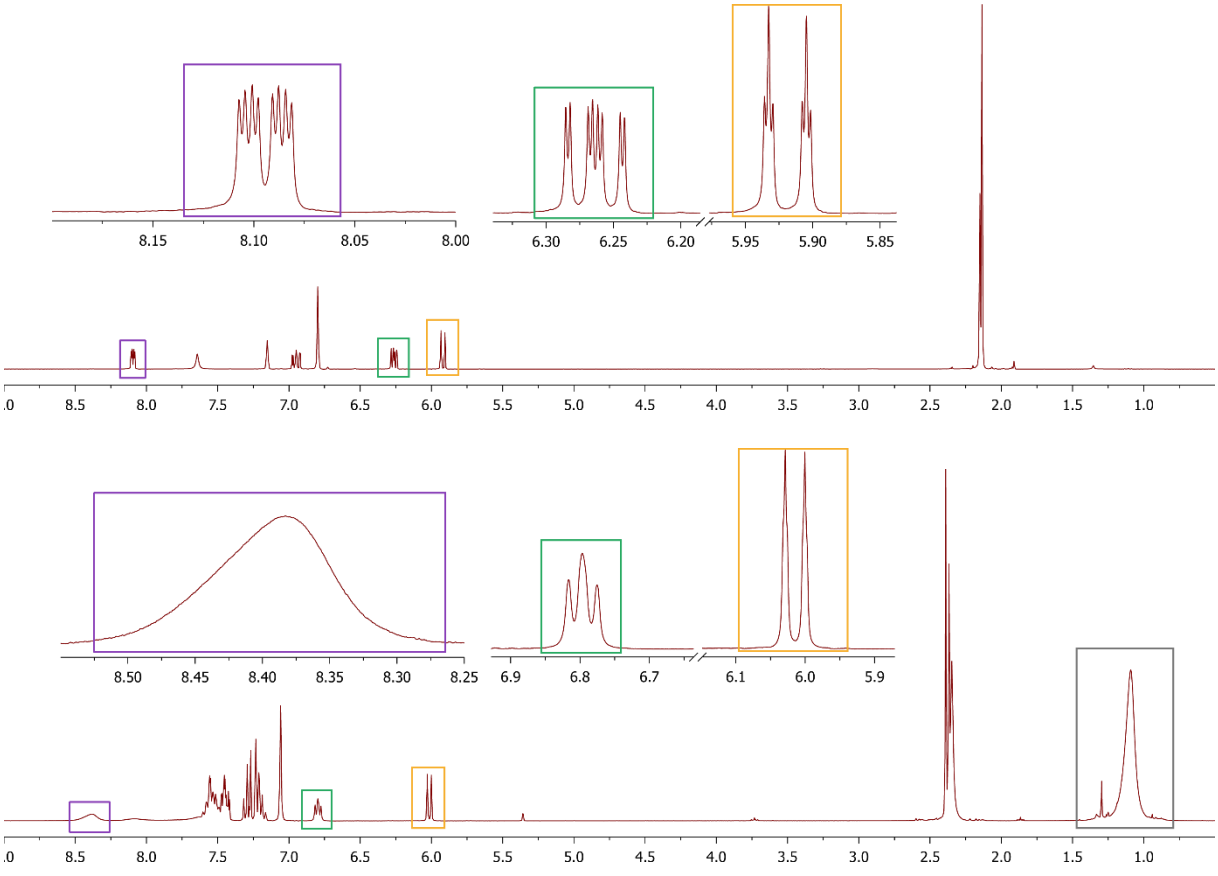

Figure 8. Comparison of the ^{1}H NMR spectrum of complex **7a** (**bottom**) and amine MesNHPy (**top**); chemical shift δ in [ppm]. The framed display details show examples of the signals derived by the pyridyl group (**purple**, **green** & **orange**) affected by the metal complexation, as well as the novel *tert*-butyl groups (**grey**).

However, the detection of ^{29}Si NMR signals remained unfortunately unattained, regardless of the chosen experimental setup (e.g. increased concentration/exposition times). The complexes **5a-c** showed already broadened signals possibly caused by relaxation effects of the metal coordination. But broadened signals are often accompanied by fluctuating effects of compounds in solution as well. In addition to the above mentioned formation of the butterfly-like composition, it is possible that the N^{Py}–Cu coordination opens up along with the transformation of the bridging halide to a terminal one. Conceiving this scenario as a dynamic ligation and dissociation in solution, the ^{29}Si signal could be heavily broadened. Therefore, it is assumed that the combination of the already low natural abundance of ^{29}Si and the aforementioned broadening effects make it nearly impossible to detect proper signals. Nevertheless, the remaining analyses confirm the existence of the silicon atoms. As already mentioned in the evaluation of complexes **5a-c**, low-temperature NMR measurements could decrease fluctuating effects, hence increasing the probability of signal detection.

The previously mentioned simultaneously published structure by *Li* and *Sun* ("**NHSiMe**", according to the syntax of this work) exhibited a ^{29}Si NMR signal of 12.0 ppm of the free ligand and 48.7/59.6 ppm of the corresponding iron complexes.[164] Secondary amine functionalized benzamidinato silylenes commonly exhibit more upfield shifted ^{29}Si NMR signals in the area of -15 ppm, thus being quite unusual. Whereas the shifts of the iron complexes show to be consistent to similar ones.[165] Although the isolation of the free NHSi ligand did not stand in focus of this thesis, it would be worthwhile if future work would concentrate on its synthesis for comparison purposes and to enhance the characterization of the hitherto discussed silylenes, especially since **NHSiMe** showed uncommonly chemical shifts of the ^{29}Si nucleus.

Even though the synthesis of the complexes **5a-c** and **7a-c** showed very good reproducibility and their analyses did not show signs of impurities or side products throughout the syntheses, taking a closer look at the reaction scheme of complexes **7a-c** by means of stoichiometry reveals that the ratio is imbalanced. Throughout optimization and reproduction processes, two additional species were revealed, giving a hint about possible byproducts (see Scheme 67). Intermittently, minor crystal growth was observed in washing, extraction or waste solutions, exhibiting two byproducts in form of yellowish crystals, which were analyzed *via* XRD experiments. Further efforts to reproduce these byproducts nor more detailed analytics did not stand in focus of this work and were not performed due to very low yields, challenging workups or high sensitivity of the products **[(NHSiMes)$_2$(CuBr)]** and **[(NHSiMes)$_2$(CuBr)$_4$]**. Nonetheless, these structures should be listed by means of completeness, especially since they give further insights to the architecture of these Cu(I) halide clusters, which were

previously discussed. These structures illustrate, that it is certainly possible to also hold a single CuBr moiety as in complex **[(NHSiMes)$_2$(CuBr)]** leaving the pyridyl groups uncoordinated. Going further, the tetranuclear complex **[(NHSiMes)$_2$(CuBr)$_4$]** shows an additional CuBr moiety to the complexes **7a-c** resulting in two shared and reflected triangles only bearing μ-bridged bromide atoms. These side products nicely elucidate the formation of different copper(I) halide complexes and the role of the novel **NHSiMes** in it.

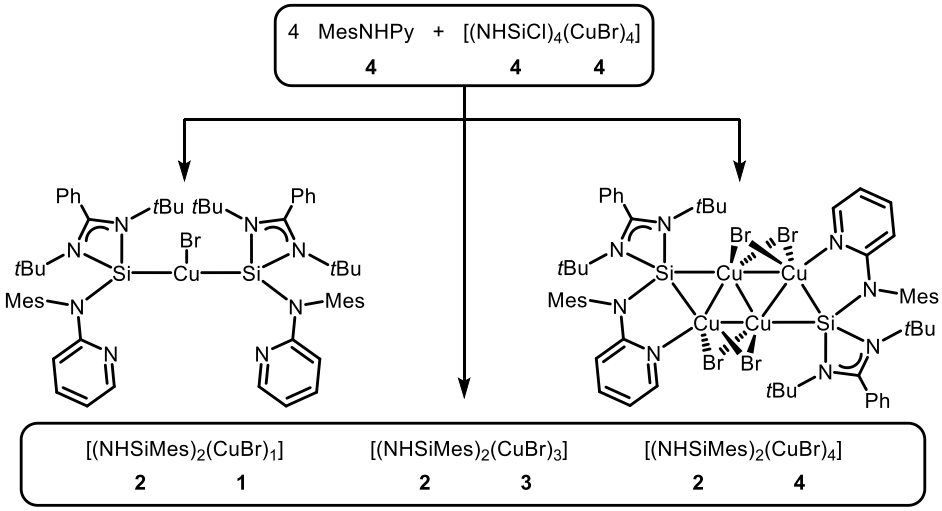

Scheme 67. Overview of the stoichiometry of the functionalization reaction and possible byproducts bis-1,3-*N*,*N*'-di-*tert*-butyl-benzamidinato-*N*-mesityl-*N*-(2-pyridyl)amino-silylene-copper(I)-bromide **[(NHSiMes)$_2$(CuBr)]** and -tetra-copper(I)-bromide **[(NHSiMes)$_2$(CuBr)$_4$]**.

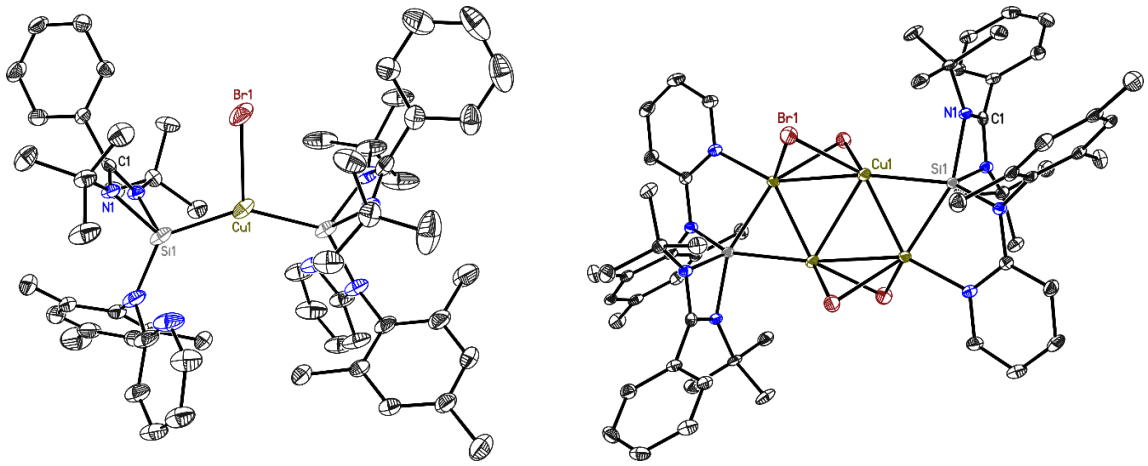

Figure 9. Crystal structures of **[(NHSiMes)$_2$(CuBr)]** and **[(NHSiMes)$_2$(CuBr)$_4$]**. **Left**: The structure crystallizes in the space group $P\bar{1}$ in a triclinic crystal system with a = 11.744(3) Å, b = 15.665(2) Å, c = 18.147(2) Å and α = 100.35(2)°, β = 102.68(3)°, γ = 100.62(2)°. **Right**: The structure crystallizes in the space group $P2_1/n$ in a monoclinic crystal system with a = 12.246(2) Å, b = 14.054(2) Å, c = 19.757(3) Å and β = 97.93(2)°. The hydrogen atoms, disorder and solvent molecules has been omitted for clarity. The anisotropic displacement parameters are depicted at the 50% probability level.

3.2.1.3. Reactivity of NHSiCl towards Organo Copper(I) Salts – $[(NHSiPh)_2(CuCl)_3]$

During the development of the new concept of the post-complex functionalization the idea grew to investigate a further method, implementing the utilization of transition metal precursors. These precursors should consist of the functional group already holding the desired transition metal atom that should be implemented in any case and check its behavior towards **NHSiCl** (**1**). This way, the alternative method of functionalizing the chloro benzamidinato silylene **1** would be enhanced to a new level, to possibly gain better control over the complexation, due to the absence of halide atoms and pre-coordinated transition metal atoms (see Scheme 68).

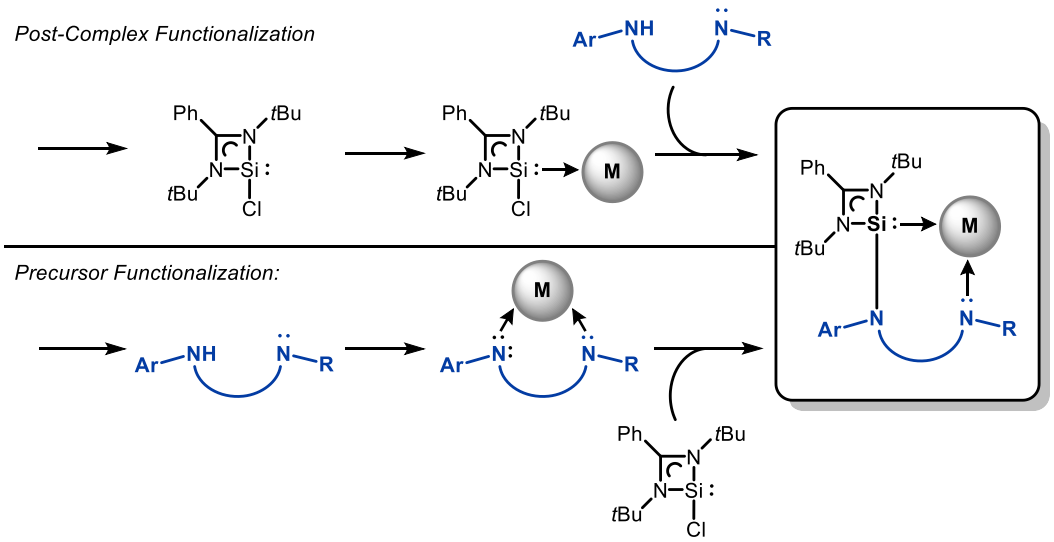

Scheme 68. Schematic illustration of changing the *Post-Complex Functionalization* to pre-coordinated transition metal atoms by the functional donor group ("*Precursor Functionalization*").

Following the concept of group 14 TM NHSi complexes, a copper(I) precursor employing the same "ArNHPy" motif should be designed, to possibly achieve another copper cluster or even a monomeric complex when adding the **NHSiCl** (**1**).

As described in the previous chapters, the salt metathesis or elimination reaction commonly works with alkali metal amides, phosphides or alkoxides, whereas the alkali metal halide salt precipitates and is removed from the reaction. Replacing the alkali metal with a transition metal, e.g. copper(I), results in an organic salt, whose application are widely spread in many fields of chemistry. However, in the case of most TM salts, the elimination of alkali metal halides will be omitted, since the TM atom will be rather coordinated by the NHSi, than precipitate in form of a halide salt. Actually, it would be most-likely that the negatively charged nitrogen atom will substitute the chloro group which will undergo a shift to the transition metal atom. In fact, such behavior was observed when the group of *P. W. Roesky* investigated the first zinc(II) silylene complexes bearing the NHSi **1** in 2014. They anticipated the coordination of the chloro benzamidinato ligand **1** at a dialkyl zinc precursor to undergo a shift of the negatively charged alkyl group with the chloro group, as shown in Scheme 69.[166] Although they did

not further investigate this observation by means of exploiting this behavior for alternative ways of functionalization, this examples illustrates the possibility of doing so.

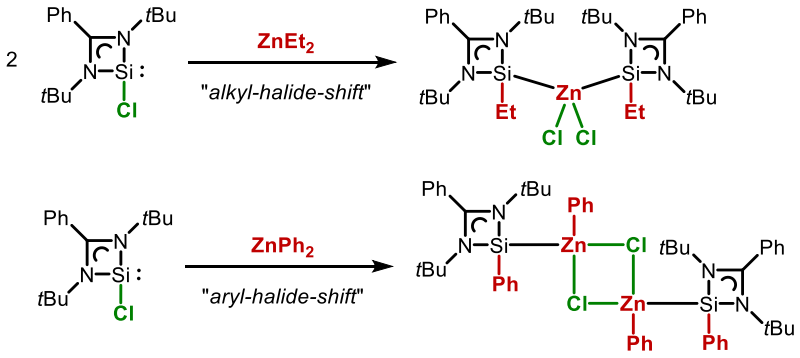

Scheme 69. Formation of the first zinc NHSi complexes by undergoing halide-alkyl-/aryl-shifts between the low-valent silicon(II) atom and zinc atom by *P. W. Roesky et al.*, 2014[166].

In 2002, *Seco* and *González Garmendia*, *inter alia*, primarily investigated the synthesis and characterization of certain copper(II) acetate salts, but also came along the synthesis of 2-anilinopyridinate copper(I) salts (see Scheme 70).[167] Due to the vanishingly low solubility, the characterization kept limited. Through the absence of a N–H stretching band in IR spectroscopic analyses, they supposed to verify the presence of the deprotonated anionic PhNPy-species. Additionally, their elemental analysis fit to the calculated values. Nevertheless, further applications could not be performed, due to the already mentioned low solubility. Throughout their investigations, they stated the assumption that the composition of the compound has to be kind of a dimeric one, whereas a polymeric structure could explain the low solubility. Indeed, this structure reminds of the previously discussed linear trinuclear Cu(I) complex by *Beck* & *Strähle* which showed one of the shortest Cu(I)–Cu(I) distances known utilizing pentaazadienides.[159]

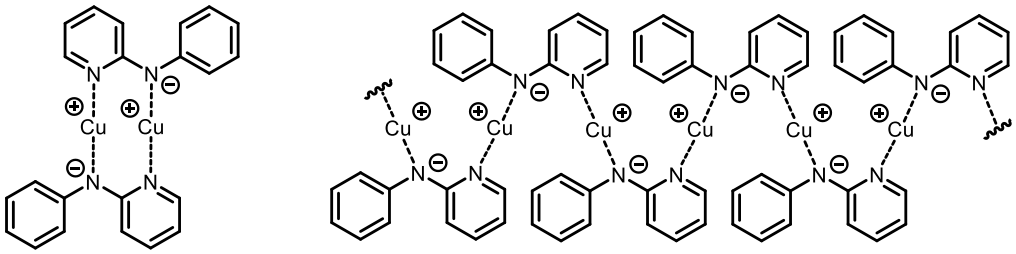

Scheme 70. Possible compositions of *N*-Phenyl-*N*-(2-pyridyl)amine-copper(I) ([(PhNPy)Cu]$_x$), by *Seco* and *González Garmendia*.[167] **Left**: chain-like structure; **right**: dimeric structure.

Following their previous results, the synthesis to *N*-Phenyl-*N*-(2-pyridyl)amine-copper(I) was slightly modified. First, **PhNHPy** was synthesized and characterized analogously to the amine **MesNHPy**, described in Chapter 3.2.1.2 (see Scheme 71).

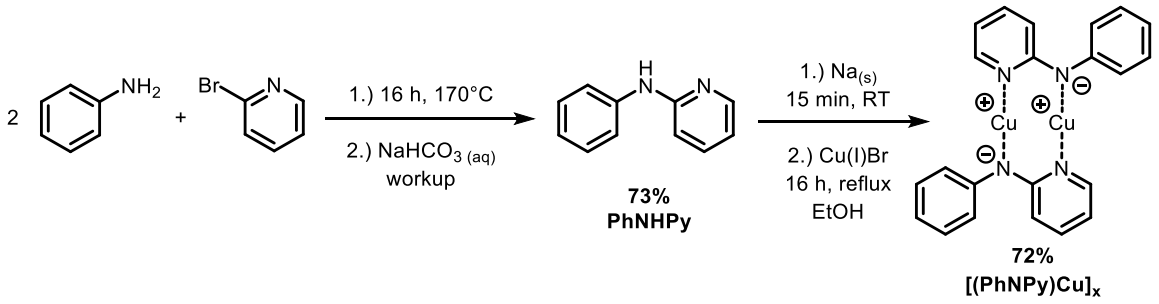

Scheme 71. Synthesis of *N*-phenyl-*N*-(2-pyridyl)amine (**PhNHPy**) *via* S_NAr reaction; followed by the synthesis of *N*-phenyl-*N*-(2-pyridyl)amine-copper(I) (**[(PhNPy)Cu]$_x$**) (yields after purification).

Under inert conditions, neat sodium was added in portions to a stirring solution of the amine **PhNHPy** in dry and degassed ethanol. Afterwards, a separately prepared solution of previously dried Cu(I)Br in ethanol was transferred to the reaction mixture and subsequently heated to reflux overnight, whereby the raw product precipitated as a very fine and bright yellow solid, as also described by *Seco* and *González Garmendia*. The powder was filtered off, washed with additional ethanol and dried under reduced pressure. Besides the characteristic color and consistency of the compound, it was analyzed *via* elemental analysis. Thereby, it emerged that the gross formula $(C_{11}H_9N_2)_4Cu_5Br$ fitted best.

Under the assumption that the ratio of PhNPy ligand to Cu atom lies at 1:1, one equivalent of **[(PhNPy)Cu)]$_x$** was added to a solution of one equivalent **1** in THF at ambient temperatures under an inert atmosphere. After 16 h the bright yellow suspension turned into a darker yellow solution that was slightly concentrated and stored for one day at -35°C to gain the target compound as yellow crystals which were filtered and dried under reduced pressure.

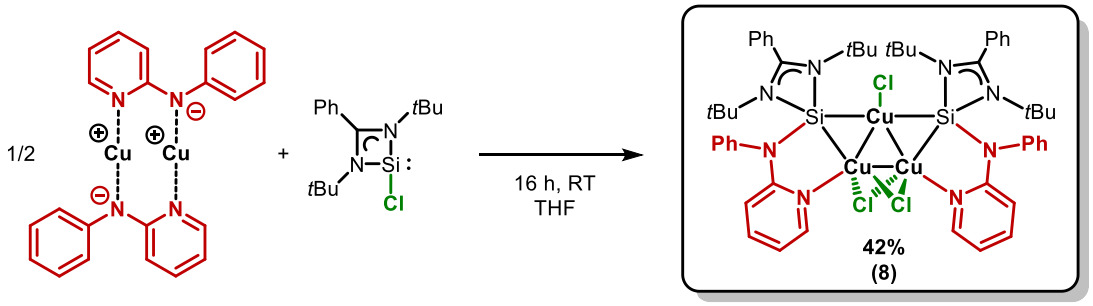

Scheme 72. Synthesis of bis-1,3-*N*,*N*'-di-*tert*-butyl-benzamidinato-*N*-phenyl-*N*-(2-pyridyl)amino-silylene-tris-copper(I)-chloride (**[(NHSiPh)$_2$(CuCl)$_3$]**, **8**) by undergoing an *amido-halide-shift*.

Remarkably, the *precursor functionalization* resulted in the exact same structure motif, as isolated and described in Chapter 3.2.1.2. The familiar trinuclear copper(I) silylene complex **8** was analyzed *via* ^1H and ^{13}C NMR spectroscopy, mass spectrometry, elemental analysis and X-ray diffraction analysis. The very fine and thin bright yellow crystalline plates melted above temperatures of approximately -10°C, which made the crystal application quite challenging. Fortunately, with the help of the cooling device *XTemp2* (see Chapter 5.4 for further details) the crystals kept stable during the application process. As

shown in Figure 10, the structure shows the exact same composition as **7a-c**, yet, looking along the Cu_3-plane the butterfly-like shape is less bend, most likely due to the sterically less demanding phenyl groups. The NMR spectroscopic analyses analogously showed a single set of signals with corresponding slightly broadened pyridyl-multiplets, yet, as already observed at complexes **7a-c**, a ^{29}Si signal could not be detected. LIFDI mass spectrometric analysis however identified the analogous complex at m/z = 1117.2.

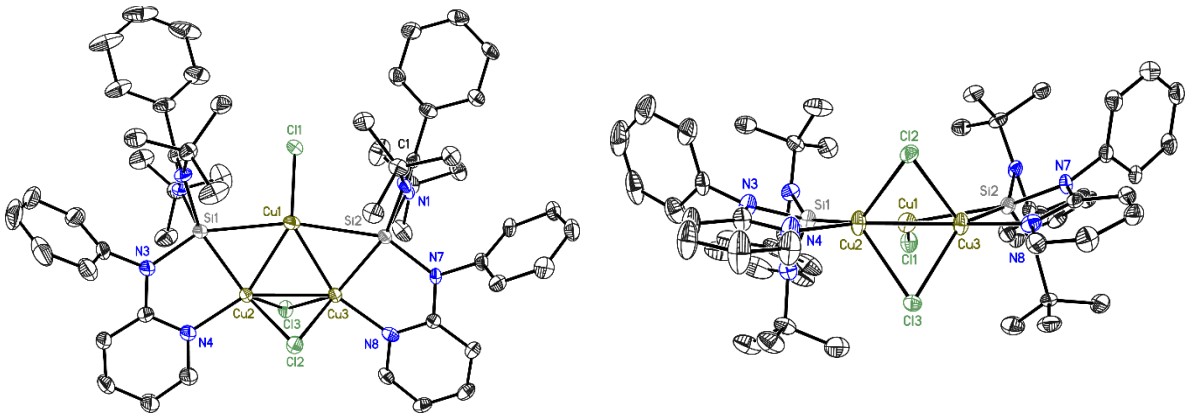

Figure 10. Crystal structure of **8**. The structure crystallizes in the space group $P2_12_12$ in an orthorhombic crystal system with a = 22.528(4) Å, b = 15.472(3) Å, c = 21.062(4) Å. The hydrogen atoms, disorder and solvent molecules has been omitted for clarity. The anisotropic displacement parameters are depicted at the 50% probability level.

Table 5. (**Left**) Selected bond lengths [Å] and angles [°] for complexes **8** and **7a**. (**Right**) Schematically visualization of the distorted triangle of **8** towards **7a** (green arrows = elongation; red arrows = shortening; no arrows = no significant changes).

	8	**7a**
Si–Cu1	2.608(2)/2.678(2)	2.5427(13)/2.5569(14)
Si-Cu2/3	2.223(2)/ 2.243(2)	2.2564(14)/2.2647(15)
Cu1-Cu2/3	2.4185(12)/2.4267(12)	2.4305(10)/2.4399(10)
Cu2-Cu3	2.5488(12)	2.5078(7)
N4-Cu2/3	1.989(6)/1.993(6)	1.995(4)/1.998(4)
N3-Si	1.814(6)/1.823(6)	1.813(4)/1.828(4)
Cu-X	2.1992(19)	2.2240(11)
Cu-(μ-X)	2.3694(19)-2.4404(18)	2.3699(13)-2.4333(13)
Cu2-Cu1-Cu3	63.48(4)	61.98(2)
Cu1-Cu2/3-Cu3/2	58.10(3)/58.42(3)	58.82(3)/ 59.19(3)
Cu1-Si-Cu2/3	58.48(5)/59.23(5)	60.41(4)/60.53(4)
Si-Cu2/3-N4	86.90(17)/87.94(18)	85.82(12)/85.94(12)
Cu-(μ-X)-Cu	63.89(5)/64.13(5)	62.64(3)/63.31(3)

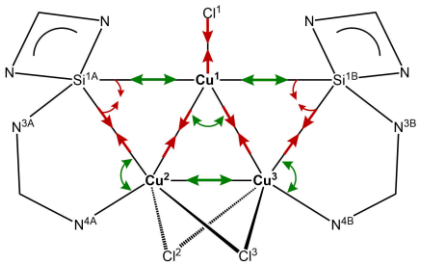

Moreover, the unit cell contains five positions of solvent molecules (THF) surrounding the compound, a rather high amount, compared to other organometallic compounds. Thus, several attempts were made to recrystallize the compound from other solvents in order to hopefully gain a different arrangement of complex and solvent molecules, resulting in a more suitable crystal growth. Unfortunately, all common solvents and methods for crystallization did not lead to crystal growth, not

even if stored for weeks at even lower temperatures, unless, one drop of THF was added, then the thin plate like crystals started to grow, *inter alia*, within seconds to minutes.

Analogously to the synthesis of **7** the stoichiometry of the reaction to **8** is imbalanced as well. Contrary to the investigations described in Chapter 3.2.1.2, there were no signs of possible byproducts while performing this reaction. Yet, the formation of similar compounds is conceivable.

In conclusion, the first successful applications of alternative methods to the synthesis of novel NHSi-TM-complexes were presented. The treatment of chloro benzamidinato silylene **1** with common copper(I) halide precursors led to the formation of the pseudocubane structures **5a-c**, which were functionalized with pyridyl-substituted secondary amines by undergoing *in situ* deprotonation reactions *via* LiHMDS (*post-complex functionalization*). The resulting compounds **7a-c** exhibited a captivating novel trinuclear constitution. In addition, with the hitherto called *precursor functionalization* it was also possible to introduce a further technique to gain NHSi-TM-complexes. Interestingly, the synthesis of compound **8** using the organo copper(I) salt **[(PhNPy)Cu)]$_x$** resulted in the same trinuclear complex, as **7a-c**. The promising alternative method should be studied on further transition metals, in order to comprehensively substantiate these results.

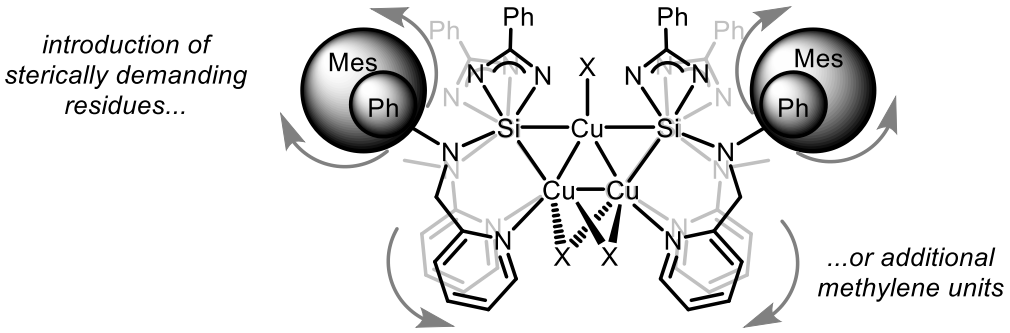

Scheme 73. Schematic illustration of possible scaffold-modifications, e.g. introducing a methylene unit between amino- and pyridyl-group to increase the biting angle or de-/increasing the bulkiness of the residue located at the amino-function.

The bond lengths and angles listed in Table 5 (left) indicate a trend, which illustrates that the phenyl-substituted version **8** of this novel class of compounds, shows an even more distorted triangle (see Table 5, right), thus signifying that the nature of this residue can influence the condition of the complexation. This feature should be intensively investigated in future works, by means of, e.g., increasing the biting angle (by introducing a methylene unit between the amino- and the pyridyl-group) or introducing different sterically demanding residues (see Scheme 73). This would be a perfect way to gain insights of how the ligand design affects the copper triangle. It is conceivable, that the ligand could be modified to a point, where the ligation would even lead to another formation than a

triangular one. This concept could also be transferred on the synthesis of modified organo copper(I) salts, in order to study the potential of this technique and expand the scope of this reaction.

Furthermore, the catalytical reactivity of complexes **5b** and **7b** were investigated by subjecting them to the copper(I)-catalyzed alkyne-azide cycloaddition (CuAAC) in Chapter 3.3ff.

3.2.2. Presentation of NHSi Silver(I) Complexes

To further investigate the potential of NHSi coinage metal complexes, the achievements of applying the *post-complex functionalization* to the synthesis of functionalized NHSi TM complexes should be transferred to the heavier congener, the silver(I) complexes. The current research of silver(I) silylene complexes is even more premature than of its lighter homologue copper, which is why to date, there are only a few examples known.

At the same time to the ascent of the famous *N*-heterocyclic silylenes, the group of *Iwamoto* investigated the synthesis and isolation of so-called dialkylsilylenes, a rather rare subclass of silylenes.[23] In this context, they have also studied the metalation of various transition metals, as well as the first silver(I) complexes in 2014.[168] By employing Ag(I) precursors bearing weakly coordinating anions, they were able to isolate and characterize a linear dimeric silver(I) complex, as shown in Scheme 74.

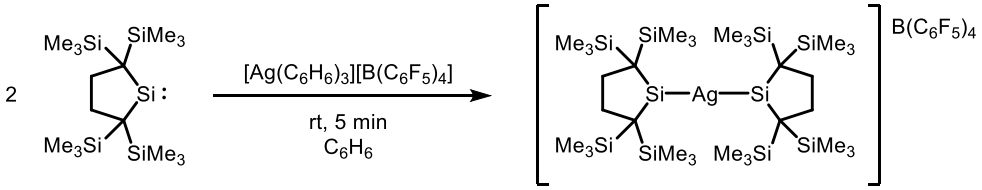

Scheme 74. Synthesis of the dialkylsilylene silver(I) complex by *Iwamoto et al*. in 2014[168].

In the following years, the group of *Khan* joined the investigations of group 11 complexes, which were primarily based on the utilization of the substituted *N*-heterocyclic silylene **NHSiHMDS**. By employing certain Ag(I) precursors bearing various counter anions, they were able to isolate three different constitutions, illustrated in Scheme 75. While the $AgNO_3$ precursor led to the formation of a monomeric species, the Ag(I) salt of triflic acid formed a dinuclear dimeric complex, with bridging counter anions.[120] The similar but rather less weakly coordinating anion SbF_6^- led to the same linear dimeric constitution as described by *Iwamoto et al*.[169]

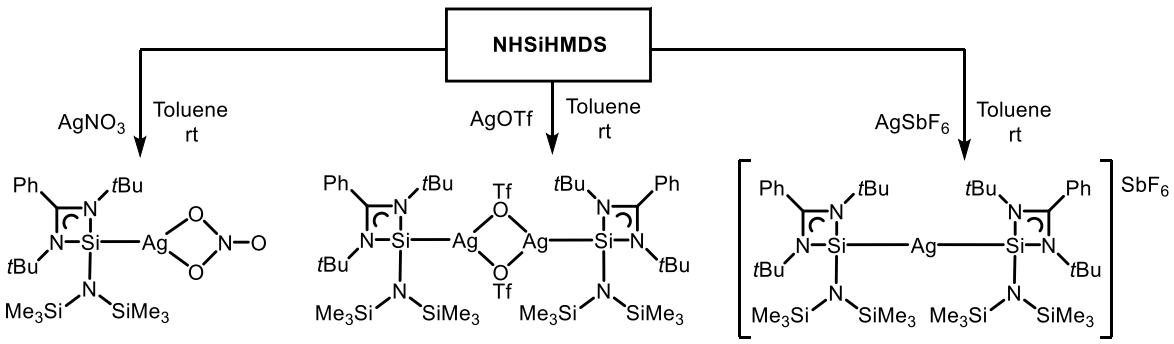

Scheme 75. Overview of the current research in the field of NHSi Ag(I) chemistry (by *Khan et al*., 2015[120]/2017[169]; the style of illustration of the depicted structures only represents the connectivities within the complex).

As these attempts indicate, the first complexes were more of a proof of principle, in order to examine the behavior of silylenes towards late transition metal atoms. Throughout the next chapters, the hitherto presented *post-complex functionalization* to novel silylenes will be investigated by employing silver(I) halides.

3.2.2.1. Synthesis of Cubane NHSiCl Ag(I)Cl Complexes – [(NHSiCl)(AgCl)]$_4$

Inspired by the success of the previously presented copper(I) complexes, the synthesis of the novel silver(I) complexes were analogously performed. Under inert conditions, a solution of the chloro benzamidinato silylene **1** in toluene was transferred to a suspension of carefully grinded silver(I) chloride in toluene at ambient temperature under the exclusion of light and was stirred overnight. The target compound precipitated in form of very fine colorless crystalline needles, which were filtrated and dried under reduced pressure. To remove traces of possible unreacted AgCl the product was redissolved in THF and filtrated again. The resulting reaction mixture was concentrated and stored at -35°C to gain the desired compound in form of colorless crystals. Concomitantly, this step provided a recrystallizing effect, since the former very fine needles grown from toluene, were now isolated as crystalline blocks already suitable for XRD analysis. The toluene- and THF-mother liquors can be again concentrated to gain more of the target compound that was worked up in the same manner, in order to increase the overall yield.

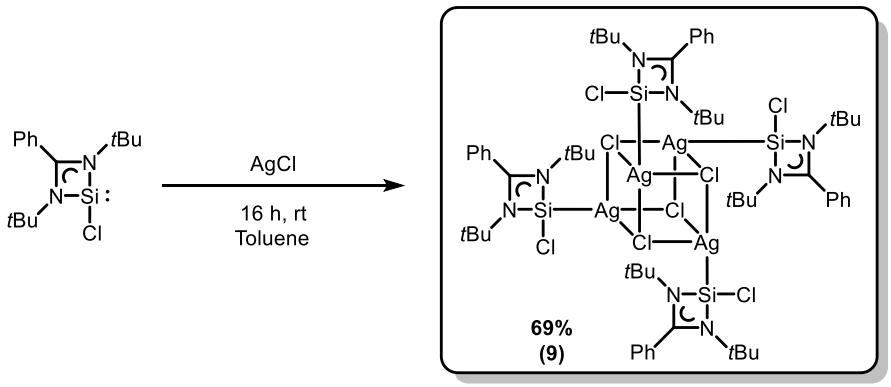

Scheme 76. Synthesis of **9** aka. tetrakis-1,3-*N*,*N*'-di-*tert*-butyl-benzamidinato-chloro-silylene-silver(I)-chloride **[(NHSiCl)(AgCl)]$_4$**.

Compound **9** was isolated and characterized *via* multinuclear NMR spectroscopy, elemental analysis and X-ray diffraction analysis. The reaction of **1** with an equimolar amount of AgCl led to the tetrameric complex [Ag$_4$(μ_3-Cl)$_4$], which alternating cubic-like structure is already known from its copper-predecessors **5a-c** described in Chapter 3.2.1.1. As already stated in that chapter, the formation of such pseudocubane-type M$_4$(μ_3-Cl)$_4$ moieties is rather common for [MX]$_4$L$_n$ complexes featuring M = Cu, Ag; X = Cl, Br, I; and L = neutral donor ligands.[129,130] Although, this structure is the first known

silver complex of that type employing *N*-heterocyclic silylenes as neutral donor ligands, the group of *Polo* published a similar compound utilizing the heavier homologues, also known as germylenes, in 2015 (see Scheme 77, right; and Table 6).[134] The $[AgCl]_4$ cubane of **9** is significantly less distorted than their copper counterparts **7a-c** and shows averaged angles of 90±5° in all planes and a narrower range of Ag–Cl-bonds of approximately ΔAg–Cl = 0.191 Å compared to ΔCu–Cl = 0.475 Å. The Si–Ag bond lengths are similar to the ones reported by *Khan et al.* in 2015,[120] which investigated the first NHSi silver complex $[(NHSiHMDS)(AgOTf)]_2$ (see Table 6), whereas the mononuclear complex $[(NHSiHMDS)_2(Ag)]SbF_6$ from 2017 exhibited a prolonged bond length of 2.4246 Å.[169]

Table 6. Selected bond lengths [Å] and angles [°] for complexes **9**, **[(NHGe*t*Bu)(AgCl)]$_4$** by *Polo et al*. (2015[134]), **[(NHSiHMDS)(AgOTf)]$_2$** by *Khan et al*. (2015[120]) and **[(NHSiHMDS)$_2$(Ag)]SbF$_6$** by *Khan et al*. (2017[169]).

	9		**[(NHGe*t*Bu)(AgCl)]$_4$**
Si–Ag	2.3363(9)-2.3522(8)	**Ge-Ag**	2.42-2.43
Ag–Cl	2.5060(8)-2.6974(9)	**Ag-Cl**	2.50-2.89
Ag–Cl–Ag	85.02(3)-96.13(3)	**Ag–Cl–Ag**	74.1-88.4
Cl–Ag–Cl	87.98(3)-98.32(3)	**Cl–Ag–Cl**	87.6-102.4

	[(NHSiHMDS)$_2$(Ag)]SbF$_6$
Si–Ag	2.4243(13)-2.4249(12)
	[(NHSiHMDS)(AgOTf)]$_2$
Si–Ag	2.337(2)-2.346(2)

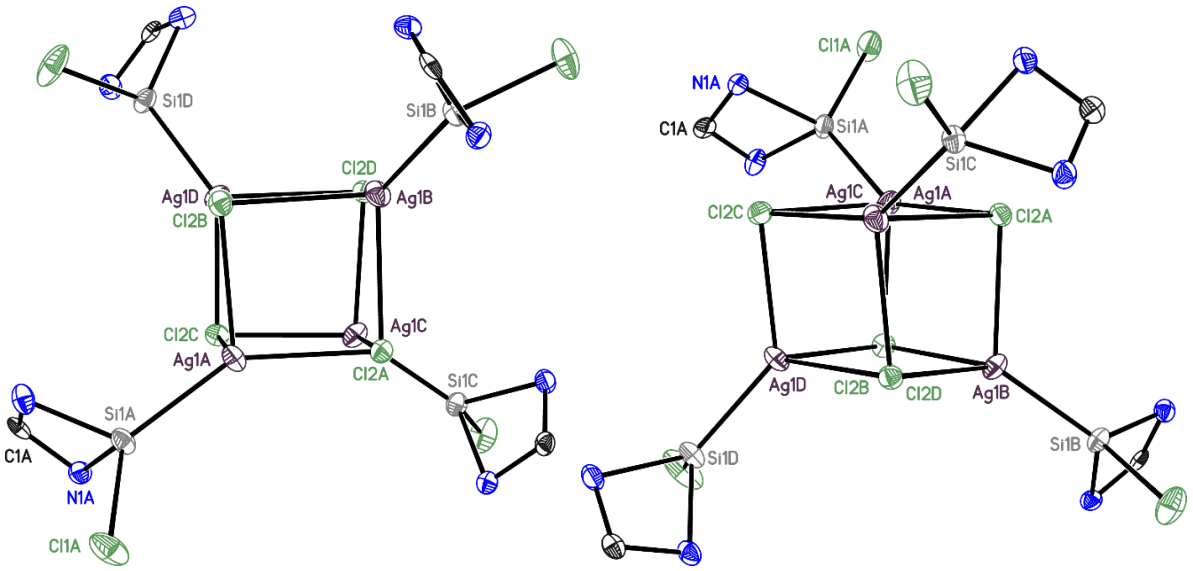

Figure 11. Crystal structures of **9** (**left**: top view; **right**: side view). The complex crystallizes in the space group $P\bar{1}$ in a triclinic crystal system with a = 13.749(2) Å, b = 14.267(2) Å, c = 25.724(3) Å and α = 82.31(3)°, β = 89.88(4)°, γ = 68.44(3)°. The *tert*-butyl-/phenyl-groups, hydrogen atoms, disorder and solvent molecules has been omitted for clarity. The anisotropic displacement parameters are depicted at the 50% probability level.

Unfortunately, mass spectrometric analysis did not show any meaningful signals, presumably due to the decomposition of the product, which turned brown under the slightest exposition of air or moisture.

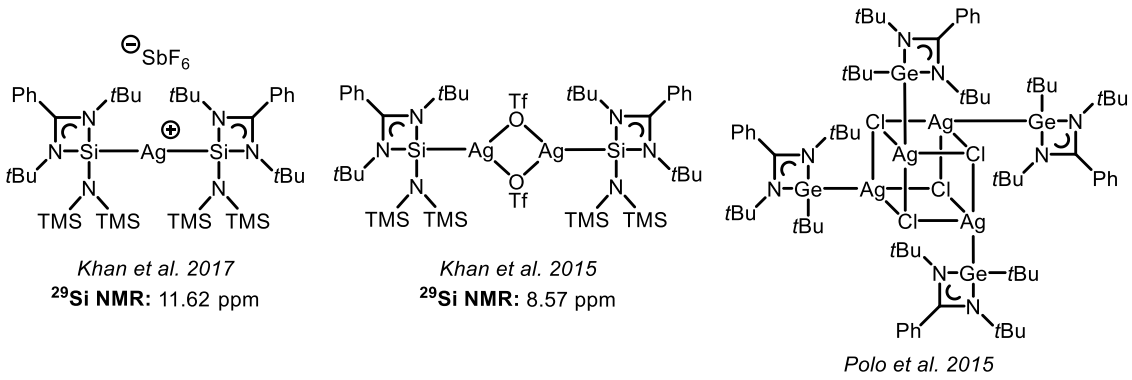

Scheme 77. Overview of similar silver(I) complexes bearing the **NHSiHMDS** investigated by *Khan et al.* (2015[120], 2017[169], **left**) and the analogues tetramer $Ag_4(\mu_3\text{-}Cl)_4$ employing the heavier homologue **NHGe*t*Bu** by *Polo et al*. (2015[134], **right**).

As expected, the ^{1}H NMR spectrum shows a slightly shifted singlet for the *tert*-butyl groups at 1.30 ppm, as well as a multiplet at 7.66-7.54 ppm deriving from the phenyl-groups, which are matching to the corresponding ^{13}C NMR signals. A rather highly concentrated solution of **9** and extended measuring times were necessary to gain a suitable ^{29}Si NMR spectrum that exhibited a solitary singlet at 37.83 ppm, significantly downfield shifted when compared to the free NHSi **1** (14.26 ppm[13]). Interestingly, comparable NHSi Ag(I) complexes showed significantly more upfield shifted ^{29}Si signals, e.g., **[(NHSiHMDS)(AgOTf)]$_2$** at 8.57 ppm and **[(NHSiHMDS)$_2$(Ag)]SbF$_6$** at 11.62 ppm (see Scheme 77). The difference could be explained by the influence of the electron releasing groups located at the low-valent silicon(II) atom. As illustrated in Scheme 78, drawing the comparison to the previously discussed copper complexes, which showed a comparable effect, the ^{29}Si signal of **[(NHSiCl)(CuI)]$_4$** (**5c**) is located at 22.62 ppm whereas the functionalized complex **[(NHSiHMDS)(CuI)]$_2$** by *Khan et al.* showed an upfield shifted signal at 16.85 ppm. The same effect works at complex **9** (37.83 ppm) bearing the chloro group and the amino-substituted complex **[(NHSiHMDS)(AgOTf)]$_2$** (8.57 ppm).

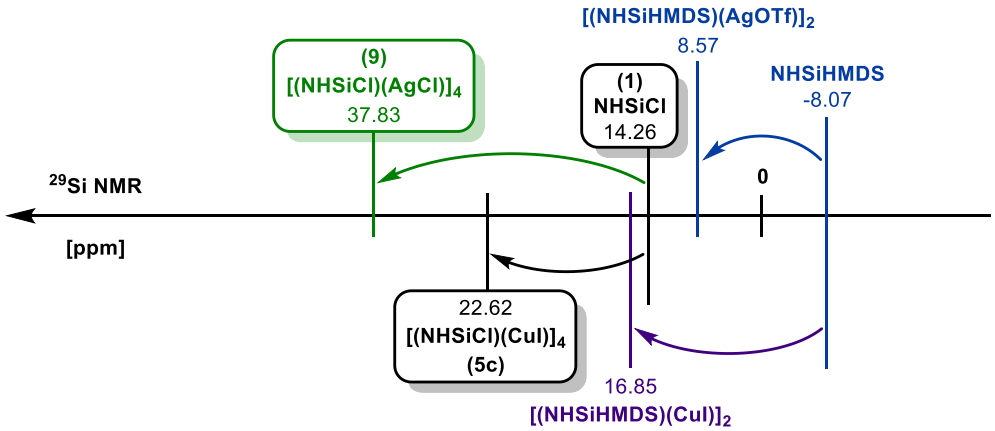

Scheme 78. Schematically illustration of the influence of a donating group adjacent to the Si(II) atom on the position of the chemical shift δ [ppm] of ^{29}Si NMR signals. The free functionalized **NHSiHMDS** towards Ag(I) and Cu(I) complexation (by *Khan et al.*, blue and purple), as well as the unsubstituted free silylene **1** towards Ag(I) and Cu(I) complexation (*this work*, black and green).

3.2.2.2. *Functionalization with Pyridyl-Substituted Amino Groups – [(NHSiMes)(AgCl)]*

In order to investigate the behavior of the novel silver(I) complex **9** towards the subsequent functionalization, the following synthesis was performed analogous to the previous achievements regarding the copper derivatives **7a-c**. The utilized amine **MesNHPy** was prepared in the same manner as described in Chapter 3.2.1.2. A solution of the complex **9** and **MesNHPy** in a mixture of diethyl ether and dichloromethane was cooled to -30°C. Subsequently neat LiHMDS was added in small portions under the exclusion of light and was stirred overnight while allowing to warm up to ambient temperature. The resulting yellow suspension was filtered and all volatiles were removed under reduced pressure. After dissolving the yellowish residue in THF and storing the resulting solution at -35°C, the target compound readily crystallized within hours in form of very thin yellow plates that were filtered and dried *i.vac*.

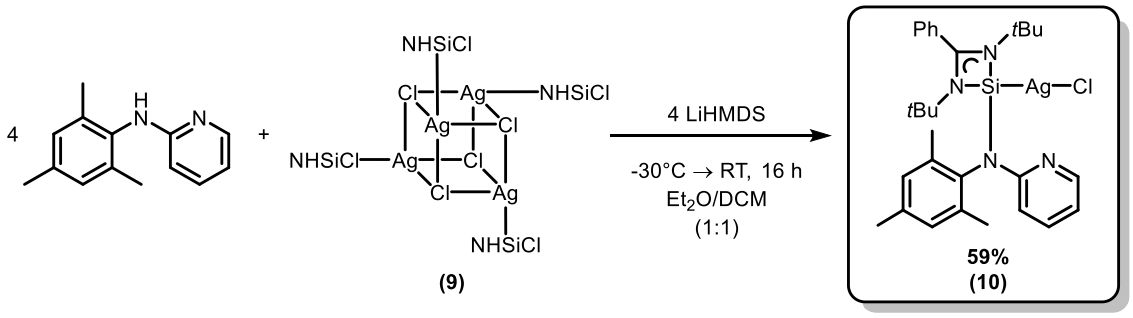

Scheme 79. Synthesis of **10** aka. 1,3-*N*,*N*'-di-*tert*-butyl-benzamidinato-*N*-mesityl-*N*-(2-pyridyl)amino-silylene-silver(I)-chloride **[(NHSiMes)(AgCl)]** *via in situ* deprotonation of the amine **MesNHPy** using LiHMDS.

As shown in Scheme 79, the functionalization of the chloro group was successful and complex **10** was verified *via* NMR spectroscopy, mass spectrometry and CHN analysis. Besides the singlet and multiplet derived by the benzamidinato scaffold, the ^{1}H and ^{13}C NMR spectra additionally exhibit one set of signals belonging to the pyridyl- and mesityl-group of the newly introduced side-arm. The ratio of the ^{1}H NMR integrals suggests a presence of 1:1, benzamidinato to amine. Furthermore, the ^{1}H pyridyl signals are significantly sharper compared to complexes **7a-c**, indicating the absence of a metal coordination (see Figure 12, top & bottom). Obviously, the singlet derived by the *tert*-butyl groups are also less broadened, in comparison to complex **7a-c.** However, similar to the functionalized copper complexes, the detection of ^{29}Si NMR signals also remained unattained, regardless of the chosen experimental setup (e.g. increased concentration/exposition times). Although LIFDI mass spectrometric analysis were not able to detect the molecular ion peak, with m/z = 505.3 it displayed the species $[M\text{-}Ag]^{+}$ and therefore supporting the successful substitution. In addition, the elemental analysis of **10** is also in line with the calculated values, thus indicating the successful synthesis and the presence of the silicon and silver atom.

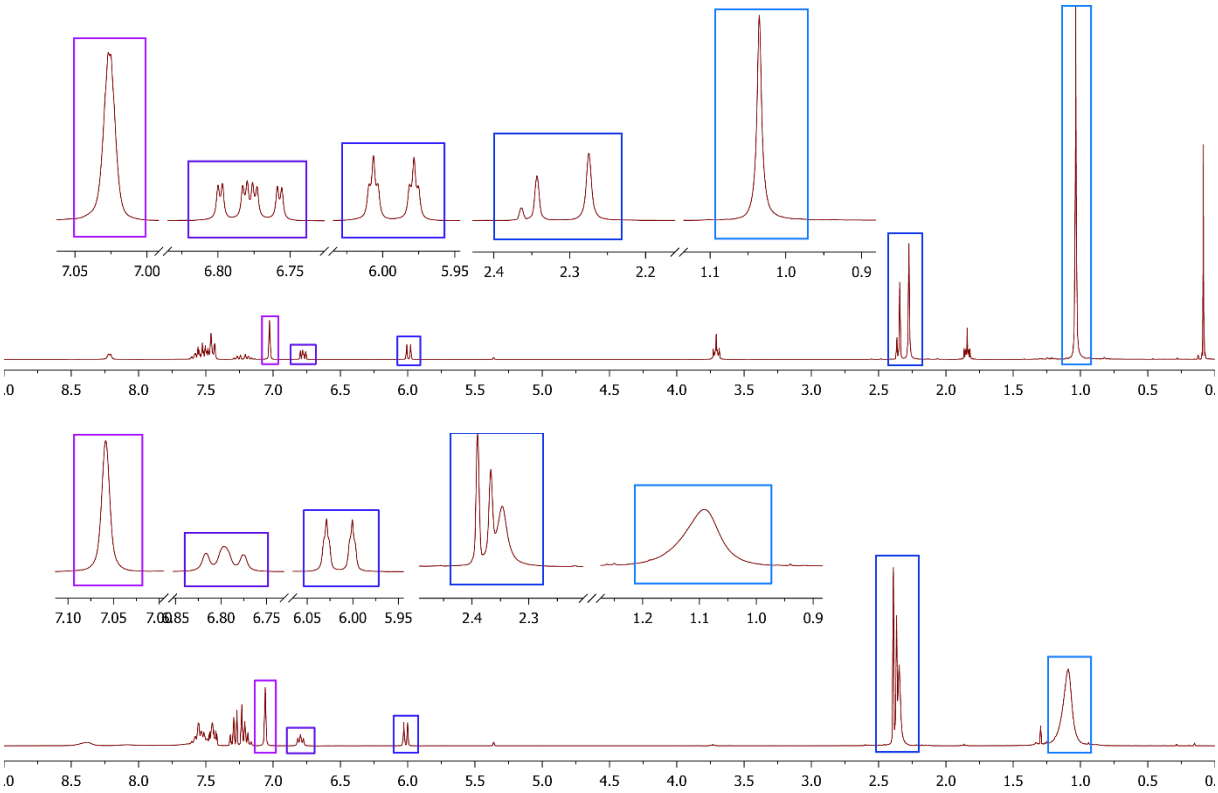

Figure 12. Comparison of the ^{1}H NMR spectrum of complex **7a** (**top**) and complex **10** (**bottom**); chemical shift δ in [ppm]. The framed display details show examples of the signals derived by the pyridyl and mesityl groups (**left**) and the *tert*-butyl and mesityl groups (**right**).

The compound proved to grow only in form of very thin crystals and crystallized only in THF, which made a determination of the absolute structure *via* X-ray diffraction analysis very challenging. Several crystals from different synthetic attempts were mounted but showed to be unsuitable to gain a decent data set.

Nevertheless, it was possible to successfully perform a functionalization of the chloro group, *via* the utilization of LiHMDS, in the presence of a NHSi Ag(I)Cl coordination, leading to a mononuclear composition. Even though the pyridyl-group kept uncoordinated, hence showing no bidentate ligation, this compound offers interesting properties, which should be the subject of future investigation. For example, removing the halide under the utilization of suitable reagents, could lead to the formation of a bidentate complexation, possibly concomitant to an oligomerization to a bigger aggregate.

In regard to the second method to functionalized NHSis presented throughout this thesis, the *precursor functionalization*, it would be very interesting to synthesize certain organo Ag(I) salts as precursors for the *in situ* functionalization of silylene **1**. The readily available and commonly utilized silver(I) oxide proved to show a higher basicity compared to other common sources of Ag(I),[170] which makes it to the reagent of choice for such purposes. The resulting silylene silver(I)-complexes could be subsequently transmetalated with other transition metal atoms, which would be a further interesting project for future work (see Scheme 80, **(A)**).

Preceding work in the area of silver(I) NHC complexes, *inter alia*, emphasized their potential as transmetalating agents.[171] The coordination to Ag(I) preserve the highly air and moisture sensitive free carbenes, featuring less stringent reaction conditions and tolerating a wider range of functionalities.[171,172,173] This can be utilized by treating silver(I) complexes with another metal precursor undergoing a substitution of the metal atom and hence improving the formation of a new stronger NHC–M bond (see Scheme 80, **(B)**).[174] Until now, such behavior did not stand in the focus of any NHSi studies, but could also be beneficial for the synthesis of novel NHSi TM metal complexes. Especially in combination with the here presented *post-complex functionalization*, enhanced new NHSis could be synthesized as silver(I) complexes, followed by a transmetalation reaction (see, **(C)**).

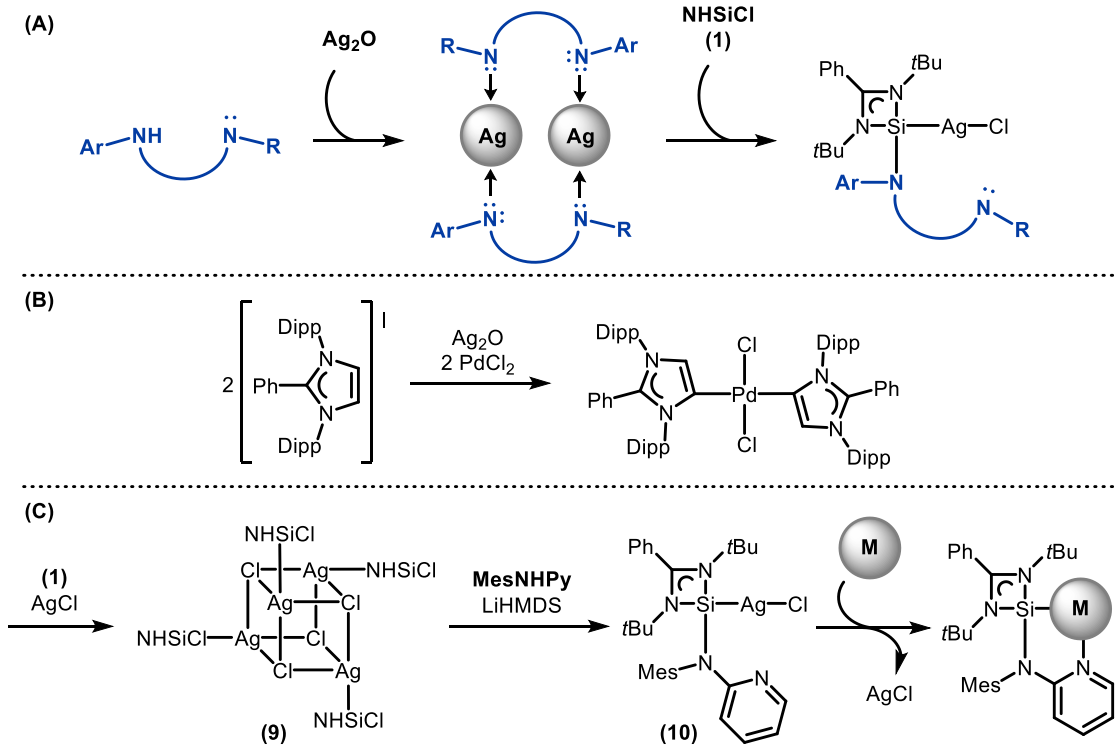

Scheme 80. (A) Possible access to organo Ag(I) salts utilizing Ag_2O for the subsequent *in situ* functionalization of **1**. **(B)** Example of the synthesis of novel aNHC-Pd(II) complexes, by the utilization of Ag_2O as a transmetalating agent by *Ghadwal et al*. **(C)** Possible application of the above-shown concept employing novel NHSi-silver(I) complexes.

3.2.3. Presentation of NHSi Gold(I) Complexes

Concomitant with the hitherto presented investigations on copper(I) and silver(I) complexes, the corresponding gold(I) compounds will be examined as well.

In fact, the first report of a silylene gold(I) complex is dated back to 1990, one year after the seminal publication of the first free silylene stable at room temperature, by the group of *Jutzi* (see Chapter 1.1, Scheme 3).[5] After the isolation of this π-coordinated decamethylsilicocen **SiCp*₂**, they tried to investigate transition metal complexes. Noteworthy, this complex was the first one they were able to isolate, after several attempts with various organometallic fragments. As shown in Scheme 81, the synthesis was performed at cryogenic temperatures, employing the carbonyl precursor (CO)Au(I)Cl. The $SiCp^*_2$ Au(I) complex proved to be highly sensitive towards air, moisture and temperature.[175]

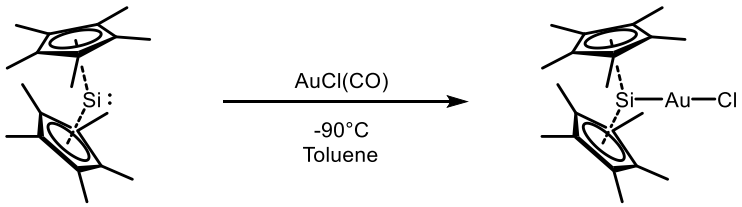

Scheme 81. Synthesis of the first Au(I) complex employing the π-coordinated decamethylsilicocen **SiCp*₂**, by *Jutzi et al*. in 1990[175].

In Chapter 3.1.3, the NHSi Au(I) complexes by *Khan et al.* were already discussed and are also subject of the discussions in the following chapters, due to their structural similarity, especially of the **NHSiNP** ligand. At the same time as these complexes were investigated, the group around *Kato* published the rather uncommon silacyclopropylidene ligand and thus certain TM complexes (see Scheme 82).[50]

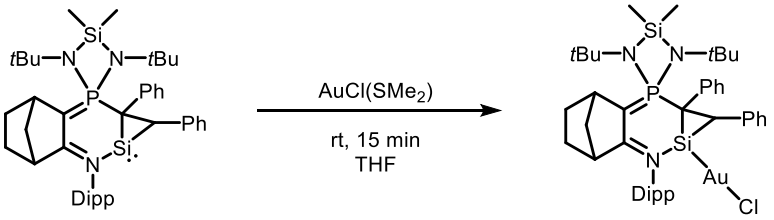

Scheme 82. Synthesis of the silacyclopropylidene gold(I) complex by *Kato et al*. in 2016[50].

Except for the studies of the aurophilic interactions discussed in the publication of *Khan et al.*,[97] these first attempts were more of a proof of principle, examining the behavior of silylenes towards late transition metal atoms. Within the next chapters, the hitherto presented *post-complex functionalization* will be investigated employing silylene gold(I) halide complexes.

3.2.3.1. Synthesis of Dimeric Aurophilic NHSiCl Au(I)Cl Complexes – $[(NHSiCl)(AuCl)]_2$

Herein, the synthesis of the novel gold(I) complex **11** as well as the succeeding functionalization to **12** will be presented, following the efforts and achievements of the aforementioned methods to the synthesis of novel copper(I) complexes (**5a-c** and **7a-c**) and silver(I) complexes (**9** and **10**), respectively. Under inert conditions, to a solution of the chloro benzamidinato silylene **1** in THF, the neat gold(I) halide precursor $AuCl(SMe_2)$ was added in small portions and kept stirring overnight at ambient temperature. The resulting black to blueish suspension was filtered and the colorless filtrate concentrated. The complex crystallized in form of colorless crystals suitable for X-ray analysis after storing the solution at -35°C. Filtration and drying *i.vac.* resulted in the target compound, as seen in Scheme 83.

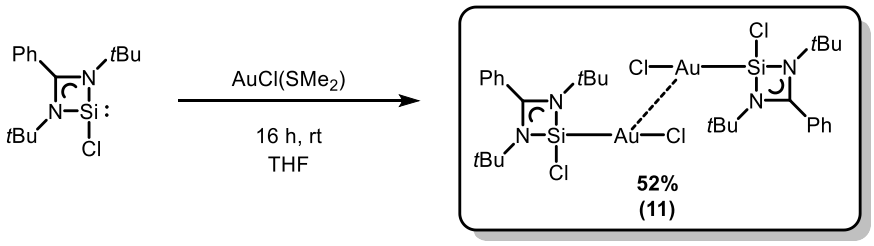

Scheme 83. Synthesis of **11** aka. bis-1,3-*N*,*N*'-di-*tert*-butyl-benzamidinato-chloro-silylene-gold(I)-chloride **$[(NHSiCl)(AuCl)]_2$**.

The colorless crystals were initially analyzed by X-ray diffraction analysis, thus revealing the most characteristic feature of **11**, the dimeric constitution of two "NHSiCl-Au-Cl" moieties, linked by aurophilic interactions. The occurrence of aurophilicity is no rare phenomenon in the field of organometallic chemistry and was already introduced in Chapter 1.5 (p.25).[86–88]

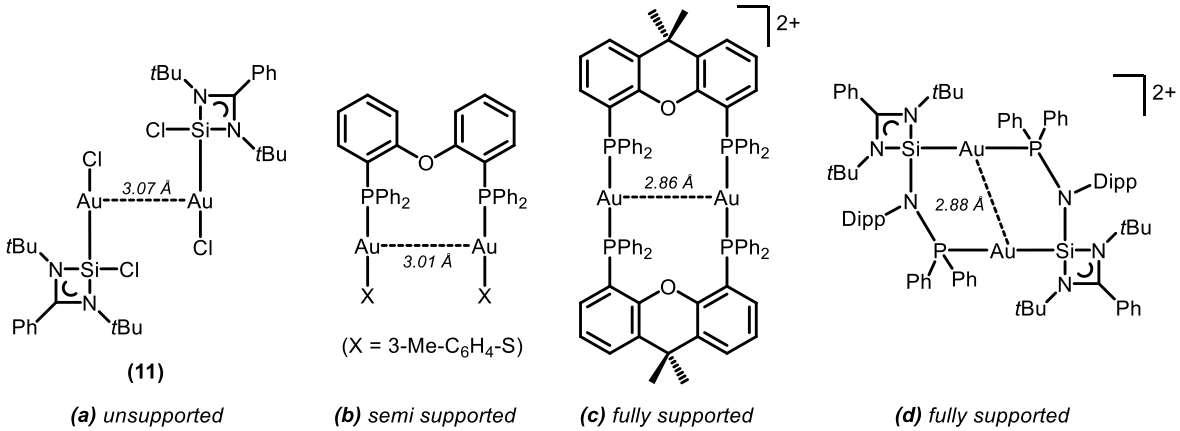

Scheme 84. Illustration of certain complexes employing *unsupported* (**(a)**, **11**), *semi supported* (**(b)**, *Lagunas et al.*, 2004[176]) and *fully supported* aurophilicity (**(c)**, *Stang et al.*, 2006[177] & **(d)** *Khan et al.*, 2016[97]).

The *unsupported* aurophilicity of **11** (compare Scheme 84, **(a)**) exhibits an Au–Au bond length of 3.0699(7) Å which lies within the aforementioned typical range of aurophilic interactions (2.5 to 3.5 Å), similar to NHC analogues employing imidazol-2-ylidenes, which show aurophilicity in the range of 3.05

to 3.20 Å.[172,178] The ligands are arranged in a so-called "*crossed-swords*" conformation, a term which was coined by *Schmidbaur* in the late 1990s and early 2000s and describes the alignment of complexes exhibiting such *unsupported* interactions.[179] This conformation shows a counter wise trend, in this case with a torsion angle of Si–Au–Au'–Si' = 133.44(2)° (see Figure 13) and seems to be favored, since the sterical repulsion of the bulky benzamidinato scaffolds is minimized, which probably optimizes the interaction energy. The somehow related dimer **[(NHSiNP)(Au)]$_2$(SbF$_6$)$_2$** presented by *Khan et al.* in 2016 reported a shortened Au–Au bond lengths of 2.873(1) Å (see Scheme 84, **(a)**),[97] which could have two reasons: on the one hand, the functional donor group, an amino-based side-arm bearing an additional P(III) donor site, increases the σ-donor strength of the Si(II) center possibly propagating on the Si–Au bond. On the other hand, the additional donor-site acts like a chelate ligand, thus ensuring a *fully supported* constitution of the complex (see Scheme 84, **(c)** & **(d)**; also compare A-frame ligands, see Chapter 3.2.1.2, p.56), which can force the gold atoms in close proximity, in comparison to the *unsupported* constitution of **11**. Similar effects were also observed in other compounds, e.g. as reported by *Lagunas et al.*[176] They published several structures based on the *Xantphos* type, which showed a rather flexible conformation bearing a *semi supported* Au–Au bond length of 3.01 Å, *versus* a related but more rigid derivative exhibiting a *fully supported* Au–Au bond length of 2.86 Å by *Stang et al.* (see Scheme 84, **(b)**).[177]

The Si–Au bond length of **11** (2.2324(17) Å) is marginally shorter than in the few existing silylene gold(I) complexes reported by *Khan et al.* (**[(NHSiHMDS)(AuCl)]**, 2.265(1) Å; **[(NHSiNP)(AuCl)]**, 2.245(2) Å), although **11** shows an unsubstituted chloro group, in comparison to the functionalized ligands **NHSiHMDS** and **NHSiNP**. Amino-substituted benzamidinato silylenes show an increased σ-donor strength, which should have an influence on the silicon(II) metal bond. However, as described above, the Si–Au bond lengths are very similar to each other, only the dimeric complex **[(NHSiNP)(Au)]$_2$(SbF$_6$)$_2$** exhibits a slightly elongated bond length (2.317(3) Å), which arises due to the simultaneous complexation of the P(III) donor site to the corresponding Au(I) atom.

Table 7. Selected bond lengths [Å], angles [°] and chemical shifts [ppm] for complexes **11**, **[(NHSiHMDS)(AuCl)]**[120], **[(NHSiNP)(AuCl)]**[97] and **[(NHSiNP)(Au)]$_2$(SbF$_6$)$_2$**[97] by *Khan et al*.

	11	**[(NHSiHMDS)(AuCl)]**	**[(NHSiNP)(AuCl)]**	**[(NHSiNP)(Au)]$_2$(SbF$_6$)$_2$**
Si–Au	2.2324(17)	2.265(1)	2.246(2)	2.317(3)
Au–Cl	2.3337(15)	2.341(1)	2.341(3)	
Si–N3		1.716(3)	1.735(7)	1.764(8)
Si–Au–Cl	174.85(5)	179.47(3)	177.39(9)	
N3–Si–Au		120.13(9)	118.2(2)	114.8
Au---Au	3.0699(7)			2.8753(1)
δ(^{29}Si)	40.06	8.76	24.73	78.05

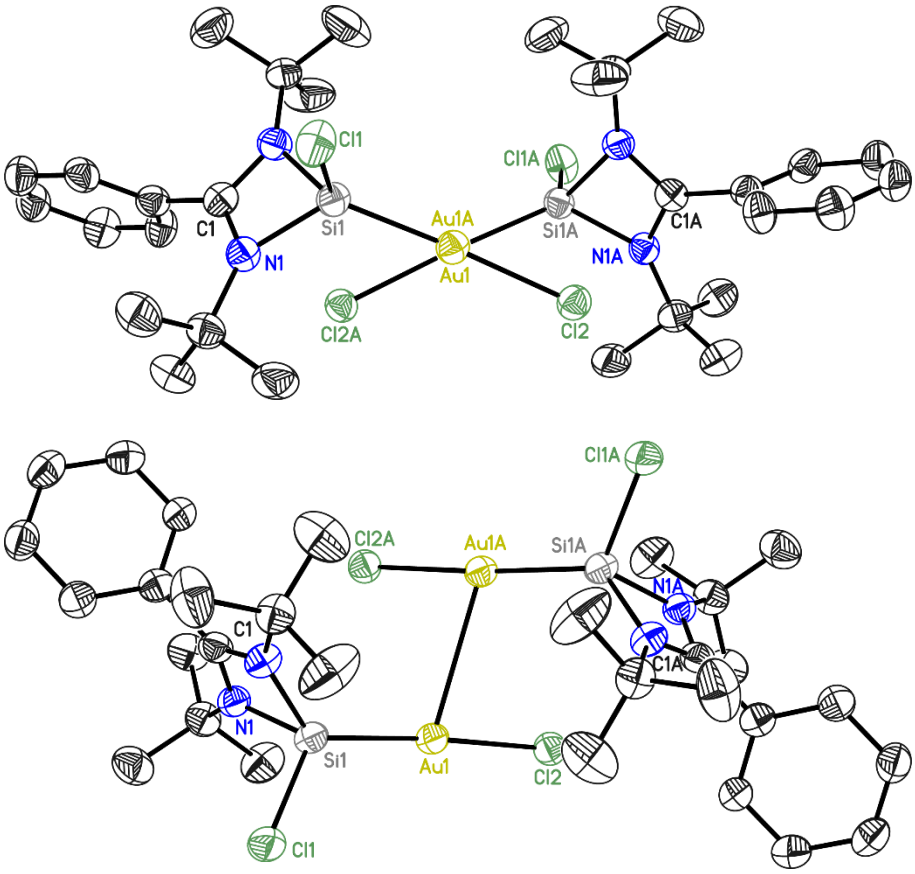

Figure 13. Crystal structures of **11** (**top**: side view; **bottom**: top view). The complex crystallizes in the space group *C*2/c in a monoclinic crystal system with a = 11.006(2) Å, b = 15.023(2) Å, c = 23.820(3) Å and β = 93.08(2)°. The hydrogen atoms, disorder and solvent molecules has been omitted for clarity. The anisotropic displacement parameters are depicted at the 50% probability level.

Furthermore, the elemental analysis, multinuclear NMR spectroscopy as well as LIFDI mass spectrometry supported the successful isolation of **11**. The ^{1}H NMR spectrum shows the expected slightly downfield shifted singlet (e.g. 1.30 ppm) and multiplet (7.83–7.77 ppm) of the benzamidinato scaffold, analogously to the predecessors **5a-c** and **9**, with corresponding ^{13}C NMR signals. The ^{29}Si NMR spectrum exhibits one single sharp peak at 40.03 ppm. This quite downfield shifted signal indicates a rather deshielded ^{29}Si nucleus. They investigated the coinage metal complexes of the conventional ligand **NHSiHMDS** and reported a shift at 8.76 ppm for the gold(I) complex.[120] The significant difference to **11** can be explained by the introduction of the functional donor group (HMDS) that shows an electron donating effect (compare Chapter 1.2), thus results in a more shielding effect on the ^{29}Si nucleus (see Scheme 85).

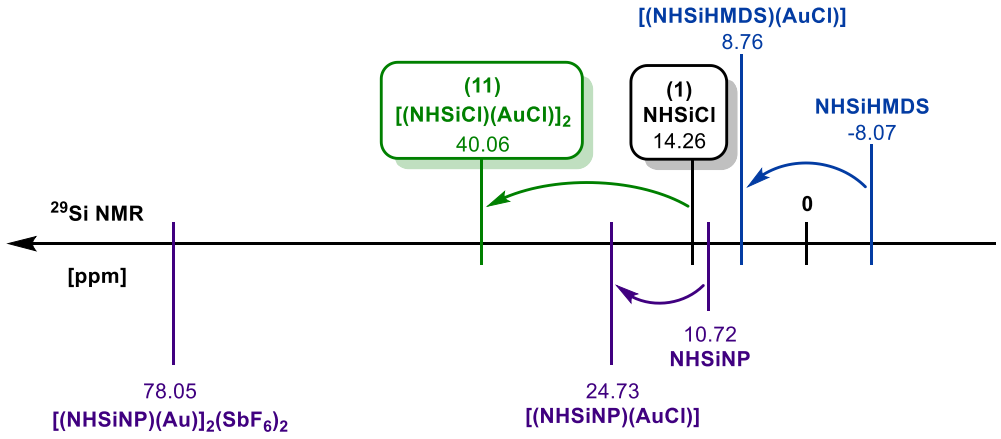

Scheme 85. Schematically illustration of the influence of a donating group adjacent to the Si(II) atom on the position of the chemical shift δ [ppm] of ^{29}Si NMR signals. The free functionalized **NHSiHMDS** and **NHSiNP** towards Au(I) complexation (by *Khan et al*. in 2015[120] & 2016[97], blue and purple), as well as the unsubstituted free silylene **1** (by *Roesky et al*. in 2006[13]) towards Au(I) complexation (*this work*, black and green).

Contrary to the results of the previously discussed solid state analyses, a molecular weight determination *via* DOSY measurements in a THF solution of **11** at ambient temperature should provide insight into its state in solution. Interestingly and contradictory to the previous analyses, the determined molecular weight rather indicates the presence of a monomeric constitution accompanied by THF molecules, than a dimeric one (see Scheme 86). Yet, it is not unusual that the aurophilic interactions of *unsupported* complexes in solution is given up.

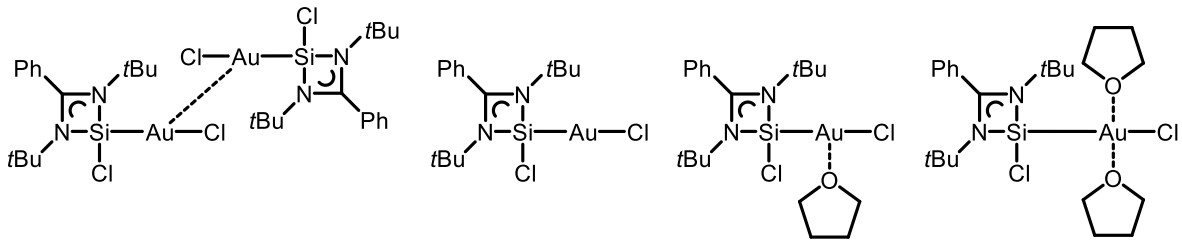

MW_{calc} = 1055 gmol^{-1}
MW_{det} = 671 gmol^{-1}
MW_{dif} = 57%

MW_{calc} = 527 gmol^{-1}
MW_{det} = 671 gmol^{-1}
MW_{dif} = -21%

MW_{calc} = 599 gmol^{-1}
MW_{det} = 630 gmol^{-1}
MW_{dif} = -5%

MW_{calc} = 672 gmol^{-1}
MW_{det} = 601 gmol^{-1}
MW_{dif} = 12%

Scheme 86. Most likely hypothetical aggregates determined by the ECC method *via* DOSY experiments. The data rather indicates the presence of a monomeric species accompanied by THF molecules, than the dimeric complex known by solid state analyses.

Remarkably, on the contrary to all novel investigated copper and silver complexes the LIFDI mass spectrometric analysis of **11** showed a solitary molecular ion peak at m/z = 1052.0, thus confirming the dimeric species. In addition, corresponding fragments of, e.g. the monomer (m/z = 491.0), were also unambiguously identified.

3.2.3.2. Functionalization with Pyridyl-Substituted Amino Groups – [(NHSiMes)(AuCl)]

The isolation of the interesting dimeric gold(I) silylene complex linked by aurophilic interactions raised the question whether the aurophilicity will be maintained after the functionalization. Therefore, the subsequent substitution was investigated following the previous efforts and methods by functionalizing the chloro group with the known amine **MesNHPy**.

Following the reaction illustrated in Scheme 87, the novel gold(I)-complex **[(NHSiCl)(AuCl)]$_2$** (**11**) was dissolved in THF and a separately prepared solution of the amine **MesNHPy** in THF was added and cooled down to -30°C. Afterwards, to the reaction mixture the solution of LiHMDS in THF was added. Under constant stirring, the resulting mixture was allowed to warm up to ambient temperature. The yellowish solution was concentrated to a minimum and a mixture of toluene and hexane was added until the crude product precipitated as a grey solid, which was subsequently filtered. The resulting raw product was dissolved in DCM and once more filtered in order to remove remaining traces of LiCl salt. The resulting clear yellowish filtrate was concentrated and stored at -35°C for crystallization. The pure product was isolated as colorless crystals, suitable for X-ray analysis.

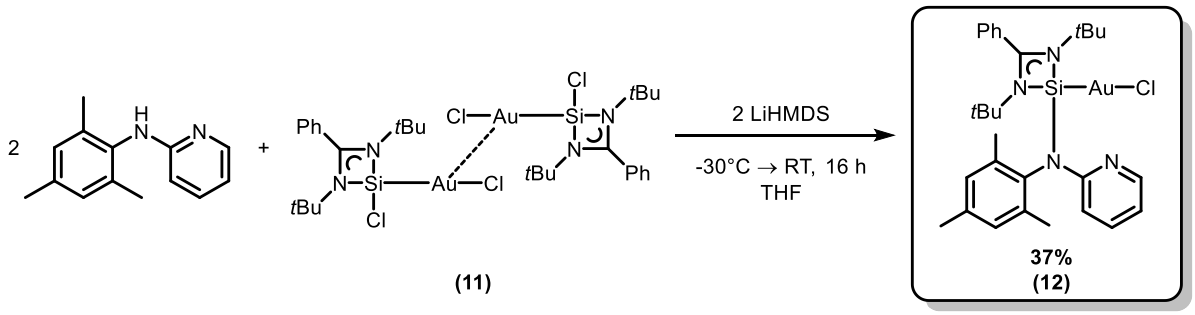

Scheme 87. Synthesis of **12** aka. 1,3-*N*,*N*'-di-*tert*-butyl-benzamidinato-*N*-mesityl-*N*-(2-pyridyl)amino-silylene-gold(I)-chloride **[(NHSiMes)(AuCl)]** *via in situ* deprotonation of the amine **MesNHPy** using LiHMDS.

^{1}H and ^{13}C NMR spectroscopic analysis of **12** showed the expected additional pyridyl-signals in the aromatic region, as well as the mesityl-group, analogues to its copper **7a-c** and silver **10** predecessors, validating the successful functionalization of the benzamidinato silylene. Unfortunately, similar to the previous isolations and analyses of the functionalized silylene metal complexes (**7a-c**, **10**), compound **12** enqueued the challenging determination of an ^{29}Si NMR signal, leading only to a flat baseline. Nevertheless, other methods support the presence of the low-valent silicon atom. Elemental analysis indicated a ligand to metal halide ratio of 1:1, which got confirmed by identifying the mass spectrometric analysis. The LIFDI mass spectrum exhibited the molecular ion peak with m/z = 702.2 and corresponding fragments (e.g. 667.2 $[M\text{-}Cl]^+$, 505.3 $[M\text{-}Au]^+$), thus confirming the successful isolation of **12** as an monomeric species.

The crystal structure determination via X-ray diffraction analysis additionally confirmed the above mentioned evaluation by elucidating the absolute structure of **12** as shown in Scheme 87 (compare

Figure 14). The newly introduced amino group shows a slightly elongated Si–N3 bond length (1.781(3) Å) compared to the aforementioned few examples by the group of *Khan* (1.716(3) to 1.764(8) Å, compare Table 8). More important, the top view of complex **12** (Figure 14, right) shows that the functional group including the free coordination site is turned roughly perpendicular to the linear Si–Au–Cl moiety, almost identically replacing the chloride substituent in **11** (see Figure 13, top view). The resulting distance between the pyridyl nitrogen atom and Au(I) atom (3.436 Å) precludes a coordination, since such binding motifs (N_{Py}–Au) usually lay in a range of 1.925 to 2.758 Å (see Chapter 3.2.4.2, p.97, for further discussion). The Si–Au bond lengths is slightly elongated compared to **11** (2.2564(11) Å), hence showing more similarity to the other functionalized examples. Since gold atoms with the oxidation state +I tend to coordinate in a linear fashion, here represented with an angle of 179.15(4)°, such a conformation and a non-coordinating pyridyl-group was expected. However, the previous aurophilicity was also cleaved and did not withstand the functionalization, which was anticipated as well, since the aurophilic interactions are rather weak.

Table 8. Selected bond lengths [Å] and angles [°] for complexes **11**, **12**, **[(NHSiHMDS)(AuCl)]**[120], **[(NHSiNP)(AuCl)]**[97] and **[(NHSiNP)(Au)]$_2$(SbF$_6$)$_2$**[97] by *Khan et al*.

	11	12	[(NHSiHMDS)(AuCl)]	[(NHSiNP)(AuCl)]	[(NHSiNP)(Au)]$_2$(SbF$_6$)$_2$
Si–Au	2.2324(17)	2.2564(11)	2.265(1)	2.246(2)	2.317(3)
Au–Cl	2.3337(15)	2.3465(11)	2.341(1)	2.341(3)	
Si–N3		1.781(3)	1.716(3)	1.735(7)	1.764(8)
Si–Au–Cl	174.85(5)	179.15(4)	179.47(3)	177.39(9)	
N3–Si–Au		122.67(12)	120.13(9)	118.2(2)	114.8
Au---Au	3.0699(7)				2.8753(1)
N_{Py}---Au		3.436			

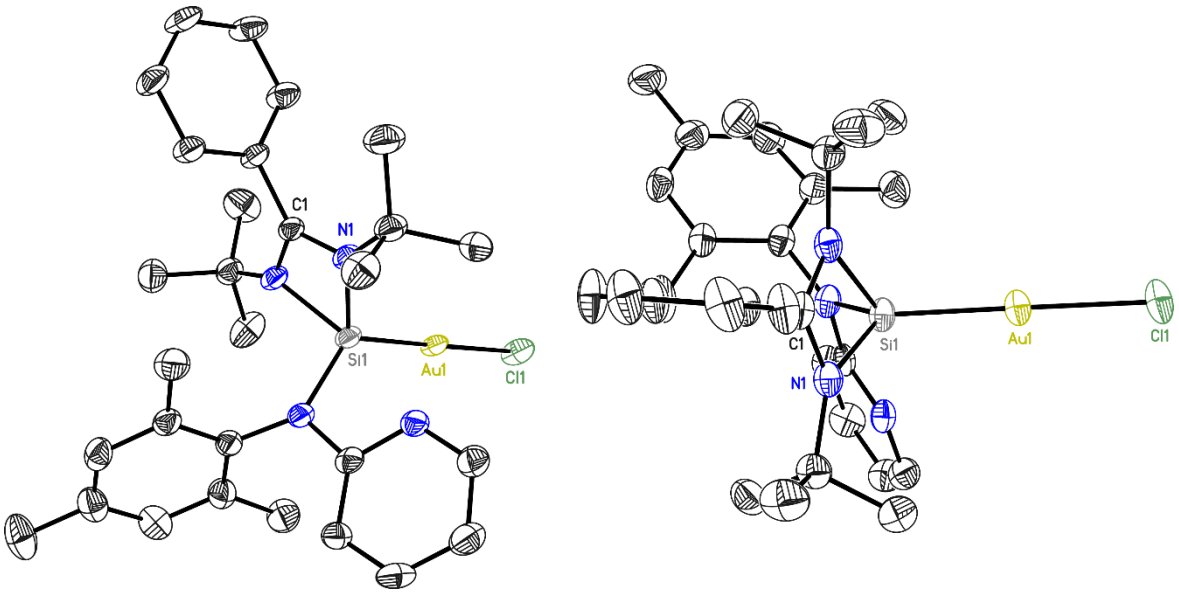

Figure 14. Crystal structures of **12** (**left**: side view; **right**: top view). The complex crystallizes in the space group $P2_1/n$ in a monoclinic crystal system with a = 11.401(2) Å, b = 16.130(3) Å, c = 18.452(3) Å and β = 105.69(2)°. The hydrogen atoms, disorder and solvent molecules has been omitted for clarity. The anisotropic displacement parameters are depicted at the 50% probability level.

In fact, *Khan et al.* observed a similar behavior as they were reporting their aurophilic interactions. The functionalized ligand **NHSiNP** occurred as a monomer when treated with the gold precursor, although a second donor-site was available, most likely due to the sterically demanding 2,6-di-*iso*-propylphenyl groups as well as the diphenylphosphine group. Only after removing the halides and introducing weakly coordinating anions, they enforced the formation of the dimeric complex featuring the *fully supported* aurophilicity (see Scheme 84).[97]

In summary, the successful application of the hitherto developed *post-complex* method to the synthesis of functionalized NHSis could once again be proven on the basis of novel Au(I) complexes. Treatment of **1** led to the formation of the dimeric complex **11**, featuring *unsupported* aurophilicity in a *crossed-swords* conformation. The subsequent functionalization *via in situ* deprotonation of **MesNHPy** utilizing LiHMDS resulted in the monomeric complex **12**, holding an Au(I)Cl with a linear geometry at the Si(II) atom, while the pyridyl donor-site remained uncoordinated, although the N points at the metal atom.

Compound **12** holds a great potential for further investigations. For example, the aforementioned behavior of the dimerization concomitant to a halide exchange to weakly coordinating anions (e.g., using $AgSbF_6$) should be checked in order to prove if the aurophilicity can be restored (see Scheme 88). Not only, but especially in this case, these compounds could be further examined by investigating their photophysical properties and possibly identify a corresponding influence of the functionalization and/or aurophilic interactions, since gold complexes often exhibit photochemical features.

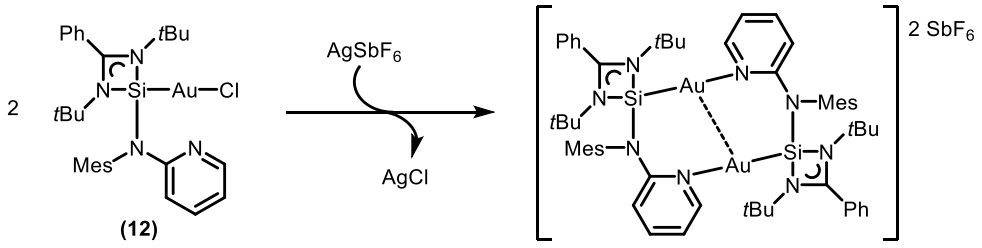

Scheme 88. Possible pathway to the formation of a dimeric complex featuring *fully supported* aurophilicity, by interchanging the halide with weakly coordinating counter anions (e.g., $AgSbF_6$).

Furthermore, certain gold complexes show catalytical behavior on the basis of an oxidative addition, exhibiting Au(I)/Au(III) equilibria.[180] The group around *Ribas* for example, focused their research on the study of such gold compounds utilizing phosphorous, nitrogenous or carbonaceous donor-groups and was able to report captivating results of oxidant free C–N or C–O cross-coupling reactions.[181] The current catalyst precursor is based on a carbene as the steering ligand (e.g., [(IPr)Au(MeCN)]), which undergoes the oxidative addition step with aryl-halides. One of the key steps of their proposed mechanism is the stabilization of the Au(III) state *via* temporary ligation of a pyridyl group, which is

part of the substrate. Compound **12** would be able to offer a strong σ-donor ability and an additional donor-site for a stabilizing transient ligation at a time, which could be beneficial regarding the reactivity and substrate scope (see Scheme 89).

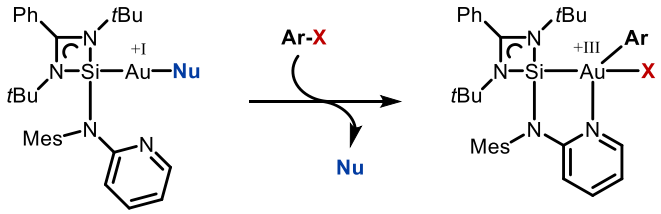

Scheme 89. Schematically illustration of a possible application of complex **12** in Au(I)/Au(III) oxidant free cross-coupling reactions.

3.2.4. Presentation of NHSi Zinc(II) Complexes

In order of finding sustainable and efficient molecular transformations, the focus of transition metal driven catalysts has to be set on cheaper, more abundant and less toxic metal centers.[182] Since one of the best ways to gain new catalysts featuring advanced properties is still to modify the ligation of transition metal atoms, the field of research regarding the closely related *N*-heterocyclic carbene zinc complexes has developed an increasing amount of catalytical applications.[183,184,185]

In the current field of *N*-heterocyclic silylene transition metal complexes, compounds employing group 12 metal centers are comparatively rare and are limited to zinc by now. The first report on such complexes was published in 2014, by the group of *P. W. Roesky*.[166] They anticipated that the coordination of **1** at a dialkyl zinc precursor undergoes a shift of the negatively charged alkyl group with the chloro group, as shown in Scheme 90. Yet, this observation was not further investigated by means of exploiting this behavior for alternative ways of functionalization. This effect was adapted in Chapter 3.2.1.3, modified and transferred, to achieve the alternative synthesis of Cu(I) complexes *via* the novel *precursor functionalization*.

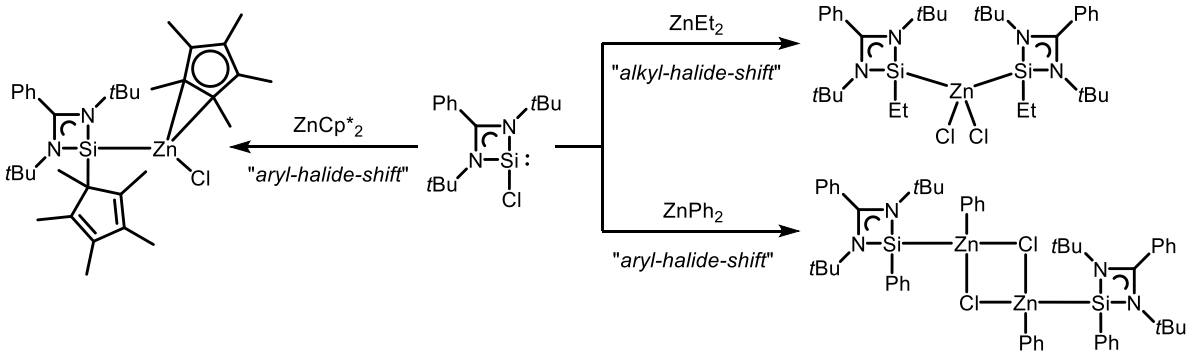

Scheme 90. Synthesis of the first NHSi Zn(II)-complexes by *P. W. Roesky et al.* in 2014[166], by undergoing halide-alkyl-/aryl-shifts between the low-valent silicon atom and zinc(II) atom, employing the **NHSiCl** (**1**) and certain zincorganyls.

Two years later, the same group further investigated NHSi Zn complexes and tried to avoid the above mentioned alkyl-/aryl-halide shift by utilizing the already functionalized NHSi, in this case the **NHSi(C_5Me_5)**, and treated it with zinc halides.[186] These attempts resulted in the formation of dimeric complexes bearing a "Zn(Cl)-(μ-Cl)$_2$-Zn(Cl)" center with a tetrahedral geometry around the Zn(II) atoms. Similar to their previous work, the formation of dimeric complexes was favored, unless the silylene **NHSi(C_5Me_5)** was treated with zincorganyls, like $ZnPh^F_2$, $ZnEt_2$ or $ZnPh_2$, which resulted in a monomeric complex with trigonal planar Zn(II) atoms.

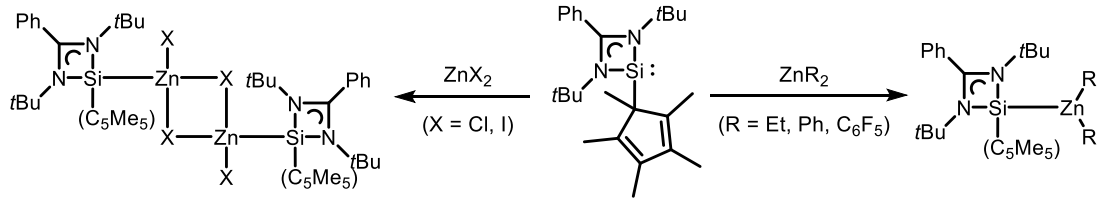

Scheme 91. Following synthetic attempts to the isolation of the **NHSi(C_5Me_5)** Zn(II)-complexes by *P. W. Roesky et al.* in 2016[186], by utilizing Zn(II) halides or zincorganyls.

At the same time, the group around *Tacke* extended their research to the synthesis of novel benzamidinato and guanidinato silylenes and related transition metal complexes and were able to report a monomeric zinc(II) halide complex employing a trigonal planar geometry instead of the formation of a μ-halide bridged dimer.[187] On the one hand, this behavior could stem from the high sterically demanding residues utilized in this NHSi (see Scheme 92, left), hence kinetically hindering the dimerization. On the other hand, throughout their investigations, the guanidinato silylene often exhibited unexpected reactivity compared to its benzamidinato congener, due to their additional resonance structures (see Chapter 1.2). For example, when treating the exact same silylene with a zincorganyl, such as $ZnEt_2$, the guanidinato scaffold undergoes a rearrangement, leading to the decomposition of the original NHSi motif (see Scheme 92, left).

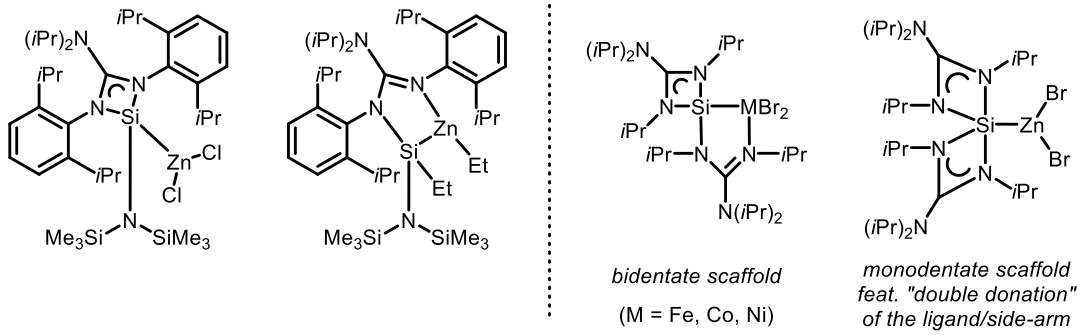

Scheme 92. Different behavior of the related guanidinato silylene towards zinc(II) halides, zincorganyls and certain 3d metal atoms, illustrated by the work of *Tacke et al.* in 2016[187] (**left**) and 2017[81] (**right**)

One year later, *Tacke et al.* further investigated the transition metal complexes of such guanidinato silylenes employing their new NHSi (see Scheme 92, right). The different reaction behavior was already highlighted in Chapter 3.1 as the first and only example of an NHSi bearing a side-arm functionalization

with an additional donor-site, even though they did not highlighted it as such a feature.[81] Interestingly, while 3d metal halides of group 8 to 10 were coordinated in a bidentate fashion (see Scheme 92, right), the complexation of the zinc halide resulted in a monodentate fashion, featuring a double donation by the side-arm to the silicon(II) atom and a trigonal planar geometry at the zinc(II) atom (see Chapter 3.1 for further information).

While *Tacke et al.* and *P. W. Roesky et al.* were investigating the subtleties of monomeric and dimeric zinc(II) complexes, the group of *Sen* published their findings, in which the choice of the solvent led to the selective formation of a dimeric or monomeric complex, respectively, employing the well-known silylene **NHSiHMDS** (see Scheme 93).[188] They initially performed the reaction in THF and recrystallized it from toluene, which led to the monomeric complex [(NHSiHMDS)(ZnI_2)(THF)], with a four-coordinated Zn(II) atom showing a tetrahedral geometry. Changing the solvent to MeCN, as well as removing the THF by carefully heating the compound, led to the dimerization, thus the formation of [(NHSiHMDS)(ZnI_2)]$_2$ bearing a μ-iodide bridged core moiety ("Zn(I)-(μ-I)$_2$-Zn(I)"). This is the first known inter-conversion of silylene transition metal adducts between a monomer and a dimer.

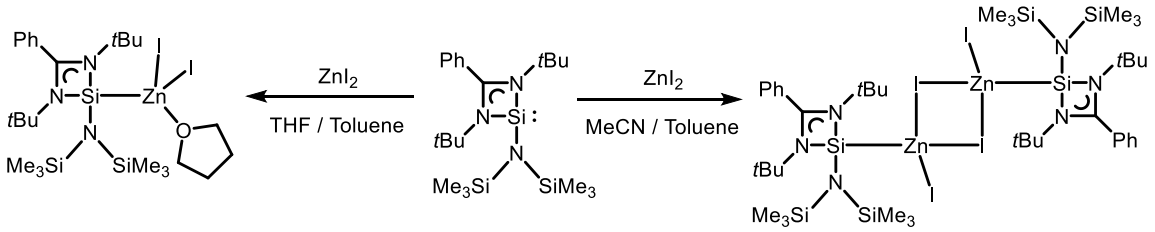

Scheme 93. Selective formation of the monomeric complex **[(NHSiHMDS)(ZnI_2)(THF)]** or the dimeric complex **[(NHSiHMDS)(ZnI_2)]$_2$** by changing the solvent from THF to MeCN, published by *Sen et al*. in 2017[188].

This previous work of the past years illustrates the different reactivity of certain NHSis towards different zinc(II) precursors and the limited understanding towards their formation. In the following chapters, the application of the preceding achievements of the *post-complex functionalization* to novel transition metal complexes will be expanded and applied to zinc(II) atoms.

3.2.4.1. Synthesis of Dimeric NHSiCl Zn(II) Halide Complexes – [(NHSiCl)($ZnCl_2$)]$_2$

Inspired by the above mentioned work, the synthesis to potential chloro benzamidinato silylene zinc(II) complexes is investigated. Under inert conditions **1** was dissolved in a mixture of THF and toluene in a ratio of 1:1. Subsequently, prior dried $ZnCl_2$ was added in small portions and left stirring overnight at ambient temperature. The clear colorless solution was concentrated and stored at -35°C for one day. The colorless crystals were filtrated and dried under reduced pressure to gain the product in high purity and good yield. The target compound showed a good solubility in THF, moderate solubility in toluene and a rather low solubility in DCM, which was quite convenient to synthetic and purification

procedures. Analysis was performed in THF, whereas recrystallization from toluene proved to be best to gain suitable crystals for single crystal analysis, and performing the above mentioned reaction in DCM, led to the precipitation of the desired product in form of a fine white solid, which was easily filtered, washed and dried for further analytics.

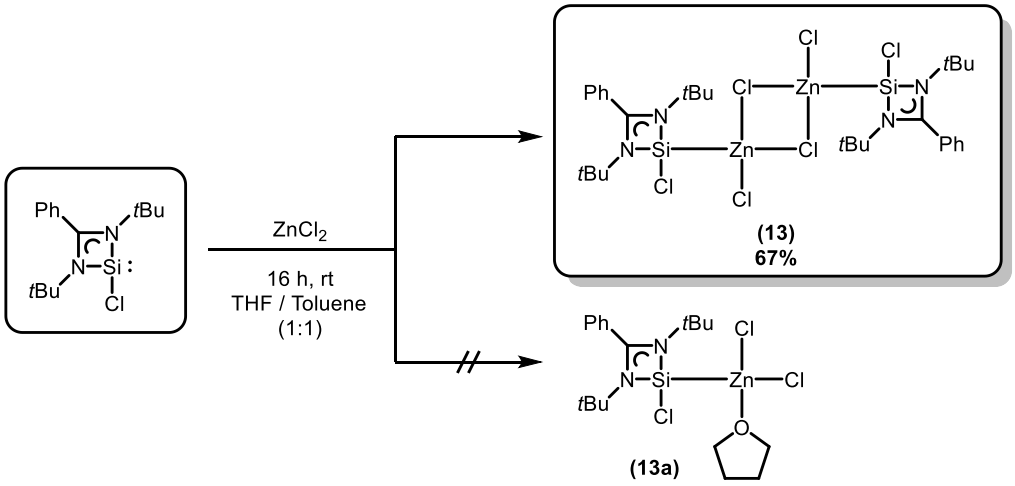

Scheme 94. Synthesis of the dimeric complex bis-1,3-*N*,*N*'-di-*tert*-butyl-benzamidinato-chloro-silylene-zinc(II)-chloride **[(NHSiCl)(ZnCl$_2$)]$_2$ 13** over the formation of the alternative monomeric complex **13a**.

Compound **13** was analyzed *via* multinuclear NMR spectroscopy, elemental and X-ray diffraction analysis. As expected, the characteristic singlets deriving from the *tert*-butyl groups of the benzamidinato scaffold were slightly downfield shifted to 1.27 ppm, as well as the aromatic signals at 7.85–7.48 ppm, analogously to the results of the previous coinage metal complexes. The ^{13}C NMR spectrum shows all corresponding signals as well. As investigated by *Sen et al.* the occurrence of coordinating THF molecules would indicate the presence of a monomer, rather than a dimer. Due to solubility reasons the measurements did take place in THF-d8 though, eventually coordinating solvent molecules could have been exchanged with deuterated ones in solution, hence vanishing the signals. Thus, the presence of a monomeric structure bearing THF molecules (see Scheme 94, **13a**) could not be unambiguously determined *via* 1D NMR spectroscopy (*vide infra* for DOSY experiments). The ^{29}Si NMR spectroscopic analysis displayed one single broadened peak at 17.81 ppm. To gain this signal, a rather highly concentrated solution was required, as well as extended measurement times that exceed the standardized acquisition times of routine experiments. The range of ^{29}Si NMR signals of NHSi Zn(II)X$_2$ complexes appeared rather wide with 60.5 to -84.3 ppm. In order to classify **13,** all relevant structures and the corresponding shifts are presented in Table 9. Ranking them by their chemical shifts, two things get obvious: first, the location of the chemical shifts of these complexes do not seem to show a big dependency on the monomer/dimer aggregation (i.e., **[(NHSiHMDS)(ZnCl$_2$)]$_2$** *vs*. **[(NHSiHMDS)(ZnCl$_2$)(THF)]**; -6.4 ppm *vs*. -9.5 ppm). Second, the chemical shift of the ^{29}Si signal rather shows to be dependent on the substituent at the low-valent Si(II) atom, than by the coordination of a

metal atom (e.g., alkyl-functionalized NHSi Zn(II) complexes show very similar chemical shifts, compared to the corresponding free ligands). In this context, the ^{29}Si signal of 17.81 ppm determined for **13** lies in the expected range for this complex, slightly downfield shifted relative to the free ligand **1** (14.26 ppm).

Table 9. Overview of the current NHSi zinc(II) halide complexes and their ^{29}Si NMR signals [ppm] as well as their Si–Zn bond lengths [Å] (m = monomer, d = dimer; color code: **bold black** = alkyl/aryl, **green** = halide, **blue** = amino donor groups).

Complex		^{29}Si NMR [ppm]	Si–Zn bond length [Å]	
[(NHSi**C$_5$Me$_5$**)(ZnCl)(C$_5$Me$_5$)]	m	60.5	2.3750(9)	*[166]*
[(NHSi**Et**)$_2$(ZnCl$_2$)]	d	59.0	2.416(2)	*[166]*
[(NHSi**C$_5$Me$_5$**)(ZnCl$_2$)]$_2$	d	51.6	2.3862(11)	*[186]*
[(NHSi**Ph**)(ZnClPh)]$_2$	d	34.2	2.4171(7)	*[166]*
[(NHSiCl)(ZnCl$_2$)]$_2$ **(13)**	d	17.8	2.380(2)	*(This work)*
[((*i*Pr)$_2$NC(NDipp)$_2$Si(HMDS))(ZnCl$_2$)]	m	17.5	2.3784(7)	*[187]*
[(NHSiHMDS)(ZnI$_2$)]$_2$	d	-6.4	2.4096(3)	*[188]*
[(NHSiHMDS)(ZnI$_2$)(THF)]	m	-9.5	2.434(2)	*[188]*
[((*i*Pr)$_2$NC(N*i*Pr)$_2$)Si)((*i*Pr)$_2$NC(N*i*Pr)$_2$)(ZnCl$_2$)]	m	-84.3	2.3531(9)	*[81]*
NHSi**C(TMS)$_3$**		72.2		*[74]*
NHSi***t*Bu**		61.5		*[74]*
NHSiCl		14.3		*[13]*

Furthermore, the fact that the monomeric and dimeric complexes **[(NHSiHMDS)(ZnCl$_2$)]$_2$** and **[(NHSiHMDS)(ZnCl$_2$)(THF)]** show very similar ^{29}Si signals (-6.4 ppm *vs*. -9.5 ppm) indicate that it might be possible that the broadening of the ^{29}Si signal of **13** stems from a fluctuating formation between a possible monomeric and dimeric constitution in solution. However, the group of *Sen* was able to isolate both structures by performing the reaction in different solvents and crystallizing them from toluene. The monomeric species was highly sensitive towards temperatures above 0°C and decomposed over time to a grey solid, which proved to be mostly elemental zinc.[188] Unfortunately, all attempts to perform the reaction from Scheme 94 in different solvents, also led to the formation of **13**, as well as all efforts in re-/crystallizing this compound (*vide infra* for further crystallographic details and discussion). To further investigate this issue, diffusion ordered spectroscopy (DOSY) analysis of a solution of **13** in THF were performed at ambient temperature. The DOSY measurements and especially the determination of the calibration curves, hence the molecular weight, proved to be very challenging, which resulted in quite high standard deviations. Nevertheless, the determined molecular weight indicates an equilibrium between the dimeric and the monomeric structure, attended by THF molecules (see Scheme 95), trending to the formation of the dimer.

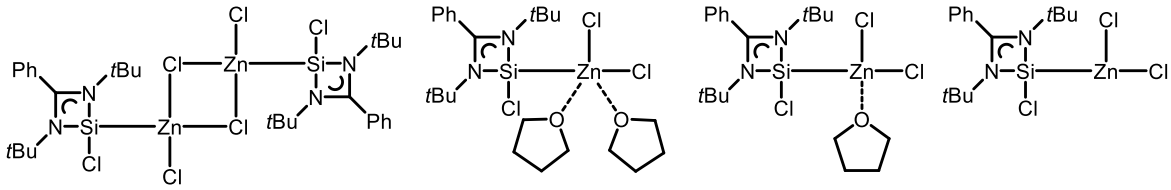

MW_{calc} = 862 gmol^{-1}
MW_{det} = 736 gmol^{-1}
MW_{dif} = 17%

MW_{calc} = 575 gmol^{-1}
MW_{det} = 690 gmol^{-1}
MW_{dif} = -17%

MW_{calc} = 503 gmol^{-1}
MW_{det} = 709 gmol^{-1}
MW_{dif} = -29%

MW_{calc} = 431 gmol^{-1}
MW_{det} = 736 gmol^{-1}
MW_{dif} = -41%

Scheme 95. Most likely hypothetical aggregates determined by the ECC method *via* DOSY experiments. The data indicates either a dimeric species or a monomeric species with possible free coordination sites that might be occupied by THF molecules.

In addition to the NMR spectroscopic studies the elemental analysis exhibited a ligand to metal halide ratio of 1:1, further suggesting the formation of the dimeric structure **13** instead of **13a**, due to the absence of coordinating solvent molecules. Yet, LIFDI mass spectrometric analyses showed no meaningful signals, probably due to the high sensibility towards air and moisture, leading to the decomposition of **13** during the process.

Table 10. Overview of the current NHSi zinc(II) halide complexes and their ^{29}Si NMR signals [ppm] as well as their Si–Zn bond lengths [Å] (m = monomer, d = dimer; color code: **bold black** = alkyl/aryl, **green** = halide, **blue** = amino donor groups).

Complex		^{29}Si NMR [ppm]	Si–Zn bond length [Å]	
[(NHSi**HMDS**)(ZnI_2)(THF)]	m	-9.5	2.434(2)	*[188]*
[(NHSi**Ph**)(ZnClPh)]$_2$	d	34.2	2.4171(7)	*[166]*
[(NHSi**Et**)$_2$($ZnCl_2$)]	d	59.0	2.416(2)	*[166]*
[(NHSi**HMDS**)(ZnI_2)]$_2$	d	-6.4	2.4096(3)	*[188]*
[(NHSi**C$_5$Me$_5$**)($ZnCl_2$)]$_2$	d	51.6	2.3862(11)	*[186]*
[(NHSi**Cl**)($ZnCl_2$)]$_2$ **(13)**	d	17.8	2.380(2)	*(This work)*
[((*i*Pr)$_2$NC(NDipp)$_2$Si(**HMDS**))($ZnCl_2$)]	m	17.5	2.3784(7)	*[187]*
[(NHSi**C$_5$Me$_5$**)(ZnCl)(C_5Me_5)]	m	60.5	2.3750(9)	*[166]*
[(((*i*Pr)$_2$NC(N*i*Pr)$_2$)Si)(**(*i*Pr)$_2$NC(N*i*Pr)$_2$**)($ZnCl_2$)]	m	-84.3	2.3531(9)	*[81]*

The solid state structure was finally determined by XRD analysis, confirming the dimeric complex showing two NHSiCl (**1**) ligands coordinated to a rhomboidal [Zn_2Cl_4] core moiety, with two terminal and two symmetrically bridging chloro anions, that form a four-membered ring with the Zn(II) atoms in a "Zn(Cl)-(μ-Cl)$_2$-Zn(Cl)" fashion. The bridging μ-Cl atoms basically behave like bidentate ligands, which is quite common in, e.g., alkaline earth metal complexes.[189] The Zn(II) atoms show a distorted tetrahedral geometry, like every dimeric composition of that type revealed. Ranking the above discussed Table 9 of NHSi Zn(II) halide complexes by their Si–Zn bond lengths (2.3531(9) to 2.434(2) Å), the trend emerges that the dimeric complexes show longer bond lengths than their monomeric congeners (see Table 10). However, there is one monomeric outlier **[(NHSiHMDS)($ZnCl_2$)(THF)]**, reported by *Sen et al*., which shows the longest Si–Zn bond length with 2.434(2) Å.[188]

Compound **13** shows the shortest Si–Zn bond lengths of the corresponding dimers with 2.380(2) to 2.385(16) Å, which is most likely traced back to the absence of an additional donating group adjacent to the low-valent silicon(II) atom. Further on, comparing the rhomboid like scaffold of the $[Zn_2Cl_2]$ moiety to the according related complexes, it appeared to be the most distorted one with Zn–μ-Cl–Zn = 86.60(8)° and μ-Cl–Zn–μ-Cl = 93.40(8)° (compare Table 11).

Table 11. Selected bond lengths [Å] and angles [°] for complexes **13**, **[(NHSiC$_5$Me$_5$)(ZnCl$_2$)]$_2$** by *P. W. Roesky et al*. (2016[186]), **[(NHSiHMDS)(ZnI$_2$)]$_2$** by *Sen et al.* (2017[188]) and **[(NHSiPh)(ZnClPh)]$_2$** by *P. W. Roesky et al*. (2014[166]).

	13	**[(NHSiC$_5$Me$_5$)(ZnCl$_2$)]$_2$**	**[(NHSiHMDS)(ZnI$_2$)]$_2$**	**[(NHSiPh)(ZnClPh)]$_2$**
Si–Zn	2.380(2)/2.385(16)	2.3862(11)	2.4096(3)	2.4171(7)
Zn–Cl	2.156(14)/2.190(2)	2.2165(12)	2.58023(16)	
Zn–μ-Cl	2.310(13)/2.385(2)	2.3491(9)/2.4081(10)	2.7223(2)/2.7373(2)	2.3826(6)/2.4944(8)
Zn–μ-Cl–Zn	86.60(8)	88.09(3)	89.138(4)	88.73(2)
μ-Cl–Zn–μ-Cl	93.40(8)	91.91(3)	90.861(4)	91.27(2)

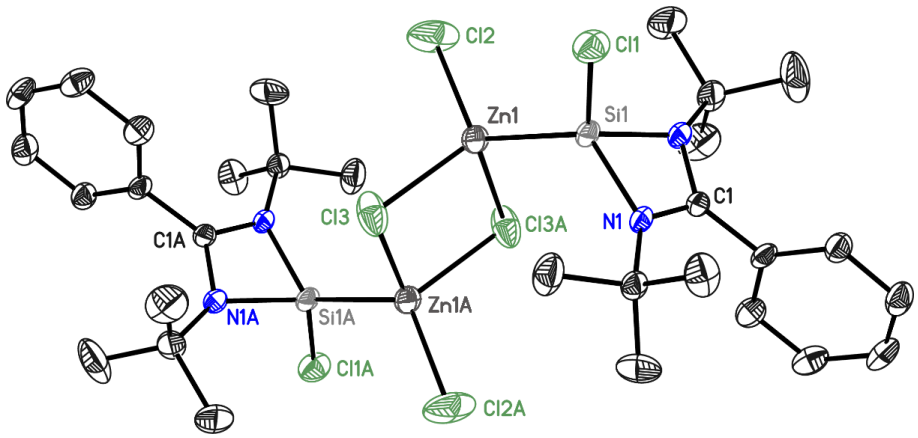

Figure 15. Crystal structure of **13**. The complex crystallizes in the space group $P2_1/n$ in a monoclinic crystal system with a = 10.6169(13) Å, b = 14.4565(17) Å, c = 12.8706(15) Å and β = 90.561(2)°. The hydrogen atoms, disorder and solvent molecules has been omitted for clarity. The anisotropic displacement parameters are depicted at the 50% probability level.

In conclusion, the isolation and predominantly full characterization of **13** was successful, whereas the question whether the complex can be present as a monomeric complex in solution is not decided yet, which would require consideration of a possible equilibrium reaction. The results of the molecular weight determination *via* DOSY measurements showed high standard deviations for the hypothetical aggregates, which illustrate an equilibrium reaction, tending to the formation of the dimer. All solid state analyses (XRD, EA) confirm the presence of a dimeric complex, too.

To further investigate this compound, low temperature NMR measurements could be meaningful, in order to see if or how the location of the ^{29}Si and ^{1}H NMR peaks would change, or even split into two species. Low temperature DOSY investigations would also be reasonable, to evaluate how this would affect the determination of the molecular weight, in order to gain better and more reliable data.

3.2.4.2. Functionalization with Pyridyl-Substituted Amino Groups – $[(NHSiMes)(ZnCl_2)]_2$

Since *Sen et al*. were able to prove that the NHSiHMDS ZnI_2 complexes are able to adopt monomer and dimer aggregation, depending on the utilized solvent (THF *vs*. MeCN), the question whether the presumed dimer **$[(NHSiCl)(ZnCl)_2]_2$** (**13**) is able to show the same transformation is not decided yet. The previously discussed results of chapter 3.2.4.1 primarily suggested the formation of the dimer, whereby the NMR spectroscopic analyses show influences of a minor equilibrium, due to broadened peaks and a challenging molecular weight determination *via* DOSY.

The current order of the novel developed synthetic strategy to functionalized silylenes provides the *in situ* deprotonation of an amine in the presence of the NHSiCl TM complex. Until now, this method proved very versatile and yielded in the isolation of interesting new compounds featuring coinage metal centers. Naturally, this method will be applied to the novel NHSiCl $ZnCl_2$ complex **13** as well, to examine its behavior towards group 12 transition metal atoms. The past years already authored certain zinc silylene complexes, which partially yielded structurally similar compounds. It was noted that one of these complexes sharing the $[Zn_2Cl_4]$ moiety, published by *P. W. Roesky et al*. in 2016, was treated with LiHMDS in order to investigate its behavior towards subsequent salt metathesis reactions.[186] As illustrated in Scheme 96, they observed the formation of the free **$NHSiC_5Me_5$** ligand and $Zn(HMDS)_2$ under the concomitant elimination of LiCl monitored *via* ^{1}H NMR spectroscopy.

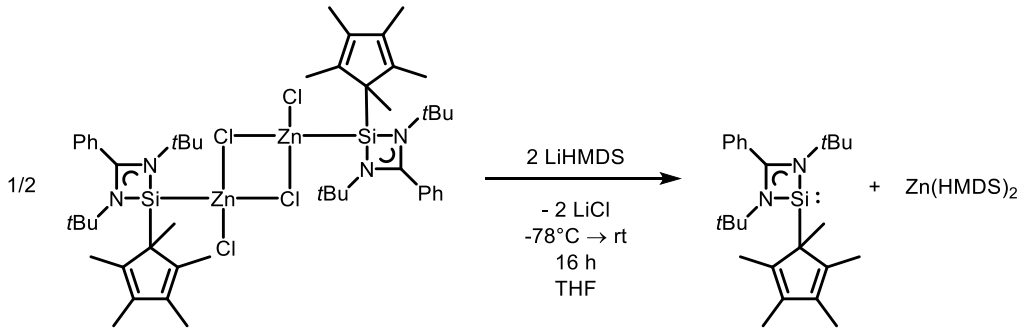

Scheme 96. Proposed reaction of **$[(NHSiC_5Me_5)(ZnCl_2)]_2$** with LiHMDS to the free ligand and $Zn(HMDS)_2$ under the formation of LiCl, by *P. W. Roesky et al*. in 2016[186].

Despite these findings, the initial method developed throughout this work, should be applied, since the deprotonation of the secondary amine should be energetically favored compared to the formation of $Zn(HMDS)_2$. Furthermore, the introduction of an additional donor-site, provided through the pyridyl-group, could lead to the formation of the monomer, by forming a bidentate complexation.

Two equivalents of the amine **MesNHPy** were added to a solution of one equivalent of the recently isolated zinc complex **13** in THF and cooled down to -30°C in order to suppress the formation of $Zn(HMDS)_2$. A solution of an equimolar amount of LiHMDS in THF was prepared separately and subsequently added dropwise to the reaction mixture under vigorous stirring. While stirring overnight, the mixture was allowed to warm up to ambient temperature. The resulting yellow solution was

concentrated and hexane and toluene were added to fully precipitate the LiCl salt, which was filtered off. After concentrating the yellow filtrate it was stored at -35°C for one day to isolate the target compound in form of colorless crystals (see Scheme 97).

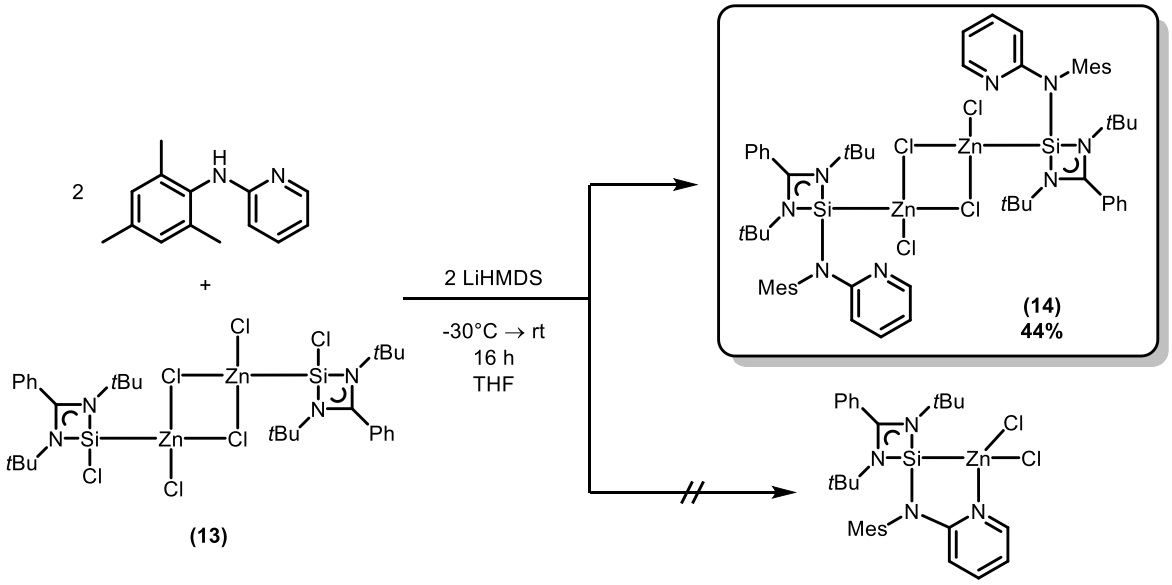

Scheme 97. Synthesis of the dimeric NHSi zinc(II) halide complex bis-1,3-*N*,*N*'-di-*tert*-butyl-benzamidinato-*N*-mesityl-*N*-(2-pyridyl)amino-silylene-zinc(II)-chloride **[(NHSiMes)(ZnCl$_2$)]$_2$** (**14**) *via in situ* deprotonation of the amine **MesNHPy** using LiHMDS.

The isolated colorless crystalline solid was fully characterized *via* CHN analysis, LIFDI mass spectrometry, multinuclear NMR spectroscopy and solid state XRD analysis. The structure of **14** is displayed in Figure 16 and shows the successful substitution of the chloro group with the amino group, further broadening the list of successfully applied *post-complex functionalization* at NHSiCl TM complexes. However, the above discussed dimeric composition featuring the rhomboid center of zinc(II) chloride was retained during the process using LiHMDS. The envisaged competing reaction to give Zn(HMDS)$_2$ could not be totally excluded, since the moderate yield of 44% would leave room for side-reactions. At least it could not impede the formation and isolation of the target compound. It is remarkable though, that the rhomboidal [Zn_2Cl_4] core with a free coordination site at the pyridyl-group dangling around seemed to be more favored than the monomerization and thus arrangement of a five-membered metallacycle. The Si–Zn bond length of **14** is just marginally shortened in comparison to **13** (2.3726(5) *vs.* 2.380(2)/5(16) Å) indicating a rather minor influence of the functionalization, however, the distortion of the rhomboid structure changed appreciable (see Table 12). While the angles got closer to an ideal right angle (86.60(8) → 88.8542(15)° and 93.40(8) → 91.457(15)°), the Zn–μ-Cl bond lengths show a noticeable elongation (2.310(13) → 2.3667(6) Å and 2.385(2) → 2.4241(5) Å) leading to an oblong rhomboid. Additionally, the Zn–Cl bond lengths to the terminal halides are elongated as well (e.g., 2.156(14) → 2.2364(5) Å). Thus, the slight shortening of the silicon(II) zinc bond and the

elongation of the rhomboid center suggests that the introduction of the donating group shows an overall weakening effect of the dimeric constitution, still favoring the dimerization, though.

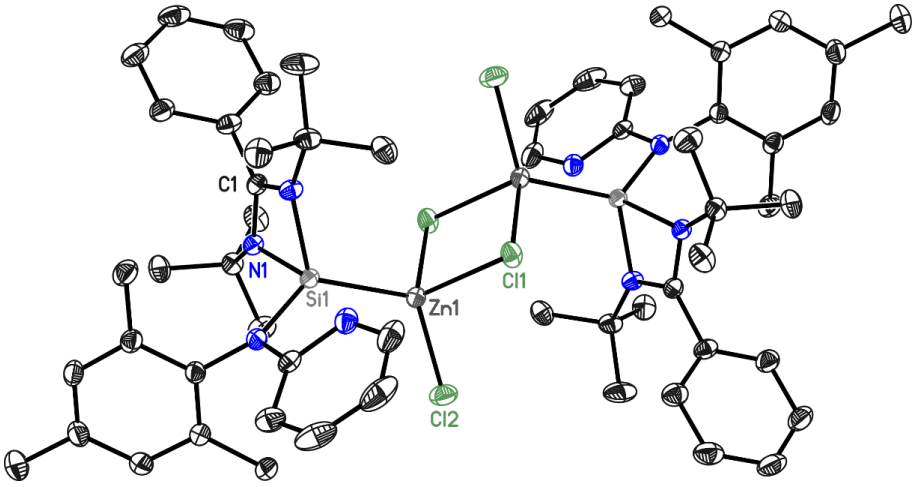

Figure 16. Crystal structure of **14**. The complex crystallizes in the space group $P2_1/c$ in a monoclinic crystal system with a = 12.968(2) Å, b = 12.560(2) Å, c = 22.982(3) Å and β = 93.73(2)°. The hydrogen atoms, disorder and solvent molecules has been omitted for clarity. The anisotropic displacement parameters are depicted at the 50% probability level.

Table 12. Selected bond lengths [Å] and angles [°] for complexes **14**, **13**, **[(NHSiHMDS)(ZnI$_2$)]$_2$** by *Sen et al.* (2017[188]) and **[(LSi(HMDS))(ZnCl$_2$)]** (with L = (*i*Pr)$_2$NC(NDipp)$_2$) by *Tacke et al*. (2016[187]).

	14	**13**	**[(NHSiHMDS)(ZnI$_2$)]$_2$**	**[(LSi(HMDS))(ZnCl$_2$)]**
Si–Zn	2.3726(5)	2.380(2)/2.385(16)	2.4096(3)	2.3784(7)
Zn–Cl	2.2364(5)	2.156(14)/2.190(2)	2.58023(16)	2.2039(11)/2.2036(10)
Zn–μ-Cl	2.3667(6)/2.4241(5)	2.310(13)/2.385(2)	2.7223(2)/2.7373(2)	
Zn–μ-Cl–Zn	88.542(15)	86.60(8)	89.138(4)	
μ-Cl–Zn–μ-Cl	91.457(15)	93.40(8)	90.861(4)	
Si–N3	1.7780(12)		1.7163(8)	1.734(2)
N$_{Py}$---Zn	3.419			

In comparison to the aforementioned structures, the shortened Si–Zn bond length of **14** is more comparable to other monomers (e.g. Table 12, 2.3784 A) and therefore further differentiating from related dimeric complexes. Although, the novel Si–N3 bond length shows to be fairly longer than other Si–N bonds of that type (e.g. 1.7780(12) → 1.7163(8) Å) it is still in the typical range of such compounds and in addition similar to the previously characterized gold(I) complex **[(NHSiMes)(AuCl)]** (**12**) (1.781(3) Å), which shows also no coordination to a metal atom by the N-donors.

Interestingly, the lone-pair of the pyridyl nitrogen atom of **14** shows a very similar orientation and distance towards the metal atom as in the Au(I)-complex **12** (3.419 vs. 3.436 Å), although the sterical constitution of the rhomboidal core is quite different, which aroused interest in the matter. A coordination can also be excluded here, since N$_{Py}$–Zn bond lengths usually range from 1.939 to 2.498 Å. However, a possible explanation for the orientation of the lone-pair located at the N$_{Py}$ of **12** and **14** could be found when considering that it is not directed towards the metal atom, but to the Si(II) atom

instead. This would indicate an interaction similar to the "double-donating" NHSis presented by *Tacke et al.*[187,190] As described in Chapter 1.5, they investigated various TM complexes of benzamidinato and guanidinato based NHSis. These silylenes showed an additional donation of the side-arm concomitant to metalation reactions. The determined Si–N bond lengths ranged from 1.798 to 2.157 Å.[20,183,191] Even though the N_{Py}---Si distances in complex **12** (2.494 Å) and **14** (2.419 Å) were significantly longer, the orientation of the functional group inclines slightly to the side, further suggesting a similar interaction of the pyridyl nitrogen lone-pair with the Si(II) atom. (see Table 13)

Table 13. Selected bond distances [Å] and angles [°] for complexes **12** and **14**. (**Left** & **Right**) Corresponding crystal structures for visual comparison purposes. The point of view was set along the M–Si bond. The hydrogen atoms, disorder, solvent molecules and anisotropic displacement has been omitted for clarity.

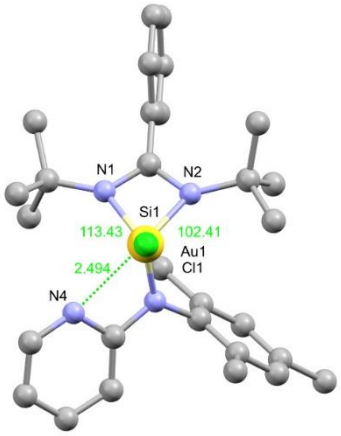

12		**14**
2.494	**N4---Si**	2.419
113.43(16)	**N1–Si1–N3**	114.29(6)
102.41(16)	**N2–Si1–N3**	102.17(5)

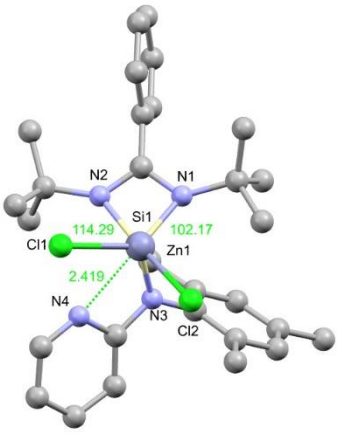

Furthermore, the group of *Tacke* discussed theoretical studies of free guanidinato NHSis in 2015 reporting Si–N bond lengths of 1.877 up to 2.461 Å which approaches the values of **14** and **15** very closely (see Scheme 98, left).[192] Drawing the comparison to the higher homologue germanium, the group of *Driess* reported the synthesis of a pincer type NHSi ligand coordinating a GeCl moiety with a N_{Py}–Ge distance of 2.594 Å and characterized this as a weakly coordinating pyridyl group (see Scheme 98, middle).[193] In 1999 the group of *Gómez* synthesized and analyzed a series of siloxanes utilizing a pincer type scaffold and reported a weakly coordinating pyridyl nitrogen to the Si(IV) atom with one of the longest N_{Py}---Si distances reported (2.790(3) Å).[194,195]

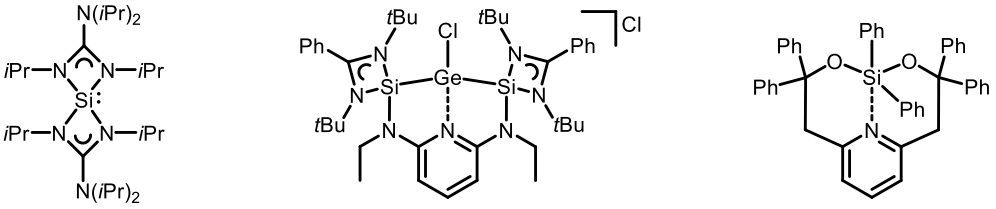

Tacke et al. *Driess et al.* *Gómez et al.*

Scheme 98. Exemplary compounds: (**left**) free guanidinato NHSi featuring "double-donation" by *Tacke et al.* in 2015[192]; (**middle**) pincer type NHSi exhibiting a weakly coordinating pyridyl group by *Driess et al.* in 2016[193]; (**right**) pincer type siloxanes with a weakly coordinating pyridyl group *Gómez et al*. in 1999[194].

Certainly, the significant distance N_{Py}---Si(II) of **12** and **14** somehow questions such interactions, yet, the aforementioned observations in related systems supports the assumption of a possible weak coordination. Nevertheless, such interactions are very challenging to verify which is why it can only be speculated about within the framework of this thesis, but should be subject of future work.

The ^{1}H and ^{13}C NMR spectra showed the corresponding additional signals derived by the introduction of the mesityl- and pyridyl-group in the aromatic region as well as the methyl groups, hence confirming the successful isolation of the above stated structure. As mentioned, while analyzing the silver(I) and gold(I) complexes **10** and **12**, the ^{1}H NMR multiplets derived by the free pyridyl-group proved to be way sharper than their bidentate complexated congeners as seen in the ^{1}H NMR spectra of **7a-c**. Unfortunately, besides this resemblance of **14** to **10** and **12**, the trend that an ^{29}Si NMR signal could not be detected continues as well. Fortunately, in addition to the XRD analysis, the LIFDI mass spectrometric spectra also confirmed the presence of the low-valent silicon(II) atom by the detection of a peak at m/z = 1177.3, which did not represent the molecular ion peak, but the equally important fragment $[M\text{-}Cl+2H]^{+}$. The elemental analysis confirmed the ligand to metal halide ratio of 1:1 as well.

In conclusion, the hitherto developed *post-complex functionalization* was successfully applied to the novel NHSiCl zinc(II) halide complex **13**. The introduction of the side-arm did not give a bidentate ligation under monomerization from the rhomboidal core. The distortion however illustrates the influence of the functionalization. Nevertheless, the question whether it is possible to synthesize and isolate a monomeric complex solitary coordinating a $ZnCl_2$ moiety in a bidentate fashion, is still under investigation. The following chapter should illustrate exactly this issue.

3.2.4.3. Reactivity of NHSiCl towards Organo Zinc(II) Salts – [(NHSiPh)(ZnCl$_2$)]

A possible pathway to monomeric NHSi Zn(II) complexes was inspired by former work of our group, who used *inter alia* M(HMDS)$_2$ precursor to *in situ* deprotonate amines to gain access to novel, e.g., amino zinc(II) complexes.[196,197] If such metal silylamides would be coordinated to the hitherto utilized starting material NHSiCl (**1**), subsequently *in situ* deprotonating the side-arm amine (ArNHPy), accompanied by the loss of HHMDS and the concurrent coordination of the amino ligand to the free coordination site at the Zn atom, this ligand could undergo an *amino-halide-shift* similar to the *alkyl-/aryl-halide-shifts* discussed in the previous chapters, leading to the desired compound (see Scheme 99).

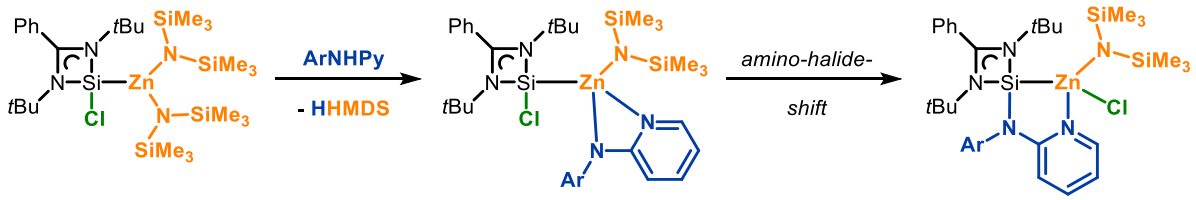

Scheme 99. Proposed synthetic route to a monomeric zinc(II) silylene complex employing a novel pyridine-based side-arm *via in situ* deprotonation of the amine utilizing a novel Zn(HMDS)$_2$ complex and taking advantage of previously shown reactivity (*alkyl-/aryl-halide-shifts*) of Zn(II) silylene complexes.

Though, it has to be noted, that such a shift could already take place after the coordination of **1** to the according zinc(II) silylamide, leading to zinc halide centers and the well-known silylene **NHSiHMDS**. Zincorganyls, especially ZnMe$_2$,[197] are also able to act as deprotonating reagents, but the aforementioned reaction behavior already proved, that alkyl-groups undergo a shift, hence disqualifying themselves for this purpose.

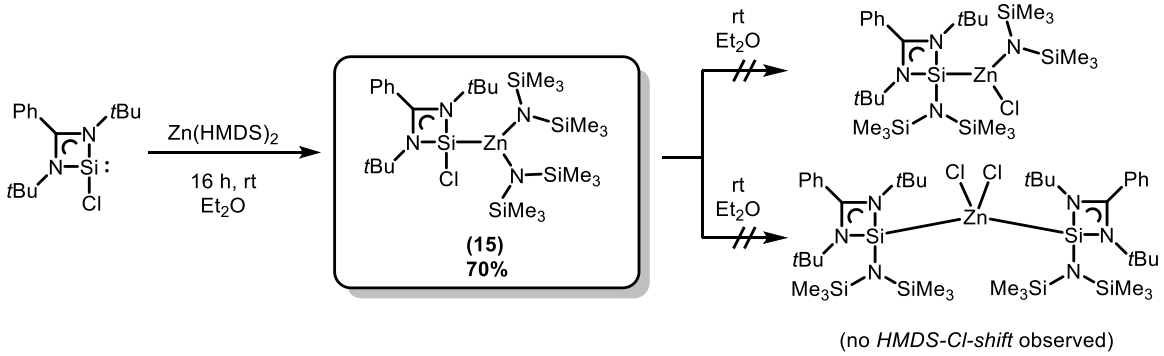

Scheme 100. Synthesis of the novel 1,3-*N*,*N*'-di-*tert*-butyl-benzamidinato-chloro-silylene-zinc(II)-bis(bis(trimethylsilyl)amide **[(NHSiCl)(Zn(HMDS)$_2$)]** (**15**). An *amino-halide-shift* as potential side reactions, hence the formation of zinc halide complexes, were not observed.

The synthesis of Zn(HMDS)$_2$ is well-known and was prepared according to existing literature procedures or are commercially available.[198,199] Two separate prepared solutions of the chloro benzamidinato silylene **1** and the precursor Zn(HMDS)$_2$ in diethyl ether were combined and stirred at ambient temperature. The solution turned slightly yellowish overnight and was concentrated

afterwards, to subsequently store it at -35°C for one day. The target compound initially crystallized in form of very fine and thin colorless needles, which were filtrated and dried under reduced pressure. In order to purify the crystalline solid, it was recrystallized from a mixture of diethyl ether and hexane (1:1) at -35°C yielding colorless blocks, which were also suitable for X-ray diffraction analysis.

As shown in Scheme 100, the isolated compound indeed turned out to be the desired complex **15**, without signs of possible pursuing reactions, such as the aforementioned amino-halide-shifts. Compound **15** appeared to be extremely sensitive towards air and moisture, but was analyzed *via* ^{1}H and ^{13}C NMR spectroscopy, CHN analysis and XRD analysis. As usual, the ^{1}H NMR spectrum showed slightly downfield shifted singlets derived by the characteristic *tert*-butyl group (1.25 ppm), as well as the aromatic signals of the phenyl-group also located at the benzamidinato scaffold (7.77 to 7.26 ppm). In addition, a singlet at 0.16 ppm was determined as the newly introduced $SiMe_3$-groups, showing a corresponding ^{1}H ratio determined by their integrals, indicating chemically equivalent TMS-groups, hence a free rotation of the residues. The ^{13}C NMR spectra exhibited the corresponding signals in appliance to the above discussed ^{1}H signals. Strangely, the ^{29}Si NMR spectrum exhibited no signals, neither from the low-valent silicon(II) atom, nor from the TMS-groups. The experimental results determined by the CHN analysis showed excellent compliance to the calculated values of the supposed structure **15** further supporting the successful synthesis and isolation.

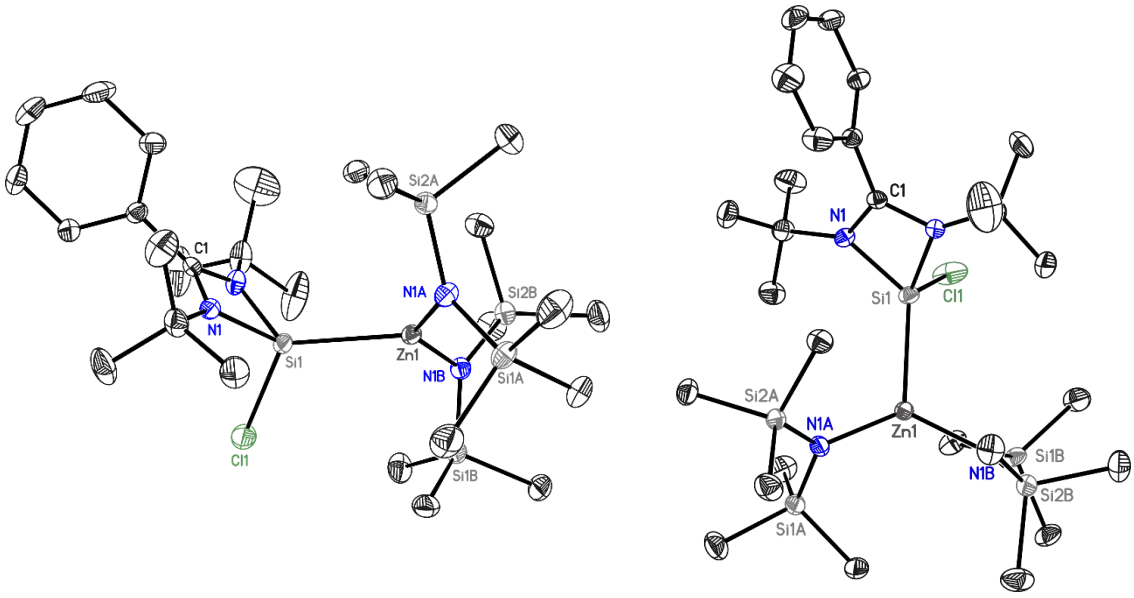

Figure 17. Crystal structure of **15** (**left**: side view; **right**: top view). The complex crystallizes in the space group $P2_1/n$ in a monoclinic crystal system with a = 20.074(3) Å, b = 10.662(2) Å, c = 21.508(3) Å and β = 114.47(2)°. The hydrogen atoms, disorder and solvent molecules has been omitted for clarity. The anisotropic displacement parameters are depicted at the 50% probability level.

Table 14. Selected bond lengths [Å] and angles [°] for complexes **15**, **[(I*t*Bu)(Zn(HMDS)$_2$)]** by *Baishya et al.* (2014[200]) and **[(*a*-IDipp)(Zn(HMDS)$_2$)]** by *Goicoechea et al*. (2014[201]).

	15	**[(I*t*Bu)(Zn(HMDS)$_2$)]**	**[(*a*-IDipp)(Zn(HMDS)$_2$)]**
Si–Zn	2.4965(7)	2.082(5)	2.008(1)
Zn–N1A/B	1.9269(11)/1.9328(11)	1.956(5)/1.985(5)	1.940(1)/2.000(1)
Si–Zn–N1A/B	112.23(4)/116.97(4)	110.90(19)/117.66(19)	107.60(6)/135.52(6)
N1A–Zn–N1B	130.79(5)	131.43(18)	116.87(5)

Due to the recrystallization from a diethyl ether/hexane mixture and the accompanied transformation of needles to block like colorless crystals suitable for single crystal X-ray diffraction analysis, it was possible to determine the solid state structure of **15** as well. As shown in Figure 17, the coordination of the NHSiCl ligand **1** to the Zn(II) atom was successful. The zinc atom unambiguously exhibits a trigonal planar geometry with a sum of the surrounding angles of approximately 360°. The Si–Zn bond length of 2.4965(7) Å is significantly longer than most of the above discussed halide complexes, but very similar to the monomeric silylene zincorganyl complex **[(NHSiC$_5$Me$_5$)(ZnEt$_2$)]** (2.4939(7) Å) by *P. W. Roesky et al*., also showing the same coordination geometry at the zinc atom.[186] Within this report, they compared *inter alia* computational studies of this Si(II)–Zn(II) bond to similar ones, concluding that bond lengths around 2.39 Å show a strong single-bond character and *vice versa*, longer bonds of 2.49 Å represent a weak single-bond. To the best of our knowledge, other low-valent silicon(II)–Zn(II)(HMDS)$_2$ bonds are not known, whereas certain structures containing the lighter homologue (NHC) were reported over the past decades. Although the NHC Zn(HMDS)$_2$ complexes by *Baishya et al.* (2014)[200] and *Waters* and *Goicoechea* (2003)[201] also hold sterically demanding residues adjacent to the low-valent atom (*tert*-butyl- and Dipp-groups), both show considerably shorter C–M bond lengths (2.082(5) and 2.008(1) Å, respectively; see Table 14). This most likely is caused by the different electronical properties of carbenes, since most NHC Zn(II) complexes show bond lengths around 2.0 Å.[185,202,203]

The following reaction step should involve the deprotonation of an amine in the presence of the novel isolated Zn(HMDS)$_2$ complex **15**. Therefore, a solution of **15** and **PhNHPy** in THF was stirred at ambient temperature. The reaction was initially monitored *via* ^{1}H NMR spectroscopy to control if the formation of novel species can be observed. When no changes could be distinguished after several days at room temperature and constant stirring, the reaction mixture was heated up to approximately 50°C. The formation of a grey solid and the detection of various insignificant ^{1}H NMR signals suggested a decomposition under the formation of elemental zinc. Further attempts showed the same behavior, which was the reason, one equivalent of LiHMDS was added to the reaction mixture at -30°C, in order to see if the deprotonation can be forced by the utilization of a strong base. Unfortunately, this procedure also led to the formation of a grey solid, which suggested another decomposition reaction.

Even after certain attempts it was not possible to isolate any meaningful products. However, at some point the formation of few crystals was observed, which showed to be suitable for single crystal analysis. The structure solution of these colorless crystals gained minor insights of possible products, as shown in Scheme 101.

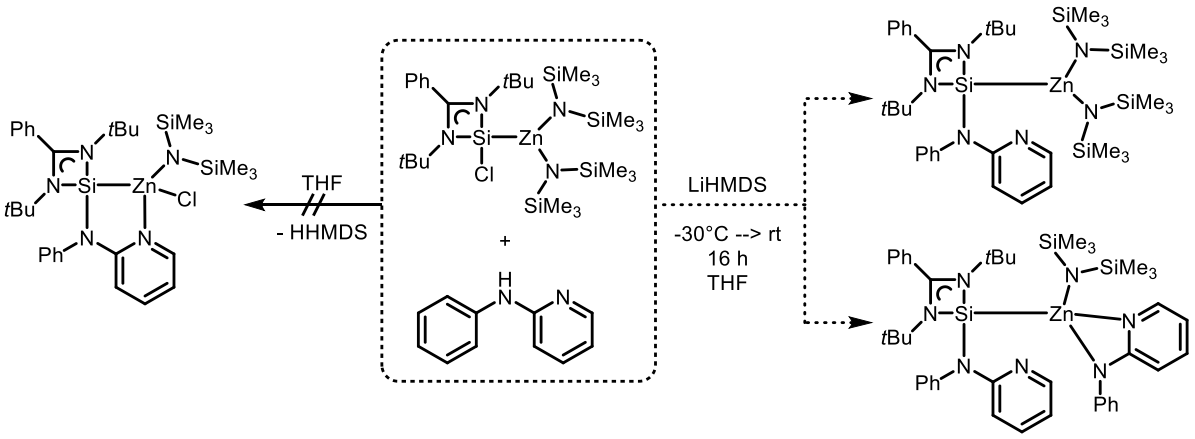

Scheme 101. Proposed synthesis of certain byproducts after treating the reaction mixture with LiHMDS.

Interestingly, the determined crystal structure revealed two compounds, the successful functionalization of the chloro-group with the amine **PhNHPy**, as well as a second structure, which arises due to a disorder of one HMDS-ligand with another PhNPy group, that is bound to the Zn(II) atom by both nitrogen atoms. The occupation of the aromatic amide substituent was determined to less than 7%. Although the isolation of the crystal was rather serendipitous, a closer look at the bond lengths and angles can provide insights into the influences that a functionalization can have (see Table 15). For example, **[(NHSiPh)(Zn(HMDS)$_2$)]** exhibits a shortened Si–Zn bond lengths (2.4644(5) compared to 2.4965(7) Å), thus indicating a strengthening influence of the substitution on the silicon(II) metal bond. Certainly, the trigonal planar geometry at the zinc atom was preserved with a total sum of 359.74° around the metal atom. The additional amino group of **[(NHSiPh)(Zn(HMDS)(PhNPy))]** located at the Zn(II) atom, expands its geometry to a tetrahedral distorted one, where the new Zn–N bonds of the amino and pyridyl nitrogen are fairly elongated in comparison to the HMDS ones. The negatively charged amino nitrogen atom shows a shorter bond to the Zn(II) atom than the pyridyl nitrogen (2.063(16) *vs*. 2.248(12) Å), but most importantly, the Si(II)–Zn(II) bond length was remarkably shortened (2.339 Å), due to the change of the HMDS by the PhNPy group.

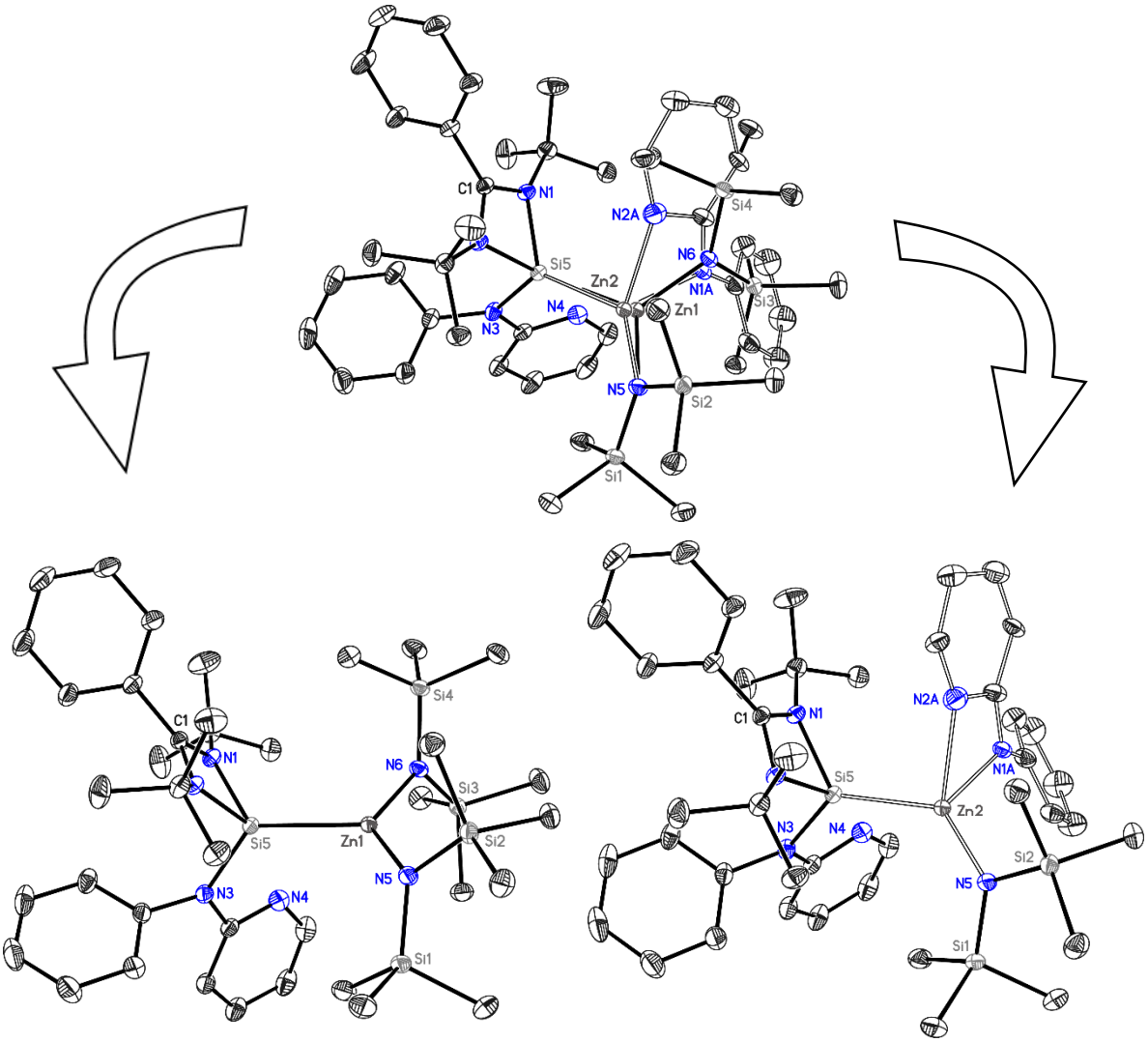

Figure 18. Crystal structure of **[(NHSiPh)(Zn(HMDS)$_2$)]** / **[(NHSiPh)(Zn(Ph)(HMDS))]**. The compound crystallizes in the space group $P2_1/n$ in a monoclinic crystal system with a = 13.075(2) Å, b = 18.707(2) Å, c = 18.776(3) Å and β = 92.05(2)°. The upper structure shows both disorders overlapped. The hydrogen atoms and solvent molecules has been omitted for clarity. The anisotropic displacement parameters are depicted at the 50% probability level.

Table 15. Selected bond lengths [Å] and angles [°] for complexes **[(NHSiPh)(Zn(HMDS)$_2$)]**, **15** and **[(NHSiPh)(Zn(HMDS)(PhNPy))]**.

	[(NHSiPh)(Zn(HMDS)$_2$)]	**15**		**[(NHSiPh)(Zn(HMDS)(PhNPy))]**
Si–Zn1	2.4644(5)	2.4965(7)	**Si–Zn2**	2.339(3)
Zn1–N5/6	1.9632(10)/1.965(8)	1.9269(11)/1.9328(11)	**Zn2–N5**	1.864(3)
			Zn2–N1A/N2A	2.063(16)/2.248(12)
Si–Zn1–N5/6	117.13(4)/119.12(3)	112.23(4)/116.97(4)	**Si–Zn2–N5**	130.85(14)
			Si–Zn2–N1A/N2A	94.4(4)/110.8(6)
N5–Zn1–N6	123.49(4)	130.79(5)	**N5–Zn2–N1A/N2A**	113.4(6)/125.3(4)

A possible reason for the competitive reaction can be found in the work of *Mulvey et al.*, who investigated the formation and reactivity of uncommon alkali-metal-zinc-reagents.[202–204] Treating Zn(HMDS)$_2$ with alkali-metal HMDS compounds, or in the presence of other nitrogenous organic bases, leads to the formation of very strong unusual bases. This could have led to the formation of unexpected

highly reactive compounds, hence unintended side-reactions, leading to the decomposition of **15**. However, since none of these compounds could be separately isolated, or detected *via* other analytical methods, the focus was set on more reproducible syntheses of novel monomeric NHSi zinc complexes bearing a pyridyl-based side-arm.

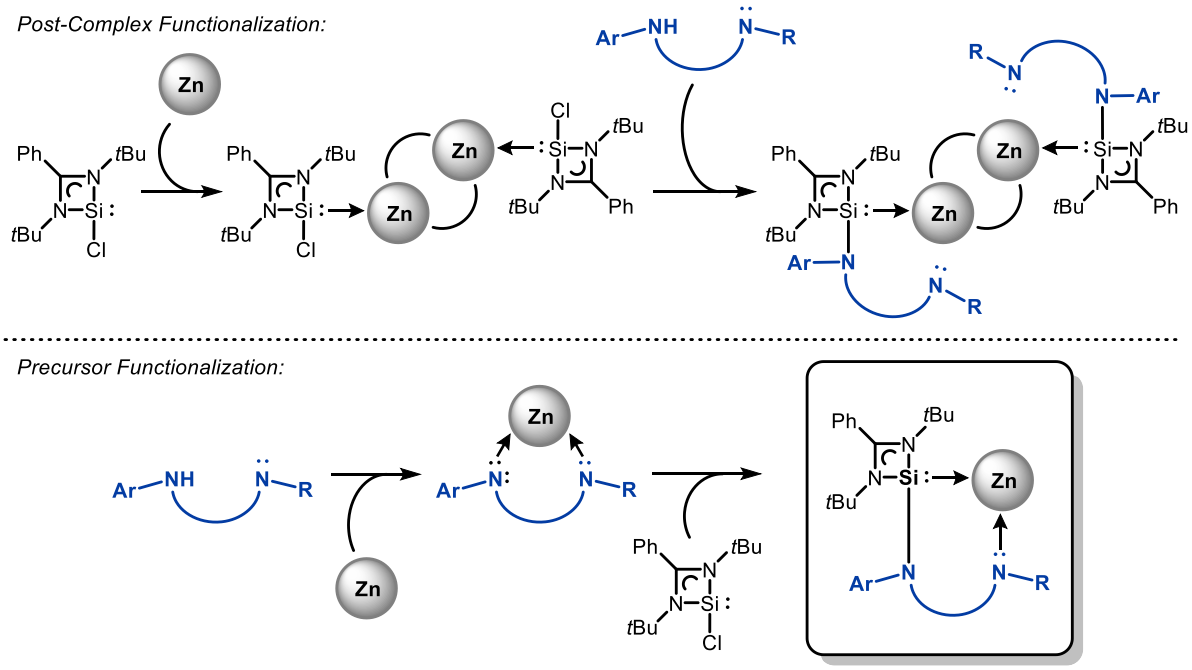

Scheme 102. Proposed application of the *precursor-method* to synthesize novel NHSi Zn(II) complexes.

In Chapter 3.2.1.3, the toolbox of synthetic methods was expanded by introducing the novel *precursor functionalization*, which, inspired by the work of *P. W. Roesky et al.*, also made use of the *ligand-halide-shift* behavior. Regarding NHSis, this method was initially illustrated by shifting carbonaceous alkyl- and aryl-groups only, but was extended to amino groups within this work, thus it proved to gain facile access to novel NHSis.

Therefore, the preceding synthesis of a suitable zinc(II) precursor is required. As already discussed in Chapter 3.2.1.3, in 2002, *Seco* and *González Garmendia*, *inter alia*, investigated the synthesis and characterization of certain copper(II) acetate salts, but also came along the synthesis of 2-anilinopyridinate copper(I) salts of the type **[(PhNPy)Cu]$_x$** (see Scheme 103, left).[167] This preceding work and the successful application to this work raised the question whether this method can be transferred to the synthesis and utilization of zinc precursors as well. The group of *Coles* and *Wheatley et al*. published the synthesis and structural characteristics of certain organo zinc complexes employing similar *N,N'*-bidentate ligands in 2004 (see Scheme 103, right).[199] They used the zincorganyl $ZnMe_2$ in order to deprotonate the amine under the release of methane to isolate the neat organo zinc(II) salt, as shown in Scheme 103. Since their presented ligand to metal atom ratio was 2:1, but a ratio of 1:1 was targeted, the two reactions should be combined or modified, respectively.

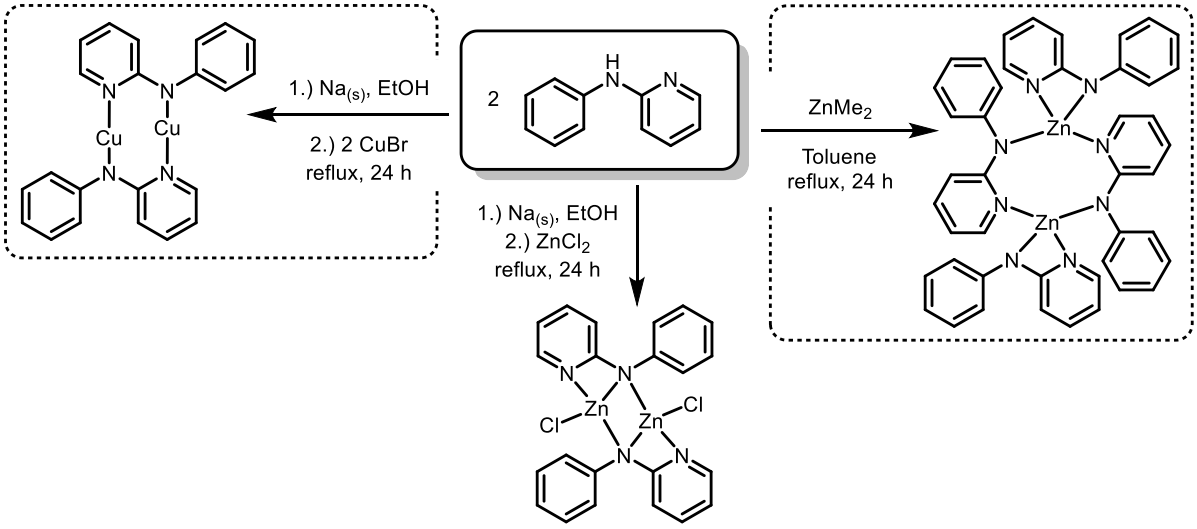

Scheme 103. Preceding work on the investigation of organo copper(I) salts, by *Seco* and *González Garmendia* (left, 2002[167]) and organo zinc(II) salts, by *Coles* and *Wheatley et al*. (right, 2004[199]), as well as the proposed combined/modified synthesis to novel organo zinc(II) salts, focused in this chapter (middle).

The required amine *N*-phenyl-*N*-(2-pyridyl)amine (**PhNHPy**) was synthesized following the procedures in Chapter 3.2.1.3. Under inert conditions, **PhNHPy** was dissolved in dry ethanol and equipped with a reflux condenser. Under vigorously stirring an equimolar amount of neat sodium was added under an argon flow in small portions and stirred for 30 min at ambient temperature. Subsequently, a separate solution of one equivalent of carefully dried $ZnCl_2$ in ethanol was transferred to the reaction mixture and heated to reflux overnight. The resulting orange suspension was filtered and all volatiles were removed under reduced pressure, resulting in an orange amorphous solid, which stayed solid under vacuum, but slowly turned to a very viscous state, when stored under argon atmosphere. It was soluble in THF, DCM and Et_2O, but formed two phases in toluene, hexane or pentane. Furthermore, it was highly sensitive towards air and moisture and quickly turned into a colorless suspension. In order to purify and analyze this compound, certain solutions employing different solvents and -mixtures were stored at -35°C to -80°C, but did not lead to the desired crystal growth or precipitation, but stayed in a viscous state. Hence, the target compound was analyzed as orange amorphous solid without further purification, *via* ^{1}H and ^{13}C NMR spectroscopy, CHN analysis and ESI mass spectrometry.

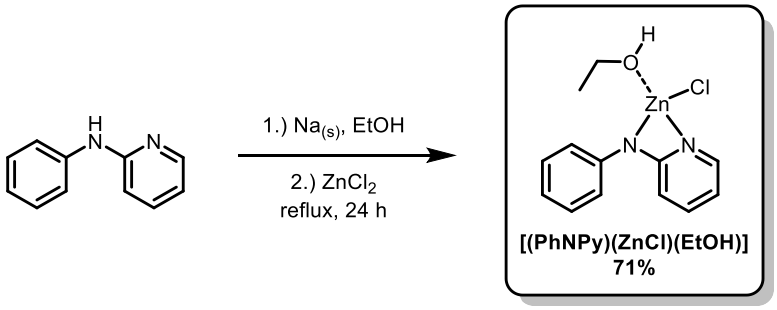

Scheme 104. Proposed synthesis of *N*-phenyl-*N*-(2-pyridyl)amine-zinc(II)-chloride ethanol **[(PhNPy)(ZnCl)(EtOH)]**.

The ^{1}H NMR spectrum was dominated by very broad signals, showing sporadic sharp signals in-between, mostly derived by traces of solvents. Although the broad peaks would not allow an assignment *via* its splitting, the integrated values and chemicals shifts fit to a deprotonated type of the utilized ligand **PhNHPy**, which endorsed the successful deprotonation. The broadened signals could suggest either a fluctuating structure and/or a successful metalation. Furthermore, there were two signals allocated in the upfield shifted region, which would fit to an ethanol molecule (5.12 ppm, O*H*; 3.97 ppm, CH_2CH_3; 1.22, CH_2CH_3). These also seriously broadened signals indicate a participation in the fluctuating structure, hence most likely coordinating a zinc(II) atom along with the amino ligand. Hence, a constitution of a deprotonated amino ligand, coordinating a zinc(II) halide core together with EtOH, or a multiple of such an aggregate can be assumed. These findings could also be a possible explanation for the highly viscous state of the compound.

Nevertheless, to gain deeper insights in the composition of this compound, low-temperature NMR studies were performed. A solution of **[(PhNPy)(ZnCl)(EtOH)]** in THF with TMB as an internal standard was monitored *via* ^{1}H NMR spectroscopy at different temperatures ([°C]: +50, +40, +25, +10, 0, -10, -20, -30, -40 , -50, -80), the results are shown in Figure 19**.** With temperatures above room temperature, the broadening of the signals increases, best to be seen at the marked peaks. Interestingly, with decreasing temperatures, the broad peaks in the area of the supposed EtOH starts to separate into two signals with different intensities, indicating an aggregate with a possible variable amount of coordinating molecules. The fact that these smaller signals show a better splitting than the rest, suggest that this molecule does not participate at the aggregation/complexation. In general, at temperatures of approximately +10 to -20°C many signals exhibit more pronounced splitting, before they undergo a very distinguished broadening, when going for temperatures towards -80°C, probably due to solubility effects.

As already mentioned and applied throughout this work, DOSY measurements can be used to determine the molecular weight of certain aggregates in solution and were also performed with compound **[(PhNPy)(ZnCl)(EtOH)]**. Unfortunately, no meaningful aggregates were determined, probably due to the highly fluctuating condition. Low-temperature DOSY measurements, to see if this potential effect can be suppressed, failed, probably due to an increased viscosity at low temperatures.

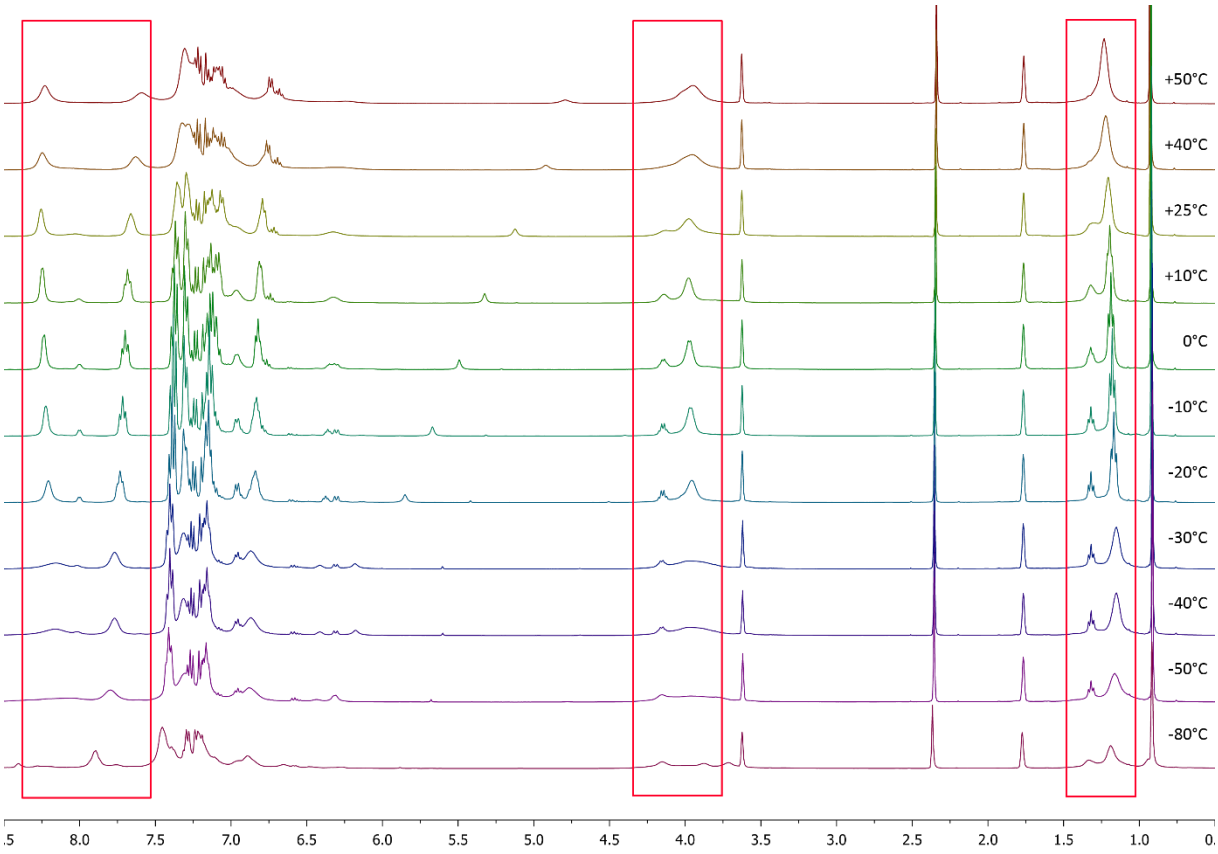

Figure 19. Temperature-depending ^{1}H NMR spectra of **[(PhNPy)(ZnCl)(EtOH)]**; chemical shift δ in [ppm].

To further investigate this challenging compound, ESI mass spectrometric analyses of **[(PhNPy)(ZnCl)(EtOH)]** were performed. The chances of detecting coordinating/accompanying solvents using such methods are rather low, but the isotope patterns of the depicted peaks at m/z = 439.1 $[(PhNPy)_2(ZnCl)+2H]^+$ and m/z = 403.1 $[(PhNPy)_2(Zn)+H]^+$ confirm the presence of a zinc halide moiety. Additionally, the ligand to metal atom ratio of these aggregates (2:1), are suggesting a dimeric constitution. However, from what is known from the ^{1}H NMR experiments, it is possible that the aggregates, derived by the mass spectra, do not have to correspond to the actual structure of this compound. It is possible, that the aggregation did undergo a change in its constitution during the process of the electrospray ionization, with a simultaneous loss of ethanol molecules. This assumption was also supported by the elemental analysis, which experimental values fit best to the calculated aggregate of **[(PhNPy)(ZnCl)(EtOH)]**, hence a ratio of 1:1:1. Future work should subject this structure to further analysis, such as thermogravimetric analysis (TGA), to determine whether and how much solvent is involved in the structure.

Under the assumption the ligand is present in a ratio of 1:1:1 the functionalization step was investigated. At -30°C a solution of the precursor **[(PhNPy)(ZnCl)EtOH]** in DCM was slowly transferred to a stirring solution of **1** in DCM. The reaction mixture quickly changed its color from deep orange to bright yellow and was left stirring overnight and allowed to warm up to ambient temperature. The

resulting clear yellowish solution was concentrated and hexane was added whereas an immediate crystal growth was observed. After storage overnight at -35°C the colorless crystals were filtrated and dried under reduced pressure (see Scheme 105).

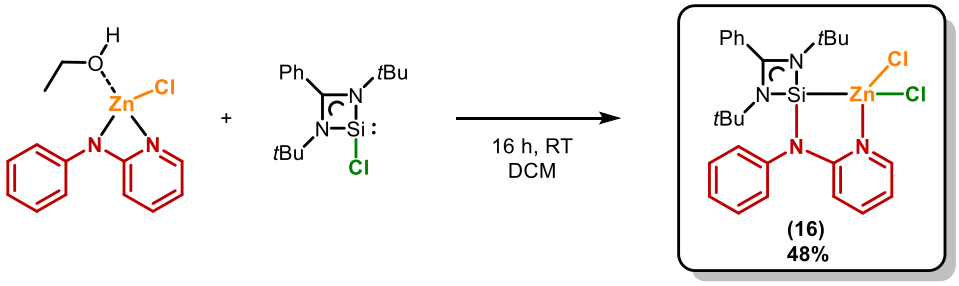

Scheme 105. Synthesis of 1,3-*N*,*N*'-di-*tert*-butyl-benzamidinato-*N*-phenyl-*N*-(2-pyridyl)amino-silylene-zinc(II)-chloride **[(NHSiPh)(ZnCl$_2$)]** (**16**) by applying the *precursor functionalization* utilizing the amino zinc(II) precursor **[(PhNPy)(ZnCl)EtOH]**.

The following analyses of the colorless crystals should confirm the successful synthesis of the monomeric NHSi Zn(II)Cl$_2$ complex as shown in Scheme 105. First and foremost, the XRD analysis elucidated the solid state structure (see Figure 20), not only illustrating the successful substitution of the chloro group with the amino group, but also the coordination of the side-arm to the zinc atom, leading to the formation of a five-membered metallacycle in a "-Si–Zn–N–C–N-" fashion. The Si–Zn bond length of 2.3822(5) Å is in fact slightly longer than the functionalized dimer of 2.3726(5) Å (**14**), whereas the Si–N bond to the side-arm is slightly shortened (1.7645(13) *vs*. 1.7780(12) Å). The geometry around the zinc(II) atom shows to be tetrahedrally distorted, which is most likely due to the bidentate coordination of **16**, which forces an unusual narrow bite angle Si–Zn–N^{Py} of 81.00(4)° on the Zn(II) atom, remarkably narrower than the ideal tetrahedral angle (109.5°) or pentagon angle (108°) (see Table 16 for the remaining angles). Comparable structures which form the same metallacycle as **16** are rare, but the comparison can be drawn to the similar five-membered metallacycles of the type "N–C–C–N–Zn(Cl$_2$)". The range of the corresponding N–Zn–N^{Py} angles lies between 72.29° and 83.74°, wherein **16** lies in the upper range.

Table 16. Selected bond lengths [Å] and angles [°] for complexes **16** and **14**.

	16	**14**		**16**
Si–Zn	2.3822(5)	2.3726(5)	**Si–Zn–Cl1**	122.987(17)
Si–N3	1.7645(13)	1.7780(12)	**Si–Zn–Cl2**	119.537(16)
Zn–N^{Py}	2.1472(12)		**Cl1–Zn–Cl2**	114.458(19)
Zn–Cl	2.2448(4)/2.2480(5)	2.2364(5)	**N^{Py}–Zn–Cl1**	104.99(4)
N3–Si–Zn	98.79(4)		**N^{Py}–Zn–Cl2**	102.03(4)
			Si–Zn–N^{Py}	81.00(4)

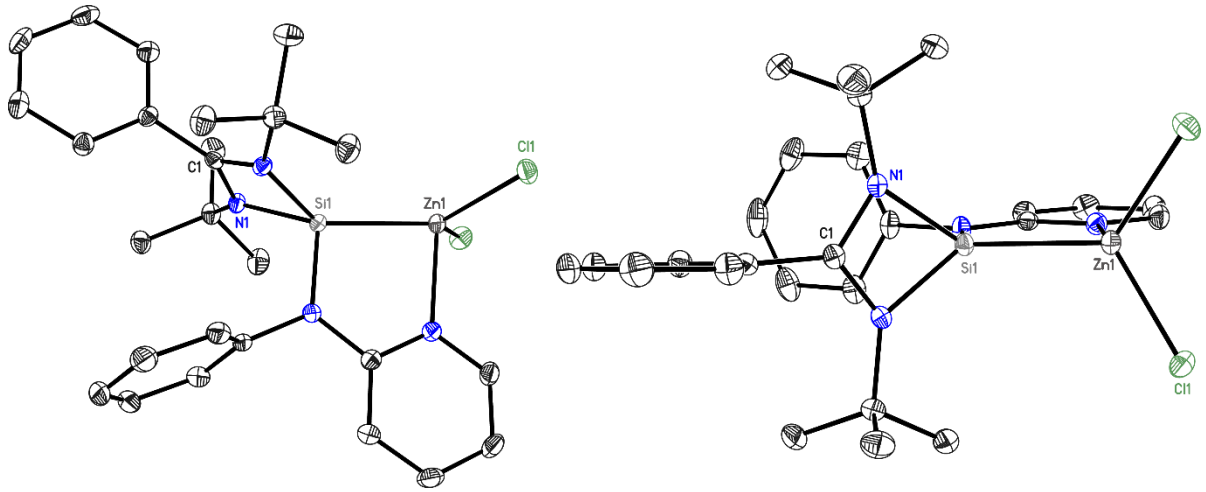

Figure 20. Crystal structure of **16** (**left**: side view; **right**: top view). The complex crystallizes in the space group *P*bca in an orthorhombic crystal system with *a* = 11.876(2) Å, *b* = 17.452(3) Å and *c* = 29.138(5) Å. The hydrogen atoms, disorder and solvent molecules has been omitted for clarity. The anisotropic displacement parameters are depicted at the 50% probability level.

The additional signals appearing in the ^{1}H and ^{13}C NMR spectra can be unambiguously assigned to the novel introduced PhNPy side-arm group and are located in the expected regions, when compared to **7a-c**, **8**, **10**, **12** and **14**. Similar to the previous functionalized complexes presented throughout this work, it was also not possible to detect any ^{29}Si signals. Still, the complementary analyses support the presence of the low-valent silicon(II) atom, as well as the LIFDI mass spectrometric analyses by identifying the m/z = 527.2 $[M\text{-}Cl]^+$ and corresponding fragments (m/z = 463.2 $[M\text{-}ZnCl]^+$, 428.3 $[M\text{-}ZnCl_2]^+$). Also the experimental values determined by the elemental analysis fit the calculated values for the shown structure of **16**. Noteworthy, that this monomer also proved to be stable towards dimerization reactions to complex **14** independently from the utilized solvent, contrary to the results described by *Sen et al*. previously discussed.

In conclusion, even though the synthesis to the novel NHSi Zn(II) complex [(NHSiCl)(Zn(HMDS)$_2$)] **15** was successful, the desired deprotonation of the amine *via* one HMDS ligand failed. Following addition of commonly used LiHMDS led primarily to the decomposition of the complex. However, the *precursor functionalization*, introduced in the synthesis of novel NHSi Cu(I) complexes in Chapter 3.2.1.3, was successfully applied to the synthesis of novel zinc(II) complexes. Therefore, leading to the isolation of the monomeric Zn(II)Cl$_2$ complex [(NHSiPh)($ZnCl_2$)] **16**, which could not be isolated by employing the previous *post-complex* method, but only the dimeric congener **14**. Thereby, it was possible to additionally isolate a novel organo zinc(II) salt **[(PhNPy)(ZnCl)(EtOH)]**, showing a challenging structure determination.

The results presented throughout Chapter 3.2.4 demonstrate the huge potential of these two methods. Depending on which method was used, it was possible to control the reactivity to form two

different complexes, either the monomeric or the dimeric complex. It illustrates the difference whether the transition metal atom is pre-coordinated by the silylene **1**, followed by the introduction of the side-arm, or if is pre-coordinated by the side-arm functionality in form of an organo TM salt (see Scheme 106).

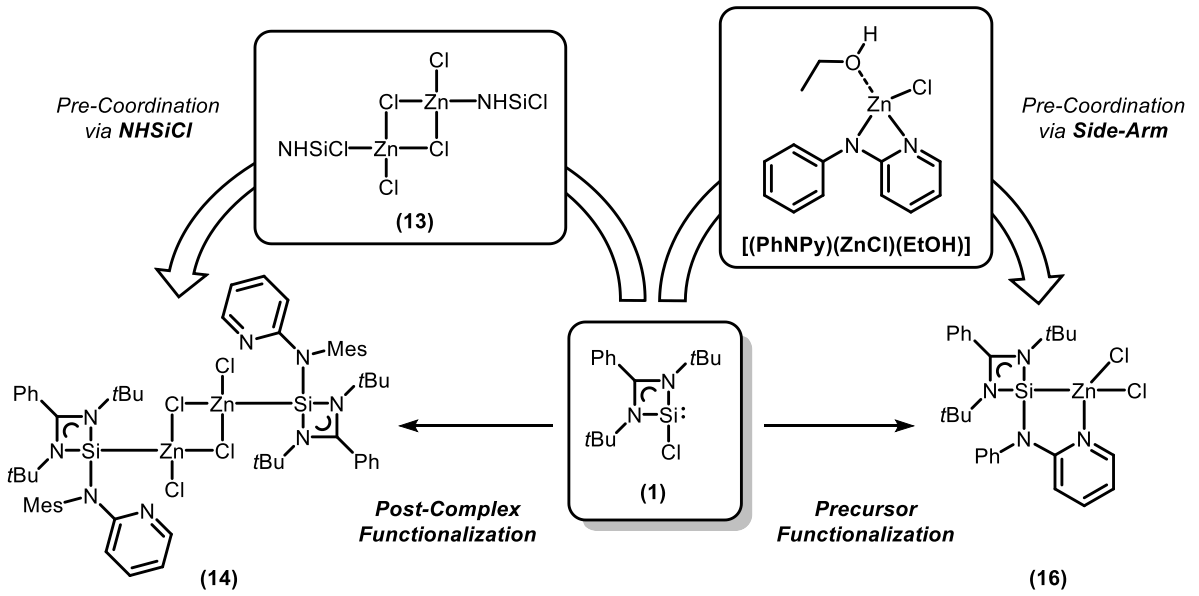

Scheme 106. Schematic overview of the different techniques applied to yield different formations.

Further efforts should concentrate on the modification of the side-arm, not only to expand the scope of amines, but also to possibly enhancing the tuning of the ligand. The bite angle could potentially be controlled by the introduction of an additional methylene unit between the amino function and the pyridyl-group. Furthermore, modifying the amine by adding bulky residues or electron donating or withdrawing substituents could not only effect the metal complexation, but also lead to an improved synthesis of the organo zinc(II) precursor, by means of isolation and workup.

3.3. Catalysis

Besides the new synthetic approaches, which were investigated and applied throughout this work, it was also the intention to investigate the reactivity of new NHSi transition metal complexes. Drawing the direct comparison to the lighter homologue, the ubiquitous *N*-heterocyclic carbenes, the applications of silylenes as ligands in organometallic catalysis are still comparatively scarce, yet emerging in various fields, depending on the employed transition metal, e.g. Co,[19,205] Rh,[68] Ir,[44,68] Fe,[67] Pd,[66,69] or Ni.[76,206] Some of these examples were already presented and discussed in the introduction of this work (see Chapter 1.3, p.16). Over the past years, certain groups have illustrated the potential of NHSi TM complexes in their studies or summed up in reviews, showing that the catalytical activity and selectivity can be increased by the utilization of NHSis, hence proving that silylenes are not only isoelectronic substitutes for phosphines or carbenes.[2,22,67,129] These up-and-coming studies inspired the examination of the catalytical potential of the hitherto isolated NHSi copper(I) complexes by checking their reactivity in the field of the renowned "Click"-chemistry. In particular, the difference in reactivity between the NHSiCl Cu(I) complexes **5a-c** and the functionalized successors **7a-c** should be emphasized, by reviewing them on a scope of commonly used azides and acetylenes at ambient temperature.

It has to be considered that the catalytical application within the framework of this thesis is not intended to be a comprehensive comparison to other literature known applications of copper(I) based catalysts, nor is it intended to provide a wide-ranging scope of subjected substrates or reaction conditions. The complexes **5b** and **7b** tested here should rather demonstrate the potential of the silylene ligands in a currently uncharted area and, above all, the influence of the functionalization on the reactivity among the two complexes.

3.3.1. Click Chemistry

In Chapter 3.2.1 and following, two alternative methods to the synthesis of the novel functionalized NHSi Cu(I) complexes **7a-c** were examined and successfully applied. After their characterization, they should be further investigated by means of focusing their reactive behavior towards possible catalytical activity. To date, there has been no catalytical application in the field of silylene copper(I) chemistry, hence potential catalytical behavior towards renowned reactions should be tested.

The copper(I)-catalyzed alkyne-azide cycloaddition (CuAAC) is based on the *Huisgen* 1,3-dipolar cycloaddition and is one of the most established and investigated transformations of the so-called "Click"-chemistry.[207,208,209] The concept behind this term was developed by *Sharpless et al.* in 2001 and describes reactions showing a high efficiency (e.g. one pot reaction, minimal harmless byproducts,

high thermodynamic driving force, high reaction specificity), to which the CuAAC reaction can be assigned.[210] The recent decades resulted in noteworthy applications in nearly every field of chemistry.[211,212] Especially NHC Cu(I) complexes have been extensively studied and applied in “Click”-chemistry, thus illustrating their huge potential in this field of catalysis.[213,214,215]

The so-called *Huisgen* reaction can be performed without any catalyst, by stirring the substrates at 100°C over several hours, yielding in the transformation of two constitutional isomers.[216] Thanks to further development of *Fokin* and *Sharpless et al*.[217] as well as *Meldal et al*.,[218] this reaction could be carried out regioselectively by the utilization of a copper(I) catalyst to 1,4-substituted 1,2,3-triazoles as the main product. Basically, any source of copper(I) can be used as a catalyst. Yet, well-designed Cu(I)-complexes can increase the selectivity, decrease catalyst loadings or establish milder reaction conditions, to improve this reaction.[214,215,219]

When *Fokin* and *Finn* revealed crucial details of the CuAAC mechanism in 2005[220] and thereby the mandatory role of copper(I), following studies increasingly focused on certain copper species as the active part and illustrated their potential.[207,212,219,221,222] The mechanism shown in Scheme 107 is based on theoretical and experimental investigations.[209,221,223]

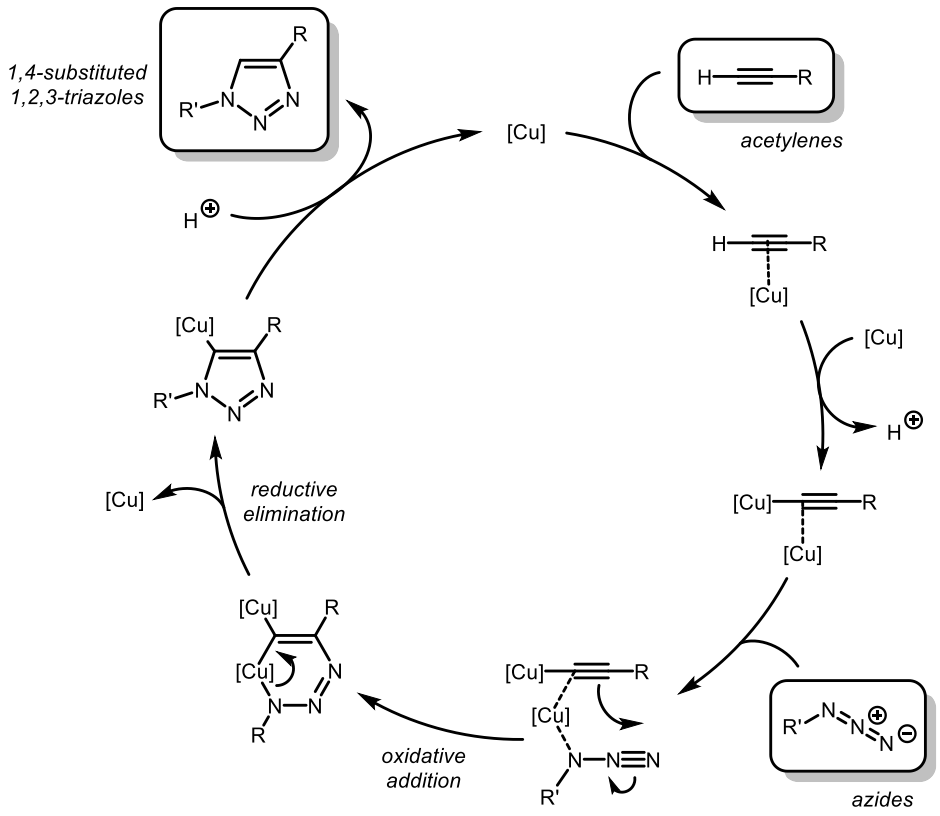

Scheme 107. Schematically illustration of the mechanism of the copper(I)-catalyzed alkyne-azide cycloaddition (CuAAC) aka. the *Huisgen* 1,3-dipolar cycloaddition ([Cu] describes a copper center with a varying number of ligands and oxidation states).

3.3.2. Catalytical Investigations of [(NHSiCl)(CuBr)]$_4$ and [(NHSiMes)$_2$(CuBr)$_3$]

The two NHSi Cu(I) complexes **[(NHSiCl)(CuBr)]$_4$** (**5b**) and **[(NHSiMes)$_2$(CuBr)$_3$]** (**7b**) were separately subjected to identical CuAAC reactions, to compare their catalytical activity to each other, in order to examine the influence of the functionalization and the side-arm coordination, respectively.

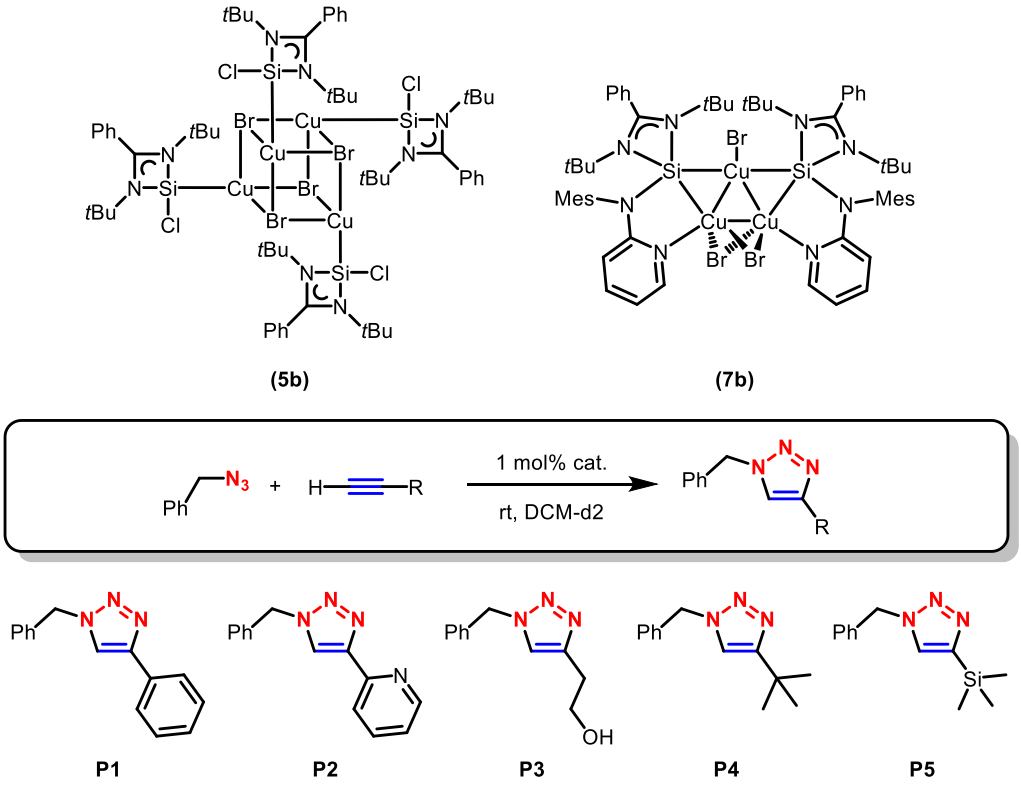

Scheme 108. General synthesis of the triazoles **P1-5** *via* the copper(I)-catalyzed alkyne-azide cycloaddition (CuAAC) conducted here (cat. = **5b**/**7b**; R = **Ph-CCH**, **Py-CCH**, **Butinol**, ***t*Bu-CCH**, **TMS-CCH**).

The progress of each reaction was monitored *via* time-scaled ^{1}H NMR spectroscopy. The corresponding solutions were prepared by adding benzyl azide (1.00 eq.), the appropriate alkyne (1.00 eq.) and adamantane as an internal standard to deuterated dichloromethane. On the basis of the internal standard the signals were normalized and the formation of byproducts was excluded. After one initial measurement of each solution, the complex **5b**/**7b** was added at ambient temperature and the measurement was started immediately (see Scheme 108). The alkyne scope comprised commonly used small alkynes (**Ph-CCH** = phenylacetylene; **Py-CCH** = 2-ethynylpyridine, **Butinol** = 3-Butyn-1-ol) and sterically more demanding ones (***t*Bu-CCH** = *tert*-butylacetylene; **TMS-CCH** = ethynyl-trimethylsilane). The results of the time-resolved measurements are depicted in Chart 1 and summarized in Table 17, respectively. Within the framework of these catalytical investigations, blank tests were performed for cross-checking to ensure that the determined conversion rates did not originate from possible traces of neat Cu(I)Br (see Chapter 5.2.2.2 for further details).

Chart 1. Time-conversion-diagram of the CuAAC reactions of benzyl azide with the corresponding alkynes (right) in the presence of 1 mol% **5b** (hollow icons) or **7b** (full icons) under inert conditions, in DCM-d2 at ambient temperature.

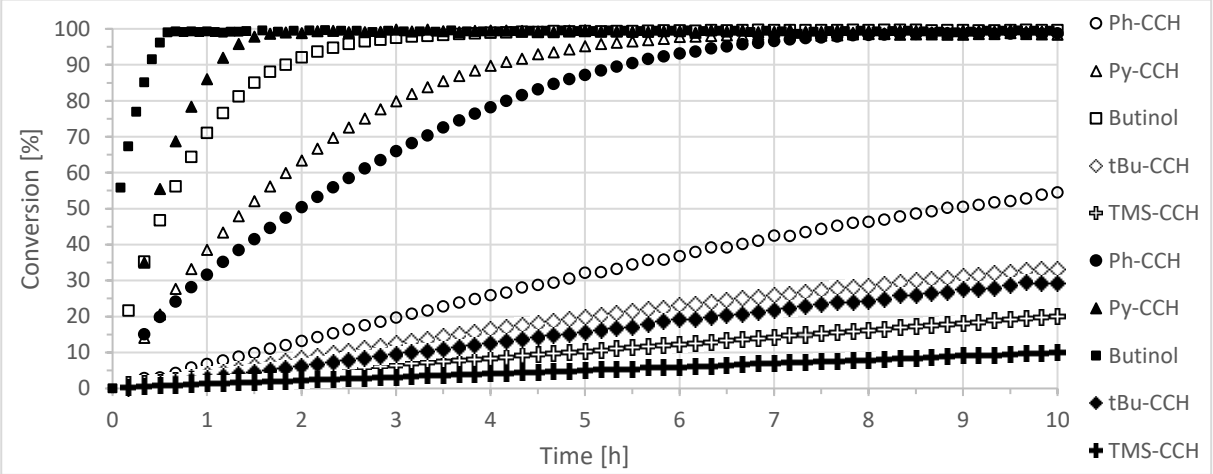

Both complexes show catalytical activity towards the transformation of 1,2,3-triazoles. Taking a closer look at the reactions to the 1,2,3-triazoles **P1-3** and comparing the corresponding curves shown in Chart 1, illustrates an overall trend that the functionalized trinuclear complex **7b** shows significantly improved conversion times than the tetrameric complex **5b**. For example, the quantitative conversion of **P2** and **P3** was already achieved after 1.5 h and 0.5 h, respectively, utilizing complex **7b** and therefore up to eight times faster as with **5b**. The formation of **P1** shows a half-conversion time of approximately 8.5 h using **5b**. Changing to complex **7b** leads to a full conversion within 8 h. At this point, it has to be noted, that conversion times in this area are not competitive when compared to the literature, since there are several examples, showing even higher conversion rates. However, these results illustrate the potential of silylenes as active catalysts and more importantly, that the functionalization, hence the introduction of the side-arm, significantly improves its reactivity.

Table 17. Conversions and conversion times of the 1,2,3-triazoles **P1-5**, monitored by ^{1}H NMR spectroscopic analysis. Yields were determined by integration of the benzyl signals of the corresponding ^{1}H NMR spectra normalized to an internal standard (adamantane).

	5b	**7b**
P1 (R = Ph)	~ 46 % (8 h)	**> 99% (8 h)**
P2 (R = Py)	> 99% (6 h)	**> 99% (1.5 h)**
P3 (R = C_2H_6OH)	> 99% (4 h)	**> 99% (0.5 h)**
P4 (R = *t*Bu)	**~ 33% (10 h)**	~ 29% (10 h)
P5 (R = TMS)	**~ 20% (10 h)**	~ 10% (10 h)

Former mechanistic investigations of dimeric NHC Cu(I) systems showed that they most likely tend to undergo decomplexation in solution during CuAAC reactions to form more reactive species.[219] Although MW determination measurements *via* DOSY NMR spectroscopy gave hints of a dimeric aggregate in a THF solution, it is questionable if the tetrameric pseudocubane **5b** undergoes similar

transformations in DCM as a solvent. Whereas the increased activity of the functionalized trinuclear complex **7b** definitely indicates an improved activity, due to enhanced ligand design. The increased activity could have different reasons: on the one hand, as described in Chapter 1.2, the introduction of electron donating groups adjacent to the low-valent silicon(II) atom leads to an increased σ-donor strength, which can show an influence on the Si–M bond and thus the reactivity of the metal center. On the other hand, in Chapter 3.2.1.2, some considerations were discussed, whether it would be possible, if the copper nitrogen coordination of the pyridyl-groups could cleave or not, in order to form reaction intermediates or transition states, respectively. Additionally, if a transformation of the tetrameric complex to smaller aggregates would be energetically inhibited, the cubane like structure could lack of suitable coordination sites.

The rather sterically demanding substrates (**P4**, **P5**) showed significantly longer conversion times in both cases. Since both catalysts show to be quite bulky, it is most likely, that the sterically demanding *tert*-butyl and TMS groups hinder the substrates from forming reactive intermediates and therefore the products. Especially since complex **7b** shows even slightly slower conversion times it is logical to assume, that the more complex design of the trinuclear compound inhibits the substrate from reacting or reaction intermediates are more shielded towards incoming substrates.

4. Summary and Outlook

While the overall objective of this thesis was to investigate novel *N*-heterocyclic silylene ligands and their transition metal complexes, the main focus laid on the development of alternative methodologies for synthesizing these functionalized NHSi TM complexes on the basis of the chloro benzamidinato silylene NHSiCl (**1**). In the context of functionalization reactions, the primary objective laid on the substitution of the chloro group of **1** with secondary amines bearing an additional donor-site, in order to serve as a side-arm adjacent to the low-valent silicon(II) atom.

Within the framework of this thesis it was possible to apply new types of donor groups to the conventional synthetic route (see Scheme 109, left), as well as develop and establish two new ways of synthesizing functionalized NHSis as TM complexes (see Scheme 109, middle & right), which will be summarized in the following.

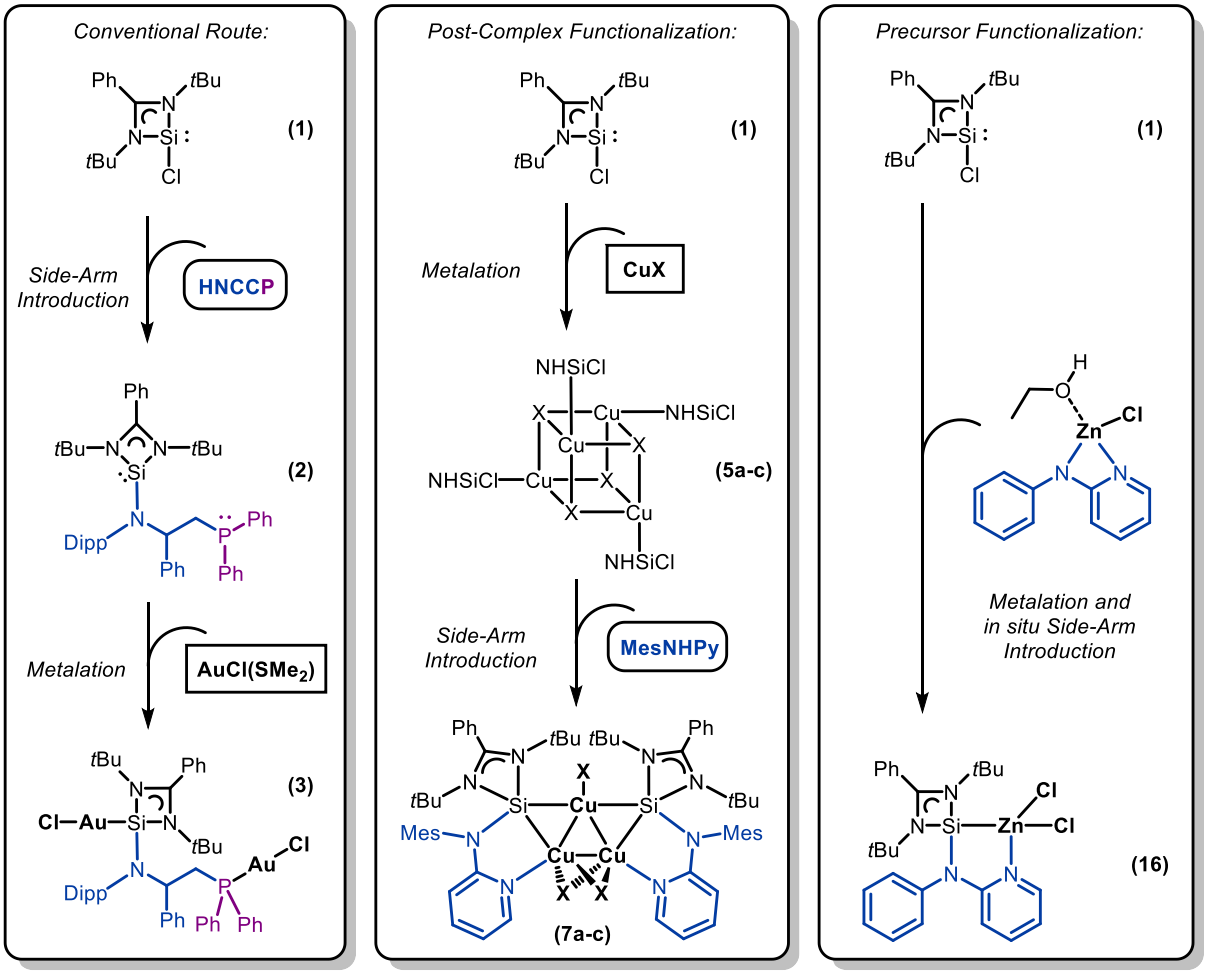

Scheme 109. Schematic overview of the hitherto applied and developed synthetic routes to the isolation of novel functionalized NHSis illustrated by certain examples. **Left**: conventional route *via* prior salt metathesis with the corresponding ligand (e.g. **HNCCP**) to the free silylene (e.g. **2**) and subsequent metalation (e.g. **3**). **Middle**: post-complex functionalization *via* prior isolation of NHSiCl TM complexes (e.g. **5a-c**), followed by the side-arm introduction *via* salt metathesis reactions of the corresponding amine (e.g. **MesNHPy**) (e.g. **7a-c**). **Right**: *In situ* substitution of the chloro group of **1** by utilizing organo TM salts in the *precursor functionalization* (e.g. **16**).

4.1. Investigating the Introduction of α-/β-Aminophosphines

The first chapters dealt with the investigation and introduction of phosphorous-based side-arms adapting the conventional method of derivatizing **1**. The corresponding α-aminophosphines (α-NP) were facile accessed by hydrophosphination reactions of the corresponding *Schiff* base and diphenylphosphine. However, subsequent salt metathesis reaction primarily led to the cleavage of the P–C bond, thus impeding the following substitution reaction, leaving the isolation of the free silylene **NHSiNCP** unattained. The β-aminophosphine **HNCCP** proved to show a diminished issue regarding the P–C bond cleavage. Following the preceding syntheses, the corresponding *Schiff* base was treated with the prior lithiated methyldiphenylphosphine resulting in the corresponding amine **HNCCP** after aqueous workup. The increased stability of the β-NP in solution led to the successful subsequent salt metathesis and hence the functionalization and isolation of the desired silylene **NHSiNCCP** (**2**), the first NHSi bearing a side-arm with an NCCP-backbone holding a phosphorous donor site.

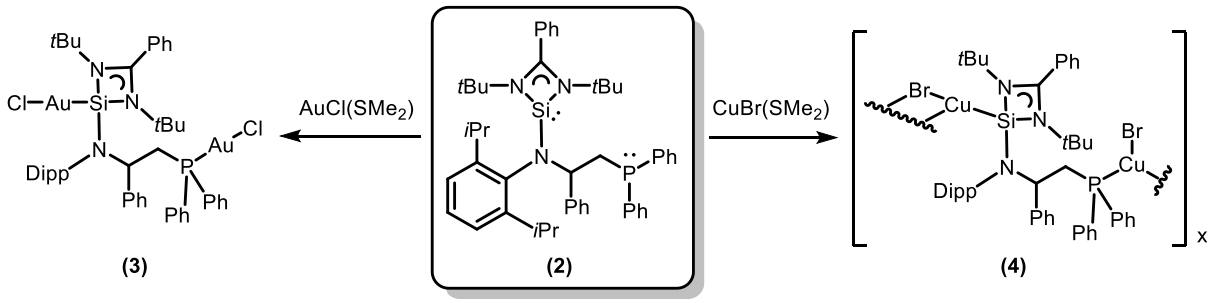

Scheme 110. Schematic overview of the novel functionalized silylene **2**, as well as its TM complexes **3** and **4**.

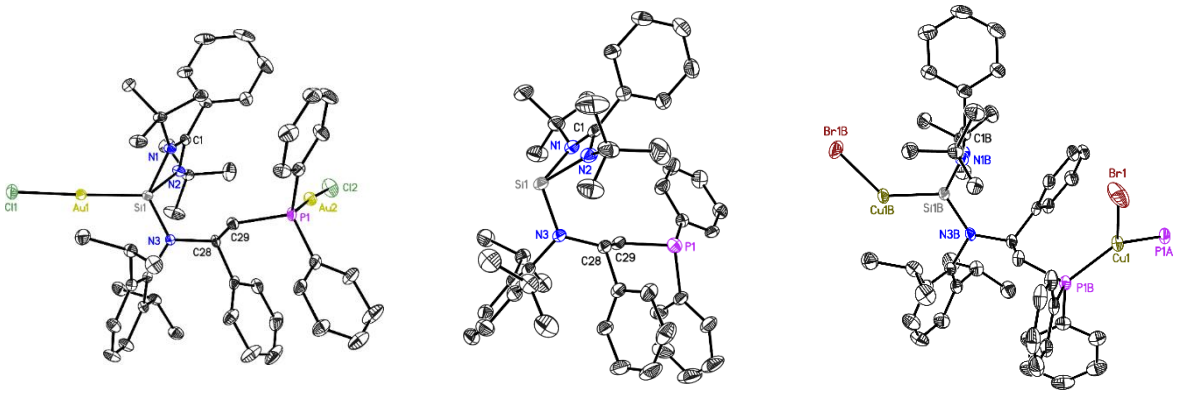

Figure 21. Crystal structures of the corresponding NHSi **2** and TM complexes **3** and **4**.

Treating silylene **2** with AuCl(SMe$_2$) led to the twofold coordination of the Si(II) and P(III) atoms forming the multinuclear complex **3** featuring linear gold(I) geometries. The reaction of **2** towards CuBr(SMe$_2$) resulted to a highly insoluble crystalline product, which challenging analysis was only accessable *via* XRD experiments, but revealed an interesting coordination polymer chain like complex **4** with a "-(head-tail-tail-head)$_x$-" constitution.

NMR spectroscopic analysis of compound **2** initially indicated the inhibited rotation of the side-arm around the new Si–N bond, to which the length of the β-NP backbone seemed to add a vital contribution as well. This constitution was pursued in the TM complexes **3** and **4**. Following efforts to generate a dimeric gold(I) complex and force the complex into a bidentate coordination by abstracting the halide using $AgSbF_6$ resulted in the decomposition of silylene **2**. Even though the bulky substituents and the length of the backbone made the ligand inflexible for bidentate complexations, its constitutions featured the formation of segregated multinuclear TM complexes.

Proceeding work could focus on the introduction of sterically less demanding substituents to get a hold on the inhibited rotation, yet, the length of the backbone seems too long to achieve such flexibility, thus it would be more promising to focus on the optimization of the shortened α-NP. At the end of Chapter 3.1.1 the synthesis of a phosphaneylidene-aniline was presented, which showed promising behavior upon following reactions and therefore could be considered as an alternative amine. Moreover, during the introduction of the α-NPs, it was stated, that an increased P–C bond formation could be observed when coordinating the ligands with copper(I) precursors. This could be advantageously used, when combining this effect with the *precursor functionalization*, which was developed in the second chapter of this thesis. Thus, it could be possible to synthesize, e.g., an organo copper(I) salt as precursor, which stabilizes the α-NP in the first place and engages an *amino-halide-shift* in the presence of **1**, leading to *in situ* functionalization under the formation of the **NHSiNCP** motif.

4.2. Developing Novel Routes to Functionalized NHSis

The difficulties, partly described above, gave the inspiration to develop alternative methods of synthesizing functionalized silylenes. These results were discussed in the main chapter of this thesis. The focus was particularly on the development and application of two new synthetic routes to functionalized NHSi TM complexes, employing secondary amines bearing pyridyl-groups for a bidentate complexation of transition metal complexes.

4.2.1. Isolation and Characterization of Novel NHSiCl TM Complexes

The first method is based on the simple yet efficient concept of changing the sequence of the conventional route. A prior metalation of **1** with the desired transition metal allows the facile isolation of NHSiCl TM complexes in good reproducible yields. For these purposes d^{10}-transition metals of group 11 (Cu(I), Ag(I), Au(I)) and group 12 (Zn(II)) were targeted. Since these NHSi complexes are still comparatively scarce, the isolated and characterized compounds are a vital contribution to silylene chemistry by means of investigating the reactive behavior towards TM coordination.

The treatment of **1** with these readily available TM halide precursors led to a series of interesting compounds. The reaction with Cu(I) halides resulted in the formation of tetrameric complexes **5a-c** bearing a pseudocubane nature of the type $\{Cu_4(\mu_3\text{-}X)_4\}$, determined *via* XRD analyses (see Scheme 111, left). The employment of different halides did not exert a great influence on the Si–Cu bonds (averaged values: **5a** (2.191 Å) < **5b** (2.208 Å) < **5c** (2.230 Å)), besides the typical changes in angles and bonds of the $[CuX]_4$ core. Additionally, the determined ^{29}Si NMR signals analogously showed only slightly downfield shifted signals (**5a**: 27.73 ppm, **5b**: 26.09 ppm, **5c**: 22.62 ppm) compared to **1** (14.26 ppm). The additional isolation of the dimeric intermediate **[(NHSiCl)(CuBrSMe$_2$)]$_2$** (**6**), broadening the list of rare copper-complexes bearing SMe_2 ligands, and the subsequent molecular weight determination analyses of **5b** in THF *via* DOSY *ECC* measurements also indicating a dimeric complex in solution, gave further insights of the behavior of NHSi TM complexes.

Since the formation of such pseudo-/cubanes is not uncommon for $[MX]_4L_n$ complexes (M = Cu, Ag; X = Cl, Br, I; and L = neutral donor ligands) the reactivity of **1** towards AgCl analogously resulted in the successful formation and subsequent isolation of the cubane like compound **9** (see Scheme 111, right).

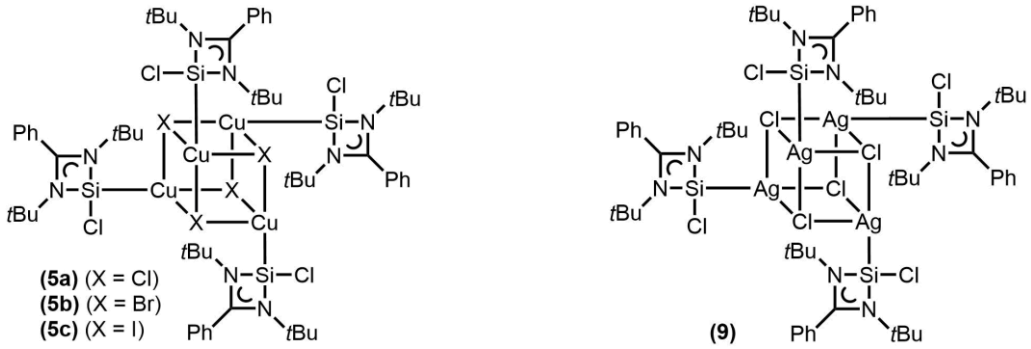

Scheme 111. Pseudo-/cubane NHSiCl Cu(I)/Ag(I) complexes **5a-c** and **9**.

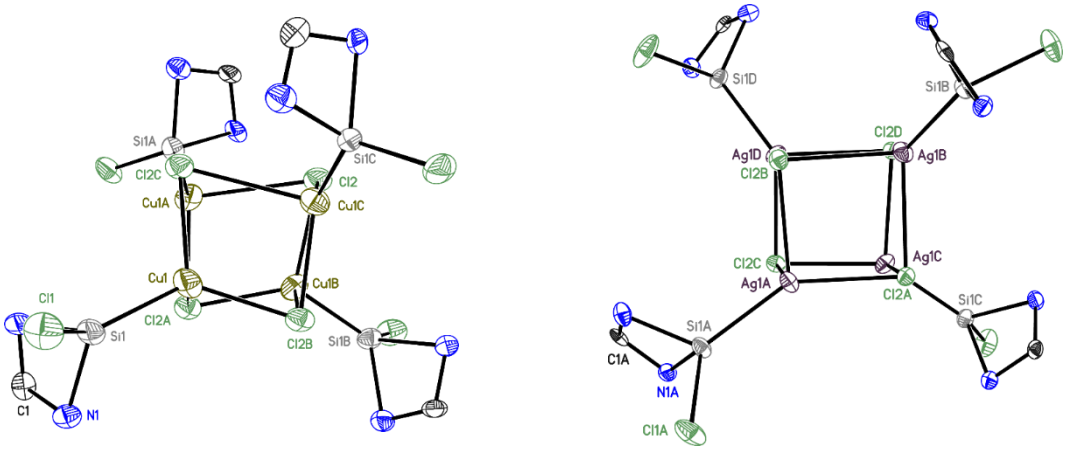

Figure 22. Crystal structures of complexes **5a** and **9** (*tert*-butyl and phenyl groups omitted for clarity).

The reaction of **1** with $AuCl(SMe_2)$ yielded in the unusual dimer **11** which exhibited aurophilic interactions in the solid state leading to a *crossed swords* conformation. Yet, the aurophilicity did not show great influence on the coordination to the metal atom. The determined averaged Si–Au bond

lengths (2.234 Å) showed to be comparable to the few previously reported Au(I) complexes, which were mostly of monomeric constitution. Contrary to the solid state analyses and in order to investigate the behavior of the aurophilic interactions in solution, DOSY measurements of **11** in THF exhibited a molecular weight which rather indicated the presence of a monomer accompanied by THF molecule(s).

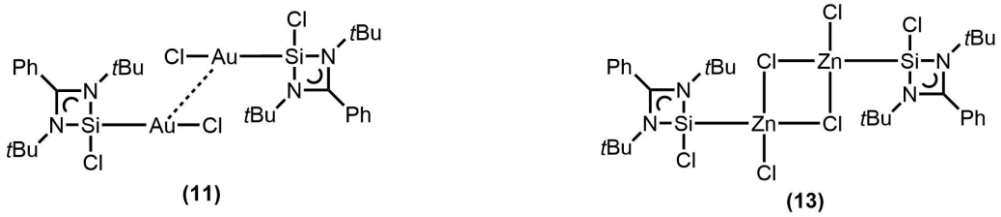

Scheme 112. Dimeric NHSi TM complexes **11** and **13**.

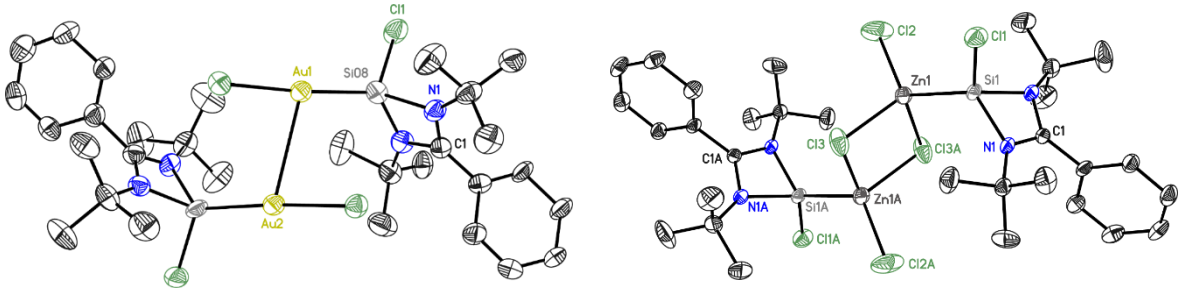

Figure 23. Crystal structures of complexes **11** and **13**.

Previous work in this field illustrated the possibility of silylene zinc halide complexes to be available as monomers as well as dimers. Treatment of **1** with the readily available Zn(II) chloride precursor resulted in compound **13**. Solid state analysis revealed a dimeric structure, regardless of the utilized solvent, whereas, for example, MW determination analysis in solution *via* DOSY spectroscopy indicated an equilibrium between the dimeric and monomeric complex, accompanied by THF molecules, respectively.

4.2.2. Reactive Behavior of NHSiCl TM Complexes towards Side-Arm Functionalization Reactions

The subsequent reaction step introduced the side-arm functionality to the readily available novel NHSiCl TM complexes. In all cases the salt metathesis of the secondary amine **MesNHPy** resulted in the intended substitution of the chloro group leading to a series of interesting functionalized NHSi TM complexes.

Performing the salt metathesis towards the precursors **5a-c** resulted in the formation of the unforeseen complexes **7a-c** which consist of two functionalized silylenes (**NHSiMes**) holding a triangular copper(I) core in a butterfly like fashion. Each silylene ligand is coordinating one Cu(I) atom in a bidentate fashion forming a metallacycle with the side-arm. Additionally, the low-valent Si(II)

atoms are coordinating a second Cu(I) atom in a shared fashion, exhibiting significantly elongated bond lengths, resulting in a unique copper-triangle in a [X-{Cu-Cu_2}(μ-$X)_2$] fashion. The exceptional ligand design and resulting complexation mode led to a slight distortion from an ideal isosceles triangle, further illustrating the influence of the ligation.

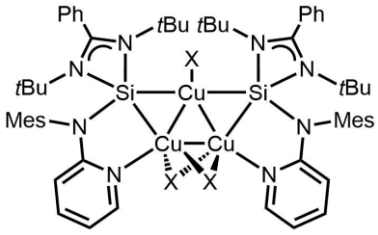

(7a) (X = Cl)
(7b) (X = Br)
(7c) (X = I)

Scheme 113. Trinuclear dimeric complexes **7a-c.**

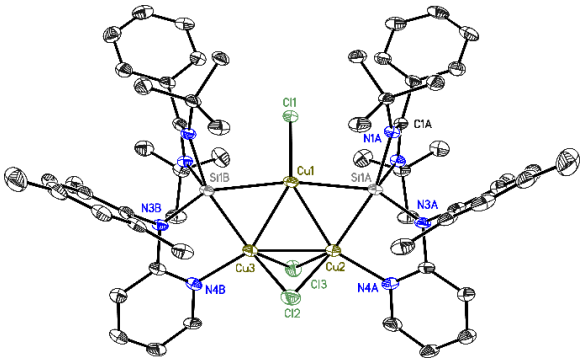

Figure 24. Crystal structure of complex **7a**.

^{1}H NMR spectroscopic analysis of **7a-c** exhibited partially seriously broadened signals, assuming possible relaxation through the metal coordination or dynamic fluctuation effects of the compounds/aggregates in solution, which was probably the reason that not any ^{29}Si NMR signals of this or any other of the following functionalized NHSi TM complexes could be detected. It is assumed that the signals vanish by the combination of these broadening effects and the already low natural abundance of the ^{29}Si nucleus. Therefore, future work should concentrate on performing temperature dependent NMR measurements of the corresponding compounds, to possibly decelerate such processes, hence determining the nature of the signal as a function of temperature.

Performing the functionalization towards the tetrameric complex **9** resulted in the monomeric complex **10** that proved to be a single functionalized **NHSiMes**, coordinating AgCl *via* the Si(II) atom in a linear geometry. Even though the challenging crystallization of **10** prevented the solid state structure determination *via* XRD analysis, the complementary analysis confirmed the isolation.

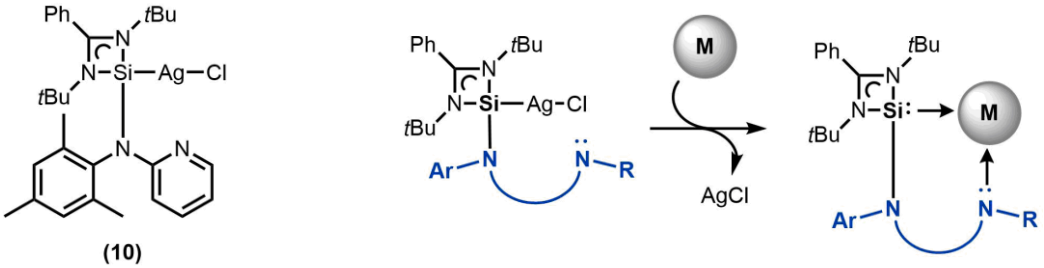

Scheme 114. (**Left**) Monomeric functionalized NHSi TM complex **10**. (**Right**) Possible utilization of Ag(I) complexes for transmetalation reactions.

As discussed in Chapter 3.2.2.2, within the field of NHC transition metal complexes it is a common method to utilize silver(I) complexes as transmetalating agents (see Scheme 114). This concept could be readily applied to the synthesis of NHSis, moreover, the hitherto generation of Ag(I) complexes and

subsequent functionalization would open passageways to transmetalating reactions, which should be subjected in future projects.

The aurophilicity of complex **[(NHSiCl)(AuCl)]$_2$** (**11**) was not preserved during the functionalization process, instead resulting in the monomeric complex **12**, which showed an analogues structure motif to **[(NHSiMes)(AgCl)]** (**10**). In addition, the solid state structure was determined *via* XRD analysis, revealing that the important bond lengths and angles are in line with comparable substituted monomeric NHSi complexes. Yet, the Si–Au bond is slightly elongated towards its unfunctionalized predecessor **11** reflecting the influence of the donor group.

The common linear geometry of the AuCl moiety should be further investigated, by means of examining the behavior of **12** towards halide abstraction reactions, in order to possibly generate a dimerization of two NHSi Au(I) ligands to conceivably restoring the aurophilicity. As discussed in Chapter 3.2.3.1 ff such compounds can exhibit fascinating luminescence properties, which is why further studies should concentrate on the investigation of the photophysical properties of such functionalized dimers and compare their properties to **11** and **12** as well.

Furthermore, the reactive behavior of complex **12** should be subjected to certain oxidative addition reactions or cycloaddition reactions, in order to check its potential catalytical reactivity. As more detailed discussed at the end of Chapter 3.2.3.2 the free donor site of the pyridyl-group could show beneficial effects in mechanistic steps stabilizing Au(III) intermediates *via* temporary ligation. Thus, compound **12** would combine a strong σ-donor ability and an additional donor-site for a stabilizing transient ligation.

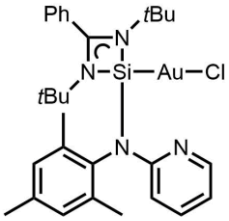

(12)

Scheme 115. Monomeric functionalized NHSi TM complex **12**

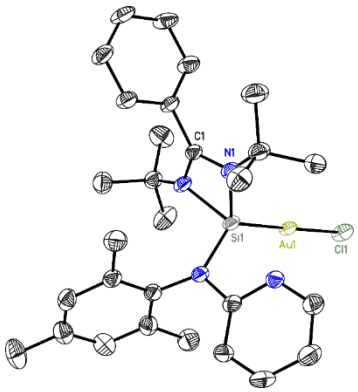

Figure 25. Crystal structure of complex **12.**

The functionalization of the zinc dimer **[(NHSiCl)(ZnCl$_2$)]$_2$** (**13**) was of special interest, since preceding work revealed the possibility of an equilibrium reaction to the monomer. With the introduction of the side-arm, the additional donor-site in direct proximity to the Zn(II) atom offered the opportunity of a bidentate coordination, hence possibly supporting a monomerization. However, analyses of complex **[(NHSiMes)(ZnCl$_2$)]$_2$** (**14**) emerged the preservation of the dimeric structure under the successful functionalization, leading to the non-bidentate ligation. Even though the modification of the silylene led to a distortion of the rhombohedral [ZnCl$_2$]$_2$ core moiety, the structure remained remarkably intact.

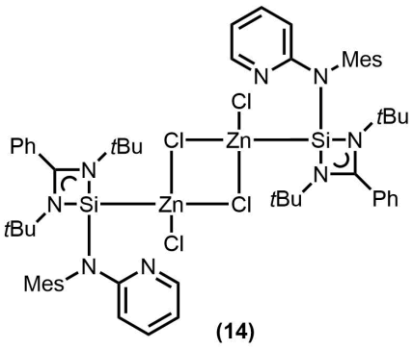

Scheme 116. Functionalized dimeric NHSi Zn(II) complex **14**.

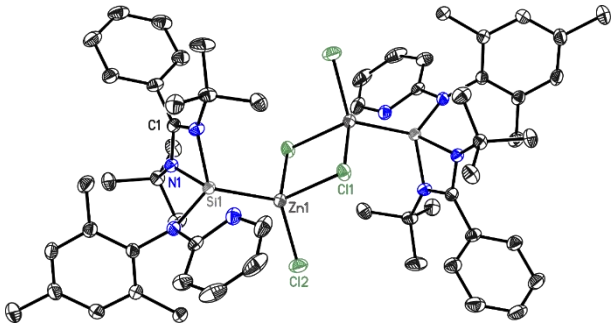

Figure 26. Crystal structure of complex **14**.

4.2.3. Utilization of Organo Transition Metal Salts for the *in situ* Functionalization of NHSiCl

The *halide-alkyl-/aryl-shift* reported by the group of *P. W. Roesky* provided the inspiration to exploit and expand this behavior by transferring it to negatively charged amino groups (PhNHPy).

Within the framework of this thesis, it was possible to illustrate the potential of this method by introducing two TM precursors, the fairly known organo copper(I) salt **[(PhNPy)Cu]$_x$** as well as the novel organo zinc(II) salt **[(PhNPy)(ZnCl)(EtOH)]**. Both precursors showed the desired behavior and led to novel NHSi TM complexes in one-pot reactions at ambient temperatures. Besides the versatile access to the utilized amine **PhNHPy** the coordination to copper(I) atoms proved to be very facile, too. Even though the resulting compound was initially deterred by extremely poor solubility, the isolation of complex **8** proved the method suitable. Interestingly, complex **8** showed exactly the same trinuclear constitution as the previous isolated complexes **7a-c**. Although the yield was initially slightly lower, the prior synthesis and workup of the tetrameric complex **5a-c** became obsolete.

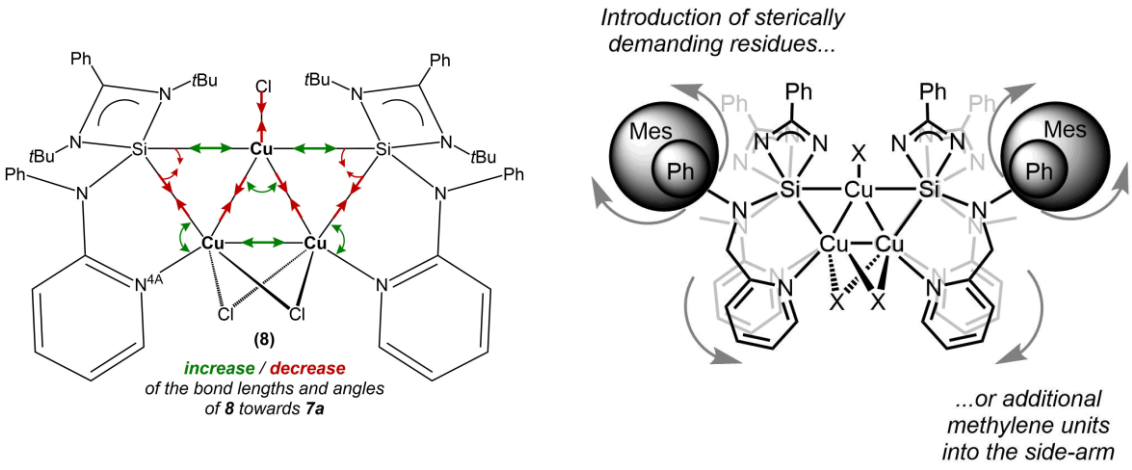

Scheme 117. (**Left**) Schematically visualized distortion of the trinuclear dimeric NHSi complex **8** towards **7a**; (**right**) schematic illustration of possible scaffold-modifications for future projects.

Remarkably, due to the employment of the sterically less demanding phenyl-group, it was possible to identify an influence of the side-arm substitution pattern on the Cu(I) triangle (see Scheme 117). This illustrates the possibility of enhanced modifications by varying the substituents at the utilized side-arm, which should be definitely further investigated, in order to examine the limits and impact of this feature.

As mentioned above, the hitherto presented *post-complex functionalization* of **1** with $ZnCl_2$ led to the dimeric complexes **13** and **14**, the idea grew if a monomeric constitution could be achieved by employing the novel *precursor functionalization*. After the non-trivial identification of the novel Zn(II) precursor **[(PhNPy)(ZnCl)(EtOH)]**, treatment of **1** with this compound resulted in the monomeric complex **16**. Not only led the aforementioned behavior to the successful functionalization, but also employing the bidentate coordination at the same time. Drawing the direct comparison to the dimeric congener, it is most likely, that the precoordinated zinc(II) atom by the pyridyl-group led to the bidentate coordination in the target compound, thus illustrating the difference between these methods.

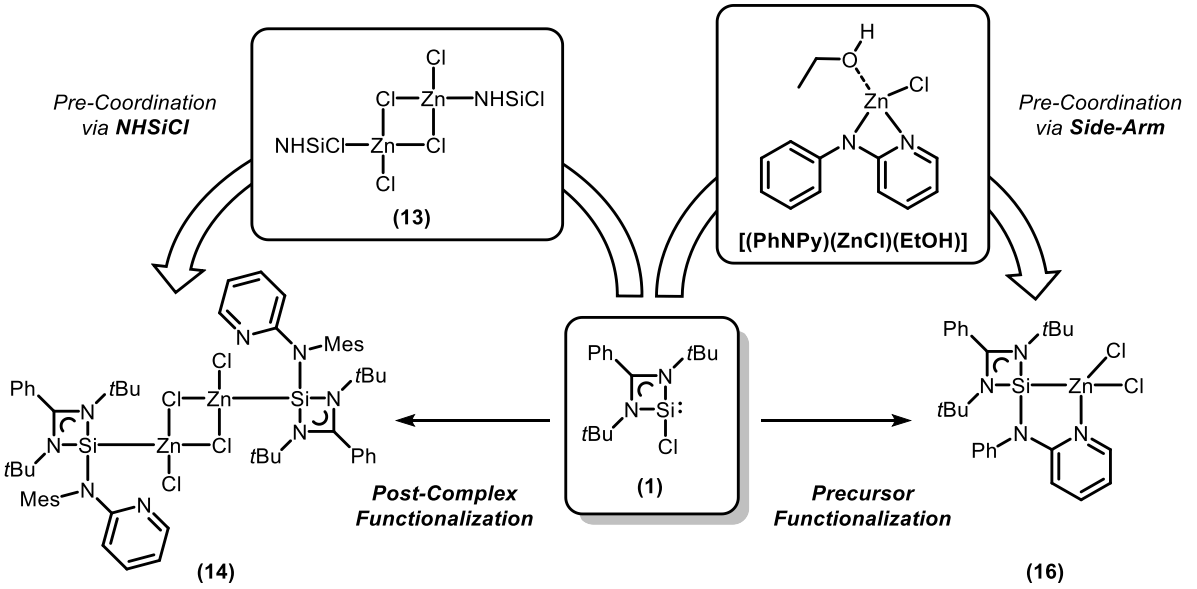

Scheme 118. Comparison of the applied methods to isolate the resulting complexes **14** and **16** utilizing different techniques to yield different formations.

These results illustrated the huge potential of this way of functionalization (see Scheme 118). While the copper(I) precursor resulted in the same enhanced triangular conformation, the zinc(II) precursor additionally exhibited the possibility to control the complexation. The *post-complex* salt metathesis led to the dimeric species, while the *precursor functionalization* resulted in the monomeric species. This concept of accessing new pathways to TM complexes and gaining control over the bidentate complexation motif should be further investigated in future works, by means of extending the scope of transition metals, as well as functional groups.

4.3. Catalytical Investigations of Complexes 5b and 7b towards the Transformation of 1,2,3-Triazoles

In the last chapter, an additional focus was set on the influence of the side-arm functionalization on catalytical reactivities, by subjecting the complexes **5b** and **7b** to the renowned copper(I)-catalyzed alkyne-azide cycloaddition (CuAAC). The catalytical investigations in the context of this work did not concentrate on extensive optimization for ideal conditions, determining the range of the substrate scope or investigating kinetic subtleties, but rather the comparison of the unfunctionalized NHSi TM complex to the side-arm introduction should stand in the focus of these reactions.

Remarkably, regarding the formation of the triazoles **P1** to **P3** it was possible to determine conversion times up to eight times higher employing the side-arm functionalized complex **7b** compared to its congener complex **5b** (see Chart 2). It remains questionable whether the increased reactivity is due to the electronical influence of the side-arm or to the presence of the multinuclear copper(I) core moiety. Either way, both explanations would be justified by the presence of the side-arm, which makes the extraordinary structural motif of **7b** possible.

Chart 2. Excerpt of the time-conversion-diagram of the CuAAC reactions discussed in Chapter 3.3.2 (1 mol% **5b** (hollow icons) or **7b** (full icons)). The graphs represent the formation of the triazoles **P1** to **P3** over time, under the utilization of the corresponding acetylenes (Ph-CCH, Py-CCH and Butinol, respectively) as well as Bn-N_3.

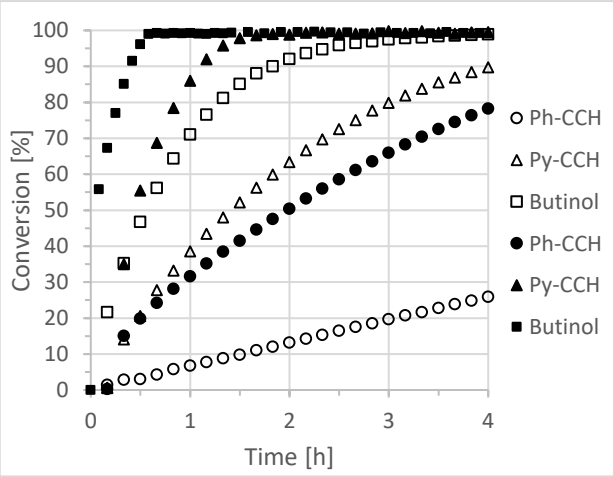

In conclusion, getting a first glimpse of the improvement through the functionalization, this project offers adequate potential to expand it in certain ways. Future work should concentrate on the expansion of the scope and the optimization of the reaction conditions, hence, it would be possible to examine the behavior of side-arm functionalized silylenes towards various functionalities. Furthermore, the substitution pattern of the side-arm can be modified in order to investigate further sterical and electronical influences towards the complex and its reactivity.

5. Experimental Section

5.1. General Procedures

Except stated otherwise, all reactions were carried out under strict exclusion of air and moisture using modified *Schlenk* techniques in a dry and purified nitrogen or argon atmosphere or in an argon glovebox *LABmaster SP* and *LABmaster eco* by *MBRAUN*.[224] All employed glass ware has been dried and heated in an oven at 120°C for at least 12 h prior to use and has been assembled under reduced pressure while still being hot. Filtration steps of air and moisture sensitive compounds were carried out using dried *Whatman* fiberglass filters (GF/B, 25 mm), which were applied with Teflon© tape and cannulas or modified syringes. All used solvents were dried using standard laboratory procedures, freshly distilled, degassed *via "pump-freeze"* method and finally stored over activated 3 Å molecular sieves prior to use (diethyl ether, *n*-pentane from sodium/potassium alloy; THF from potassium; *n*-hexane, toluene from sodium; DCM from phosphorous pentoxide). All commercially available reactants were used without further purification; all starting materials were synthesized according to the given literature procedures.

5.2. Analytical Methods

5.2.1. Mass Spectrometry

Mass spectrometry has been carried out by the Central Analytical Unit of the *Institute of Organic and Biomolecular Chemistry* at the *Georg-August-University*, Göttingen. EI spectra were recorded using a *MAT 95* device with electron ionization (EI-MS: 70 eV). High-resolution ESI spectra were recorded either with a *Bruker Daltronics microTOF Q II* or a *maXis ESI-QTOF-MS*. LIFDI-MS spectra were measured on a *Jeol AccuTOF* spectrometer. The peaks are given as a mass to charge ratio m/z of the fragment ions, based on the molecular mass of the isotopes with the highest natural abundance (e.g. ^{1}H, ^{12}C, ^{14}N, ^{16}O, ^{28}Si, ^{31}P, ^{35}Cl, $^{79/81}Br$, ^{127}I).

5.2.2. NMR Spectroscopy

All NMR spectra were recorded at room temperature, except stated otherwise, on either a *BRUKER Avance III 300*, *Avance III 400* or an *Avance 500* NMR spectrometer. The measurements were carried out with 1-15% solutions of deuterated solvents. The chemical shifts δ are given in ppm, relative to the residual proton signal of the deuterated solvent.[225,226] The coupling constant *J* is reported in Hz and the abbreviations for multiplicity are used as follows: s = singlet, d = doublet, t = triplet, q = quartet, sept = septet m = multiplet, br = broad; and their corresponding combinations: dd = doublet of doublets, etc.[225] Tetramethylsilane was used as an external standard for ^{1}H and ^{13}C spectra and

orthophosphoric acid for ^{31}P spectra, respectively, while the residual proton signal of the deuterated solvent was used as an internal standard. Respective shift assignments were determined *via* 2D correlation spectrums (HSQC, HMBC, COSY).[227] Processing of the spectra was done using *MestReNova 10.0.2-15465* by *Mestrelab Research*.

5.2.2.1. ^{1}H-DOSY-ECC-MW Estimation: Sample Preparation and Measuring Parameters

^{1}H-DOSY-ECC-MW measurements and calculations were carried out in collaboration with *Anne Kreyenschmidt* from the group of *Prof. Dr. Dietmar Stalke*. All samples for a ^{1}H-DOSY-ECC-estimation were prepared by the addition of an equimolar amount of 2,2,3,3-tetramethylbutane (TMB) or adamantane (ADAM) as internal reference to a solution of the substrate in C_6D_6, DCM-d2 or THF-d8, respectively. All spectra were recorded either on a Bruker Avance III 400 MHz spectrometer with a BBFO probe, z-gradient (maximum gradient strength: 57 G/cm) or on a Bruker Ascend 400 MHz spectrometer with a BBI probe, z-gradient (maximum gradient strength: 51 G/cm). If not indicated otherwise experiments were done at ambient temperature and without spinning. Relevant parameters are given in Table 18 Spectra processing was carried out using Topspin 3.5. The diffusion coefficients were determined with the T1/T2 relaxation module.[136,228,229]

Table 18. Parameters of the DOSY-NMR-Experiments.

PulseProgram	**dstebpgp3s**
Δ	1.1 – 3.4 ms
δ	0.1 s

Data evaluation was performed using the *MW* Estimation Software Version 1.3 in consideration of the van-der-Waals corrected ECC-DOSY.[230]

Table 19. Linear fit parameters (log(*K*) and α) as well as log($D_{ref,fix}$) for THF-d_8.[137]

	THF-d_8
log($D_{ref,fix}$)	−8.7749 (TMB)
log(*K*)	−7.60
−α	−0.553

Equation 1. $$X_{cor} = \frac{a}{(1+\exp(-k(MD_W - xc)))}$$

Table 20. Fit parameters of the van-der-Waals corrected ECC-DOSY for THF-d_8 with the general formula.[228]

Parameter	
a	2.255
k	$2.97 \cdot 10^{-30}$
xc	$5.12 \cdot 10^{29}$
cor. R^2	0.93

5.2.2.1.1. ECC-*MW* Estimation of [(NHSiCl)(CuBr)]$_4$

Table 21. ^{1}H-DOSY-ECC-*MW* estimation regarding the ECC-MD_W correction of **5b** in a solution of benzene-d_6 and THF-d_8. Adamantane ($\log D_{ref,fix} = -8{,}8025$) was used as internal reference. Hypothetical aggregates are marked from A to D. However, the data indicate a decomposition of the one known from X-ray experiments determined tetrameric species D in solution into a bimetallic species (A - C). Free coordination sites might be occupied by solvent molecules as the slightly elevated molecular weight compared to the solvent free aggregate A indicates.

		^{1}H-DOSY				
		Aggregate	**MW_{det} [g/mol]**	**MW_{dif} [%]**	**MD_W [gmol^{-1}m^{-3}]**	**X_{cor}**
D_x [m^2/s]	5.92E–10	A	1023	–14	6.21E+29	1.3556
log(D_x)	–9.2277	B	998	–5	6.02E+29	1.3222
log($D_{x,norm}$)	–9.2261	C	997	4	5.86E+29	1.2852
D_{ref} (ADAM) [m^2/s]	1.57E–09	D	1023	71	6.21E+29	1.3556
log(D_{ref})(ADAM)	–8.8041					

Hypothetical aggregate	Structure	Hypothetical aggregate	Structure
A (MW_{calc} = 877 gmol^{-1})	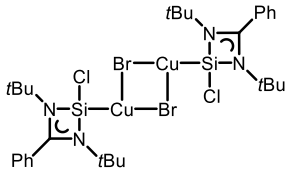	**C (MW_{calc} = 021 gmol^{-1})**	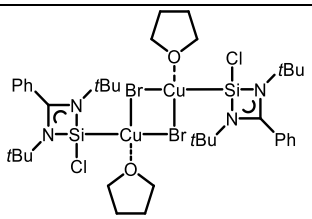
B (MW_{calc} = 949 gmol^{-1})	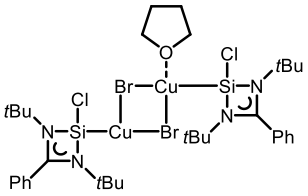	**D (MW_{calc} = 1753 gmol^{-1})**	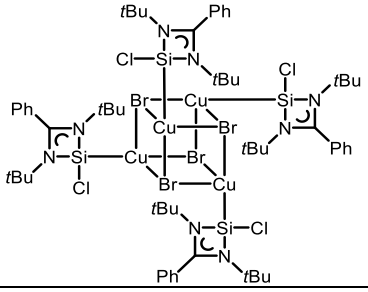

5.2.2.1.2. ECC-*MW* Estimation of $[(NHSiCl)(AuCl)]_2$

Table 22. ^{1}H-DOSY-ECC-*MW* estimation regarding the ECC-MD_W correction of **11** in THF-d_8. TMB ($\log D_{ref,fix}$ = -8.7749) was used as internal reference. Hypothetical aggregates are marked from A to D. The diffusion data indicate decomposition of the bimetallic complex in solution (C and D).

		^{1}H-DOSY				
		Aggregate	MW_{det} **[g/mol]**	MW_{dif} **[%]**	MD_W **[gmol^{-1}m^{-3}]**	X_{cor}
D_x **[m^2/s]**	8.1488E-10	A	671	57	7.53E+29	1.5151
log(D_x)	-9.0889	B	671	-21	7.53E+29	1.5151
log($D_{x,norm}$)	-9.0633	C	601	12	6.53E+29	1.3586
D_{ref} **(TMB) [m^2/s]**	1.58E-09	D	630	-5	6.93E+29	1.4235
log(D_{ref})(TMB)	-9.8005					

Hypothetical aggregate	**Structure**	**Hypothetical aggregate**	**Structure**
A (MW_{calc} = 1055 gmol^{-1})	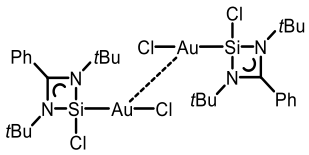	**C (MW_{calc} = 672 gmol^{-1})**	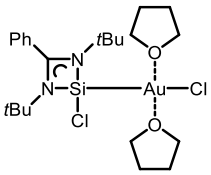
B (MW_{calc} = 527 gmol^{-1})	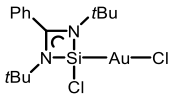	**D (MW_{calc} = 599 gmol^{-1})**	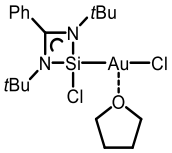

5.2.2.1.3. ECC-*MW* Estimation of $[(NHSiCl)(ZnCl_2)]_2$

Table 23. ^{1}H-DOSY-ECC-*MW* estimation regarding the ECC-MD_W correction of **13** in THF-d_8. TMB ($\log D_{ref,fix}$ = -8.7749) was used as internal reference. Hypothetical aggregates are marked from A to D. Despite the high standard deviations of the hypothetical aggregates A and C, the data indicate an equilibrium in solution between those two species. Free coordination sites might be occupied by solvent molecules as the slightly elevated molecular weight compared to the solvent free aggregates indicate.

		^{1}H-DOSY				
		Aggregate	MW_{det} **[g/mol]**	MW_{dif} **[%]**	MD_W **[gmol^{-1}m^{-3}]**	X_{cor}
D_x **[m^2/s]**	6.8423E-10	A	736	17	5.91E+29	1.2584
log(D_x)	–9.1648	B	736	–41	5.91E+29	1.2584
log($D_{x,norm}$)	–9.1303	C	690	–17	5.43E+29	1.1790
D_{ref} **(TMB) [m^2/s]**	1.55E-09	D	709	–29	5.62E+29	1.2115
log(D_{ref})(TMB)	–8.8094					

Hypothetical aggregate	**Structure**	**Hypothetical aggregate**	**Structure**
A (MW_{calc} = 856 gmol^{-1})	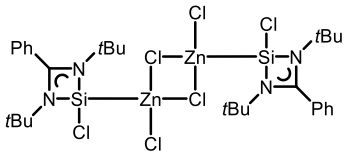	**C (MW_{calc} = 503 gmol^{-1})**	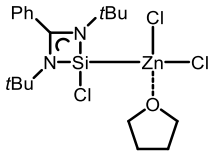
B (MW_{calc} = 575 gmol^{-1})	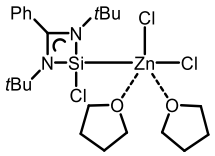	**D (MW_{calc} = 431 gmol^{-1})**	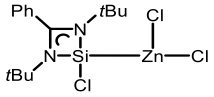

5.2.2.2. ^{1}H NMR Click-Chemistry Experiments: Sample Preparation, Measuring Parameters and Processing

For the corresponding time-resolved measurements of the CuCAAC reactions, discussed in Chapter Catalysis3.3, a NMR Young tube was charged with benzyl azide (1.00 eq.), the appropriate alkyne (1.00 eq), adamantane (1/8 eq) as an internal standard and deuterated dichloromethane. After an initial measurement of the neat reactants, the complex **5b**/**7b** was added. The progress of the reaction was monitored *via* ^{1}H NMR spectroscopic measurements in 5 and/or 10 min steps for at least 10 h at room temperature. All spectra were recorded on a *BRUKER Avance III 400* and processed with *MestReNova 10.0.2-15465* by *Mestrelab Research* (e.g. referencing, normalizing and integration of multiple spectra) and further processing was done with *Microsoft Excel*.

Table 24. Summary of the integrated values.

Conversion (Integrated values; ≈ 0 – 100.000)											
Time [h]	**2b PhCCH**	**2b PyCCH**	**2b Butinol**	**2b *t*BuCCH**	**2b TMSCCH**	**3b PhCCH**	**3b PyCCH**	**Time [h]**	**3b Butinol**	**3b *t*BuCCH**	**3b TMSCCH**
0.167	1.451	0.641	21.626	0.120	1.075	0.327	0.539	0.083	55.853	0.123	0.185
0.333	2.833	14.059	35.238	1.150	1.497	15.048	35.035	0.167	67.359	0.513	0.509
0.5	3.087	20.600	46.761	1.686	1.816	19.859	55.498	0.250	76.988	1.218	0.733
0.667	4.260	27.749	56.201	2.366	2.124	24.195	68.760	0.333	85.144	1.790	0.933
0.833	5.774	33.267	64.405	3.093	2.445	28.166	78.410	0.417	91.523	2.363	1.115
1	6.752	38.578	71.068	3.852	2.761	31.642	85.994	0.500	96.190	2.885	1.277
1.167	7.781	43.416	76.588	4.585	3.068	35.184	91.974	0.583	99.025	3.357	1.451
1.333	8.824	47.959	81.234	5.310	3.369	38.487	95.785	0.667	99.306	3.928	1.613
1.5	9.845	52.147	85.084	6.043	3.711	41.501	97.864	0.750	99.082	4.457	1.734
1.667	11.078	56.236	88.087	6.766	4.005	44.607	98.666	0.833	99.312	4.972	1.936
1.833	12.044	59.931	90.017	7.543	4.330	47.521	98.983	0.917	99.148	5.578	2.057
2	13.174	63.423	92.054	8.274	4.645	50.420	98.829	1.000	99.263	6.135	2.237
2.167	14.262	66.715	93.689	8.986	4.944	53.245	99.392	1.083	99.070	6.704	2.409
2.333	15.306	69.759	94.725	9.671	5.267	55.968	99.439	1.167	98.974	7.216	2.587
2.5	16.446	72.608	95.853	10.461	5.592	58.551	99.126	1.250	99.234	7.802	2.745
2.667	17.550	75.101	96.500	11.098	5.909	61.179	99.110	1.333	99.181	8.372	2.866
2.833	18.505	77.692	96.998	11.795	6.221	63.541	99.229	1.417	99.390	8.859	2.946
3	19.707	79.852	97.478	12.417	6.542	65.960	99.808	1.583	99.519	9.452	3.168
3.167	20.802	81.899	97.881	13.131	6.875	68.254	99.301	1.750	99.198	10.007	3.327
3.333	21.686	83.778	98.035	13.750	7.178	70.393	99.824	1.917	99.501	10.415	3.474
3.5	22.790	85.528	98.349	14.439	7.507	72.552	99.351	2.083	99.521	10.925	3.714
3.667	23.845	86.903	98.598	15.096	7.837	74.555	99.131	2.250	99.607	11.384	3.856
3.833	24.875	88.436	98.783	15.619	8.160	76.393	99.468	2.417	99.429	12.023	3.921
4	25.909	89.726	98.930	16.296	8.483	78.227	99.541	2.583	99.442	12.370	4.120
4.167	26.609	90.872	99.007	16.885	8.793	79.959	99.570	2.750	99.078	13.078	4.302
4.333	28.036	91.738	99.181	17.487	9.117	81.611	99.490	2.917	99.485	13.703	4.390
4.5	28.804	92.950	99.140	18.168	9.421	83.207	99.250	3.083	99.264	14.276	4.520
4.667	29.421	93.519	99.383	18.619	9.731	84.715	99.105	3.250	99.317	14.604	4.725
4.833	30.604	94.299	99.272	19.277	10.064	85.988	99.570	3.417	99.226	15.105	4.876
5	32.142	95.161	99.342	19.674	10.412	87.211	99.660	3.583	99.553	15.696	5.069
5.167	32.363	95.852	99.276	20.407	10.700	88.451	99.280	3.750	99.318	16.158	5.153
5.333	33.269	96.198	99.380	20.842	11.078	89.523	99.251	3.917	99.252	16.783	5.261
5.5	34.497	96.540	99.413	21.362	11.352	90.508	99.212	4.083	99.292	17.062	5.403
5.667	35.727	96.868	99.500	21.891	11.679	91.619	99.192	4.250	99.396	17.710	5.772
5.833	35.805	97.285	99.528	22.386	11.989	92.328	99.397	4.417	99.494	18.543	5.779
6	36.833	97.742	99.526	23.000	12.333	93.168	99.399	4.583	99.484	19.095	5.922
6.167	37.975	97.826	99.457	23.427	12.672	93.724	98.905	4.750	99.590	19.153	6.108
6.333	39.233	98.058	99.632	24.065	12.980	94.535	99.671	4.917	99.407	19.924	6.261
6.5	39.154	98.195	99.578	24.461	13.342	95.130	99.290	5.083	99.412	20.411	6.533
6.667	40.220	98.001	99.643	24.913	13.623	95.762	99.583	5.250	99.543	20.603	6.728
6.833	41.087	98.390	99.709	25.405	13.948	96.072	99.070	5.417	99.426	21.044	6.847
7	42.496	97.885	99.607	25.793	14.269	96.637	99.227	5.583	99.390	21.582	6.885
7.167	42.424	98.234	99.628	26.304	14.617	97.043	99.699	5.750	99.492	22.301	7.113

7.333	43.449	98.279	99.637	26.695	14.917	97.455	99.169	5.917	99.474	22.888	7.172
7.5	44.320	98.122	99.605	27.299	15.268	97.640	99.165	6.083	99.515	23.332	7.407
7.667	45.247	98.194	99.652	27.813	15.563	97.844	99.556	6.250	99.372	23.831	7.531
7.833	46.013	98.497	99.775	28.011	15.888	98.180	98.968	6.417	99.457	24.034	7.789
8	46.318	98.578	99.687	28.506	16.197	98.284	99.398	6.583	99.510	24.207	7.847
8.167	46.943	98.588	99.693	29.050	16.526	98.423	98.773	6.750	99.135	24.797	8.141
8.333	47.829	98.430	99.717	29.460	16.845	98.602	99.532	6.917	99.457	25.743	8.306
8.5	48.624	98.477	99.752	29.896	17.229	98.554	99.437	7.083	99.258	25.751	8.499
8.667	49.270	98.487	99.594	30.234	17.515	98.636	99.041	7.250	98.562	26.402	8.694
8.833	50.209	98.357	99.689	30.633	17.817	98.719	98.972	7.417	99.171	26.707	8.820
9	50.543	98.427	99.684	31.092	18.208	98.537	99.526	7.583	99.412	27.476	9.075
9.167	50.996	98.596	99.597	31.346	18.454	98.654	99.354	7.750	99.370	27.662	9.118
9.333	51.759	98.580	99.570	31.857	18.857	98.688	99.318	7.917	99.509	27.920	9.230
9.5	52.127	98.838	99.672	32.259	19.116	98.705	99.717	8.083	99.325	28.715	9.405
9.667	52.851	98.556	99.691	32.714	19.461	98.696	99.213	8.250	99.393	29.464	9.641
9.833	53.898	98.482	99.688	33.160	19.786	98.684	99.294	8.417	99.457	29.281	9.794
10	54.548	98.356	99.616	33.248	20.101	98.767	100.187	8.583	99.324	29.339	9.988
								8.750	99.190		
								8.917	99.065		
								9.083	99.186		
								9.250	99.484		
								9.417	99.504		
								9.583	99.558		
								9.750	99.441		
								9.917	99.486		
								10.083	99.422		

Within the framework of these catalytical investigations, blank tests were performed for cross-checking to ensure that the determined conversion rates did not originate from possible traces of neat Cu(I)Br. Therefore, under the same conditions mentioned above, 1 mol% of $CuBr(SMe_2)$ was added instead of complex **5b**/**7b** and the resulting reaction mixture was monitored *via* ^1H NMR measurements periodic intervals. The conversion times to the formation of the triazoles **P1-3** were partly significantly longer (**P1**: 40 h, 96%; **P2**: 16 h, 100%; **P3**: 40 h, 67%), whereas the formation of **P4-5** showed similar conversion times (**P4**: 40 h; 96%; **P5**: 40 h; 82%).

5.2.3. Elemental Analysis

Elemental analyses (C, H, N) were carried out on a *VARIO EL III* at the *Analytical Laboratory of Institute of Inorganic Chemistry*, Georg-August-University Göttingen.

5.3. Synthesis and Characterization

5.3.1. HNCP – (1-Anilino-1-phenyl-methyl)diphenylphosphine

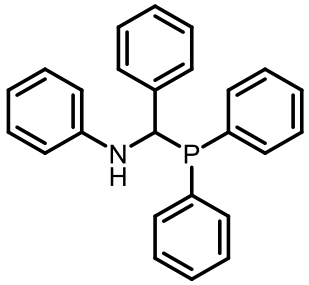

The synthesis of (1-anilino-1-phenyl-methyl)diphenylphosphine is done in two consecutive reaction steps.

Procedure 1. A 250 mL round bottom flask equipped with a *Dean-Stark* apparatus was charged with aniline (3.060 g, 32.9 mmol, 3.00 ml), benzaldehyde (3.487 g, 32.9 mmol, 3.32 ml) and toluene (100 mL) and heated to reflux for approximately 24 h. The solvent was removed under reduced pressure and the resulting brown oil was destilled *via* a *Kugelrohr* apparatus to isolate the intermediate (*E*)-*N*,1-diphenylmethanimine in form of a yellowish crystalline solid.

Empirical formula: $C_{13}H_{11}N$

Molecular weight: 181.24 g/mol

Yield: 5.682 g, 31.4 mmol, 95%

^{1}H-NMR (300.13 MHz, DCM-*d2*): δ [ppm] = 8.13 (s, 1H, NC*H*), 7.86–7.78 (m, 2H, C*Ph* / N*Ph*), 7.23–7.09 (m, 7H, C*Ph* / N*Ph*), 7.08–7.00 (m, 1H, C*Ph* / N*Ph*).

^{13}C{^{1}H}-NMR (75.48 MHz, DCM-*d2*): δ [ppm] = 159.64 (s, NCH), 152.46 (s, C*Ph* / N*Ph*), 136.64 (s, C*Ph* / N*Ph*), 130.92 (s, C*Ph* / N*Ph*), 129.01 (s, C*Ph* / N*Ph*), 128.79 (s, C*Ph* / N*Ph*), 128.47 (s, C*Ph* / N*Ph*), 125.70 (s, C*Ph* / N*Ph*), 120.95 (s, C*Ph* / N*Ph*).

ESI–HRMS: m/z: 182.0961 (100) $[M]^+$ (Calcd: 182.0964).

Procedure 2. Under inert conditions, diphenyl phosphine (931 mg, 5.00 mmol, 0.87 mL) was added dropwise to a solution of (*E*)-*N*,1-diphenylmethanimine (906 mg, 5.00 mmol) in hexane (5 mL) and stirred overnight at ambient temperature. The resulting suspension was filtered and the white solid was dried under reduced pressure. Further purification was not necessary, but could be performed by washing the solid with hexane (3 x 3mL).

Empirical formula: C_{25} H_{22} N P

Molecular weight: 367.43 g/mol

Yield: 1.479 g, 4.03 mmol, 81%

^{1}H-NMR (300.13 MHz, DCM-*d2*): δ [ppm] = 7.54–6.55 (m, 20H, *aromatics*), 5.23 (dd, *J* = 7.3, 3.8 Hz, 1H, NC*H*P), 4.53 (dd, *J* = 7.4, 3.8 Hz, 1H, *H*NCP).

^{13}C{^{1}H}-NMR (75.48 MHz, DCM-*d2*): δ [ppm] = 147.56–114.17 (*aromatics*), 57.59 (d, *J* = 12.3 Hz, N*C*P).

^{31}P{^{1}H}-NMR (121.49 MHz, DCM-*d2*): δ [ppm] = 4.48.

ESI–HRMS: m/z: 390.1380 (40) $[M+Na]^+$ (Calcd: 390.1382).

5.3.2. $H^{Py}NCP$ – (1-(2-Pyridylamino)-1-phenyl-methyl)diphenylphosphine

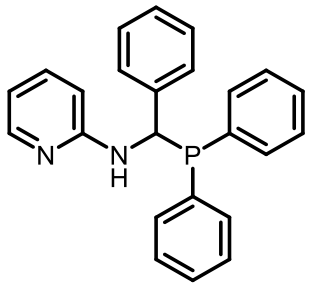

The synthesis of (1-(2-pyridylamino)-1-phenyl-methyl)diphenylphosphine is done in two consecutive reaction steps.

Procedure 1. A 250 mL round bottom flask equipped with a *Dean-Stark* apparatus was charged with 2-aminopyridine (8.87 g, 94.2 mmol), benzaldehyde (10.0 g, 94.2 mmol, 9.52 ml) and toluene (100 mL) and heated to reflux for approximately 24 h. The solvent was removed under reduced pressure and the resulting brown oil was destilled *via* a *Kugelrohr* apparatus to isolate the intermediate (*E*)-1-phenyl-*N*-(pyridin-2-yl)methanimine in form of a yellow crystalline solid.

Empirical formula: $C_{12}H_{10}N_2$

Molecular weight: 182.23 g/mol

Yield: 15.793 g, 86.7 mmol, 92%

^{1}H-NMR (300.13 MHz, C_6D_6): δ [ppm] = 9.43 (s, 1H, NC*H*), 8.36 (ddd, *J* = 4.8, 2.0, 0.9 Hz, 1H, N*Py*^{5}), 7.95–7.87 (m, 2H, C*Ph*), 7.30 (dt, *J* = 7.9, 1.0 Hz, 1H, N*Py*^{2}), 7.13 (ddd, *J* = 7.9, 7.4, 2.0 Hz, 1H, N*Py*^{3}), 7.09–7.05 (m, 2H, C*Ph*), 6.61 (ddd, *J* = 7.4, 4.8, 1.1 Hz, 1H, N*Py*^{4}).

^{13}C{^{1}H}-NMR (75.48 MHz, C_6D_6): δ [ppm] = 162.44 (s, NCH), 161.01 (s, N*Py*^{1}), 148.81 (s, N*Py*^{5}), 137.45 (s, N*Py*^{3}), 136.38 (s, C*Ph*), 131.42 (s, C*Ph*), 129.48 (s, C*Ph*), 128.51 (s, C*Ph*), 121.58 (s, N*Py*^{4}), 120.59 (s, N*Py*^{2}).

Procedure 2. Under inert conditions, diphenyl phosphine (931 mg, 5.00 mmol, 0.87 mL) was added dropwise to a solution of (*E*)-1-phenyl-*N*-(pyridin-2-yl)methanimine (911 mg, 5.00 mmol) in hexane (5 mL) and stirred overnight at ambient temperature. The resulting suspension was filtered and the white solid was dried under reduced pressure. Further purification was not necessary, but could be performed by washing the solid with hexane (3 x 3mL).

Empirical formula: $C_{24}H_{21}N_2P$

Molecular weight: 368.42 g/mol

Yield: 1.472 g, 4.00 mmol, 80%

^{1}H-NMR (300.13 MHz, $CDCl_3$): δ [ppm] = 8.20 (ddd, *J* = 5.0, 1.9, 0.9 Hz, 1H, N*Py*^{5}), 7.57–7.23 (m, 15H, aromatics), 7.42–7.37 (m, 1H, N*Py*^{3}), 6.65 (ddd, *J* = 7.2, 5.0, 0.9 Hz, 1H, N*Py*^{2}), 6.38 (dt, *J* = 8.4, 1.0 Hz, 1H, N*Py*^{4}), 5.69 (dd, *J* = 8.0, 2.8 Hz, 1H, N*CH*P), 5.43 (dd, *J* = 8.1, 3.5 Hz, 1H, *HN*CP).

^{13}C{^{1}H}-NMR (75.48 MHz, $CDCl_3$): δ [ppm] = 157.82 (s, N*Py*^{1}), 148.28 (s, N*Py*^{5}), 140.11–126.95 (aromatics), 137.62 (s, N*Py*^{3}), 113.58 (s, N*Py*^{2}), 107.40 (s, N*Py*^{4}), 54.91 (d, *J* = 15.1 Hz, N*C*P).

^{31}P{^{1}H}-NMR (121.49 MHz, $CDCl_3$): δ [ppm] = 5.19.

ESI–HRMS: m/z: 369.1517 $[M+H]^+$ (Calcd: 369.1515).

5.3.3. $H^{Py}N^{Py}CP$ – (1-(2-Pyridylamino)-1-(2-pyridyl)-methyl)diphenylphosphine

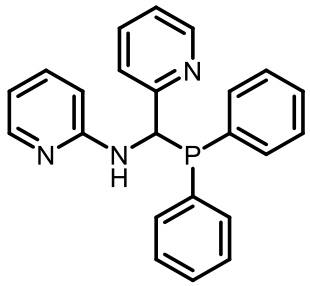

The synthesis of (1-(2-pyridylamino)-1-(2-pyridyl)-methyl)diphenylphosphine is done in two consecutive reaction steps.

Procedure 1. A 250 mL round bottom flask equipped with a *Dean-Stark* apparatus was charged with 2-aminopyridine (1.58 g, 16.8 mmol), 2-pyridinecarboxaldehyde (1.80 g, 16.8 mmol, 1.60 ml) and toluene (100 mL) and heated to reflux for approximately 24 h. The solvent was removed under reduced pressure and the resulting brown oil was destilled *via* a *Kugelrohr* apparatus to isolate the intermediate (*E*)-*N*,1-di(pyridin-2-yl)methanimine in form of a yellow crystalline solid.

Empirical formula: $C_{11}H_9N_3$

Molecular weight: 183.21 g/mol

Yield: 2.801 g, 15.29 mmol, 91%

^{1}H-NMR (300.13 MHz, C_6D_6): δ [ppm] = 9.82 (d, *J* = 0.7 Hz, 1H, NC*H*), 8.46 (ddd, *J* = 4.8, 1.8, 1.0 Hz, 1H, N*Py*^{5}), 8.33–8.26 (m, 2H, N*Py*^{3} / C*Py*^{5}), 7.24 (dt, *J* = 7.9, 1.0 Hz, 1H, C*Py*^{3}), 7.12–7.06 (m, 1H, C*Py*^{2}), 7.06–7.00 (m, 1H, N*Py*^{2}), 6.62–6.58 (m, 1H, N*Py*^{4}), 6.58–6.54 (m, 1H, C*Py*^{4}).

^{13}C{^{1}H}-NMR (75.48 MHz, C_6D_6): δ [ppm] = 163.83 (s, N*C*H), 160.48 (s, N*Py*^{1}), 155.15 (s, C*Py*^{1}), 149.64 (s, N*Py*^{5}), 149.02 (s, C*Py*^{5}), 137.40 (s, C*Py*^{2}), 135.65 (s, N*Py*^{2}), 124.75 (s, N*Py*^{4}), 122.03 (s, C*Py*^{4}), 121.38 (s, N*Py*^{3}), 120.38 (s, C*Py*^{3}).

ESI–HRMS: m/z: 184.0869 $[M+H]^+$ (Calcd: 184.0869).

Procedure 2. Under inert conditions, diphenyl phosphine (931 mg, 5.00 mmol, 0.87 mL) was added dropwise to a solution of (*E*)-*N*,1-di(pyridin-2-yl)methanimine (916 mg, 5.00 mmol) in hexane (5 mL) and stirred overnight at ambient temperature. The resulting suspension was filtered and the white solid was dried under reduced pressure. Further purification was not necessary, but could be performed by washing the solid with hexane (3 x 3mL).

Empirical formula: $C_{23}\,H_{20}\,N_3\,P$

Molecular weight: 369.41 g/mol

Yield: 1.507 g, 4.10 mmol, 82%

^{1}H-NMR (300.13 MHz, $CDCl_3$): δ [ppm] = 8.55 (ddd, *J* = 4.9, 1.8, 0.9 Hz, 1H, N*Py*^{5}), 8.13 (ddd, *J* = 5.0, 1.9, 0.9 Hz, 1H, C*Py*^{5}), 7.58–7.50 (m, 2H, *aromatics*), 7.46–7.40 (m, 1H, N*Py*^{3}), 7.39–7.21 (m, 9H, C*Py*^{3} / *aromatics*), 7.07 (ddt, *J* = 7.3, 4.8, 1.1 Hz, 1H, N*Py*^{2}), 6.98 (dq, *J* = 7.9, 1.1 Hz, 1H, N*Py*^{4}), 6.59 (ddd, *J* = 7.1, 5.0, 1.0 Hz, 1H, C*Py*^{2}), 6.42 (dt, *J* = 8.4, 0.9 Hz, 1H, C*Py*^{4}), 6.04 (dd, *J* = 8.8, 2.7 Hz, 1H, NC*H*P), 5.52 (dd, *J* = 9.0, 2.0 Hz, 1H, *H*NCP).

^{13}C{^{1}H}-NMR (75.48 MHz, $CDCl_3$): δ [ppm] = 159.77 (s, N*Py*^{1}), 157.76 (s, C*Ph*^{1}), 149.21 (s, N*Py*^{5}), 148.07 (s, C*Py*^{5}), 137.25 (s, C*Py*^{3}), 135.91 (s, N*Py*^{3}), 135.33–127.51 (*aromatics*), 122.49 (s, N*Py*^{4}), 121.70 (s, N*Py*^{2}), 113.57 (s, C*Ph*^{2}), 108.43 (s, C*Py*^{4}), 56.61 (d, *J* = 13.0 Hz, NC*P*).

^{31}P{^{1}H}-NMR (121.49 MHz, $CDCl_3$): δ [ppm] = 4.49.

ESI–HRMS: m/z: 370.1486 $[M+H]^+$ (Calcd: 370.1468).

5.3.4. $HN^{Py}CP$ – (1-Anilino-1-(2-pyridyl)-methyl)diphenylphosphine

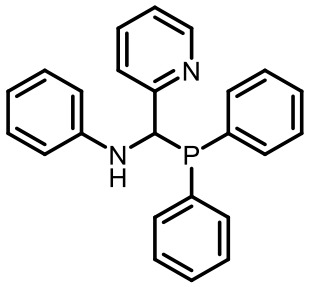

The synthesis of (1-anilino-1-(2-pyridyl)-methyl)diphenylphosphine is done in two consecutive reaction steps.

Procedure 1. A 250 mL round bottom flask equipped with a *Dean-Stark* apparatus was charged with aniline (8.70 g, 93.4 mmol, 8.52 mL), 2-pyridinecarboxaldehyde (10.0 g, 93.4 mmol, 8.88 ml) and toluene (100 mL) and heated to reflux for approximately 24 h. The solvent was removed under reduced pressure and the resulting brown oil was destilled *via* a *Kugelrohr* apparatus to isolate the intermediate (*E*)-*N*-phenyl-1-(pyridin-2-yl)methanimine in form of a yellow crystalline solid.

Empirical formula: $C_{12}\,H_{10}\,N_2$

Molecular weight: 182.23 g/mol

Yield: 16.00 g, 87.80 mmol, 94%

^{1}H-NMR (300.13 MHz, C_6D_6): δ [ppm] = 8.72 (d, *J* = 0.7 Hz, 1H, NC*H*), 8.47 (ddd, *J* = 4.8, 1.8, 1.0 Hz, 1H, C*Py*^{5}), 8.22 (dt, *J* = 7.9, 1.1 Hz, 1H, C*Py*^{3}), 7.18–7.09 (m, 4H, N*Ph*), 7.09–7.02 (m, 2H, C*Py*^{2}), 7.02–6.95 (m, 1H, N*Ph*), 6.63 (ddd, *J* = 7.5, 4.8, 1.2 Hz, 1H, C*Py*^{4}).

^{13}C{^{1}H}-NMR (75.48 MHz, C_6D_6): δ [ppm] = 160.97 (s, N*C*H), 155.20 (s, C*Py*^{1}), 151.34 (s, N*Ph*), 149.44 (s, C*Py*^{5}), 135.75 (s, C*Py*^{2}), 129.09 (s, N*Ph*), 126.38 (s, N*Ph*), 124.47 (s, C*Py*^{4}), 121.13 (s, C*Py*^{3}), 120.98 (s, N*Ph*).

Procedure 2. Under inert conditions, diphenyl phosphine (931 mg, 5.00 mmol, 0.87 mL) was added dropwise to a solution of (*E*)-*N*-phenyl-1-(pyridin-2-yl)methanimine (911 mg, 5.00 mmol) in hexane (5 mL) and stirred overnight at ambient temperature. The resulting suspension was filtered and the white solid was dried under reduced pressure. Further purification was not necessary, but could be performed by washing the solid with hexane (3 x 3mL).

Empirical formula: $C_{24}H_{21}N_2P$

Molecular weight: 368.42 g/mol

Yield: 1.309 g, 3.60 mmol, 72%

^{1}H-NMR (300.13 MHz, C_6D_6): δ [ppm] = 8.28 (ddd, *J* = 4.8, 1.7, 1.1 Hz, 1H, C*Py*^{5}), 7.56 (m, 2H, *aromatics*), 7.39–7.30 (m, 2H, *aromatics*), 7.05–6.86 (m, 8H, *aromatics*), 6.82–6.72 (m, 2H, C*Py*^{3,2}), 6.65–6.55 (m, 3H, *aromatics*), 6.38 (dddd, *J* = 6.7, 4.8, 1.9, 1.0 Hz, 1H, C*Py*^{4}), 5.55 (dd, *J* = 8.4, 2.8 Hz, 1H, NC*H*P), 4.85 (dd, *J* = 8.4, 2.8 Hz, 1H, *H*NCP).

^{13}C{^{1}H}-NMR (75.48 MHz, C_6D_6): δ [ppm] = 160.09 (s, C*Py*^{1}), 149.02 (s, C*Py*^{5}), 147.37–114.09 (*aromatics*), 135.14 (s, C*Py*^{3}), 122.08 (s, C*Py*^{2}), 121.14 (s, C*Py*^{4}), 59.79 (d, *J* = 12.7 Hz, N*C*P).

^{31}P{^{1}H}-NMR (121.49 MHz, C_6D_6): δ [ppm] = 4.04.

ESI–HRMS: m/z: 385.1469 $[M+O]^+$ (Calcd: 385.1464).

5.3.5. HNCCP – (2-(2,6-Di-*iso*-propylanilino)-2-phenylethyl)diphenylphosphine

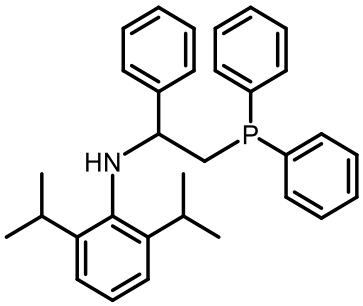

The synthesis of (2-(2,6-di-*iso*-propylanilino)-2-phenylethyl)diphenylphosphine is done in two consecutive reaction steps.

Procedure 1. A 250 mL round bottom flask equipped with a *Dean-Stark* apparatus was charged with 2,6-di-*iso*-propylaniline (16.707 g, 94.2 mmol, 17.77 ml), benzaldehyde (10.0 g, 94.2 mmol, 9.52 ml) and toluene (100 mL) and heated to reflux for approximately 24 h. The solvent was removed under reduced pressure and the resulting brown oil was destilled *via* a *Kugelrohr* apparatus to isolate the intermediate (*E*)-*N*-(2,6-di-*iso*-propylphenyl)-1-phenylmethanimine in form of a yellow oil which crystallized after a while.

Empirical formula: $C_{19}H_{23}N$

Molecular weight: 265.40 g/mol

Yield: 20.213 g, 76.2 mmol, 81%

^{1}H-NMR (300.13 MHz, $CDCl_3$): δ [ppm] = 8.31 (s, 1H, NC*H*), 8.06–7.99 (m, 2H, C*Ph*), 7.63–7.56 (m, 3H, C*Ph*), 7.32–7.15 (m, 3H, N*Ph*), 3.10 (sept, *J* = 6.9 Hz, 2H, C*H*$(CH_3)_2$), 1.28 (d, *J* = 6.9 Hz, 12H, CH*(*$CH_3)_2$).

Procedure 2. Under inert conditions a solution of *n*-butyllithium in hexane (1.57 M, 1.602 g, 25.0 mmol, 15.92 mL) and TMEDA (2.906 g, 25.0 mmol, 3.75 mL) were combined and stirred for 15 min at ambient temperature. Subsequently methyldiphenylphosphine (5.0 g, 25.0 mmol, 4.65 mL) was added and stirred for further 30 min until a yellowish precipitate was formed, which was dissolved with THF (5 mL). After 15 min a separately prepared solution of (*E*)-*N*-(2,6-di-*iso*-propylphenyl)-1-phenylmethanimine (4.976 g, 18.8 mmol) in THF (5 mL) was transferred to the reaction mixture and stirred overnight. The resulting dark red solution was quenched with degassed water (20 mL) and

resulted in two yellowish layers. The organic layer was separated via cannula and the aqueous phase was washed with THF (2 x 20 mL). The combined layers were dried over $MgSO_4$, filtered and concentrated under reduced pressure. After addition of degassed methanol (10 mL) the product began to precipitate after a few minutes and was stirred overnight. The resulting suspension was filtered, washed with methanol (3 x 4 mL) and dried *i.vac.* to isolate the target compound as a fine white powder.

Empirical formula: $C_{32}\ H_{36}\ N\ P$

Molecular weight: 465.62 g/mol

Yield: 3.941 g, 8.46 mmol, 45%

^{1}H-NMR (300.13 MHz, C_6D_6): δ [ppm] = 7.46–7.31 (m, 4H, *aromatics*), 7.09–6.98 (m, 14H, *aromatics*), 4.10 (dq, *J* = 9.9, 7.2 Hz, 1H, NC*H*Ph), 3.48 (dd, *J* = 9.9, 1.2 Hz, 1H, N*H*), 3.18 (sept, *J* = 6.7 Hz, 2H, C*H*$(CH_3)_2$), 2.93–2.56 (m, 2H, C*H*$_2$PPh_2), 1.00 (dd, *J* = 26.4, 6.8 Hz, 12H, CH*(CH$_3$)$_2$*).

^{13}C{^{1}H}-NMR (75.48 MHz, C_6D_6): δ [ppm] = 143.18–123.47 (*aromatics*), 62.62 (d, *J* = 16.6 Hz, N*C*HPh), 36.37 (d, *J* = 15.1 Hz, *C*H$_2$P$Ph_2$15), 27.78 (d, *J* = 1.6 Hz, *C*H$(CH_3)_2$), 24.02 (s, CH*(CH$_3$)$_2$*), 23.83 (s, CH*(CH$_3$)$_2$*).

^{31}P{^{1}H}-NMR (121.49 MHz, C_6D_6): δ [ppm] = -23.76 (d, *J* = 7.2 Hz).

ESI–HRMS: m/z: 466.2634 $[M+H]^+$ (Calcd: 466.2658).

5.3.6. MesNHPy – *N*-Mesityl-*N*-(2-pyridyl)amine

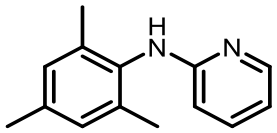

Under inert conditions, a high-pressure flask was charged with 2,4,6-trimethylaniline (17.12 g, 126.58 mmol, 17.83 ml) and 2-bromopyridine (10.00 g, 63.29 mmol, 6.17 ml), sealed and stirred for 16 h at 170°C. The mixture was allowed to cool down to under 100°C and subsequently quenched with a saturated aqueous solution of $NaHCO_3$ (30 mL). Potentially formed solids were dissolved in diethyl ether (30 mL). The mixture was transferred into a separating funnel and another portion of saturated aqueous $NaHCO_3$ solution (250 mL) was added. The resulting solution was extracted with diethyl ether (3 x 200 mL), the combined organic layers were dried over $MgSO_4$ and all volatiles were removed *i.vac*. During this process, the raw product precipitates in form of colorless crystals, which were washed with hexane (3 x 20 mL) and dried *i.vac*. If further purification steps are needed the product can be recrystallized from hot toluene or *via* a *Kugelrohr* apparatus.

Empirical formula: $C_{14}\,H_{16}\,N_2$

Molecular weight: 212.29 g/mol

Yield: 8.7 g, 41 mmol, 65%

^{1}H-NMR (300.13 MHz, C_6D_6): δ [ppm] = 8.09 (ddd, *J* = 5.0, 2.0, 0.9 Hz, 1H, N*Py*^{5}), 7.64 (s, 1H, N*H*), 6.95 (ddd, *J* = 8.4, 7.1, 1.9 Hz, 1H, N*Py*^{3}), 6.80 (q, *J* = 0.7 Hz, 2H, N*Mes*^{3,5}), 6.26 (ddd, *J* = 7.1, 5.0, 1.0 Hz, 1H, N*Py*^{4}), 5.92 (dt, *J* = 8.4, 0.9 Hz, 1H, N*Py*^{2}), 2.15 (s, 3H, N*Mes-4-CH*$_3$), 2.14 (s, 6H, N*Mes-2,6-CH*$_3$).

^{13}C{^{1}H}-NMR (75.48 MHz, C_6D_6): δ [ppm] = 158.83 (s, N*Py*^{1}), 148.45 (s, N*Py*^{5}), 137.32 (s, N*Py*^{3}), 136.55 (s, N*Mes*^{2,6}), 135.70 (s, N*Mes*^{1}), 134.57 (s, N*Mes*^{4}), 129.19 (s, N*Mes*^{3,5}), 112.88 (s, N*Py*^{4}), 105.08 (s, N*Py*^{2}), 20.64 (s, N*Mes-4-CH*$_3$), 17.99 (s, N*Mes-2,6-CH*$_3$).

ESI–HRMS: m/z: Calcd.: 213.1386; found: 213.1388 $[M]^+$.

5.3.7. PhNHPy – *N*-Phenyl-*N*-(2-pyridyl)amine

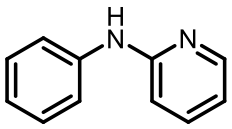

Under inert conditions, a high-pressure flask was charged with phenylaniline (10.7 g, 115.0 mmol, 10.5 ml) and 2-bromopyridine (9.1 g, 57.4 mmol, 5.6 ml), sealed and stirred for 16 h at 170°C. The mixture was allowed to cool down to under 100°C and subsequently quenched with a saturated aqueous solution of $NaHCO_3$ (30 mL). Potentially formed solids were dissolved in diethyl ether (30 mL). The mixture was transferred into a separating funnel and another portion of saturated aqueous $NaHCO_3$ solution (100 mL) was added. The resulting solution was extracted with diethyl ether (3 x 30 mL), the combined organic layers were dried over $MgSO_4$ and all volatiles were removed *i.vac*. During this process, the raw product precipitates in form of colorless crystals, which were washed with hexane (3 x 20 mL) and dried *i.vac*. If further purification steps are needed the product can be recrystallized from hot toluene or *via* a *Kugelrohr* apparatus.

Empirical formula: $C_{11}H_{10}N_2$

Molecular weight: 170.21 g/mol

Yield: 7.096 g, 41.69 mmol, 73%

^{1}H-NMR (300.13 MHz, C_6D_6): δ [ppm] = 8.18 (ddd, *J* = 5.0, 2.0, 0.9 Hz, 1H, N*Py*^{5}), 7.81 (s, 1H, N*H*), 7.28 – 7.20 (m, 2H, N*Ph*^{3,5}), 7.17 – 7.07 (m, 2H, N*Ph*^{2,6}), 6.99 (ddd, *J* = 8.5, 7.1, 2.0 Hz, 1H, N*Py*^{3}), 6.91 – 6.83 (m, 1H, N*Ph*^{4}), 6.55 (dt, *J* = 8.5, 0.9 Hz, 1H, NPy^4), 6.34 (ddd, *J* = 7.2, 5.0, 0.9 Hz, 1H, N*Py*^{2}).

^{13}C{^{1}H}-NMR (75.48 MHz, C_6D_6): δ [ppm] = 156.63 (s, N*Py*^{1}), 148.29 (s, N*Py*^{5}), 141.10 (s, N*Ph*^{1}), 137.11 (s, N*Py*^{3}), 129.05 (s, N*Ph*^{2,6}), 122.36 (s, N*Ph*^{4}), 120.43 (s, N*Ph*^{3,5}), 114.36 (s, N*Py*^{2}), 107.95 (s, N*Py*^{4}).

ESI–HRMS: m/z: Calcd.: 171.0917; found: 171.0917 $[M]^+$.

5.3.8. NHSiCl – 1,3-*N*,*N'*-Di-*tert*-butyl-benzamidinato-chloro-silylene

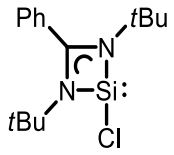

The synthesis of 1,3-*N*,*N'*-di-*tert*-butyl-benzamidinato-chloro-silylene is done in two consecutive reaction steps.

Under inert conditions a 250 mL Schlenk flask is charged with *N*,*N'*-di-*tert*-butyl-carbodiimide (6.00 g, 38.90 mmol, 7.50 ml) and diethyl ether (150 mL) and cooled down to -78°C. A solution of phenyllithium in dibutyl ether (1.9 M, 3.43 g, 40.85 mmol, 21.50 ml) is added dropwise over a period of 1 h under vigorously stirring. The reaction mixture is warmed up to ambient temperature and stirred for another 4 h to complete the lithiation. The solution is cooled to -78°C again and trichlorosilane (6.59 g, 48.63 mmol, 4.91 ml) is added dropwise in the same manner over a period of 30 min. The resulting solution is allowed to warm up to room temperature and stirred overnight. The yellow suspension is filtrated, the residue washed with diethyl ether (20 mL) and concentrated until crystal growth starts. The resulting mixture is filtrated at -78°C and the colorless crystals are getting dried *i.vac*. afterwards. To prevent decomposition the raw intermediate NHSiCl is used without further purification or analysis.

In a glovebox, LiHMDS (6.23 g, 37.23 mmol) was added to the previously dried intermediate (11.76 g, 35.46 mmol). At -78°C the substrates were flushed with toluene (150 mL) and stirred overnight while allowed to warm up to ambient temperature. The orange suspension was filtered *via* Whatman or over a thin layer of Celite. The resulting orange filtrate was concentrated whereby a crystal growth of colorless needles can be observed. The flask is stored at -30°C overnight and cold filtrated. For further purification, the colorless crystals were washed with cold toluene (20 mL), filtrated and dried *i.vac.* The mother liquor can be again concentrated and worked up in the same manner to improve the yield.

Empirical formula: $C_{15}H_{23}N_2ClSi$

Molecular weight: 294.90 g/mol

Yield: 9.52 g, 32.27 mmol, 91 %

^{1}H-NMR (300.13 MHz, C_6D_6): δ [ppm] = 6.89 (m, 5H, CPh), 1.09 (s, 18H, N^t*Bu*).

$^{13}C\{^1H\}$-NMR (75.48 MHz, C_6D_6): δ [ppm] = 166.56 (s, *C*Ph), 132.52 (s, C*Ph*), 129.69 (s, C*Ph*), 127.99 (s, C*Ph*), 127.76 (s, C*Ph)*, 127.67 (s, C*Ph)*, 127.35 (s, C*Ph*), 53.43 (s, N*C*$(CH_3)_3$), 31.04 (s, NC*$(CH_3)_3$*).

$^{29}Si\{^1H\}$-NMR (59.63 MHz, C_6D_6): δ [ppm] = 14.26.

ESI–HRMS: m/z: Calcd.: 294.1319; found: 294.1320 $[M]^+$.

5.3.9. NHSiNCCP – 1,3-*N*,*N*'-Di-*tert*-butyl-benzamidinato-*N*-(2-(2,6-di-*iso*-propylanilino)-2-phenylethyl)diphenylphosphine)-silylene

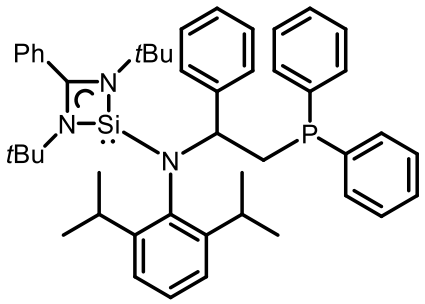

A solution of *n*-butyllithium in hexane (1.59 M, 259 mg, 4.04 mmol, 2.54 mL) was added dropwise to a vigorously stirring suspension of (2-(2,6-di-*iso*-propylanilino)-2-phenylethyl)-diphenylphosphine (HNCCP) (1.879 g, 4.04 mmol) in diethyl ether (30 mL) at -20°C. After 30 min, the reaction mixture was allowed to warm up to ambient temperature and stirred for another 2 h. Meanwhile a solution of the chloro benzamidinate NHSiCl (1.190 g, 4.04 mmol) in toluene (20 mL) was separately prepared and subsequently transferred to the reaction mixture at -78°C and stirred overnight while warming up to ambient temperature again. All volatiles of the reaction mixture were removed under reduced pressure and the resulting brownish oil was extracted with hexane. After filtrating the suspension over *Celite* the filtrate was concentrated and stored at -26°C for three days. The colorless to slightly brownish crystals were filtrated, washed with cold hexane (3 x 10 mL) and dried under reduced pressure.

Empirical formula: $C_{47}\,H_{58}\,N_3\,P\,Si$

Molecular weight: 724.06 g/mol

Yield: 968 mg, 1.337 mmol, 33%

^{1}H-NMR (300.13 MHz, C_6D_6): δ [ppm] = 7.46–7.43 (m, 2H, *aromatics*), 7.17–7.09 (m, 2H, *aromatics*), 7.05–6.64 (m, 19H, *aromatics*), 4.82 (ddd, *J* = 13.1, 6.1, 3.3 Hz, 1H, NC*H*Ph), 3.82 (sept, *J* = 6.9 Hz, 1H, C*H*$(CH_3)_2$), 3.54 (ddd, *J* = 13.2, 4.4, 3.4 Hz, 1H, C*H*$_2$PPh$_2$), 3.40 (sept, *J* = 6.7 Hz, 1H, C*H*$(CH_3)_2$), 3.31–3.18 (m, 1H, C*H*$_2$PPh$_2$), 1.27 (d, *J* = 6.7 Hz, 3H, CH(CH_3)$_2$), 1.18 (s, 3H, N*tBu*), 1.13 (d, *J* = 6.8 Hz, 3H, CH(CH_3)$_2$) 1.12 (s, 3H, N*tBu*), 0.83 (d, *J* = 6.8 Hz, 3H, CH(CH_3)$_2$), 0.60 (d, *J* = 6.8 Hz, 3H, CH(CH_3)$_2$).

$^{13}C\{^1H\}$-NMR (75.48 MHz, C_6D_6): δ [ppm] = 163.19 (s, N*C*N), 149.69–124.34 (*aromatics*), 67.62 (s, N*C*HPh), 67.27 (s, N*C*HPh), 53.86 (s, N*C*$(CH_3)_3$), 53.74 (s, N*C*$(CH_3)_3$), 35.38 (s, *C*H_2PPh_2) 35.20 (s, *C*H_2PPh_2), 32.96 (s, N*tBu*), 32.87 (s, N*tBu*), 28.44 (s, *C*$(CH_3)_2$), 28.32 (s, *C*$(CH_3)_2$), 27.72 (s, C(*CH*$_3)_2$), 27.70 (s, C(*CH*$_3)_2$), 23.93 (s, C(*CH*$_3)_2$), 23.50 (s, C(*CH*$_3)_2$).

$^{29}Si\{^1H\}$-NMR (59.63 MHz, C_6D_6): δ [ppm] = -11.96.

$^{31}P\{^1H\}$-NMR (121.49 MHz, C_6D_6): δ [ppm] = -20.05.

LIFDI–MS: m/z: 740.4 $[M+O]^+$, 724.4 $[M]^+$.

Elemental analysis for $C_{47}H_{58}N_3PSi$ (found (calc.) [%]): C 77.62 (77.97), H 7.72 (8.07), N 5.95 (5.80).

5.3.10. $[(NHSiCl)(AuCl)]_2$ – Bis-1,3-*N*,*N'*-di-*tert*-butyl-benzamidinato-chloro-silylene-gold(I)-chloride

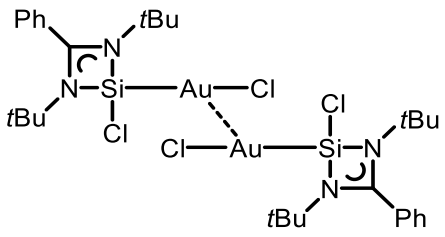

Under inert conditions the chloro silylene NHSiCl (495 mg, 1.67 mmol) was dissolved in a mixture of toluene (5 mL) and THF (5 mL) in a ratio of 1:1. The gold(I)-precursor $AuCl(SMe_2)$ (493 mg, 1.67 mmol) was added in small portions and stirred over night at ambient temperature. The resulting suspension was filtered and the filtrate was concentrated. The complex crystallized in form of colorless crystals suitable for X-ray analysis after storing the solution at -35°C over night. Filtration and drying *i.vac.* resulted in the target compound.

Empirical formula: $C_{30}H_{46}N_4Si_2Au_2Cl_4$

Molecular weight: 1054.63 g/mol

Yield: 0.4625 g, 0.439 mmol, 52%

^{1}H-NMR (400.13 MHz, THF-*d8*): δ [ppm] = 7.83–7.77 (m, 2H, C*Ph*), 7.73–7.68 (m, 2H, C*Ph*), 7.67–7.60 (m, 6H, C*Ph*), 1.30 (s, 36H, N^t*Bu*).

^{13}C{^{1}H}-NMR (100.62 MHz, THF-*d8*): δ [ppm] = 177.05 (s, *C*Ph), 131.58 (s, C*Ph*), 129.36 (s, C*Ph*), 128.58 (s, C*Ph*), 128.50 (s, C*Ph*), 128.22 (s, C*Ph*), 127.78 (s, C*Ph*), 55.24 (s, N*C*$(CH_3)_3$), 30.34 (s, N^t*Bu*).

^{29}Si{^{1}H}-NMR (59.63 MHz, THF-*d8*): δ [ppm] = 40.03.

LIFDI–MS: m/z: 1052.0 $[M]^+$, 1017.0 $[M\text{-}Cl]^+$, 491.0 [M-(NHSiCl-Au-Cl)(Cl)]$^+$, 329.1 [M-(NHSiCl-Au-Cl)(Au)]$^+$.

Elemental analysis for $C_{30}H_{46}N_4Si_2Au_2Cl_4$ (found (calc.) [%]): C 34.35 (34.17), H 4.24 (4.40), N 5.45 (5.31).

5.3.11. [(NHSiMes)(AuCl)] – 1,3-*N*,*N'*-Di-*tert*-butyl-benzamidinato-*N*-mesityl-*N*-(2-pyridyl)amino-silylene-gold(I)-chloride

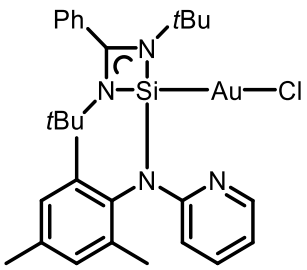

The gold-complex $[(NHSiCl)(AuCl)]_2$ (200 mg, 0.190 mmol) was dissolved in THF (2 mL). Alongside the amine MesNHPy (80.5 mg, 0.379 mmol) was dissolved in THF (3 mL) separately, subsequently added to the first solution and cooled to -30°C. Meanwhile LiHMDS (63.4 mg, 0.379 mmol) was taken up in THF (2 mL) and added dropwise to the cooled solution. The reaction mixture was allowed to warm up to ambient temperature overnight under constant stirring. The resulting yellowish solution was concentrated to a minimum and a mixture of toluene (2 mL) and hexane (2 mL) was added until the crude product precipitated as a grey solid, which was subsequently filtered. The resulting crude product was dissolved in DCM (2.5 mL) and once more filtered to remove the rest of LiCl salt. The clear yellowish filtrate was concentrated and stored at -35°C for crystallization. The pure product was isolated as colorless crystals, suitable for X-ray analysis.

Empirical formula: $C_{29}H_{38}N_4SiAuCl$

Molecular weight: 703.15 g/mol

Yield: 0.0995 g, 0.142 mmol, 37 %

^{1}H-NMR (300.13 MHz, THF-*d8*): δ [ppm] = 8.32 (dt, *J* = 5.1, 1.6 Hz, 1H, N*Py*), 7.77 7.70 (m, 1H, C*Ph*), 7.65 7.48 (m, 4H, C*Ph*, 1H, N*Py*), 7.05 (s, 2H, N*Mes*), 6.85 (ddd, *J* = 7.2, 5.2, 0.9 Hz, 1H, N*Py*), 6.02 (dt, *J* = 8.4, 1.0 Hz, 1H, N*Py*), 2.36 (s, 6H, o-Mes*CH$_3$*), 2.34 (s, 3H, p-Mes*CH$_3$*), 1.09 (s, 18H, N*tBu*).

^{13}C{^{1}H}-NMR (75.48 MHz), THF-*d8*): δ [ppm] = 173.72 (s, *C*Ph), 158.94 (s, N*Py*^{1}), 144.73 (s, N*Py*^{5}), 139.40 (s, C*Ph*^{3,4}), 137.43 (s, N*Mes*^{2,6}), 136.82 (s, N*Mes*^{1}), 136.44 (s, N*Mes*^{4}), 132.02 (s, C*Ph*^{1}), 130.69 (s, N*Py*^{3}), 129.36 (s, N*Mes*^{3,5}), 129.24 (s, C*Ph*^{4}), 127.86 (s, C*Ph*^{2,6}), 114.35 (s, NPy^4), 106.19 (s, N*Py*^{2}), 55.08 (s, N*C*(CH$_3$)$_3$), 31.03 (s, N*tBu*), 20.09 (s, NMes*Me*^{4}), 18.68 (s, NMes*Me*^{2,6}).

^{29}Si{^{1}H}-NMR (59.63 MHz, THF-*d8*): δ [ppm] = n/a.

LIFDI–MS: m/z: 702.2 $[M]^+$, 667.2 $[M\text{-}Cl]^+$, 505.3 $[M\text{-}Au]^+$.

Elemental analysis for $C_{29}H_{38}N_4SiAuCl(CH_2Cl_2)$ (found (calc.) [%]): C 46.41 (45.72), H 4.99 (5.12), N 7.52 (7.11).

5.3.12. $[(NHSiCl)(AgCl)]_4$ – Tetrakis-1,3-*N*,*N'*-di-*tert*-butyl-benzamidinato-chloro-silylene-silver(I)-chloride

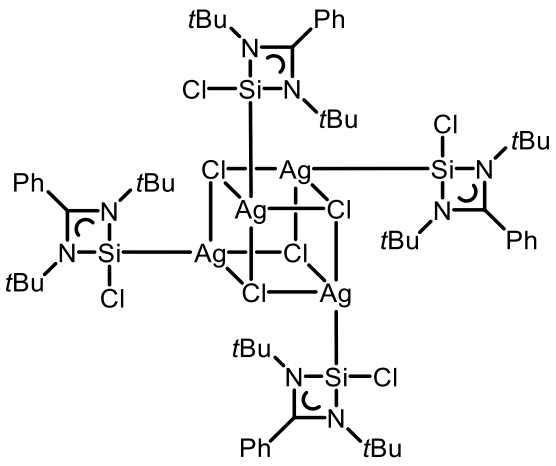

A solution of the chloro benzamidinato chloro silylene NHSiCl (500 mg, 1.695 mmol) in toluene (2 mL) was transferred to a suspension of silver(I) chloride (243 mg, 1.695 mmol) in toluene (2 mL) at ambient temperature under the exclusion of light and was stirred overnight. The target compound precipitated in form of very fine colorless crystalline needles, which were filtrated and dried under reduced pressure. Further purification was not necessary. The mother liquor was concentrated to gain more of the target compound that was worked up in the same manner.

Empirical formula: $C_{60}\,H_{92}\,N_8\,Si_4\,Cl_8\,Ag_4$

Molecular weight: 1752.86 g/mol

Yield: 514 mg, 1.17 mmol, 69%

^{1}H-NMR (300.13 MHz, DCM-*d2*): δ [ppm] = 7.66–7.54 (m, 20H, C*Ph*), 1.30 (s, 72H, N*tBu*).

^{13}C{^{1}H}-NMR (75.48 MHz, DCM-*d2*): δ [ppm] = 172.29 (s, N*C*N), 137.91 (s, C*Ph*), 130.93 (s, C*Ph*), 130.53 (s, C*Ph*), 128.33 (s, C*Ph*), 128.14 (s, C*Ph*), 54.82 (s, *C*$(CH_3)_3$), 30.97 (s, N*tBu*).

^{29}Si{^{1}H}-NMR (59.63 MHz, DCM-*d2*): δ [ppm] = 37.83.

Elemental analysis for $C_{60}H_{92}N_8Si_4Cl_8Ag_4(C_7H_8)$ (found (calc.) [%]): C 43.37 (43.62), H 5.61 (5.46), N 6.17 (6.07).

5.3.13. [(NHSiMes)(AgCl)] – 1,3-*N*,*N*'-Di-*tert*-butyl-benzamidinato-*N*-mesityl-*N*-(2-pyridyl)amino-silylene-silver(I)-chloride

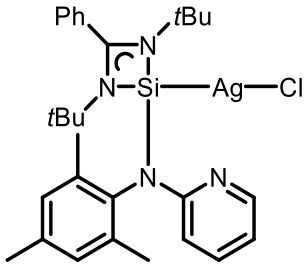

A solution of tetrakis-1,3-*N*,*N*'-di-*tert*-butyl-benzamidinato-chloro-silylene-silver(I)-chloride (252 mg, 0.575 mmol) and *N*-mesityl-*N*-(2-pyridyl)amine (122 mg, 0.575 mmol) in a mixture of diethyl ether (3 mL) and dichloromethane (3 mL) was cooled to -30°C. Subsequently LiHMDS (96 mg, 0.575 mmol) was added in small portions under the exclusion of light and stirred overnight while warming up to ambient temperature. The resulting yellow suspension was filtered and all volatiles were removed under reduced pressure. After the addition of THF (1 mL) and storage at -35°C the target compound readily crystallized within hours in form of very thin yellow plates that were filtered and dried *i.vac*.

Empirical formula: $C_{29}H_{38}N_4SiAgCl$

Molecular weight: 614.05 g/mol

Yield: 209.5 mg, 0.341 mmol, 59%

^{1}H-NMR (300.13 MHz, DCM-*d2*): δ [ppm] = 8.22 (d, *J* = 5.1 Hz, 1H, N*Py*^{5}), 7.67–7.40 (m, 6H, N*Py*^{3} / C*Ph*), 7.12–6.95 (s, 2H, N*Mes*), 6.78 (ddd, *J* = 7.2, 5.1, 0.9 Hz, 1H, N*Py*^{2}), 5.99 (dt, *J* = 8.4, 1.0 Hz, 1H, N*Py*^{4}), 2.34 (s, 3H, NMes-*p*-*CH*$_3$), 2.27 (s, 6H, NMes-*o*-*CH*$_3$), 1.03 (s, 18H, N*tBu*).

^{13}C{^{1}H}-NMR (75.48 MHz, DCM-*d2*): δ [ppm] = 171.49 (s, N*C*N), 158.81 (s, N*Py*^{1}), 144.96 (s, N*Py*^{5}), 138.77 (s, N*Py*^{3}), 137.18 (s,N*Mes*^{2,6}), 136.94 (s, N*Mes*^{1}), 136.81(s, N*Mes*^{4}), 131.98 (s, C*Ph*^{1}), 130.70 (s, C*Ph*^{3,5}), 129.50 (s, N*Mes*^{3,5}), 128.36 (s, C*Ph*^{4}), 128.16 (s, C*Ph*^{2,6}), 114.23 (s, N*Py*^{4}), 106.87 (s, N*Py*^{2}), 55.15 (s, *C*(CH$_3$)$_3$), 31.51 (s, N*tBu*), 20.68 (s, NMes-*p*-*CH*$_3$), 19.05 (s, NMes-*p*-*CH*$_3$).

^{29}Si{^{1}H}-NMR (59.63 MHz, DCM-*d2*): δ [ppm] = n/a.

LIFDI–MS: m/z: 505.3 $[M\text{-}Ag]^+$.

Elemental analysis for $C_{29}H_{38}N_4SiAgCl(C_4H_8O)$ (found (calc.) [%]): C 57.49 (57.77), H 5.93 (6.76), N 8.20 (8.17).

5.3.14. $[(NHSiCl)(CuCl)]_4$ – Tetrakis-1,3-*N*,*N'*-di-*tert*-butyl-benzamidinato-chloro-silylene-copper(I)-chloride

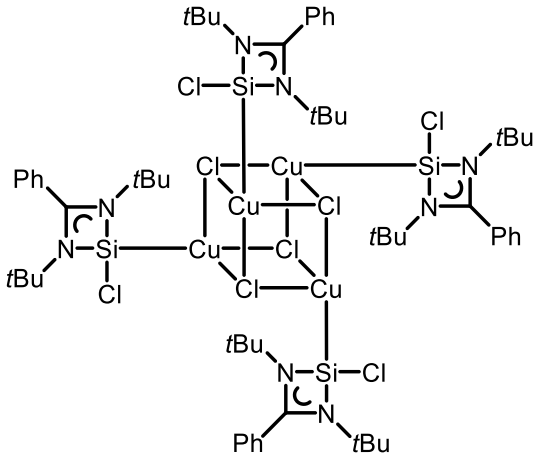

The chloro silylene NHSiCl (500 mg, 1.695 mmol) was dissolved in THF (8 mL), whereupon the copper precursor CuCl (167.8 mg, 1.695 mmol) was added in small portions to the stirring solution at ambient temperature. The white suspension turned into a yellowish clear solution after approximately one hour but kept stirring for further 16 h. The reaction mixture was filtered to remove suspended particles and was concentrated right afterwards. Subsequent addition of *n*-hexane (3 mL) to the concentrate resulted in an immediate crystal growth at room temperature. The resulting yellow crystals were filtered and dried under reduced pressure to gain the pure target compound.

Empirical formula: $C_{60}\ H_{92}\ N_8\ Si_4\ Cl_8\ Cu_4$

Molecular weight: 1575.58 g/mol

Yield: 448.8 mg, 0.285 mmol, 67%

^{1}H-NMR (300.13 MHz, DCM-d2): δ [ppm] = 7.72–7.69 (m, 4H, C*Ph*), 7.60–7.49 (m, 16H, C*Ph*), 1.26 (s, 72H, N^t*Bu*).

^{13}C{^{1}H}-NMR (75.48 MHz, DCM-d2): δ [ppm] = 172.11 (*C*Ph), 131.21 (C*Ph*), 130.59 (C*Ph*), 128.68 (C*Ph*), 128.38 (C*Ph*), 128.07 (C*Ph*), 54.33 (N*C*(CH$_3$)$_3$), 30.53 (N^t*Bu*).

^{29}Si{^{1}H}-NMR (59.63 MHz, DCM-d2): δ [ppm] = 27.73.

Elemental analysis for $C_{60}H_{92}N_8Si_4Cl_8Cu_4$ (found (calc.) [%]): C, 45.44 (45.74); H, 5.65 (5.89); N, 7.31 (7.11).

5.3.15. [(NHSiCl)(CuBr)]$_4$ – Tetrakis-1,3-*N*,*N*'-di-*tert*-butyl-benzamidinato-chloro-silylene-copper(I)-bromide

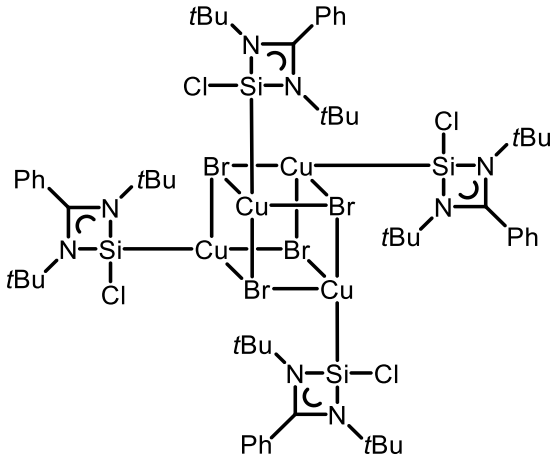

The chloro silylene NHSiCl (500 mg, 1.695 mmol) was dissolved in THF (8 mL), whereupon the copper precursor CuBr(SMe_2) (349 mg, 1.695 mmol) was added in small portions to the stirring solution at ambient temperature. The white suspension turned into a yellowish clear solution after approximately one hour but kept stirring for further 16 h. The reaction mixture was filtered to remove suspended particles and was concentrated right afterwards. Subsequent addition of *n*-hexane (3 mL) to the concentrate resulted in an immediate crystal growth at room temperature. The resulting yellow crystals were filtered and dried under reduced pressure to gain the pure target compound.

Empirical formula: $C_{60}H_{92}N_8Si_4Br_4Cl_4Cu_4$

Molecular weight: 1753.39 g/mol

Yield: 550.0 mg, 0.302 mmol, 71%

^{1}H-NMR (400.13 MHz, C_6D_6): δ [ppm] = 7.35 (d, *J* = 8.1 Hz, 4H, C*Ph*), 7.13–6.98 (m, 16H, C*Ph*), 1.21 (s, 36H, N^t*Bu*).

^{13}C{^{1}H}-NMR (100.62 MHz, C_6D_6): δ [ppm] = 171.52 (s, *C*Ph), 131.08 (s, C*Ph*), 130.09 (s, C*Ph*), 128.35 (s, C*Ph*), 128.32 (s, C*Ph*), 127.66 (s, C*Ph*), 54.29 (s, N*C*$(CH_3)_3$), 30.75 (s, N^t*Bu*).

^{29}Si{^{1}H}-NMR (59.63 MHz, C_6D_6): δ [ppm] = 26.09.

ESI–HRMS: m/z: 2144.78 (<5) [M - Br^- + 2 SbF_6^-]$^+$. (Calcd: 2144.7821; Found: 2144.7776.)

Elemental analysis for $C_{60}H_{92}N_8Si_4Br_4Cl_4Cu_4(C_7H_8)$ (found (calc.) [%]): C, 43.00 (43.60); H, 5.40 (5.46); N, 5.96 (6.07).

5.3.16. $[(NHSiCl)(CuI)]_4$ – Tetrakis-1,3-*N*,*N*'-di-*tert*-butyl-benzamidinato-chloro-silylene-copper(I)-iodide

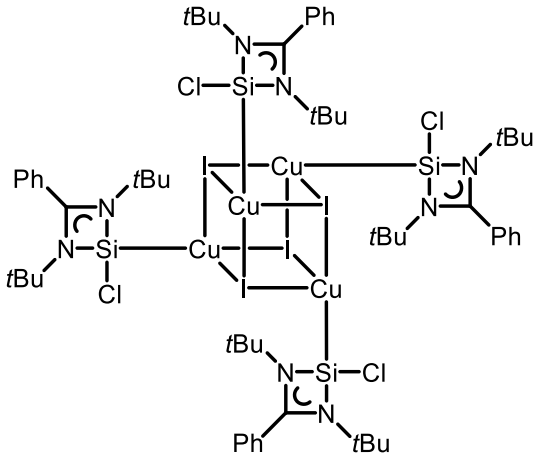

The chloro silylene NHSiCl (500 mg, 1.695 mmol) was dissolved in THF (8 mL), whereupon the copper precursor CuI (322,8 mg, 1.695 mmol) was added in small portions to the stirring solution at ambient temperature. The white suspension turned into a yellowish clear solution after approximately one hour but kept stirring for further 16 h. The reaction mixture was filtered to remove suspended particles and was concentrated right afterwards. Subsequent addition of *n*-hexane (3 mL) to the concentrate resulted in an immediate crystal growth at room temperature. The resulting yellow crystals were filtered and dried under reduced pressure to gain the pure target compound.

Empirical formula: $C_{60}\ H_{92}\ N_8\ Si_4\ Cl_4\ I_4\ Cu_4$

Molecular weight: 1941.38 g/mol

Yield: 454.0 mg, 0.234 mmol, 55%

^{1}H-NMR (300.13 MHz, DCM-d2): δ [ppm] = 7.66–7.48 (m, 20H, C*Ph*), 1.30 (s, 36H, N^t*Bu*).

^{13}C{^{1}H}-NMR (75.48 MHz, DCM-d2): δ [ppm] = 172.14 (*C*Ph), 130.87 (C*Ph*), 130.63 (C*Ph*), 128.63 (C*Ph*), 128.50 (C*Ph*), 128.16 (C*Ph*), 54.58 (N*C*$(CH_3)_3$), 31.11 (N^t*Bu*).

^{29}Si{^{1}H}-NMR (59.63 MHz, DCM-d2): δ [ppm] = 22.62.

Elemental analysis for $C_{60}H_{92}N_8Si_4I_4Cl_4Cu_4(C_7H_8)$ (found (calc.) [%]): C, 38.92 (39.57); H, 4.61 (4.96); N, 5.42 (5.51).

5.3.17. [(NHSiMes)$_2$(CuCl)$_3$] – Bis-1,3-*N*,*N'*-di-*tert*-butyl-benzamidinato-*N*-mesityl-*N*-(2-pyridyl)amino-silylene-tris-copper(I)-chloride

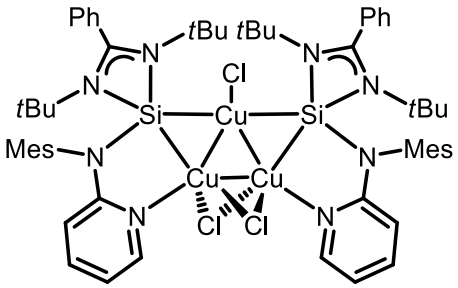

The copper precursor [(NHSiCl)(CuCl)]$_4$ (213 mg, 0.135 mmol) and the amine MesNHPy (115 mg, 0.540 mmol) were dissolved in a mixture of toluene (3 mL) and THF (3 mL) in a ratio of 1:1 and cooled down to -30°C. A separately prepared solution of LiHMDS (90.4 mg, 0.540 mmol) in THF (2 mL) was added dropwise and subsequently allowed to warm up to ambient temperature under constant stirring for approximately 16 h. The resulting suspension was concentrated until a yellowish solid precipitated which was filtered off and dissolved in DCM in order to remove the LiCl salt in another filtration step. The concentrated solution was stored at -35°C for one day. The target compound was isolated in form of yellow crystals suitable for X-ray analysis.

Empirical formula: $C_{58}H_{76}N_8Si_2Cl_3Cu_3$

Molecular weight: 1238.45 g/mol

Yield: 183.0 mg, 0.148 mmol, 55%

^{1}H-NMR (300.13 MHz, DCM-*d2*): δ [ppm] = 8.39 (br s, 2H, N*Py*), 7.61–7.42 (m, 10H, C*Ph*), 7.45 (ddd, *J* = 8.8 Hz, 6.2, 1.9 Hz, 2H, N*Py*), 7.06 (s, 4H, N*Mes*), 6.80 (t, *J* = 6.2 Hz, 2H, N*Py*), 6.01 (dt, *J* = 8.5, 1.0 Hz, 2H, N*Py*), 2.39–2.35 (m, 18H, Mes*CH$_3$*), 1.11 (br s, 36H, N^t*Bu*).

^{13}C{^{1}H}-NMR (75.48 MHz), DCM-*d2*): δ [ppm] = 172.09 (*C*Ph), 160.05 (N*Py*), 146.05 (N*Py*), 138.71 (N*Mes*), 137.92 (N*Mes*), 137.24 (N*Mes*), 136.46 (N*Mes*), 130.57 (N*Py*), 129.62 (C*Ph*), 128.96 (N*Mes*), 128.38 (C*Ph*), 128.15 (C*Ph*), 128.00 (C*Ph*), 114.42 (N*Py*), 108.16 (N*Py*), 54.73 (N*C*(CH$_3$)$_3$), 31.32 (N^t*Bu*), 20.66 (Mes*Me*), 19.38 (Mes*Me*).

^{29}Si{^{1}H}-NMR (59.63 MHz, DCM-*d2*): δ [ppm] = n/a.

LIFDI–MS: m/z: 1117.2 (5) [M-Cl]$^+$, 919.4 (100) [M-Cu$_2$Cl$_3$]$^+$.

Elemental analysis for $C_{58}H_{76}N_8Si_2Cl_3Cu_3(C_7H_8)_2$ (found (calc.) [%]): C, 61.83 (60.78); H, 6.33 (6.52); N, 7.70 (7.88).

5.3.18. [(NHSiMes)$_2$(CuBr)$_3$] – Bis-1,3-*N*,*N*'-di-*tert*-butyl-benzamidinato-*N*-mesityl-*N*-(2-pyridyl)amino-silylene-tris-copper(I)-bromide

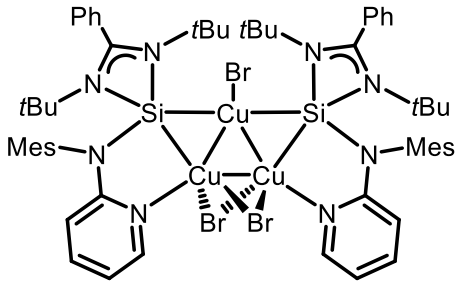

Method A:

The copper precursor [(NHSiCl)(CuBr)]$_4$ (234 mg, 0.134 mmol) and the amine MesNHPy (114 mg, 0.535 mmol) were dissolved in a mixture of toluene (3 mL) and THF (3 mL) in a ratio of 1:1 and cooled down to -30°C. A separately prepared solution of LiHMDS (89.5 mg, 0.535 mmol) in THF (2 mL) was added dropwise and subsequently allowed to warm up to ambient temperature under constant stirring for approximately 16 h. The resulting suspension was concentrated until a yellowish solid precipitated which was filtered off and dissolved in DCM in order to remove the LiCl salt in another filtration step. The concentrated solution was stored at -35°C for one day. The target compound was isolated in form of yellow crystals suitable for X-ray analysis.

Method B:

The copper precursor [(NHSiCl)(CuBr)]$_4$ (200.8 mg, 0.115 mmol) was dissolved in THF (1.5 mL) and cooled down to -30°C. A separately prepared solution of the lithiated amine MesNLiPy (100.0 mg, 0.229 mmol) in THF (1.5 mL) was added dropwise and subsequently allowed to warm up to ambient temperature under constant stirring for approximately 16 h. Hexane (2 mL) and toluene (2 mL) were added to the resulting yellow solution and the precipitated LiCl salt was filtered off. The reaction mixture was concentrated and stored at -35°C for one day. The target compound was isolated in form of yellow crystals suitable for X-ray analysis.

Empirical formula: $C_{58}H_{76}N_8Si_2Br_3Cu_3$

Molecular weight: 1371.82 g/mol

Yield: *Method A:* 77.8 mg, 0.0567 mmol, 42%

Method B: 77.0 mg, 0.0561 mmol, 49%

^{1}H-NMR (300.13 MHz, DCM-*d2*): δ [ppm] = 8.41 (br s, 2H, N*Py*), 7.55–7.36 (m, 10H, C*Ph*), 7.42–7.34 (m, 2H, N*Py*), 7.00 (s, 4H, N*Mes*), 6.73 (t, *J* = 6.2 Hz, 2H, N*Py*), 5.93 (d, *J* = 8.3 Hz, 2H, N*Py*), 2.32–2.29 (m, 18H, Mes*CH*$_3$), 1.04 (br s, 36H, N^t*Bu*).

^{13}C{^{1}H}-NMR (75.48 MHz), DCM-*d2*): δ [ppm] = 172.12 (*C*Ph), 160.65 (N*Py*), 148.25 (N*Py*), 140.13 (N*Mes*), 138.64 (N*Py*), 137.30 (N*Mes*), 136.46 (N*Mes*), 130.45 (C*Ph*),129.56 (N*Mes*), 128.78 (C*Ph*), 127.90 (C*Ph*), 125.09 (C*Ph*), 114.19 (N*Py*), 110.37 (N*Py*), 54.64 (N*C*(CH$_3$)$_3$), 31.21 (N^t*Bu*), 20.39 (Mes*Me*), 19.36 (Mes*Me*).

^{29}Si{^{1}H}-NMR (59.63 MHz, DCM-*d2*): δ [ppm] = none.

LIFDI–MS: m/z: 1435.0 (100) [M-Br+2THF]$^+$, 1291.2 (5) [M-Br]$^+$.

Elemental analysis for $C_{58}H_{76}N_8Si_2Br_3Cu_3(C_7H_8)_2$ (found (calc.) [%]): C, 58.26 (55.57); H, 5.71 (5.96); N, 7.20 (7.19).

5.3.19. $[(NHSiMes)_2(CuI)_3]$ – Bis-1,3-*N*,*N*'-di-*tert*-butyl-benzamidinato-*N*-mesityl-*N*-(2-pyridyl)amino-silylene-tris-copper(I)-iodide

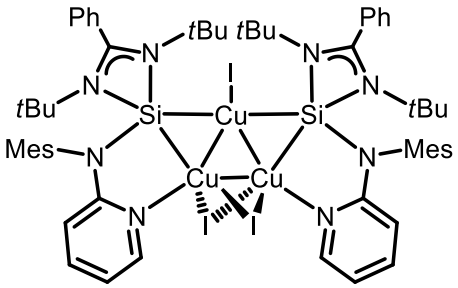

The copper precursor $[(NHSiCl)(CuI)]_4$ (334 mg, 0.172 mmol) and the amine MesNHPy (146 mg, 0.688 mmol) were dissolved in a mixture of toluene (3 mL) and THF (3 mL) in a ratio of 1:1 and cooled down to -30°C. A separately prepared solution of LiHMDS (115 mg, 0.688 mmol) in THF (2 mL) was added dropwise and subsequently allowed to warm up to ambient temperature under constant stirring for approximately 16 h. The resulting suspension was concentrated until a yellowish solid precipitated which was filtered off and dissolved in DCM in order to remove the LiCl salt in another filtration step. The concentrated solution was stored at -35°C for one day. The target compound was isolated in form of yellow crystals suitable for X-ray analysis.

Empirical formula: $C_{58}\ H_{76}\ N_8\ Si_2\ I_3\ Cu_3$

Molecular weight: 1512.80 g/mol

Yield: 159 mg, 0.105 mmol, 31%

^{1}H-NMR (300.13 MHz, DCM-*d2*): δ [ppm] = 8.72 (br s, 2H, N*Py*), 7.59–7.40 (m, 10H, C*Ph*), 7.48–7.42 (m, 2H, N*Py*), 7.08 (s, 4H, N*Mes*), 6.79 (ddd, *J* = 6.8, 5.4, 1.1 Hz, 2H, N*Py*), 6.00 (d, *J* = 8.5 Hz, 2H, N*Py*), 2.41–2.37 (m, 18H, Mes*CH₃*), 1004 (s, 36H, N^t*Bu*).

^{13}C{^{1}H}-NMR (75.48 MHz), DCM-*d2*): δ [ppm] = 172.68 (*C*Ph), 161.13 (N*Py*), 148.57 (N*Py*), 139.93 (N*Mes*), 138.96 (N*Py*), 137.93 (N*Mes*), 137.34 (N*Mes*), 131.68 (C*Ph*), 130.47 (C*Ph*), 129.82 (N*Mes*), 128.96 (C*Ph*), 128.15 (C*Ph*), 114.46 (N*Py*), 110.31 (N*Py*), 54.68(N*C*(CH$_3$)$_3$), 31.28 (N^t*Bu*), 20.60 (Mes*Me*), 20.12 (Mes*Me*).

^{29}Si{^{1}H}-NMR (59.63 MHz, DCM-*d2*): δ [ppm] = none.

LIFDI–MS: m/z: 1385.3 (10) $[M\text{-}I]^+$, 1003.6 (< 5) $[M\text{-}Cu_2I_3]^+$.

Elemental analysis for $C_{58}H_{76}N_8Si_2I_3Cu_3(C_7H_8)$ (found (calc.) [%]): C, 53.53 (48.64); H, 5.21 (5.28); N, 7.11 (6.98).

5.3.20. $[(PhNPy)Cu]_x$ – *N*-Phenyl-*N*-(2-pyridyl)amine-copper(I)

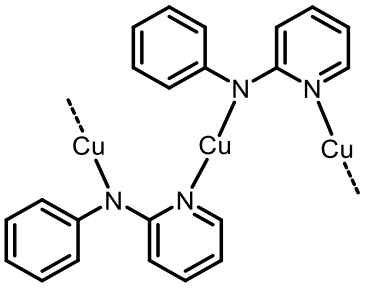

Under inert conditions, sodium (176 mg, 12.3 mmol) was added portion wise to a stirring solution of PhNHPy (2.10 g, 12.3 mmol) in ethanol (50 mL). After 15 min a separately prepared solution of Cu(I)Br (1.68 g, 12.3 mmol) in ethanol (25 mL) was transferred to the reaction mixture and subsequently heated to reflux for approximately 18 h. The bright yellow precipitate, which formed during the reaction, was filtered off, washed with ethanol (3 x 10 mL) and dried under reduced pressure. The target compound was isolated as a fine bright yellow powder.

Empirical formula: $C_{11}\,H_9\,N_2\,Cu$

Molecular weight: 232.76 g/mol

Yield: 2.07 g, 8.89 mmol, 72%

Elemental analysis for $(C_{11}H_9N_2)_4Cu_5Br$ (found (calc.) [%]): C 50.29 (49.19), H 3.34 (3.38), N 10.66 (10.43).

5.3.21. $[(NHSiPh)_2(CuCl)_3]$ – Bis-1,3-*N*,*N*'-di-*tert*-butyl-benzamidinato-*N*-phenyl-*N*-(2-pyridyl)amino-silylene-tris-copper(I)-chloride

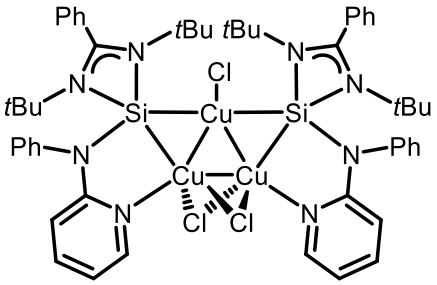

The copper(I) precursor $(PhNPyCu)_x$ (158 mg, 0.678 mmol) was added to a stirring solution of NHSiCl (200 mg, 0.678 mmol) in THF (2 mL) at ambient temperature. After 16 h the yellow solution was slightly concentrated and stored at -35°C for one day to gain the target compound as yellow crystals which were filtered and dried under reduced pressure.

Empirical formula: $C_{52}H_{64}N_8Cl_3Cu_3Si_2$

Molecular weight: 1154.30 g/mol

Yield: 114.5 mg, 0.0992 mmol, 42%

^{1}H-NMR (300.13 MHz, DCM-*d2*): δ [ppm] = 8.42 (br s, 2H, N*Py*), 7.51 (t, *J* = 7.7 Hz, 4H, N*Ph*), 7.42 (dd, *J* = 5.6, 3.3 Hz, 4H, N*Ph*), 7.36–7.30 (m, 2H, N*Py*, 10H, C*Ph*), 6.99 (d, *J* = 7.6 Hz, 2H, N*Ph*), 6.72–6.68 (m, 2H, N*Py*), 6.19–6.07 (br s, 2H, N*Py*), 1.06 (s, 36H, N^t*Bu*).

^{13}C{^{1}H}-NMR (75.48 MHz, DCM-*d2*): δ [ppm] = 174.40 (*C*Ph), 163.82 (N*Py*), 149.76 (N*Py*), 144.82 (N*Ph*), 140.05 (N*Py*), 132.91 (C*Ph*), 132.09 (N*Ph*), 131.45 (N*Ph*), 130.39 (C*Ph*), 130.09 (N*Ph*), 129.71 (C*Ph*), 128.50 (C*Ph*), 116.39 (N*Py*), 112.60 (N*Py*), 55.93 (N*C*$(CH_3)_3$), 32.47 (N^t*Bu*).

^{29}Si{^{1}H}-NMR (59.63 MHz, DCM-*d2*): δ [ppm] = n/a.

LIFDI–MS: m/z: 1117.2 (< 5) $[M\text{-}Cl]^+$, 919.4 (100) $[M\text{-}Cu_2Cl_3]^+$.

Elemental analysis for $C_{52}H_{64}N_8Cl_3Cu_3Si_2(C_4H_8O)$ (found (calc.) [%]): C 55.09 (54.84), H 5.68 (5.92), N 9.19 (9.14).

5.3.22. $[(NHSiCl)(CuBr(SMe_2))]_2$ – Bis-1,3-*N*,*N*'-di-*tert*-butyl-benzamidinato-chloro-silylene-copper(I)-(dimethylsulfide)-bromide

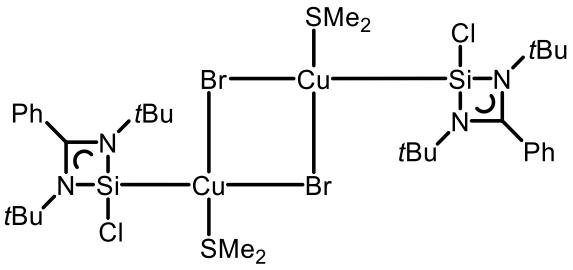

The chloro silylene NHSiCl (500 mg, 1.695 mmol) was dissolved in THF (5 mL) and cooled to -30°C. Under heavy stirring the neat copper(I) precursor $CuBr(SMe_2)$ (349 mg, 1.695 mmol) was slowly added in small portions. After the reaction mixture was allowed to warm up to ambient temperature over night the resulting greenish suspension was filtered to gain a pale green solid and a yellow filtrate. The solid was dissolved in DCM (2 mL) and stored at -35°C for overnight. The target compound was isolated as yellow-greenish crystals suitable for X-ray analysis.

Empirical formula: $C_{34}\ H_{58}\ N_4\ S_2\ Si_2\ Br_2\ Cl_2\ Cu_2$

Molecular weight: 1000.96 g/mol

Yield: 197.8 mg, 0.1976 mmol, 12%

^{1}H-NMR (300.13 MHz, DCM-d_2): δ [ppm] = 7.67–7.42 (m, 10H, C*Ph*), 2.25 (s, 12H, S*Me*$_2$), 1.27 (s, 36H, N*tBu*).

^{13}C{^{1}H}-NMR (75.48 MHz), DCM-d_2): δ [ppm] = 172.40 (s, NCN), 130.83 (s, C*Ph*), 130.70 (s, C*Ph*), 128.54 (s, C*Ph*), 128.20 (s, C*Ph*), 128.08 (s, C*Ph*), 54.57 (s, *C*$(CH_3)_3$), 30.90 (s, N*tBu*), 19.14 (s, S*Me*$_2$).

^{29}Si{^{1}H}-NMR (59.63 MHz, DCM-d_2): δ [ppm] = n/a.

5.3.23. $[(NHSiCl)(ZnCl_2)]_2$ – Bis-1,3-*N*,*N*'-di-*tert*-butyl-benzamidinato-chloro-silylene-zinc(II)-chloride

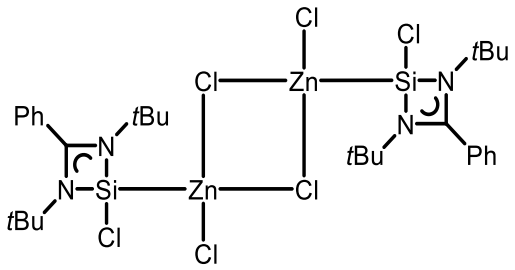

Under inert conditions the neat chloro benzamidinato NHSiCl (496 mg, 1.676 mmol) was dissolved in a mixture of THF (3 mL) and toluene (3 mL) in a ratio of 1:1. Subsequently dried $ZnCl_2$ (228 mg, 1.676 mmol) was added in small portions and left stirring overnight at ambient temperature. The clear colorless solution was concentrated and stored at -35°C for one day. The colorless crystals were filtrated and dried under reduced pressure.

Empirical formula: $C_{30}\ H_{46}\ N_4\ Cl_6\ Si_2\ Zn_2$

Molecular weight: 862.36 g/mol

Yield: 484 g, 0.561 mmol, 67%

^{1}H-NMR (300.13 MHz, THF-*d8*): δ [ppm] = 7.85–7.48 (m, 10H, C*Ph*), 1.27 (s, 36H, N^t*Bu*).

^{13}C{^{1}H}-NMR (75.48 MHz, THF-*d8*): δ [ppm] = 158.04 (s, *C*Ph), 132.35 (s, C*Ph*), 130.99 (s, C*Ph*), 129.88 (s, C*Ph*), 129.54 (s, C*Ph*), 129.53 (s, C*Ph*), 129.34 (s, C*Ph*), 56.25 (s, N*C*$(CH_3)_3$), 31.43 (s, N^t*Bu*).

^{29}Si{^{1}H}-NMR (59.63 MHz, THF-*d8*): δ [ppm] = 17.81.

Elemental analysis for $C_{30}H_{46}N_4Cl_6Si_2Zn_2$ (found (calc.) [%]): C 42.92 (41.78), H 5.29 (5.38), N 6.55 (6.50).

5.3.24. [(NHSiMes)($ZnCl_2$)]$_2$ – Bis-1,3-*N*,*N'*-di-*tert*-butyl-benzamidinato-*N*-mesityl-*N*-(2-pyridyl)amino-silylene-zinc(II)-chloride

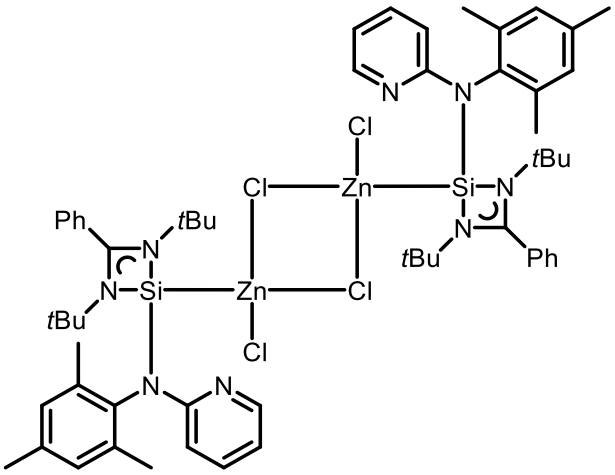

The amine MesNHPy (98.5 mg, 0.464 mmol) was added to a solution of the zinc complex [(NHSiCl)($ZnCl_2$)]$_2$ (200 mg, 0.232 mmol) in THF (3 mL) and cooled to -30°C. Separately a solution of LiHMDS (77.6 mg, 0.464 mmol) was prepared in THF (2 mL) and subsequently added dropwise to the reaction mixture under vigorously stirring. While stirring overnight, the mixture was allowed to warm up to ambient temperature. The yellow solution was concentrated and hexane (2 m L) and toluene (2 mL) were added to precipitate the LiCl salt, which were filtered off afterwards. After concentrating the resulting yellow filtrate, it was stored at -35°C for one day, to isolate the target compound in form of colorless crystals, after filtering and drying under reduced pressure.

Empirical formula: $C_{58}\ H_{76}\ N_8\ Cl_4\ Si_2\ Zn_2$

Molecular weight: 1214.03 g/mol

Yield: 124.1 g, 0.102 mmol, 44%

^{1}H-NMR (300.13 MHz, DCM-*d2*): δ [ppm] = 8.41 (ddd, *J* = 5.3, 1.9, 0.9 Hz, 1H, N*Py*), 7.66–7.50 (m, 5H, N*Py* / C*Ph*), 7.40–7.32 (m, 1H, C*Ph*), 7.04 (s, 2H, N*Mes*), 6.90 (ddd, *J* = 7.3, 5.3, 1.0 Hz, 1H, N*Py*), 6.18 (dt, *J* = 8.5, 1.0 Hz, 1H, N*Py*), 2.34 (s, 3H, p-Mes*CH$_3$*), 2.29 (s, 6H, o-Mes*CH$_3$*), 1.04 (s, 18H, N*tBu*).

$^{13}C\{^1H\}$-NMR (75.48 MHz, DCM-*d2*): δ [ppm] = 173.82 (s, *C*Ph), 160.67 (s, N*Py*), 146.27 (s, N*Py*), 140.49 (s, C*Ph*), 137.12 (s, N*Mes*), 136.85 (s, N*Mes*), 136.48 (s, N*Mes*), 131.05 (s, C*Ph*), 130.55 (s, N*Py*), 129.90 (s, C*Ph*), 128.39 (s, C*Ph*), 128.06 (s, C*Ph*), 115.54 (s, N*Py*), 110.62 (s, N*Py*), 54.97 (s, N*C*$(CH_3)_3$), 30.76 (s, N*tBu*), 20.50 (s, NMes-p-*Me*), 19.34 (s, NMes-o-*Me*).

$^{29}Si\{^1H\}$-NMR (59.63 MHz, DCM-*d2*): δ [ppm] = n/a.

LIFDI–MS: m/z: 1177.3 $[M\text{-}Cl+2H]^+$.

Elemental analysis for $C_{58}H_{76}N_8Cl_4Si_2Zn_2$ (found (calc.) [%]): C 57.36 (57.38), H 6.11 (6.31), N 9.28 (9.23).

5.3.25. [(PhNPy)(ZnCl)(EtOH)] – *N*-Phenyl-*N*-(2-pyridyl)amine-zinc(II)-chloride ethanol

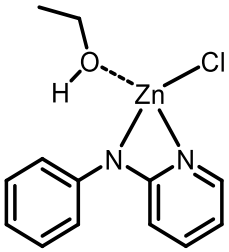

Under inert conditions, the amine PhNHPy (2.0 g, 11.7 mmol) was dissolved in dry ethanol (25 mL) and equipped with a reflux condenser. Under vigorously stirring neat sodium (270 mg, 11.7 mmol) was added in small portions and stirred for 30 min at ambient temperature. Afterwards a separate solution of dry $ZnCl_2$ (1.6 g, 11.7 mmol) in ethanol (25 mL) was transferred to the reaction mixture and heated to reflux for overnight. The resulting orange suspension was filtered and all volatiles were removed under reduced pressure. The target compound was isolated as an orange amorphous solid which was used without further purification.

Empirical formula: $C_{13}\,H_{15}\,N_2\,Cl\,O\,Zn$

Molecular weight: 316.11 g/mol

Yield: 2.6 g, 8.3 mmol, 71%

^{1}H-NMR (300.13 MHz, THF-*d8*): δ [ppm] = 8.25 (s br, 1H, N*Py*), 7.66 (s br, 1H, N*Py*), 7.47 – 6.92 (m, 6H, N*Py* / N*Ph*), 6.87 – 6.66 (m, 1H, N*Py*), 5.12 (s, 1H, O*H*), 3.97 (s br, 2H, CH_2CH_3), 1.22 (s br, 3H, CH_2CH_3).

^{13}C{^{1}H}-NMR (75.48 MHz, THF-*d8*): δ [ppm] = 156.92 (s, N*Py*), 147.20 (s, N*Py*), 139.97 (s, N*Py*), 139.49(s, N*Ph*), 123.61 (s, N*Ph*), 129.16 (s, N*Ph*), 121.34 (s, N*Ph*), 114.44 (s, N*Py*), 109.52 (s, N*Py*), 62.41 (s, CH_2CH_3), 19.53 (s, CH_2CH_3).

ESI–MS: m/z: 439.1 (10) $[2M\text{-}ZnCl\text{-}2EtOH+2H]^+$, 403.1 (20) $[2M\text{-}ZnCl_2\text{-}2EtOH+H]^+$.

Elemental analysis for $C_{13}H_{15}N_2ClOZn$ (found (calc.) [%]): C 51.3 (49.4), H 4.82 (4.78), N 8.82 (8.86).

5.3.26. [(NHSiPh)($ZnCl_2$)] – 1,3-*N*,*N*'-Di-*tert*-butyl-benzamidinato-*N*-phenyl-*N*-(2-pyridyl)amino-silylene-zinc(II)-chloride

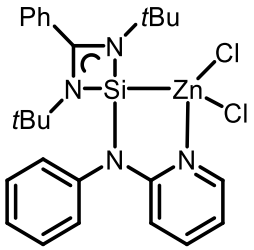

At -30°C [(PhNPy)(ZnCl)EtOH] (231 mg, 0.731 mmol) was added to a stirring solution of NHSiCl (216 mg, 0.731 mmol) in DCM (1 mL). The reaction mixture quickly changed its color from deep orange to bright yellow and was left stirring overnight and allowed to warm up to ambient temperature. The resulting solution was concentrated and hexane (1 mL) was added whereas crystal growth started readily. After storage for one day at -35°C the colorless crystal were filtrated and dried under reduced pressure.

Empirical formula: $C_{26}H_{32}N_4Cl_2SiZn$

Molecular weight: 564.94 g/mol

Yield: 197 mg, 0.349 mmol, 48%

^{1}H-NMR (300.13 MHz, DCM-*d2*): δ [ppm] = 8.35 (ddd, *J* = 5.4, 2.0, 0.8 Hz, 1H, N*Py*), 7.68–7.57 (m, 5H, N*Py* / C*Ph*), 7.56–7.46 (m, 3H, C*Ph* / N*Ph*), 7.43–7.32 (m, 3H, C*Ph* / N*Ph*) 7.05–6.91 (m, 2H, N*Py* / N*Ph*), 6.52 (dt, *J* = 8.6, 1.0 Hz, 1H, N*Py*), 1.15 (s, 18H, N*tBu*).

^{13}C{^{1}H}-NMR (75.48 MHz, DCM-*d2*): δ [ppm] = 176.41 (s, *C*Ph), 161.10 (N*Py*), 146.78 (s, N*Py*), 140.70 (s, N*Py*), 131.44 (s, C*Ph*), 130.12 (s, C*Ph*), 129.39 (s, C*Ph*), 128.55 (s, N*Ph*) 128.43 (s, N*Ph*), 127.62 (s, N*Ph*), 127.24 (s, N*Ph*), 116.68 (s, NPy), 112.32 (s, NPy), 54.87 (s, N*C*(CH_3)$_3$), 30.42 (s, N*tBu*).

^{29}Si{^{1}H}-NMR (59.63 MHz, DCM-*d2*): δ [ppm] = n/a.

LIFDI–MS: m/z: 527.2 $[M\text{-}Cl]^+$, 463.2 $[M\text{-}ZnCl]^+$, 428.3 $[M\text{-}ZnCl_2]^+$.

Elemental analysis for $C_{26}H_{32}N_4Cl_2SiZn(CH_2Cl_2)$ (found (calc.) [%]): C 50.17 (49.90), H 5.01 (5.27), N 8.77 (8.62).

5.3.27. [(NHSiCl)(ZnHMDS$_2$)] – 1,3-*N*,*N'*-Di-*tert*-butyl-benzamidinato-chloro-silylene-zinc(II)-bis(bis(trimethylsilyl)amide)

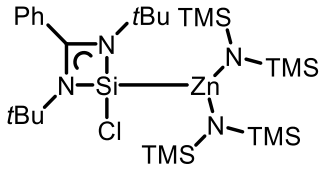

Two separate prepared solutions of the chloro benzamidinato silylene NHSiCl (500 mg, 1.69 mmol) and the precursor Zn(II)HMDS$_2$ (652 mg, 1.69 mmol, 0.68 mL) in diethyl ether (each 2 mL) were transferred into each other and stirred at ambient temperature. The solution turned slightly yellowish overnight and was concentrated afterwards, to store it at -35°C. The target compound crystallized in form of colorless needles, which were filtrated and dried *i.vac*. Recrystallization in a mixture of diethyl ether and hexane (1:1) yields in colorless blocks.

Empirical formula: $C_{27}\,H_{59}\,N_4\,Si_5\,Cl\,Zn$

Molecular weight: 681.05 g/mol

Yield: 806.9 mg, 1.183 mmol, 70%

^{1}H-NMR (300.13 MHz, DCM-*d2*): δ [ppm] = 7.77–7.26 (m, 5H, C*Ph*), 1.25 (s, 18H, N*tBu*), 0.16 (s, 36H, N(Si*Me*$_3$)$_2$).

^{13}C{^{1}H}-NMR (75.48 MHz, DCM-*d2*): δ [ppm] = 179.22 (s, NCN), 131.96 (s, C*Ph*), 128.60 (s, C*Ph*), 127.85 (s, C*Ph*), 57.18 (s, *C*(CH$_3$)$_3$), 31.13 (s, N*tBu*), 5.10 (s, N(Si*Me*$_3$)$_2$).

^{29}Si{^{1}H}-NMR (59.63 MHz, DCM-*d2*): δ [ppm] = n/a.

Elemental analysis for $C_{27}H_{59}N_4Si_5ClZn$ (found (calc.) [%]): C 47.72 (47.62), H 8.28 (8.28), N 8.34 (8.34).

5.3.28. [(ClAu)(NHSiNCCP)(AuCl)] – 1,3-*N*,*N'*-Di-*tert*-butyl-benzamidinato-*N*-(2-(2,6-di-*iso*-propylanilino)-2-phenylethyl)diphenylphosphine-silylene-*Si*,*P*-di-gold(I)-chloride

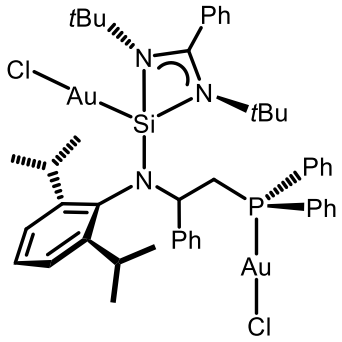

To a solution of 1,3-*N*,*N'*-di-*tert*-butyl-benzamidinato-*N*-(2-(2,6-di-*iso*-propylanilino)-2-phenylethyl)diphenylphosphine)-silylene (NHSiNCCP) (50.0 mg, 0.0691 mmol) in deuterated benzene (0.5 mL) the gold(I) precursor $AuCl(SMe_2)$ (40.7 mg, 0.1382 mmol) was added at ambient temperature and stirred overnight. Traces of black precipitate were filtered off and the colorless filtrate was concentrated under reduced pressure until a crystal growth could be observed. The target compound was isolated as colorless needless.

Empirical formula: $C_{47}\ H_{58}\ N_3\ P\ Si\ Cl_2\ Au_2$

Molecular weight: 1188.89 g/mol

Yield: 40.3 mg, 0.0339 mmol, 49%

^{1}H-NMR (300.13 MHz, C_6D_6): δ [ppm] = 7.29–7.24 (m, 2H, *aromatics*), 7.08–6.50 (m, 21H, *aromatics*), 4.76 (dt, *J* = 10.9, 5.3 Hz, 1H, NC*H*Ph), 3.62 (sept, *J* = 6.6 Hz, 1H, C*H*$(CH_3)_2$), 3.15–2.93 (m, 3H, C*H*$(CH_3)_2$ / C*H*$_2$PPh_2), 1.31 (d, *J* = 6.8 Hz, 3H, CH(*CH*$_3$)$_2$), 1.22 (d, *J* = 6.5 Hz, 3H, CH(*CH*$_3$)$_2$), 1.04 (s, 9H, N*tBu*), 0.97 (d, *J* = 6.6 Hz, 3H, CH(*CH*$_3$)$_2$), 0.94 (s, 9H, N*tBu*), 0.30 (d, *J* = 6.9 Hz, 3H, CH(*CH*$_3$)$_2$).

^{13}C{^{1}H}-NMR (75.48 MHz, C_6D_6): δ [ppm] = 176.02 (s, N*C*N), 149.83–124.83 (*aromatics*), 65.82 (s, NCHPh), 55.45 (s, *C*$(CH_3)_3$), 55.41 (s, *C*$(CH_3)_3$), 37.69 (d, *J* = 10.4 Hz, *C*H$_2$PPh_2), 32.43 (s, N*tBu*), 32.29 (s, N*tBu*), 28.61 (s, C(*CH*$_3$)$_2$), 28.47 (s, *C*$(CH_3)_2$), 28.44 (s, *C*$(CH_3)_2$), 28.30 (s, C(*CH*$_3$)$_2$), 24.04 (s, C(*CH*$_3$)$_2$), 22.62 (s, C(*CH*$_3$)$_2$).

^{29}Si{^{1}H}-NMR (59.63 MHz, C_6D_6 / THF-*d8*): δ [ppm] = n/a.

^{31}P{^{1}H}-NMR (121.49 MHz, THF-*d8*): δ [ppm] = 25.82.

LIFDI–MS: m/z: 990.4 $[M\text{-}Au]^+$.

5.3.29. [(BrCu)(NHSiNCCP)(CuBr)] – 1,3-*N*,*N*‘-Di-*tert*-butyl-benzamidinato-*N*-(2-(2,6-di-*iso*-propylanilino)-2-phenylethyl)diphenylphosphine-silylene-*Si*,*P*-di-copper(I)-bromide

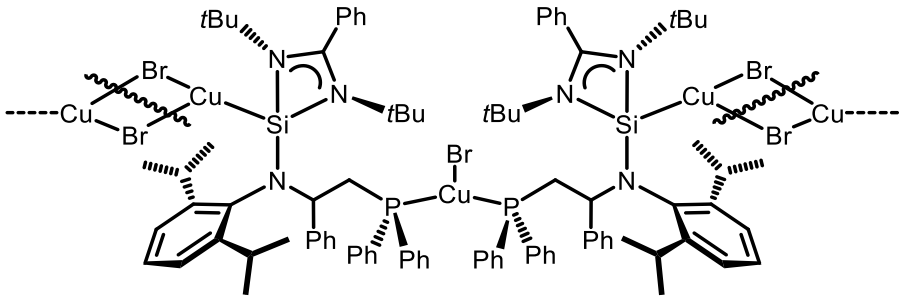

To a solution of 1,3-*N*,*N*‘-di-*tert*-butyl-benzamidinato-*N*-(2-(2,6-di-*iso*-propylanilino)-2-phenylethyl)diphenylphosphine)-silylene (NHSiNCCP) (45.0 mg, 0.0695 mmol) in deuterated benzene (0.5 mL) the copper(I) precursor $CuBr(SMe_2)$ (14.3 mg, 0.0695 mmol) was added at ambient temperature and stirred overnight. The resulting white precipitate was filtered and dried under reduced pressure. It showed to be nearly insoluble in common solvents. Through slow vapor diffusion tiny colorless crystals could be isolated, which could be analyzed via XRD analysis.

Empirical formula: $C_{94}\,H_{116}\,N_6\,P_2\,Si_2\,Br_3\,Cu_3$

Molecular weight: 1878.47 g/mol

Yield: 25.1 mg, 0.0267 mmol, 38% (white precipitate)

5.4. Crystallographic Section

5.4.1. Crystal Selection and Handling

Suitable crystals for single crystal X-ray diffraction analysis of the presented compounds were either preselected from a *Schlenk* flask under an argon gas flow and were quickly transferred into perfluorated oil on a microscope slide, or they were preselected under an argon atmosphere in a glovebox and were directly covered in perfluorated oil on a microscope slide. The final selection was done using a polarizer microscope with additionally cooling for thermally unstable compounds with a nitrogen gas flow by the *X-TEMP2* device.[231,232] The selected crystals were mounted to the tip of a *MiTeGen©MicroMount*, fixed to a goniometer head and shock cooled to 100(2) K by the corresponding crystal cooling device.[232]

5.4.2. Data Collection and Processing

Data collection was performed either on a *BRUKER Smart APEX* diffractometer with an *Incoatec IμS*-Mo-Microsource (λ = 0.71073 Å), a *BRUKER TXS* rotating-Mo-anode (λ = 0.71073 Å) or a *BRUKER Smart APEX* with an *Incoatec IμS*-Ag-Microsource (λ = 0.56086 Å).[233] All diffractometers were equipped with an *Oxford Cryosystems* crystal cooling device, an *APEX II CCD* detector and either *Incoatec Quazar* or *Helios* mirror optics, mounted on a D8-goniometer.

All diffractometers were controlled by the *APEX2* program suite.[234] Prior to each experiment a *matrix-scan* was recorded to check the crystal quality, cell parameters and to determine the required exposure time. Measurements were conducted in a ω-scan mode with a step width of 0.5°. Determination and refinement of the unit cell was also done with the *APEX2* program suite. All data were integrated with *SAINT*[235] and a semi-empirical absorption correction was applied with *SADABS*[236] or in the case of non-merohedral twinning with TWINABS.[237] Additional 3λ correction of the data was carried out if necessary.[238] Data statistics and preliminary space group determination as well as file setup for structure solution and refinement was carried out with *XPREP*.[239]

5.4.3. Structure Solution and Refinement

All structures have been solved by direct methods using *SHELXT* within *SHELXTL*.[240] Structure solution was performed on F_0^2, which are directly proportional to the measured integrities, via *SHELXL* within *SHELXTL* using the *ShelXle GUI*.[241] If not stated otherwise all C-bonded hydrogen atoms were refined isotropically on calculated positions using a riding model. The positions were geometrically optimized and the U_{iso} were constrained to 1.2 U_{eq} of the pivot atom or 1.5 U_{eg} of the methyl carbon atom. All

refinements were carried out to minimize the function $M(p_i, k)$ shown in Equation 2 using the weights w_H defined in Equation 3.

Equation 2. $$\boldsymbol{M(p_i, k) = \sum_H w_h [k|F_{obs}(H)|^2 - |F_{calc}(H)|^2]^2 = min}$$

Equation 3. $$\boldsymbol{w_H^{-1} = \sigma_H^2 F_{obs}^2 + (g1 \cdot P)^2 + g2 \cdot P \; with \; P = \frac{F_{obs}^2 + 2F_{calc}^2}{3}}$$

The results of the refinements were verified by comparison of the calculated and the observed structure factors. Commonly used criteria are the residuals *R1* shown in Equation 4 and *wR2* shown in Equation 5 with *wR2* being more significant since the model is refined against F^2.

Equation 4. $$\boldsymbol{R1 = \frac{\sum_H w_H (|F_{obs}| - |F_{calc}|)}{\sum_H w_H |F_{obs}|}}$$

Equation 5. $$\boldsymbol{wR2 = \frac{\sum_H w_H (|F_{obs}|^2 - |F_{calc}|^2)^2}{\sum_H w_H |F_{obs}|^4}}$$

Furthermore, the goodness of fit (GooF, S), a figure of merit showing the relation between deviation of F_{calc} from F_{obs} and the over-determination of refined parameters is calculated with Equation 6.

Equation 6. $$\boldsymbol{S = \sqrt{\frac{\sum (w_H (F_{obs}^2 - F_{calc}^2)^2)}{(n-p)}}}$$

Residual densities from the different Fourier analyses should be small. These residuals are usually found in the bonding regions due to the model restrictions. Higher residuals for heavy scatterers are acceptable as they arise mainly from absorption effects and Fourier truncation errors due to the limited recorded resolution range. The highest peak and deepest hole from difference Fourier analysis are listed in the crystallographic tables. The quality of the model is depicted by the size, ellipticity and orientation of the ADPs. These ADPs should be equal in size with little ellipticity and oriented perpendicular to the bonds. All graphics were generated and plotted with the *xp*[242] program with the anisotropic displacement parameters at the 50 % probability level unless stated otherwise.

5.4.4. Treatment of Disorder

Structure solutions with disordered moieties were refined using constraints and restraints by employing common distance restraints like *SADI* and *SAME* and additionally anisotropic displacement parameter (ADP) restraints like *SIMU*, *DELU* and *RIGU*. These restraints are treated as additional experimental observations, increasing the data to refine against. Thus the minimization function changes to Equation 7**.**

Equation 7. $$\boldsymbol{M = \sum w(F_{obs}^2 - F_{calc}^2)^2 + \sum w_r(R_{target} - R_{calc})^2}$$

Constraints such as the site occupation factor and AFIX instruction have been used during refinement of the disorder.

5.5. Determined Structures

5.5.1. Structures of Self-Synthesized Compounds

5.5.1.1. Crystal structure of NHSiNCCP – 1,3-N,N'-di-tert-butyl-benzamidinato-N-(2-(2,6-di-iso-propylanilino)-2-phenylethyl)diphenylphosphine)-silylene

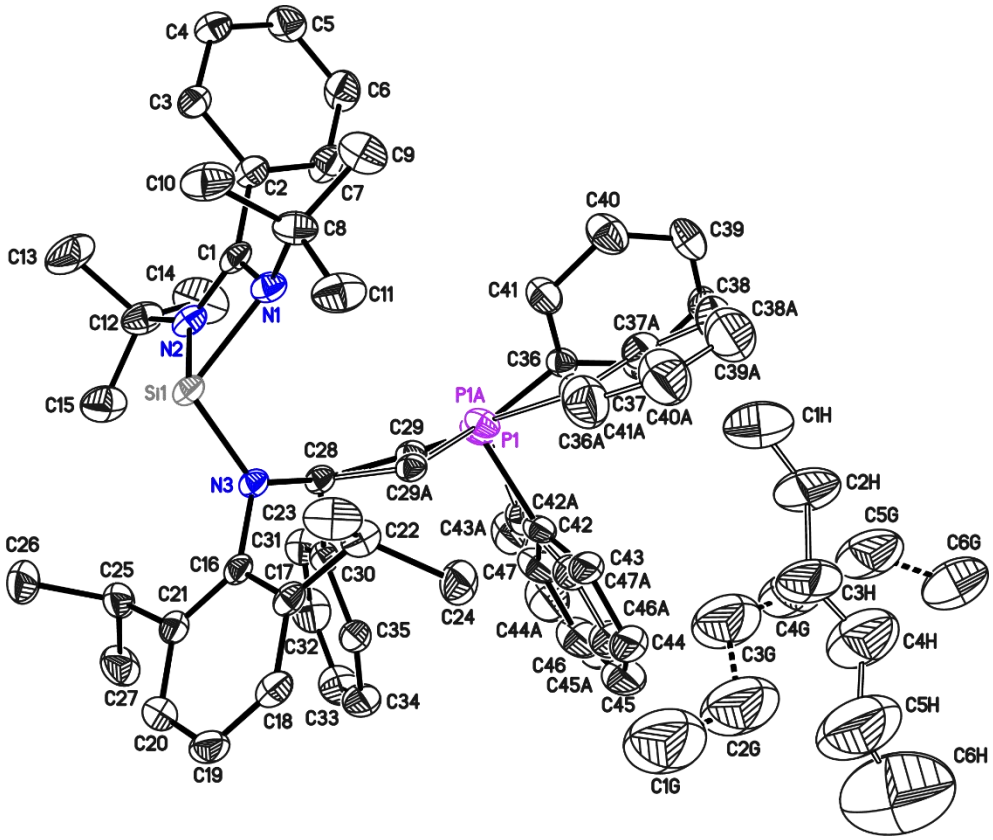

Figure 27. Asymmetric unit of **2**. The anisotropic displacement parameters are depicted at the 50% probability level. The hydrogen atoms are omitted for clarity.

Table 25. Crystal data of **2**.

Structure Code	AP066	Z	4
Empirical formula	$C_{50}H_{65}N_3PSi$	ρ_{calc}	1.104
Formula weight [g/mol]	773.11	μ [mm^{-1}]	0.121
Temperature [K]	100(2)	F(000)	1660
Wavelength [Å]	0.71073	θ range [°]	1.906 to 25.364
Crystal system	$P2_1/c$	Reflections collected	80269
space group	Monoclinic	Independent reflections	8471
a [Å]	20.289(3)	R(int)	0.0319
b [Å]	10.643(2)	Max. / min. transmission	0.7749 / 0.7279
c [Å]	21.683(2)	Restraints / parameter	1405 / 703
α [°]	90	GooF	1.031
β [°]	99.780(10)	R1 / *w*R2 (I > 2σ(I))	0.0445 / 0.1144
γ [°]	90	R1 / *w*R2 (all data)	0.0512 / 0.1201
Volume [$Å^3$]	4614.1(12)	max. diff peak / hole [e $Å^{-3}$]	0.468 / -0.328

5.5.1.2. Crystal structure of $[(NHSiCl)(AuCl)]_2$ – Bis-1,3-N,N'-di-tert-butyl-benzamidinato-chloro-silylene-gold(I)-chloride

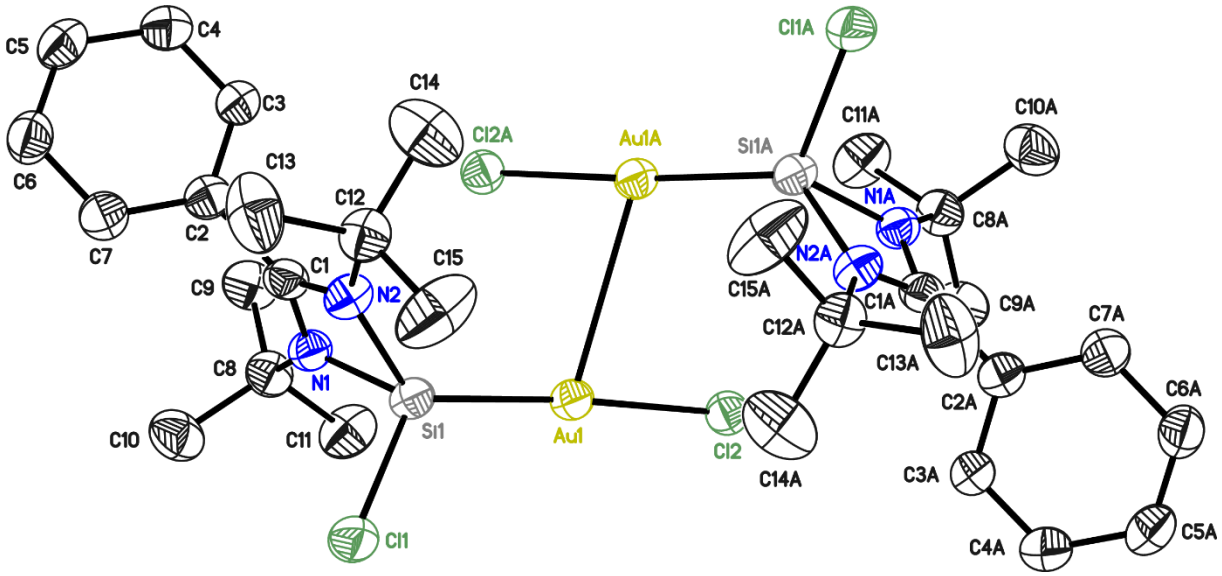

Figure 28. Asymmetric unit of **11**. The anisotropic displacement parameters are depicted at the 50% probability level. The hydrogen atoms are omitted for clarity.

Table 26. Crystal data of **11**.

Structure Code	AP182	Z	8
Empirical formula	$C_{15}H_{23}N_2SiCl_2Au$	ρ_{calc}	1.781
Formula weight [g/mol]	527.31	μ [mm^{-1}]	7.810
Temperature [K]	100(2)	F(000)	2032
Wavelength [Å]	0.71073	θ range [°]	1.712 to 26.460
Crystal system	Monoclinic	Reflections collected	50980
space group	*Cc*	Independent reflections	4057
a [Å]	11.006(2)	R(int)	0.0273
b [Å]	15.023(2)	Max. / min. transmission	0.4296 / 0.2741
c [Å]	23.820(3)	Restraints / parameter	0 / 196
α [°]	90	GooF	1.384
β [°]	93.08(2)	R1 / *w*R2 (I > 2σ(I))	0.0253 / 0.0595
γ [°]	90	R1 / *w*R2 (all data)	0.0260 / 0.0597
Volume [$Å^3$]	3932.8(10)	max. diff peak / hole [e $Å^{-3}$]	1.561 / -2.260

5.5.1.3. Crystal structure of [(NHSiMes)(AuCl)] – 1,3-N,N'-di-tert-butyl-benzamidinato-N-mesityl-N-(2-pyridyl)amino-silylene-gold(I)-chloride

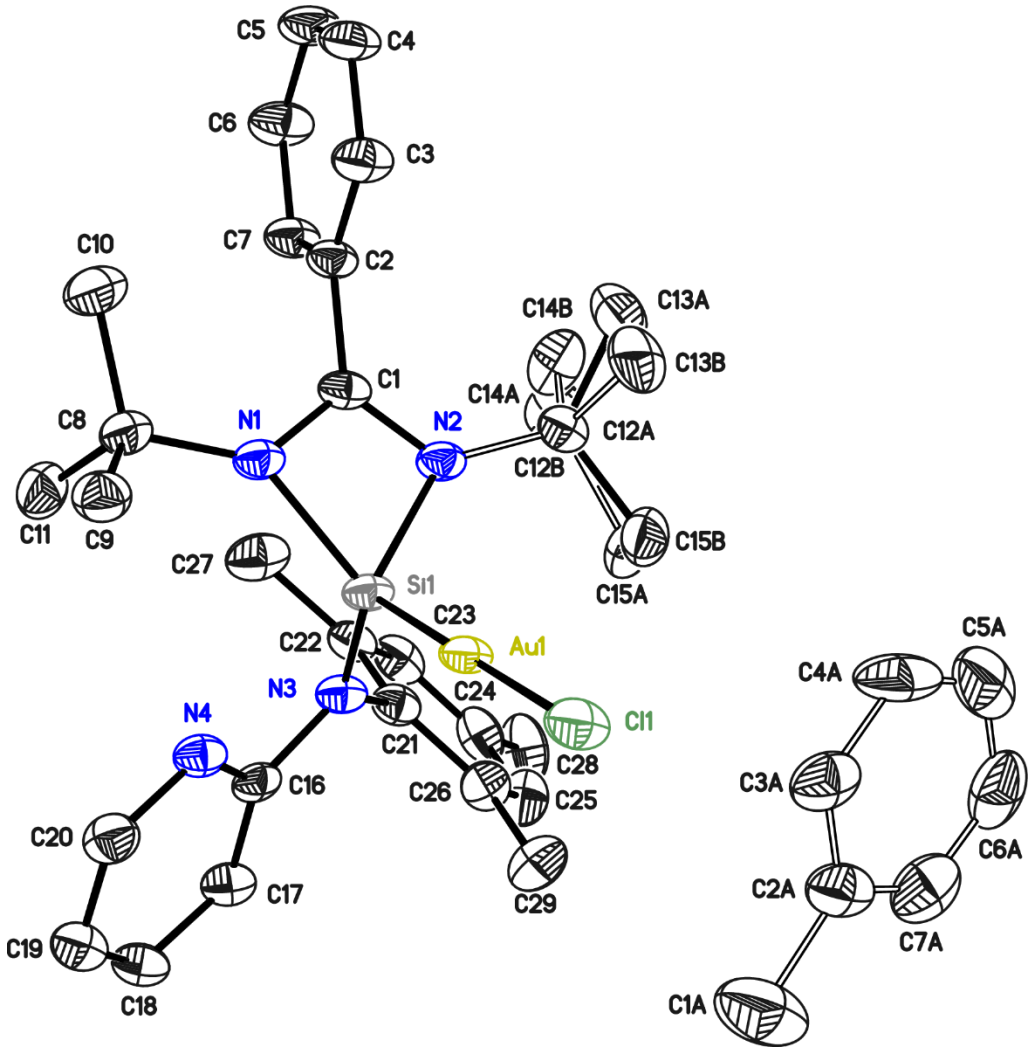

Figure 29. Asymmetric unit of **12**. The anisotropic displacement parameters are depicted at the 50% probability level. The hydrogen atoms are omitted for clarity.

Table 27. Crystal data of **12**.

Structure Code	AP192	Z	2
Empirical formula	$C_{65}H_{84}N_8Si_2Cl_2Au_2$	ρ_{calc}	1.523
Formula weight [g/mol]	1498.41	μ [mm^{-1}]	4.649
Temperature [K]	100(2)	F(000)	1500
Wavelength [Å]	0.71073	θ range [°]	1.705 to 25.360
Crystal system	$P2_1/n$	Reflections collected	59250
space group	Monoclinic	Independent reflections	5990
a [Å]	11.401(2)	R(int)	0.0468
b [Å]	16.130(3)	Max. / min. transmission	0.4288 / 0.3402
c [Å]	18.452(3)	Restraints / parameter	655 /423
α [°]	90	GooF	1.110
β [°]	105.69(2)	R1 / *w*R2 (I > 2σ(I))	0.0273 / 0.0578
γ [°]	90	R1 / *w*R2 (all data)	0.0370 / 0.0612
Volume [$Å^3$]	3266.9(10)	max. diff peak / hole [e $Å^{-3}$]	1.749 / -0.855

5.5.1.4. Crystal structure of $[(NHSiCl)(AgCl)]_4$ – Tetrakis-1,3-N,N'-di-tert-butyl-benzamidinato-chloro-silylene-silver(I)-chloride

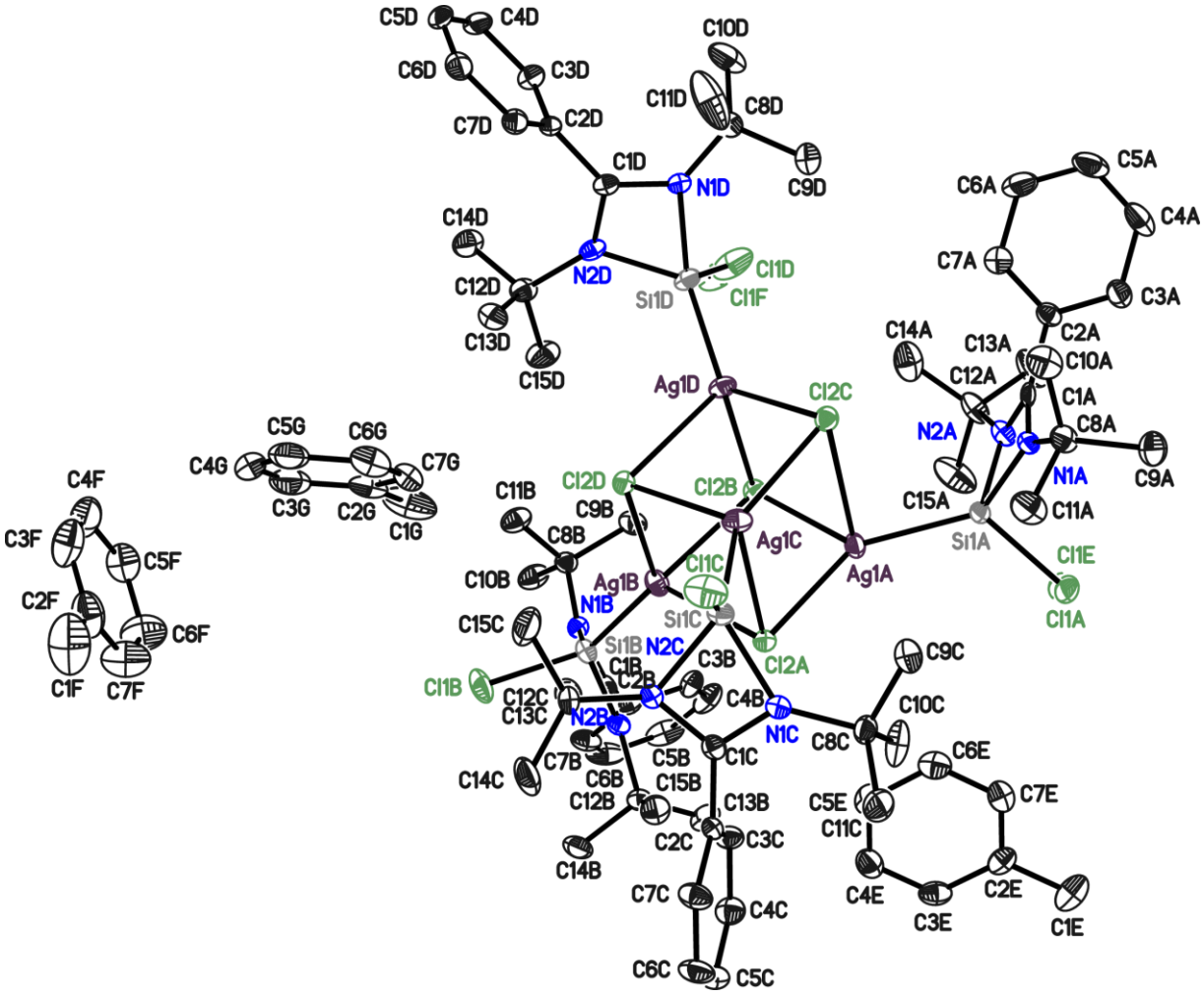

Figure 30. Asymmetric unit of **9**. The anisotropic displacement parameters are depicted at the 50% probability level. The hydrogen atoms are omitted for clarity.

Table 28. Crystal data of **9**.

Structure Code	AP246	Z	2
Empirical formula	$C_{81}H_{116}N_8Si_4Cl_8Ag_4$	ρ_{calc}	1.451
Formula weight [g/mol]	2029.25	μ [mm^{-1}]	0.610
Temperature [K]	100(2)	F(000)	2076
Wavelength [Å]	0.56086	θ range [°]	1.483 to 20.611
Crystal system	$P\bar{1}$	Reflections collected	133900
space group	Triclinic	Independent reflections	19156
a [Å]	13.749(2)	R(int)	0.0456
b [Å]	14.267(2)	Max. / min. transmission	0.7444 / 0.7029
c [Å]	25.724(3)	Restraints / parameter	96 / 981
α [°]	82.31(3)	GooF	1.028
β [°]	89.88(4)	R1 / *w*R2 (I > 2σ(I))	0.0265 / 0.0491
γ [°]	68.44(3)	R1 / *w*R2 (all data)	0.0398 / 0.0535
Volume [$Å^3$]	4644.6(14)	max. diff peak / hole [e $Å^{-3}$]	0.470 / -0.454

5.5.1.5. Crystal structure of $[(NHSiCl)(CuCl)]_4$ – Tetrakis-1,3-N,N'-di-tert-butyl-benzamidinato-chloro-silylene-copper(I)-chloride

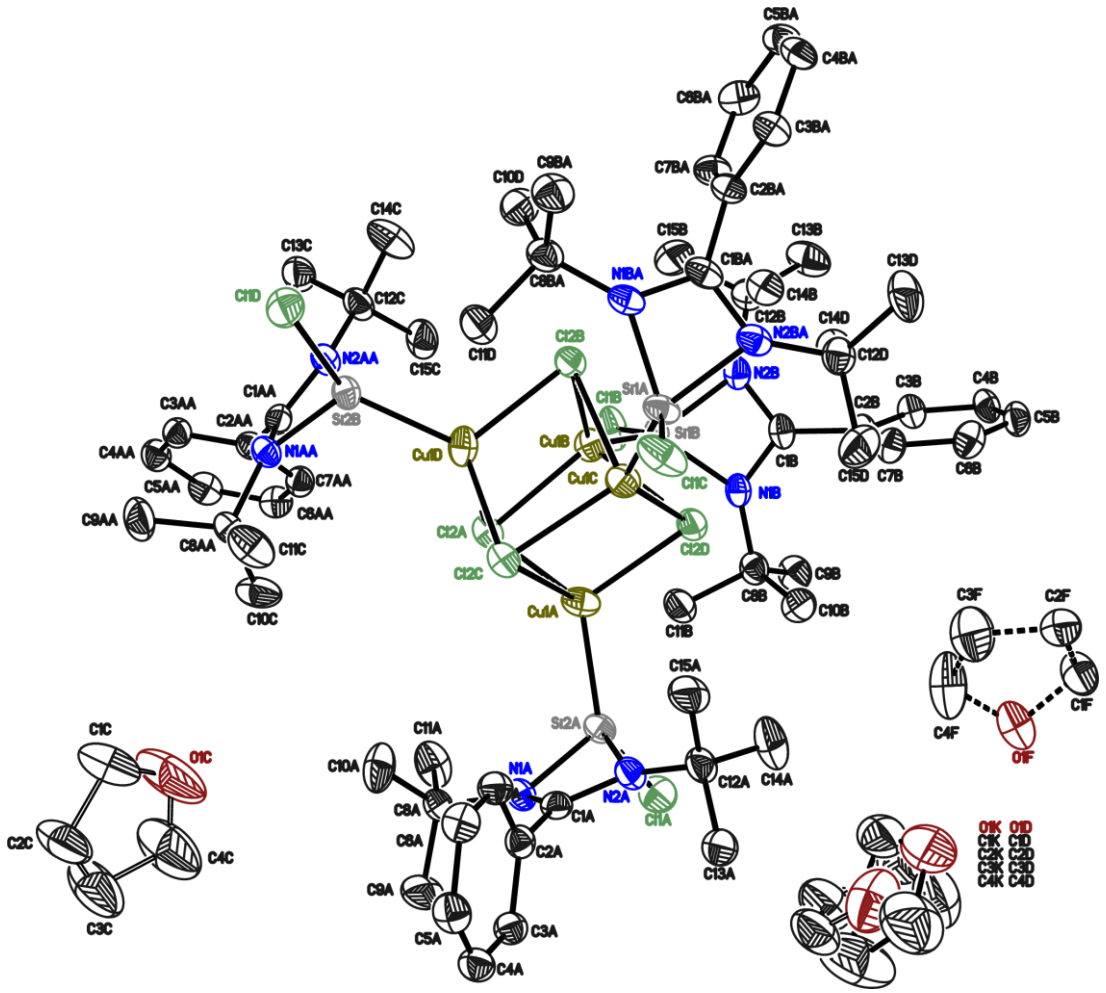

Figure 31. Asymmetric unit of **5a**. The anisotropic displacement parameters are depicted at the 50% probability level. The hydrogen atoms are omitted for clarity.

Table 29. Crystal data of **5a**.

Structure Code	AP231	Z	4
Empirical formula	$C_{76}H_{124}Cl_8Cu_4N_8O_4Si_4$	ρ_{calc}	1.384
Formula weight [g/mol]	1863.94	μ [mm^{-1}]	1.280
Temperature [K]	100(2)	F(000)	3904
Wavelength [Å]	0.71073	θ range [°]	1.867 to 25.420
Crystal system	Monoclinic	Reflections collected	109474
space group	*C*2/c	Independent reflections	8240
a [Å]	19.064(2)	R(int)	0.0300
b [Å]	18.785(2)	Max. / min. transmission	0.7452 / 0.6383
c [Å]	25.746(3)	Restraints / parameter	466 / 573
α [°]	90	GooF	1.150
β [°]	103.96(2)°.	R1 / *w*R2 (I > 2σ(I))	0.0377 / 0.0972
γ [°]	90	R1 / *w*R2 (all data)	0.0435 / 0.1005
Volume [$Å^3$]	8947.8(19)	max. diff peak / hole [e $Å^{-3}$]	0.474 / -0.387

5.5.1.6. Crystal structure of $[(NHSiCl)(CuBr)]_4$ – Tetrakis-1,3-N,N'-di-tert-butyl-benzamidinato-chloro-silylene-copper(I)-bromide

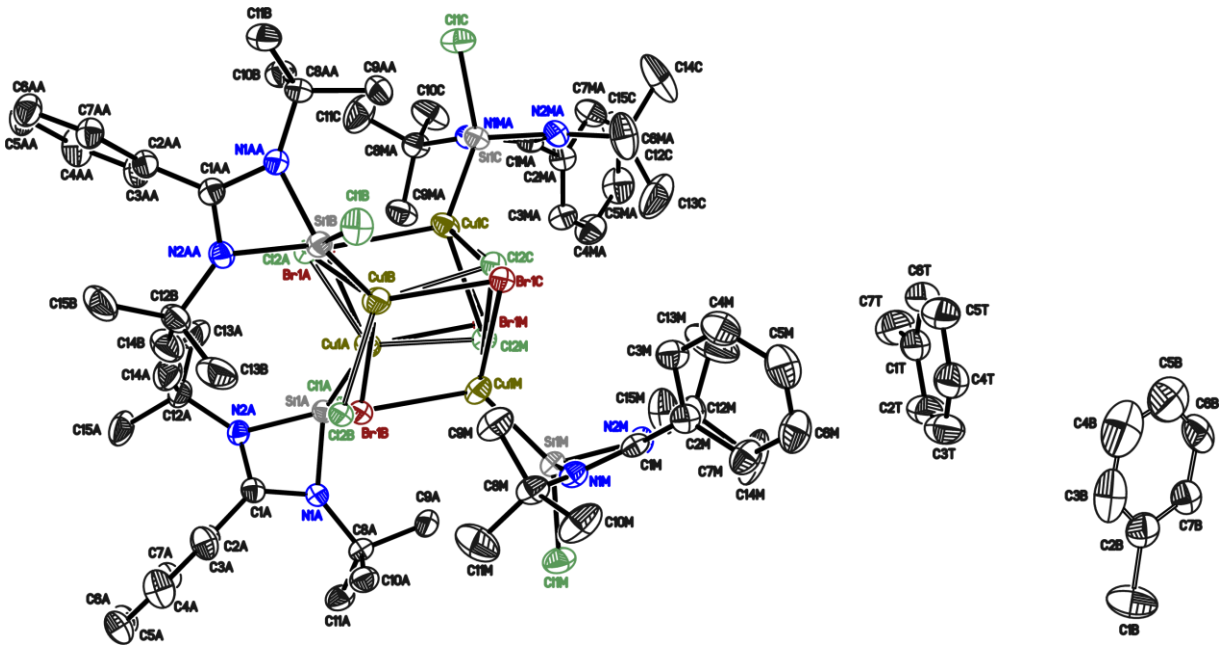

Figure 32. Asymmetric unit of **5b**. The anisotropic displacement parameters are depicted at the 50% probability level. The hydrogen atoms are omitted for clarity.

Table 30. Crystal data of **5b**.

Structure Code	AP189	Z	4
Empirical formula	$C_{81}H_{116}N_8Si_4Cl_{4.25}Br_{3.75}Cu_4$	ρ_{calc}	1.438
Formula weight [g/mol]	2018.44	μ [mm^{-1}]	2.722
Temperature [K]	100(2)	F(000)	4134
Wavelength [Å]	0.71073	θ range [°]	1.538 to 26.363
Crystal system	Monoclinic	Reflections collected	136628
space group	*C*2/c	Independent reflections	9521
a [Å]	20.130(3)	R(int)	0.0334
b [Å]	18.444(2)	Max. / min. transmission	0.4296 / 0.3752
c [Å]	26.594(3)	Restraints / parameter	230 / 527
α [°]	90	GooF	1.088
β [°]	109.17(3)	R1 / *w*R2 (I > 2σ(I))	0.0262 / 0.0649
γ [°]	90	R1 / *w*R2 (all data)	0.0326 / 0.0677
Volume [$Å^3$]	9326(3)	max. diff peak / hole [$eÅ^{-3}$]	0.933 / -0.400

5.5.1.7. Crystal structure of $[(NHSiCl)(CuI)]_4$ – Tetrakis-1,3-N,N'-di-tert-butyl-benzamidinato-chloro-silylene-copper(I)-iodide

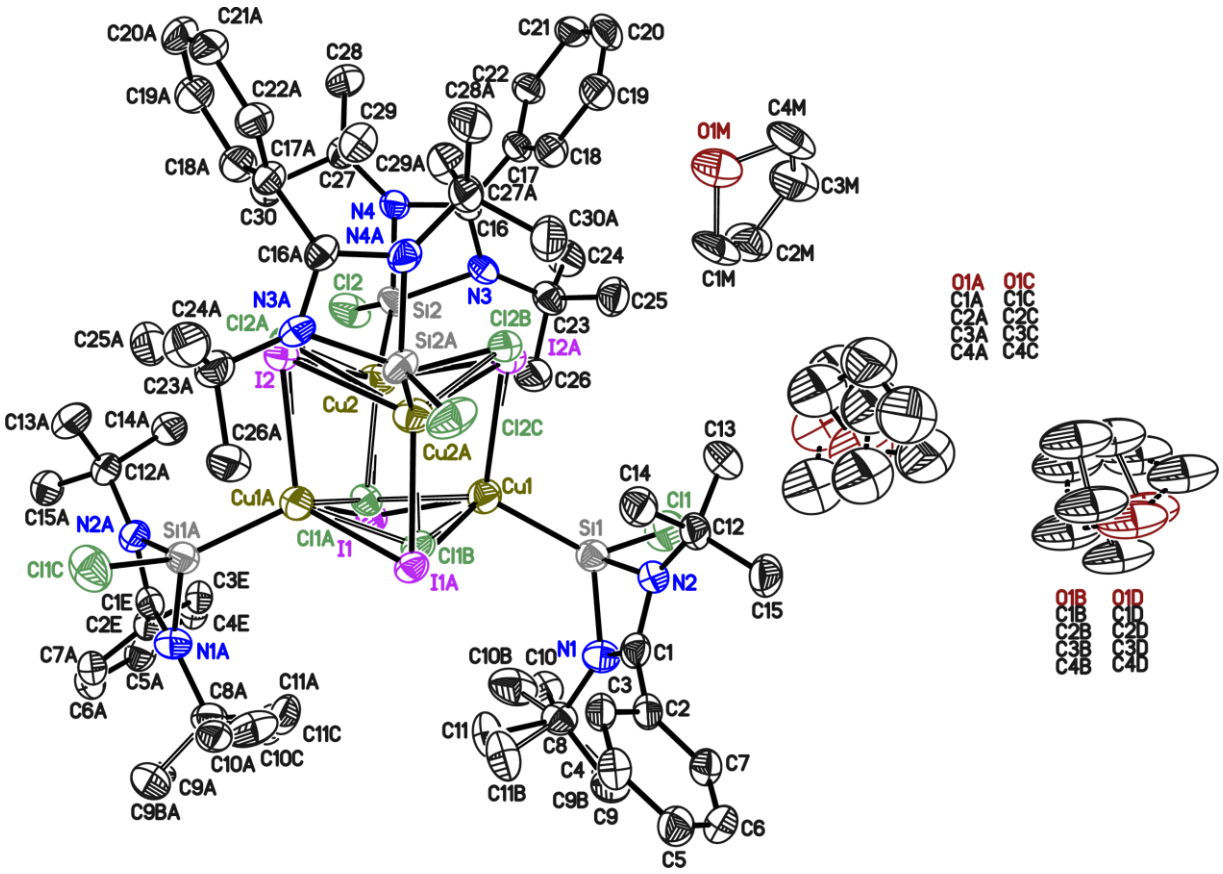

Figure 33. Asymmetric unit of **5c**. The anisotropic displacement parameters are depicted at the 50% probability level. The hydrogen atoms are omitted for clarity.

Table 31. Crystal data of **5c**.

Structure Code	APCuI	Z	4
Empirical formula	$C_{76}H_{124}Cl_{4.57}Cu_4I_{3.43}N_8O_4Si_4$	ρ_{calc}	1.566
Formula weight [g/mol]	2177.32	μ [mm^{-1}]	1.206
Temperature [K]	100(2)	F(000)	4397
Wavelength [Å]	0.56086	θ range [°]	1.196 / 19.823
Crystal system	Monoclinic	Reflections collected	130581
space group	*C*2/c	Independent reflections	8542
a [Å]	19.751(2)	R(int)	0.0391
b [Å]	18.807(2)	Max. / min. transmission	0.7444 / 0.6457
c [Å]	25.572(3)	Restraints / parameter	897 / 651
α [°]	90	GooF	1.157
β [°]	103.53(2)	R1 / *w*R2 (I > 2σ(I))	0.0349 / 0.0793
γ [°]	90	R1 / *w*R2 (all data)	0.0468 / 0.0893
Volume [$Å^3$]	9235.3(19)	max. diff peak / hole [e $Å^{-3}$]	1.061 / -0.763

5.5.1.8. Crystal structure of $[(NHSiMes)_2(CuCl)_3]$ – Bis-1,3-N,N'-di-tert-butyl-benzamidinato-N-mesityl-N-(2-pyridyl)amino-silylene-tris-copper(I)-chloride

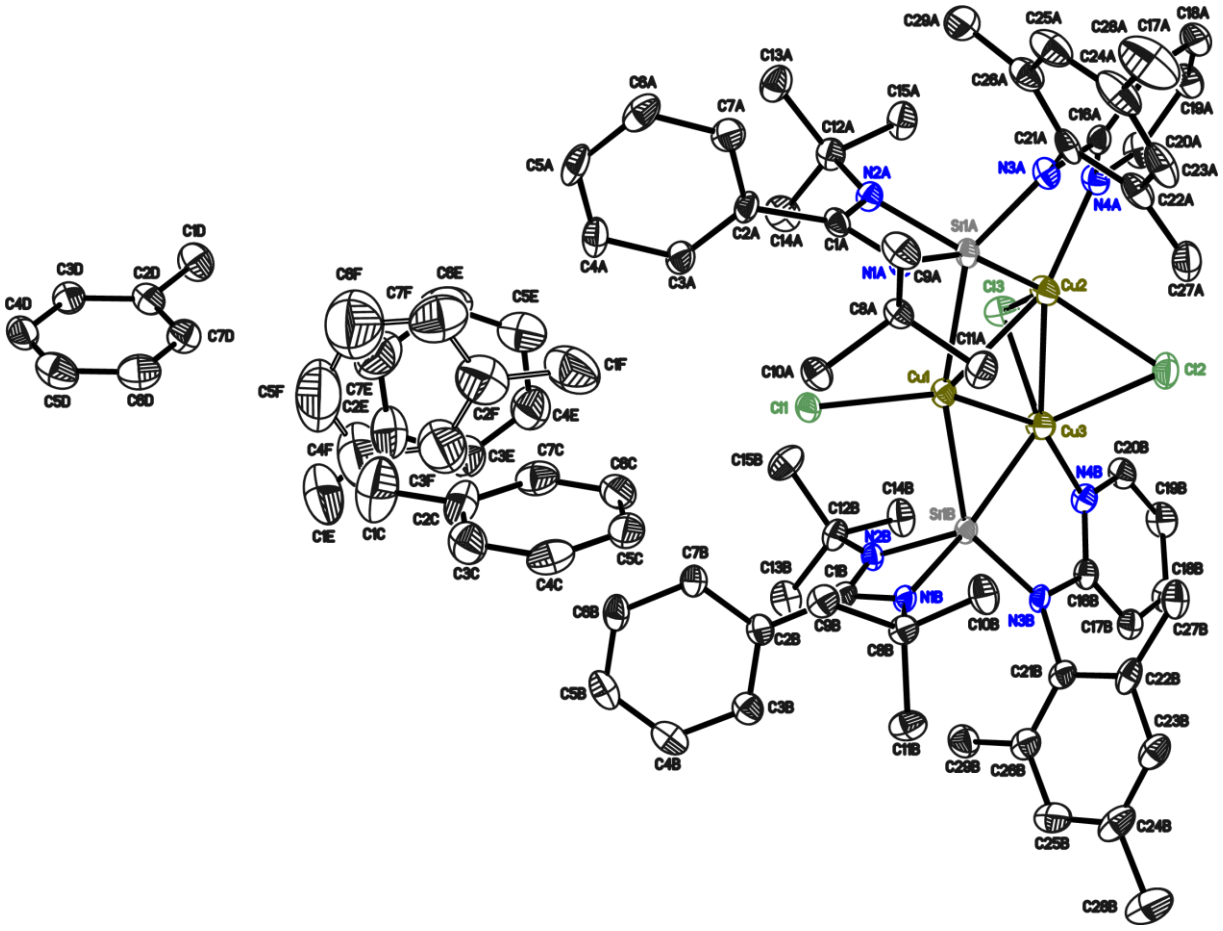

Figure 34. Asymmetric unit of **7a**. The anisotropic displacement parameters are depicted at the 50% probability level. The hydrogen atoms are omitted for clarity.

Table 32. Crystal data of **7a**.

Structure Code	AP234B	Z	2
Empirical formula	$C_{79}H_{100}N_8Si_2Cl_3Cu_3$	ρ_{calc}	1.341
Formula weight [g/mol]	1514.81	μ [mm^{-1}]	1.030
Temperature [K]	100(2)	F(000)	1592
Wavelength [Å]	0.71073	θ range [°]	1.122 to 25.455
Crystal system	Triclinic	Reflections collected	99149
space group	$P\bar{1}$	Independent reflections	13774
a [Å]	10.376(2)	R(int)	0.0401
b [Å]	18.154(2)	Max. / min. transmission	0.6937 / 0.5970
c [Å]	20.423(3)	Restraints / parameter	913 / 941
α [°]	89.56(2)	GooF	1.072
β [°]	77.14(2)	R1 / *w*R2 (I > 2σ(I))	0.0509 / 0.1390
γ [°]	89.75(3)	R1 / *w*R2 (all data)	0.0549 / 0.1432
Volume [$Å^3$]	3750.4(10)	max. diff peak / hole [e $Å^{-3}$]	1.095 / -1.461

5.5.1.9. Crystal structure of [(NHSiMes)$_2$(CuBr)$_3$] – Bis-1,3-N,N'-di-tert-butyl-benzamidinato-N-mesityl-N-(2-pyridyl)amino-silylene-tris-copper(I)-bromide

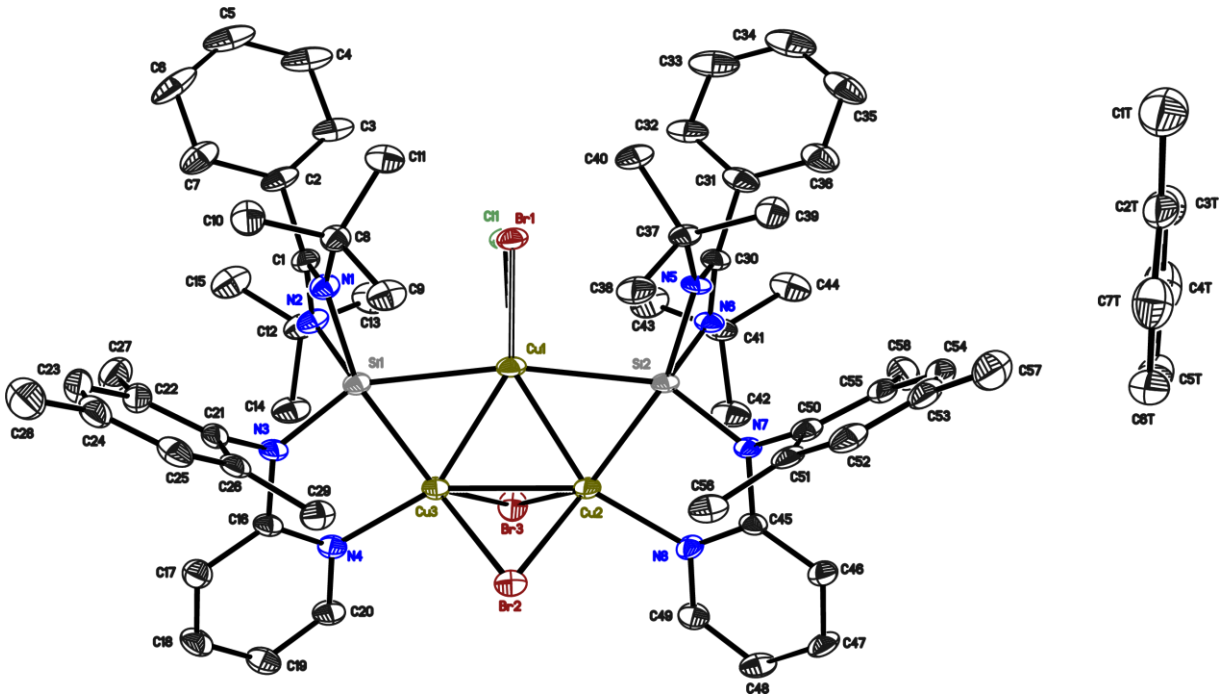

Figure 35. Asymmetric unit of **7b**. The anisotropic displacement parameters are depicted at the 50% probability level. The hydrogen atoms are omitted for clarity.

Table 33. Crystal data of **7b**.

Structure Code	AP200	Z	2
Empirical formula	$C_{65}H_{84}Br_{2.57}Cl_{0.43}Cu_3N_8Si_2$	ρ_{calc}	1.259
Formula weight [g/mol]	1444.76	μ [mm^{-1}]	2.262
Temperature [K]	100(2)	F(000)	1484
Wavelength [Å]	0.71073	θ range [°]	1.017 to 25.455
Crystal system	Triclinic	Reflections collected	14039
space group	$P\bar{1}$	Independent reflections	14039
a [Å]	10.460(2)	R(int)	
b [Å]	18.205(4)	Max. / min. transmission	
c [Å]	20.522(4)	Restraints / parameter	0 / 754
α [°]	88.29(3)	GooF	1.048
β [°]	77.36(2)	R1 / *w*R2 (I > 2σ(I))	0.0450 / 0.1171
γ [°]	89.01(3)	R1 / *w*R2 (all data)	0.0555 / 0.1236
Volume [Å^3]	3811.2(14)	max. diff peak / hole [e Å^{-3}]	1.274 / -0.670

5.5.1.10. Crystal structure of $[(NHSiMes)_2(CuI)_3]$ – Bis-1,3-N,N'-di-tert-butyl-benzamidinato-N-mesityl-N-(2-pyridyl)amino-silylene-tris-copper(I)-iodide

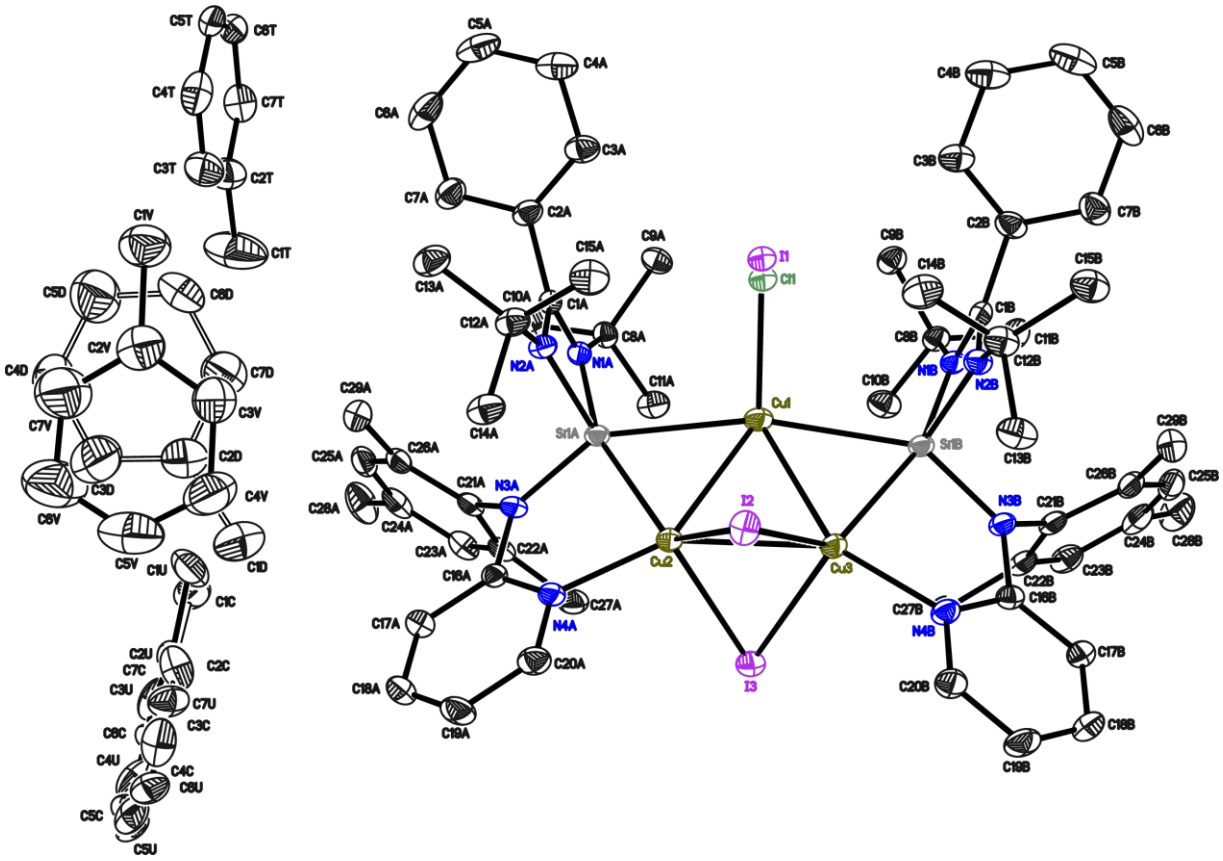

Figure 36. Asymmetric unit of **7c**. The anisotropic displacement parameters are depicted at the 50% probability level. The hydrogen atoms are omitted for clarity.

Table 34. Crystal data of **7c**.

Structure Code	AP233	Z	2
Empirical formula	$C_{79}H_{100}Cl_{0.92}Cu_3I_{2.08}N_8Si_2$	ρ_{calc}	1.489
Formula weight [g/mol]	1704.96	μ [mm^{-1}]	0.947
Temperature [K]	100(2)	F(000)	1742
Wavelength [Å]	0.56086	θ range [°]	1.570 to 19.827
Crystal system	Triclinic	Reflections collected	99962
space group	$P\bar{1}$	Independent reflections	14073
a [Å]	10.498(3)	R(int)	0.0376
b [Å]	18.205(2)	Max. / min. transmission	0.7444 / 0.6750
c [Å]	20.437(2)	Restraints / parameter	1593 / 1008
α [°]	87.32(2)	GooF	1.071
β [°]	77.16(2)	R1 / *w*R2 (I > 2σ(I))	0.0270 / 0.0693
γ [°]	88.91(3)	R1 / *w*R2 (all data)	0.0340 / 0.0748
Volume [$Å^3$]	3803.9(13)	max. diff peak / hole [e $Å^{-3}$]	1.187 / -0.605

5.5.1.11. Crystal structure of $[(NHSiPh)_2(CuCl)_3]$ – Bis-1,3-N,N'-di-tert-butyl-benzamidinato-N-phenyl-N-(2-pyridyl)amino-silylene-tris-copper(I)-chloride

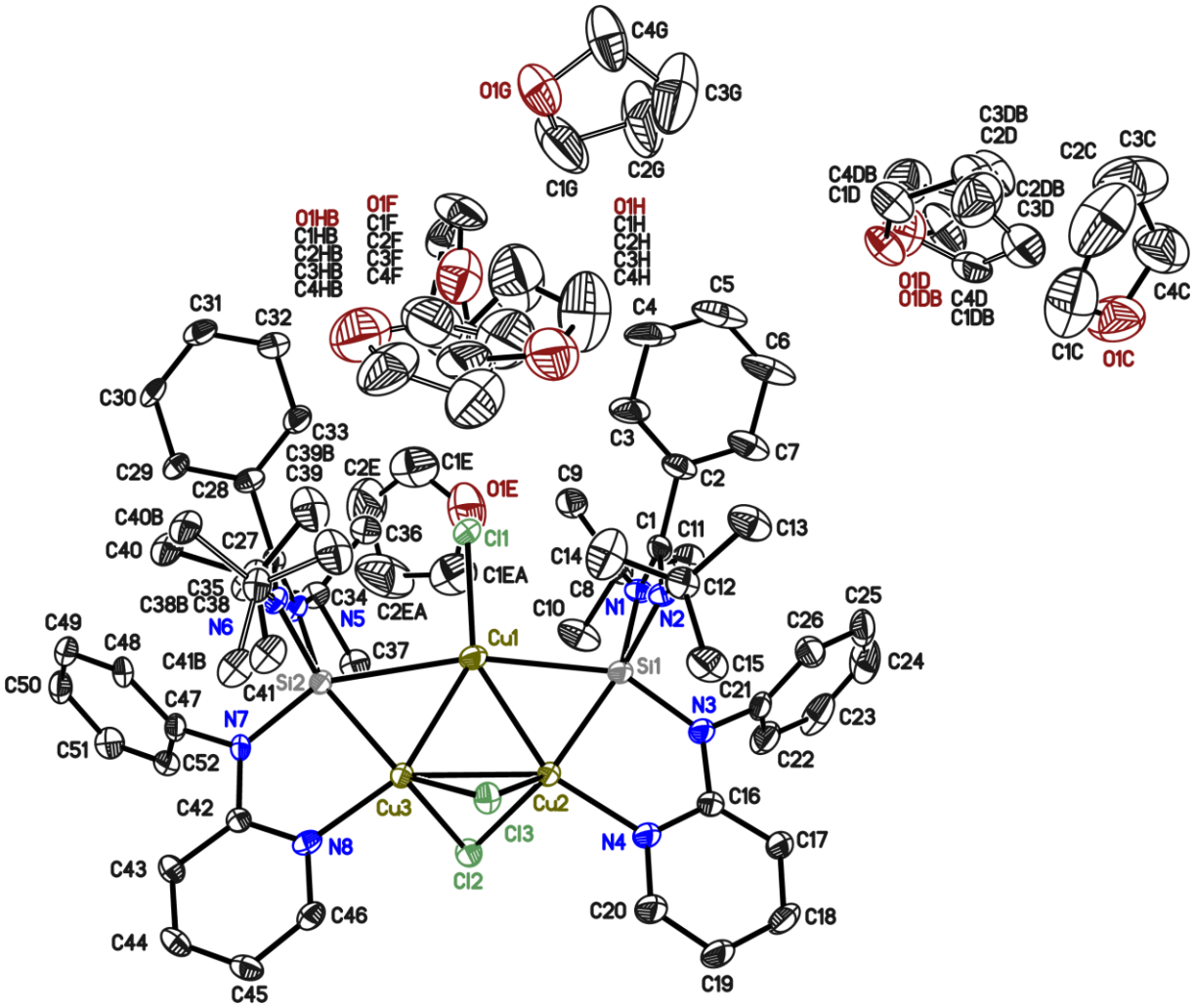

Figure 37. Asymmetric unit of **8**. The anisotropic displacement parameters are depicted at the 50% probability level. The hydrogen atoms are omitted for clarity.

Table 35. Crystal data of **8**.

Structure Code	AP_SR25B	Z	4
Empirical formula	$C_{72}H_{104}Cl_3Cu_3N_8O_5Si_2$	ρcalc	1.371
Formula weight [g/mol]	1514.78	μ [mm-1]	1.057
Temperature [K]	100(2)	F(000)	3192
Wavelength [Å]	0.71073	θ range [°]	1.324 to 25.402
Crystal system	Orthorhombic	Reflections collected	116068
space group	$P2_12_12$	Independent reflections	13509
a [Å]	22.528(4)	R(int)	0.0948
b [Å]	15.472(3)	Max. / min. transmission	0.7452 / 0.6603
c [Å]	21.062(4)	Restraints / parameter	2256 / 982
α [°]	90	GooF	1.128
β [°]	90	R1 / wR2 (I > 2σ(I))	0.0509 / 0.0961
γ [°]	90	R1 / wR2 (all data)	0.0693 / 0.1024
Volume [Å3]	7341(2)	max. diff peak / hole [e Å-3]	0.539 / -0.592

5.5.1.12. Crystal structure of $[(NHSiCl)(CuBr(SMe_2))]_2$ – Bis-1,3-N,N'-di-tert-butyl-benzamidinato-chloro-silylene-copper(I)-(dimethylsulfide)-bromide

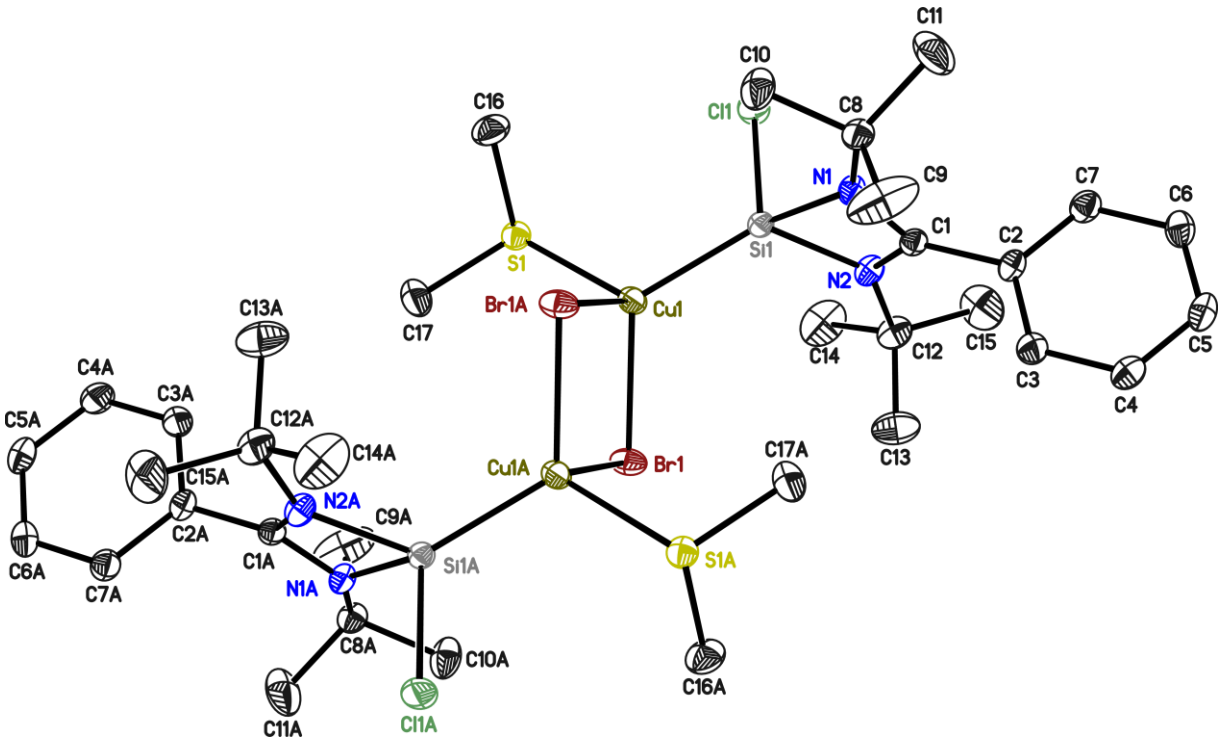

Figure 38. Asymmetric unit of **6**. The anisotropic displacement parameters are depicted at the 50% probability level. The hydrogen atoms are omitted for clarity.

Table 36. Crystal data of **6**.

Structure Code	AP216	Z	2
Empirical formula	$C_{34}H_{58}Br_2Cl_2Cu_2N_4S_2Si_2$	ρ_{calc}	1.483
Formula weight [g/mol]	1000.94	μ [mm^{-1}]	3.024
Temperature [K]	100(2)	F(000)	1024
Wavelength [Å]	0.71073	θ range [°]	1.413 to 27.503
Crystal system	Monoclinic	Reflections collected	58507
space group	$P2_1/c$	Independent reflections	5144
a [Å]	9.265(2)	R(int)	0.0236
b [Å]	28.831(3)	Max. / min. transmission	0.2080 / 0.1598
c [Å]	8.806(2)	Restraints / parameter	0 / 225
α [°]	90	GooF	1.109
β [°]	107.60(2)	R1 / *w*R2 (I > 2σ(I))	0.0208 / 0.0501
γ [°]	90	R1 / *w*R2 (all data)	0.0223 / 0.0507
Volume [$Å^3$]	2242.1(8)	max. diff peak / hole [e $Å^{-3}$]	0.489 / -0.234

5.5.1.13. Crystal structure of [(NHSiMes)$_2$(CuBr)] – Bis-1,3-N,N'-di-tert-butyl-benzamidinato-N-mesityl-N-(2-pyridyl)amino-silylene-copper(I)-bromide

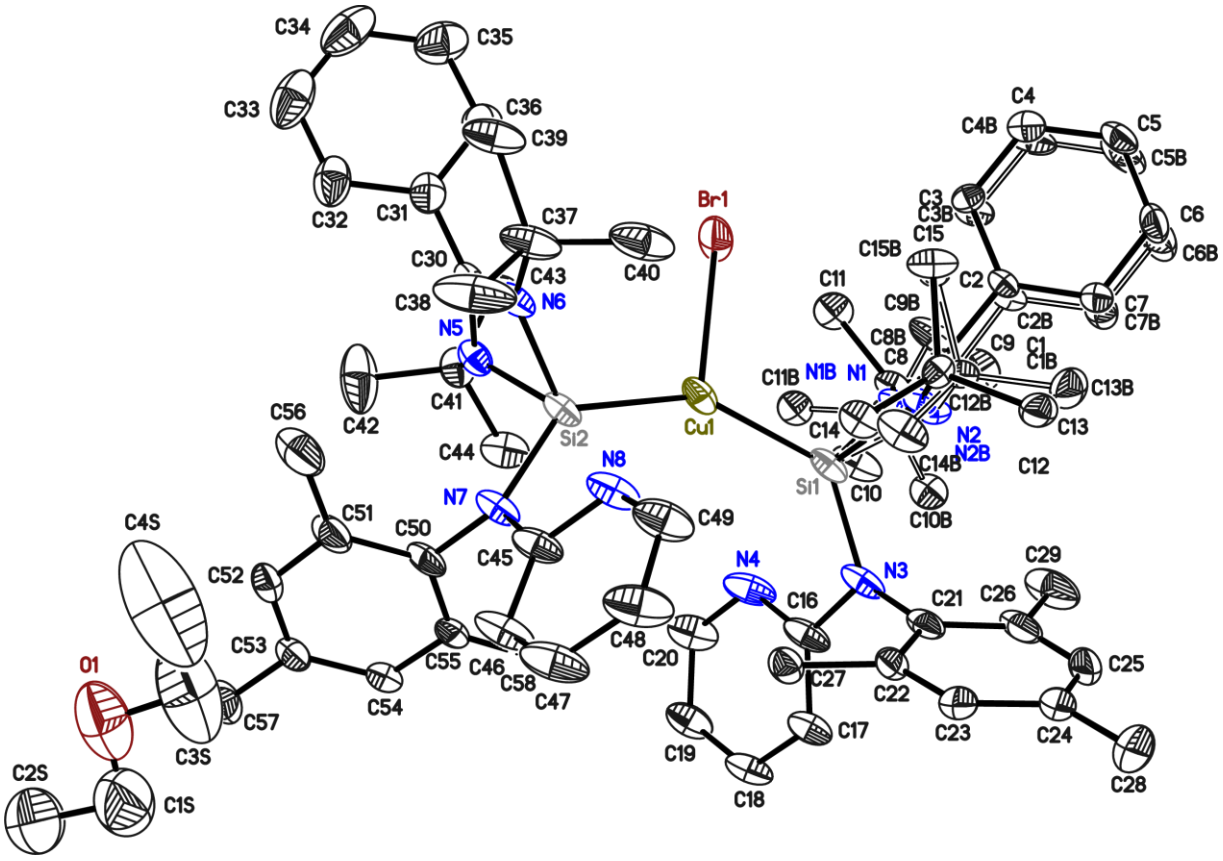

Figure 39. Asymmetric unit of **[(NHSiMes)$_2$(CuBr)]**. The anisotropic displacement parameters are depicted at the 50% probability level. The hydrogen atoms are omitted for clarity.

Table 37. Crystal data of **[(NHSiMes)$_2$(CuBr)]**.

Structure Code	AP220	Z	2
Empirical formula	$C_{62}H_{86}N_8Si_2BrCuO$	ρ_{calc}	1.235
Formula weight [g/mol]	1159.01	μ [mm^{-1}]	0.578
Temperature [K]	100(2)	F(000)	1228
Wavelength [Å]	0.56086	θ range [°]	0.932 to 19.818
Crystal system	$P\bar{1}$	Reflections collected	100327
space group	Triclinic	Independent reflections	11502
a [Å]	11.744(3)	R(int)	0.0430
b [Å]	15.665(2)	Max. / min. transmission	0.7444 / 0.7083
c [Å]	18.147(2)	Restraints / parameter	2326 / 854
α [°]	100.35(2)	GooF	1.091
β [°]	102.68(3)	R1 / *w*R2 (I > 2σ(I))	0.0410 / 0.0902
γ [°]	100.62(2)	R1 / *w*R2 (all data)	0.0658 / 0.1089
Volume [Å^3]	3115.8(11)	max. diff peak / hole [e Å^{-3}]	0.808 / -1.782

5.5.1.14. Crystal structure of [(NHSiMes)$_2$(CuBr)$_4$] – Bis-1,3-N,N'-di-tert-butyl-benzamidinato-N-mesityl-N-(2-pyridyl)amino-silylene-tetra-copper(I)-bromide

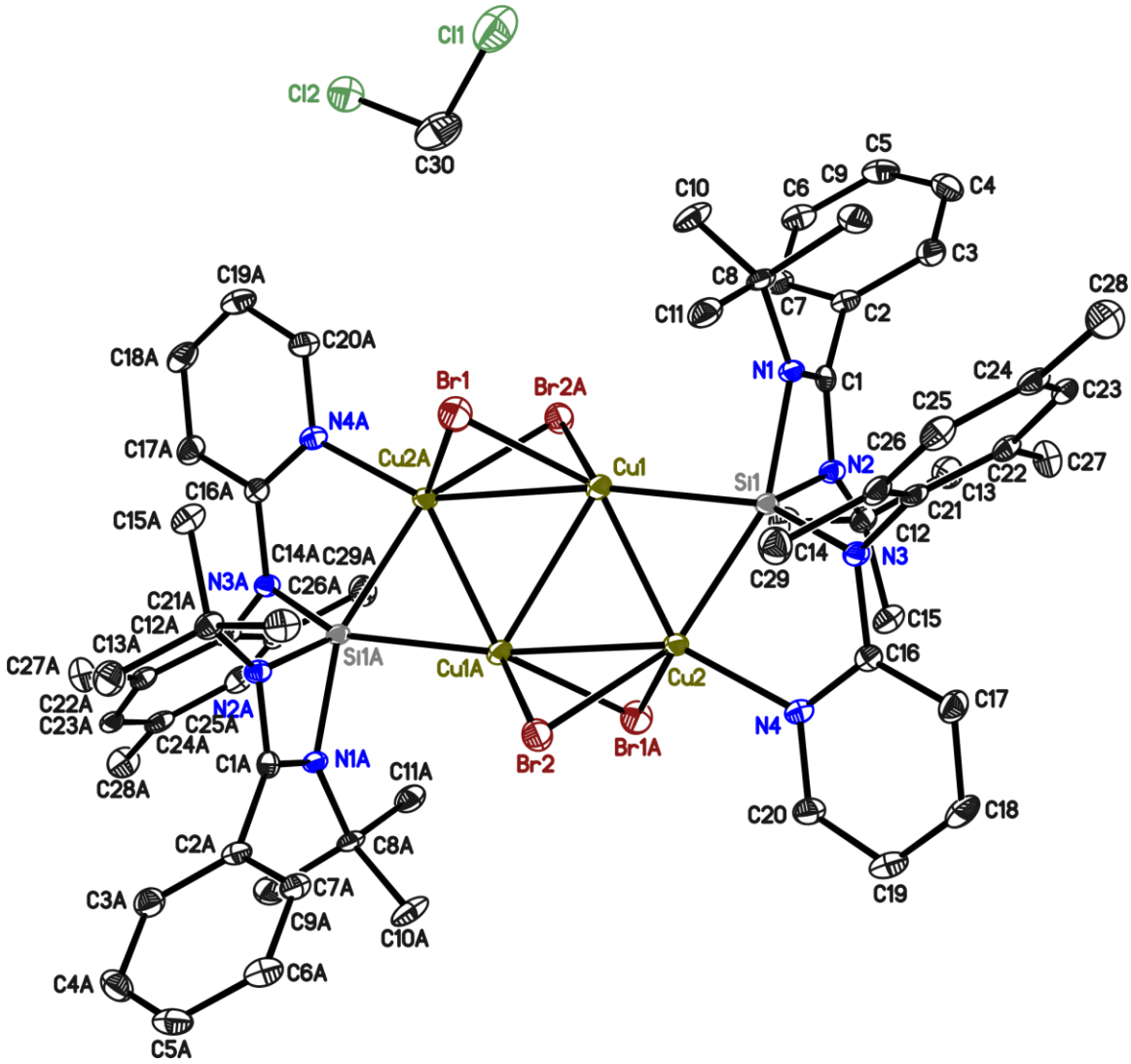

Figure 40. Asymmetric unit of **[(NHSiMes)$_2$(CuBr)$_4$]**. The anisotropic displacement parameters are depicted at the 50% probability level. The hydrogen atoms are omitted for clarity.

Table 38. Crystal data of **[(NHSiMes)$_2$(CuBr)$_4$]**.

Structure Code	AP224	Z	2
Empirical formula	$C_{60}H_{80}N_8Si_2Cl_4Br_4Cu_4$	ρ_{calc}	1.662
Formula weight [g/mol]	1685.10	μ [mm^{-1}]	3.857
Temperature [K]	100(2)	F(000)	1696
Wavelength [Å]	0.71073	θ range [°]	1.784 to 25.369
Crystal system	monoclinic	Reflections collected	63012
space group	$P2_1/n$	Independent reflections	6172
a [Å]	12.246(2)	R(int)	0.0354
b [Å]	14.054(2)	Max. / min. transmission	0.8747 / 0.8073
c [Å]	19.757(3)	Restraints / parameter	0 / 379
α [°]	90	GooF	1.043
β [°]	97.93(2)	R1 / *w*R2 (I > 2σ(I))	0.0261 / 0.0692
γ [°]	90	R1 / *w*R2 (all data)	0.0327 / 0.0722
Volume [Å^3]	3367.8(9)	max. diff peak / hole [e Å^{-3}]	1.012 / -0.835

5.5.1.15. Crystal structure of $[(NHSiCl)(ZnCl_2)]_2$ – Bis-1,3-N,N'-di-tert-butyl-benzamidinato-chloro-silylene-zinc(II)-chloride

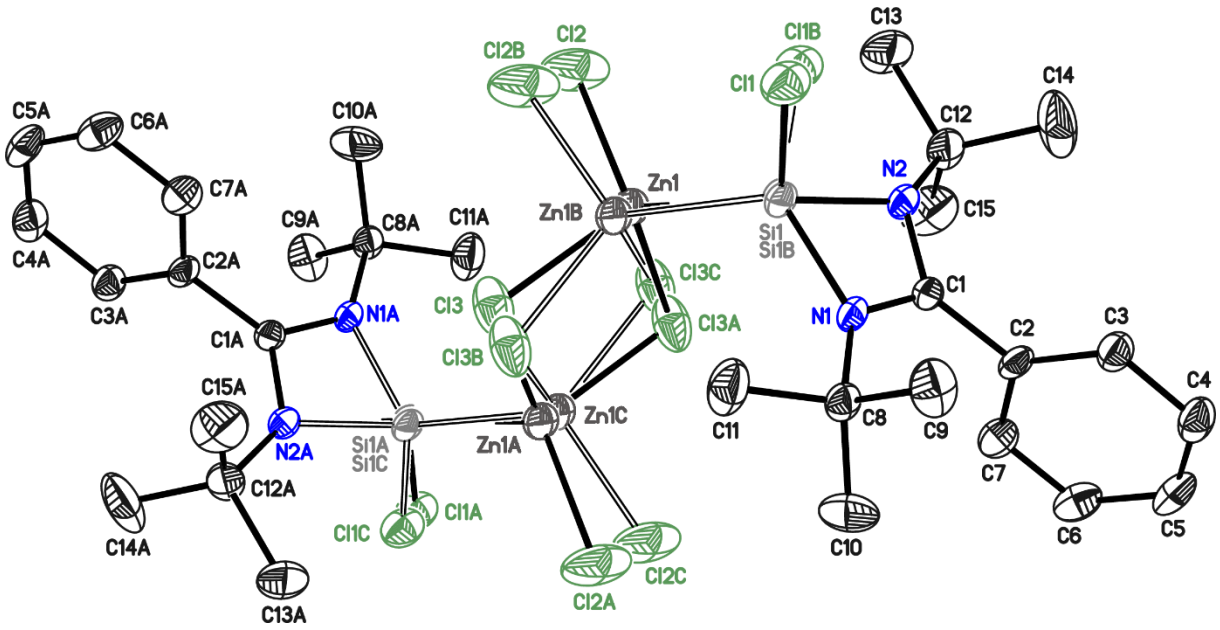

Figure 41. Asymmetric unit of **13**. The anisotropic displacement parameters are depicted at the 50% probability level. The hydrogen atoms are omitted for clarity.

Table 39. Crystal data of **13**.

Structure Code	AP181	Z	2
Empirical formula	$C_{30}H_{46}N_4Si_2Cl_6Zn_2$	ρ_{calc}	1.450
Formula weight [g/mol]	862.33	μ [mm^{-1}]	1.707
Temperature [K]	100(2)	F(000)	888
Wavelength [Å]	0.71073	θ range [°]	2.119 to 25.385
Crystal system	$P2_1/n$	Reflections collected	37200
space group	Monoclinic	Independent reflections	3627
a [Å]	10.6169(13)	R(int)	0.0540
b [Å]	14.4565(17)	Max. / min. transmission	0.6108 / 0.5236
c [Å]	12.8706(15)	Restraints / parameter	84 / 221
α [°]	90	GooF	1.099
β [°]	90.561(2)	R1 / *w*R2 (I > 2σ(I))	0.0490 / 0.1248
γ [°]	90	R1 / *w*R2 (all data)	0.0597 / 0.1308
Volume [$Å^3$]	1975.3(4)	max. diff peak / hole [e $Å^{-3}$]	1.247 / -0.512

5.5.1.16. Crystal structure of $[(NHSiMes)(ZnCl_2)]_2$ – Bis-1,3-N,N'-di-tert-butyl-benzamidinato-N-mesityl-N-(2-pyridyl)amino-silylene-zinc(II)-chloride

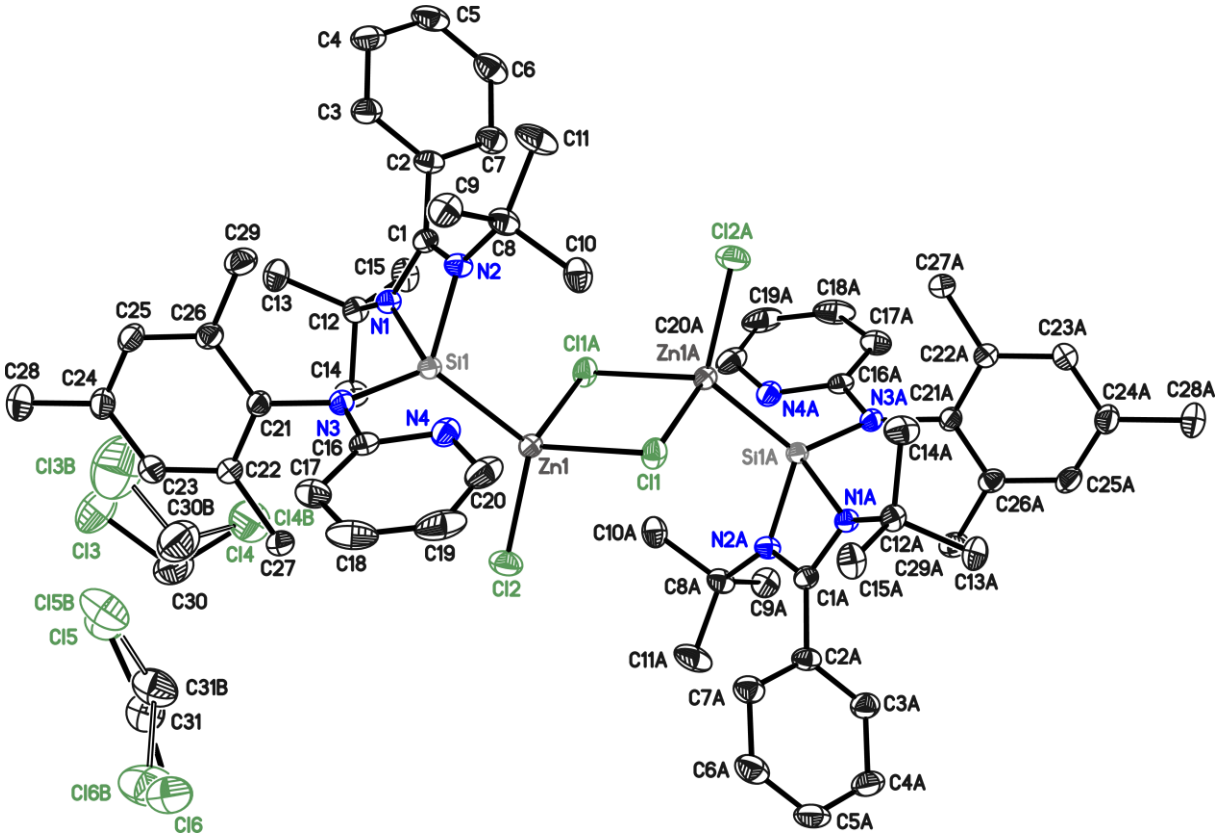

Figure 42. Asymmetric unit of **14**. The anisotropic displacement parameters are depicted at the 50% probability level. The hydrogen atoms are omitted for clarity.

Table 40. Crystal data of **14**.

Structure Code	AP193	Z	2
Empirical formula	$C_{62}H_{54}N_8Si_2Cl_{12}Zn_2$	ρ_{calc}	1.381
Formula weight [g/mol]	1553.69	μ [mm^{-1}]	1.146
Temperature [K]	100(2)	F(000)	1608
Wavelength [Å]	0.71073	θ range [°]	1.574 to 26.400
Crystal system	$P2_1/c$	Reflections collected	89790
space group	Monoclinic	Independent reflections	7663
a [Å]	12.968(2)	R(int)	0.0241
b [Å]	12.560(2)	Max. / min. transmission	0.2185 / 0.1791
c [Å]	22.982(3)	Restraints / parameter	160 / 453
α [°]	90	GooF	1.041
β [°]	93.73(2)	R1 / *w*R2 (I > 2σ(I))	0.0231 / 0.0629
γ [°]	90	R1 / *w*R2 (all data)	0.0249 / 0.0641
Volume [Å^3]	3735.3(10)	max. diff peak / hole [e Å^{-3}]	0.481 / -0.384

5.5.1.17. Crystal structure of [(NHSiPh)($ZnCl_2$)] – 1,3-N,N'-di-tert-butyl-benzamidinato-N-phenyl-N-(2-pyridyl)amino-silylene-zinc(II)-chloride

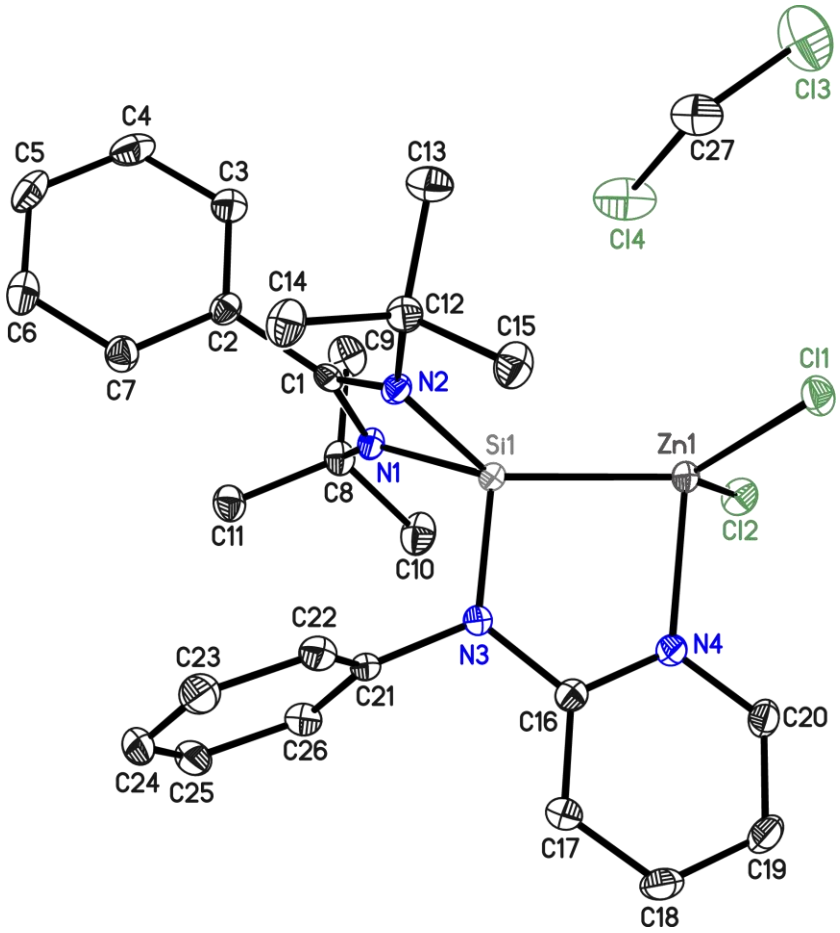

Figure 43. Asymmetric unit of **16**. The anisotropic displacement parameters are depicted at the 50% probability level. The hydrogen atoms are omitted for clarity.

Table 41. Crystal data of **16**.

Structure Code	AP178187	Z	8
Empirical formula	$C_{27}H_{34}N_4SiCl_4Zn$	ρ_{calc}	1.429
Formula weight [g/mol]	649.84	μ [mm^{-1}]	1.231
Temperature [K]	100(2)	F(000)	2688
Wavelength [Å]	0.71073	θ range [°]	1.398 to 25.390
Crystal system	orthorhombic	Reflections collected	128838
space group	*P*bca	Independent reflections	5551
a [Å]	11.876(2)	R(int)	0.0331
b [Å]	17.452(3)	Max. / min. transmission	0.6462 / 0.5639
c [Å]	29.138(5)	Restraints / parameter	0 / 340
α [°]	90	GooF	1.044
β [°]	90	R1 / *w*R2 (I > 2σ(I))	0.0207 / 0.0528
γ [°]	90	R1 / *w*R2 (all data)	0.0233 / 0.0543
Volume [$Å^3$]	6039.1(18)	max. diff peak / hole [e $Å^{-3}$]	0.329 /-0.283

5.5.1.18. Crystal structure of [(NHSiCl)(Zn(HMDS)$_2$)] – 1,3-N,N'-di-tert-butyl-benzamidinato-chloro-silylene-zinc(II)-bis(bis(trimethylsilyl)amide)

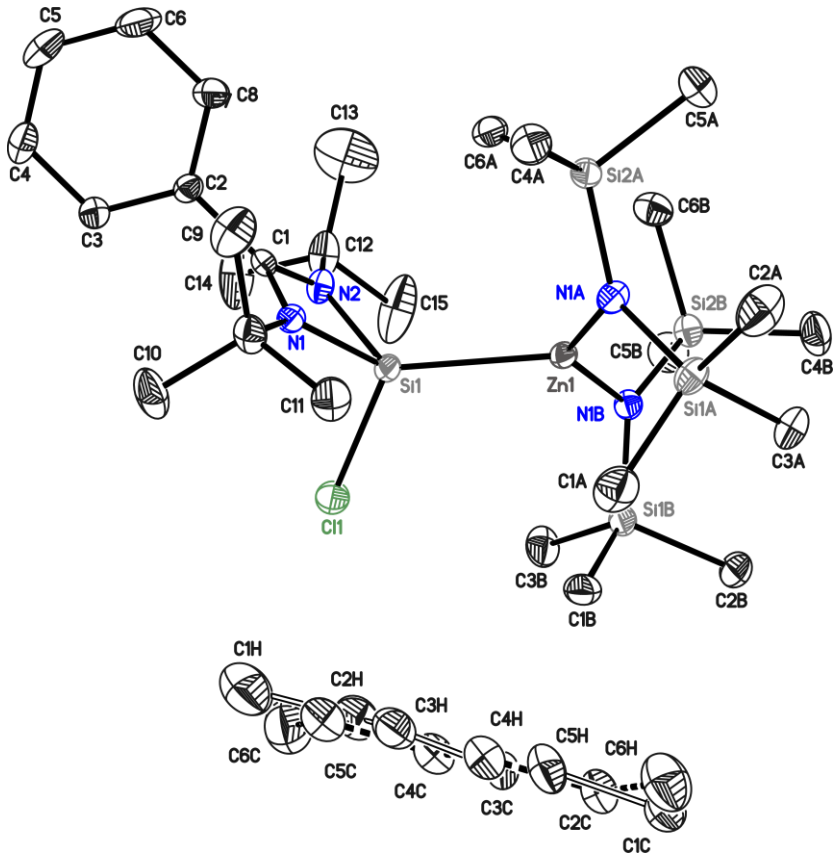

Figure 44. Asymmetric unit of **15**. The anisotropic displacement parameters are depicted at the 50% probability level. The hydrogen atoms are omitted for clarity.

Table 42. Crystal data of **15**.

Structure Code	AP217	Z	4
Empirical formula	$C_{30}H_{66}N_4Si_5ClZn$	ρ_{calc}	1.148
Formula weight [g/mol]	724.13	μ [mm^{-1}]	0.817
Temperature [K]	100(2)	F(000)	1564
Wavelength [Å]	0.71073	θ range [°]	1.812 to 27.506
Crystal system	monoclinic	Reflections collected	137907
space group	$P2_1/n$	Independent reflections	9605
a [Å]	20.074(3)	R(int)	0.0416
b [Å]	10.662(2)	Max. / min. transmission	0.7041 / 0.6495
c [Å]	21.508(3)	Restraints / parameter	283 / 470
α [°]	90	GooF	1.046
β [°]	114.47(2)	R1 / *w*R2 (I > 2σ(I))	0.0243 / 0.0627
γ [°]	90	R1 / *w*R2 (all data)	0.0293 / 0.0656
Volume [Å^3]	4189.9(13)	max. diff peak / hole [e Å^{-3}]	0.375 to -0.291

5.5.1.19. Crystal structure of [(NHSiPh)(Zn(HMDS)$_2$)] – 1,3-N,N'-di-tert-butyl-benzamidinato-N-phenyl-N-(2-pyridyl)amino-silylene-zinc(II)-bis(bis(trimethylsilyl)amide)

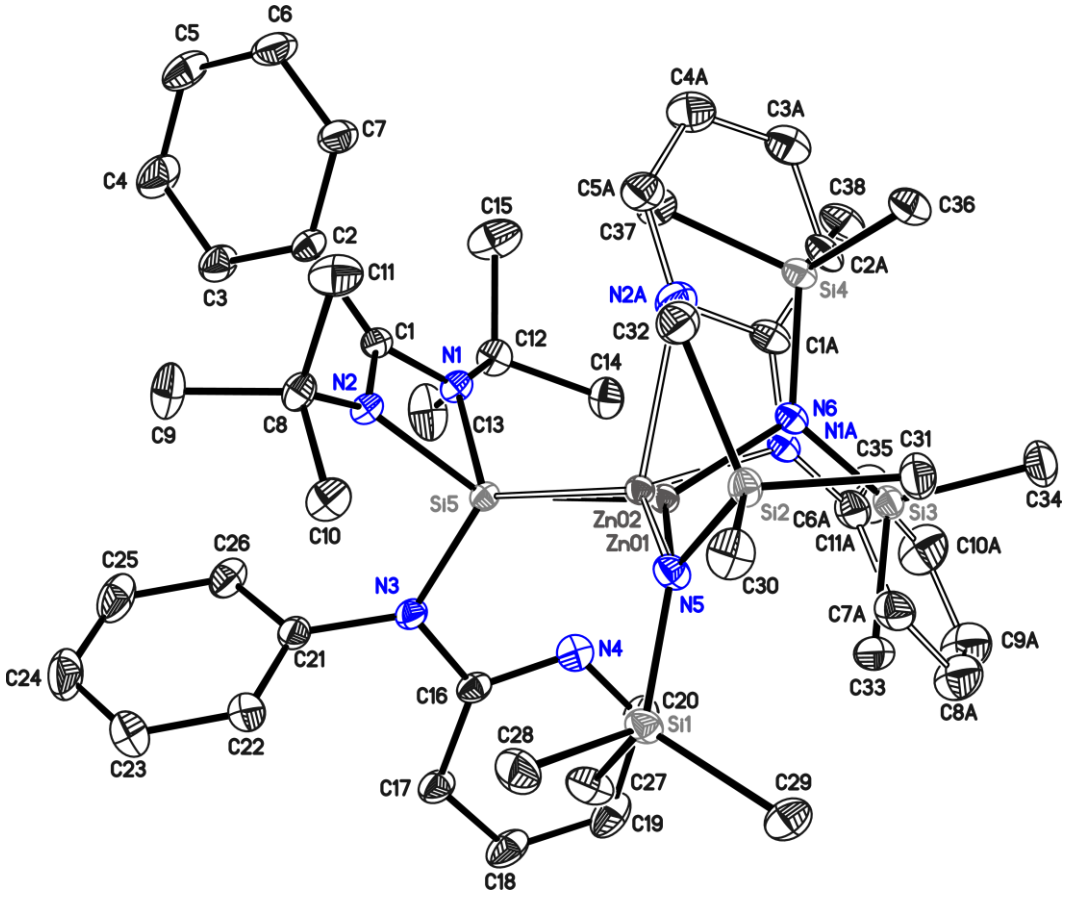

Figure 45. Asymmetric unit of **[(NHSiPh)(Zn(HMDS)$_2$)]**. The anisotropic displacement parameters are depicted at the 50% probability level. The hydrogen atoms are omitted for clarity.

Table 43. Crystal data of **[(NHSiPh)(Zn(HMDS)$_2$)]**.

Structure Code	AP178	Z	4
Empirical formula	$C_{38.33}H_{67.41}N_{6.07}Si_{4.87}Zn$	ρ_{calc}	1.180
Formula weight [g/mol]	815.38	μ [mm^{-1}]	0.695
Temperature [K]	100(2)	F(000)	1752
Wavelength [Å]	0.71073	θ range [°]	1.537 to 32.203
Crystal system	monoclinic	Reflections collected	266735
space group	$P2_1/n$	Independent reflections	16104
a [Å]	13.075(2)	R(int)	0.0323
b [Å]	18.707(2)	Max. / min. transmission	0.7463 / 0.7081
c [Å]	18.776(3)	Restraints / parameter	708 / 578
α [°]	90	GooF	1.059
β [°]	92.05(2)	R1 / *w*R2 (I > 2σ(I))	0.0246 / 0.0644
γ [°]	90	R1 / *w*R2 (all data)	0.0294 / 0.0668
Volume [Å^3]	4589.6(11)	max. diff peak / hole [e Å^{-3}]	0.485 / -0.280

5.5.1.20. Crystal structure of [(ClAu)(SiNCCP)(AuCl)] – 1,3-N,N'-di-tert-butyl-benzamidinato-N-(2-(2,6-di-iso-propylanilino)-2-phenylethyl)diphenylphosphine-silylene-Si,P-di-gold(I)-chloride

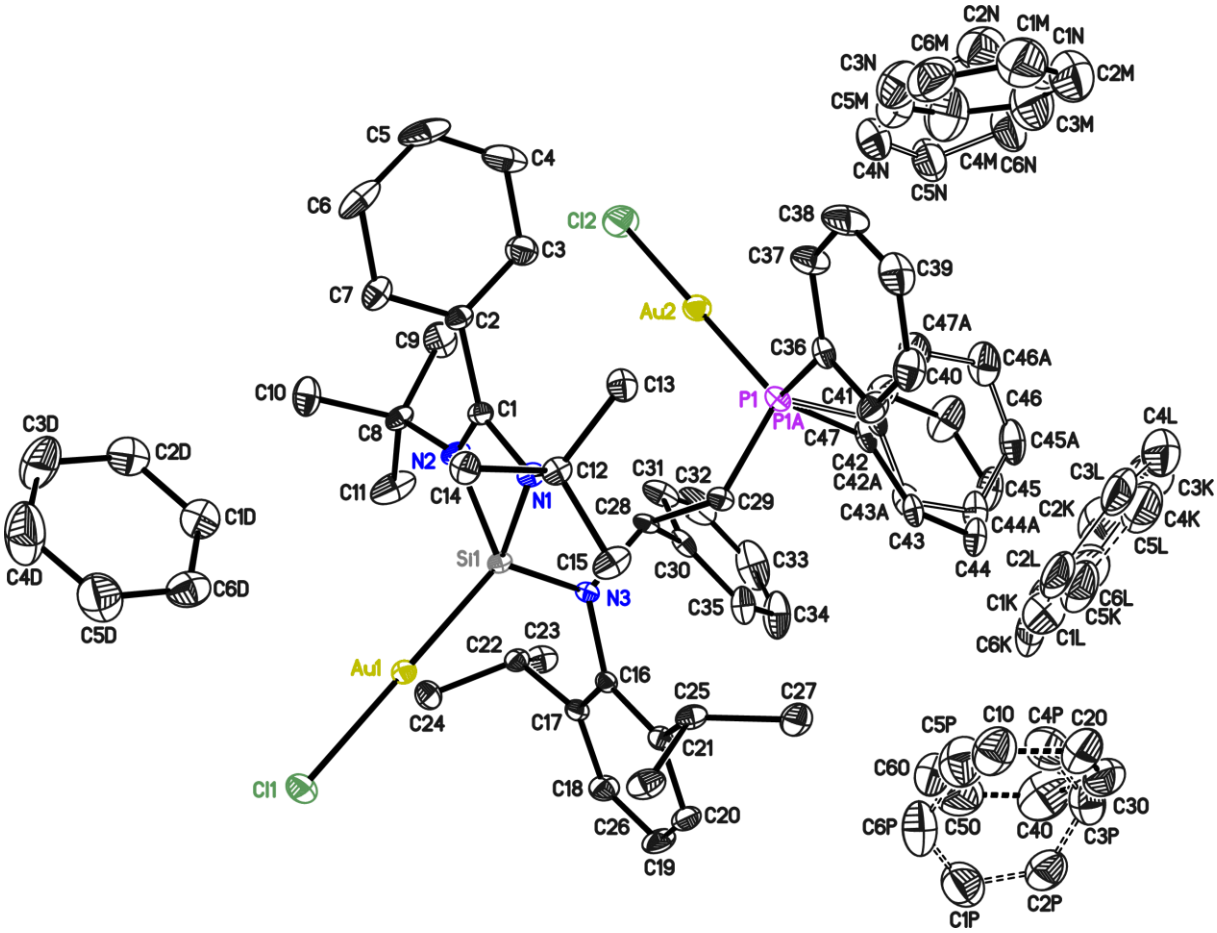

Figure 46. Asymmetric unit of **3**. The anisotropic displacement parameters are depicted at the 50% probability level. The hydrogen atoms are omitted for clarity.

Table 44. Crystal data of **3**.

Structure Code	AP066	Z	4
Empirical formula	$C_{71}H_{82}N_3PSiCl_{1.89}Au_{1.89}$	ρ_{calc}	1.514
Formula weight [g/mol]	1475.47	μ [mm^{-1}]	4.442
Temperature [K]	100(2)	F(000)	2957
Wavelength [Å]	0.71073	θ range [°]	1.079 to 27.497
Crystal system	Monoclinic	Reflections collected	142999
space group	$P2_1/c$	Independent reflections	14822
a [Å]	19.201(4)	R(int)	0.0318
b [Å]	13.865(3)	Max. / min. transmission	0.2012 / 0.1548
c [Å]	24.736(5)	Restraints / parameter	3609 / 949
α [°]	90	GooF	1.114
β [°]	100.62(2)	R1 / *w*R2 (I > 2σ(I))	0.0178 / 0.0382
γ [°]	90	R1 / *w*R2 (all data)	0.0212 / 0.0391
Volume [$Å^3$]	6472(2)	max. diff peak / hole [e $Å^{-3}$]	0.824 / -0.386

5.5.1.21. Crystal structure of [(BrCu)(SiNCCP)(CuBr)] – 1,3-N,N'-di-tert-butyl-benzamidinato-N-(2-(2,6-di-iso-propylanilino)-2-phenylethyl)diphenylphosphine-silylene-Si,P-di-copper(I)-bromide

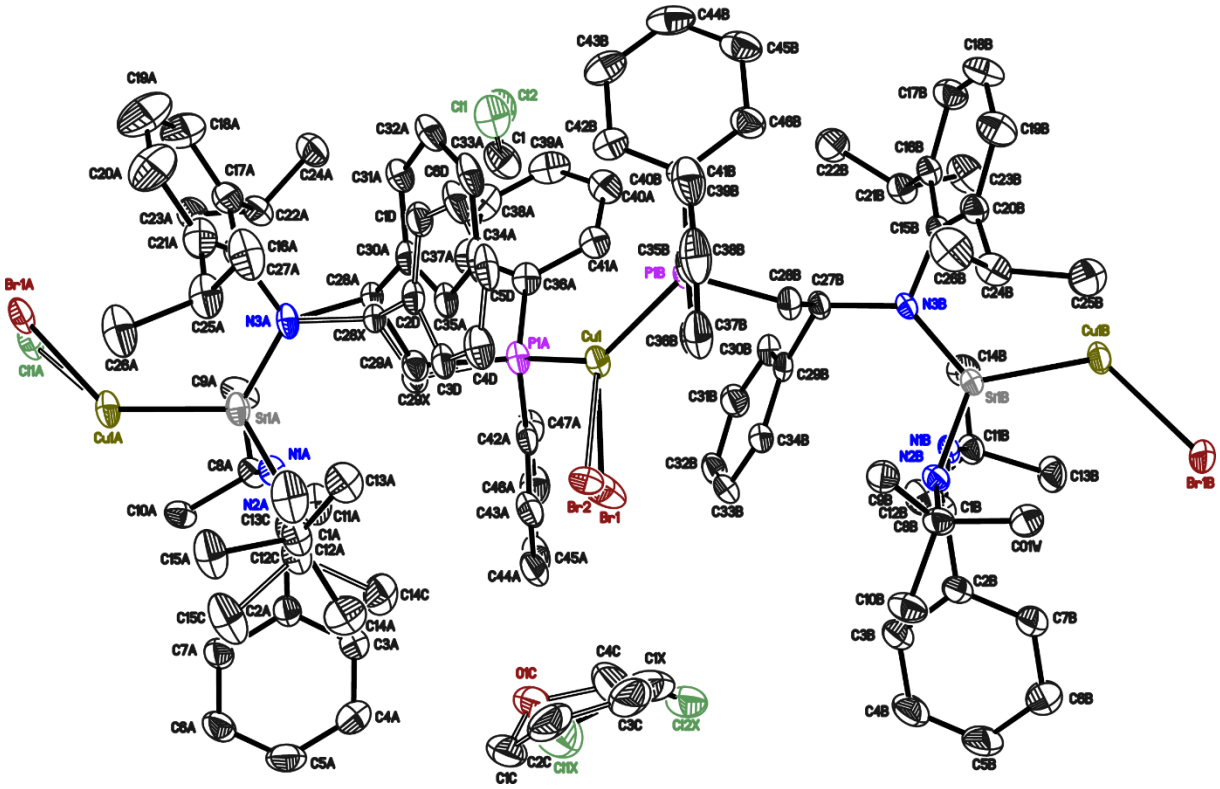

Figure 47. Asymmetric unit of **4**. The anisotropic displacement parameters are depicted at the 50% probability level. The hydrogen atoms are omitted for clarity.

Table 45. Crystal data of **4**.

Structure Code	AP_Cu_2	Z	2
Empirical formula	$C_{96.60}H_{121.19}N_6O_{0.43}P_2Si_2Cl_{1.90}Br_{2.84}Cu_3$	ρ_{calc}	1.398
Formula weight [g/mol]	1976.13	μ [mm^{-1}]	2.044
Temperature [K]	100(2)	F(000)	2046
Wavelength [Å]	0.71073	θ range [°]	0.879 to 25.525
Crystal system	$P\bar{1}$	Reflections collected	127488
space group	Triclinic	Independent reflections	17314
a [Å]	13.171(2)	R(int)	0.0478
b [Å]	15.396(2)	Max. / min. transmission	0.7452 / 0.6484
c [Å]	23.231(3)	Restraints / parameter	1005 / 1209
α [°]	92.20(2)	GooF	1.140
β [°]	93.61(3)	R1 / *w*R2 (I > 2σ(I))	0.0484 / 0.1049
γ [°]	92.28(2)	R1 / *w*R2 (all data)	0.0657 / 0.1129
Volume [Å^3]	4693.8(11)	max. diff peak / hole [e Å^{-3}]	0.820 / -0.829

5.5.2. Crystallographic Cooperation

5.5.2.1. Structures determined with Rajendra S. Ghadwal

Reference: Dennis Rottschäfer, Christian J. Schürmann, Jan-Hendrik Lamm, Alexander N. Paesch, Beate Neumann, and Rajendra S. Ghadwal, *Organometallics* **2016**, *35*, 3421−3429, 10.1021/acs.organomet.6b00662.

CCDC number(s): 1487623, 1494820, 1498255

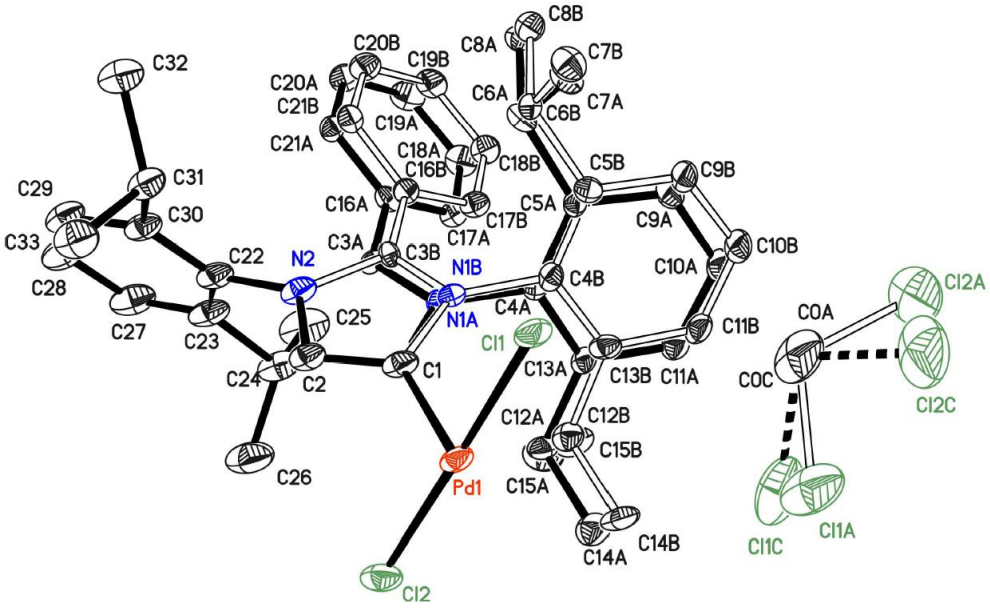

Figure 48. Asymmetric unit of CCDC no. **1487623**. The anisotropic displacement parameters are depicted at the 50% probability level. The hydrogen atoms are omitted for clarity.

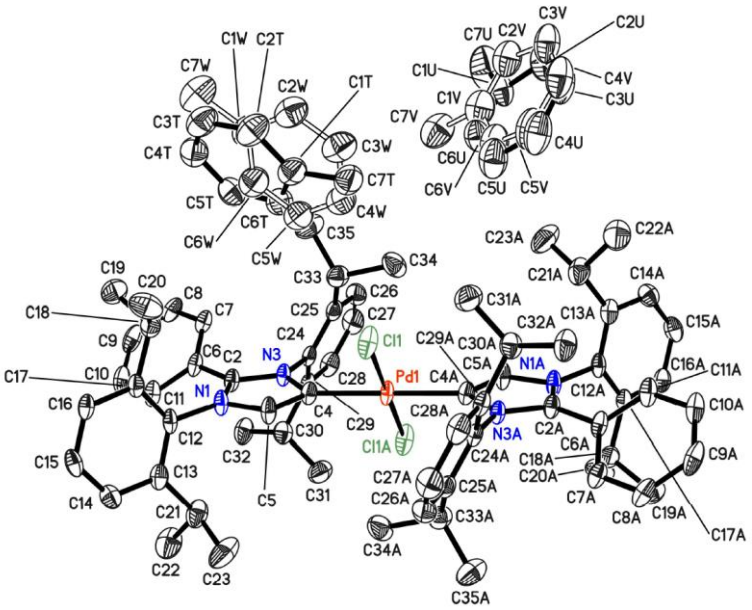

Figure 49. Asymmetric unit of CCDC no. **1487623**. The anisotropic displacement parameters are depicted at the 50% probability level. The hydrogen atoms are omitted for clarity.

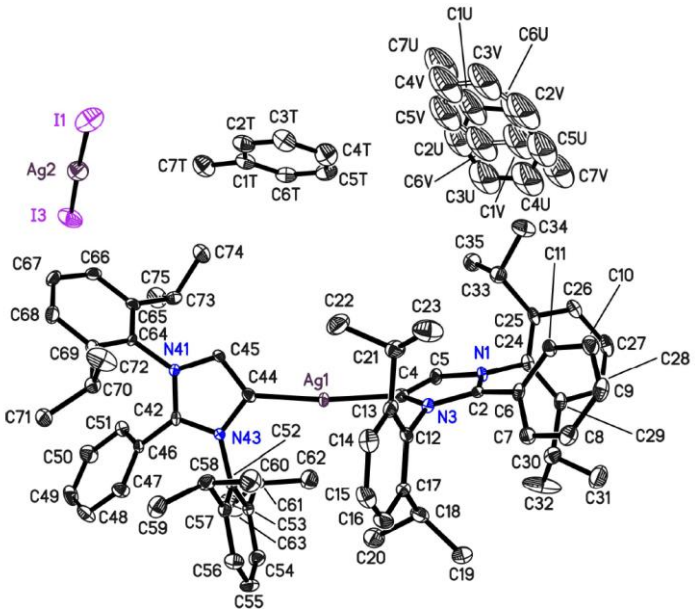

Figure 50. Asymmetric unit of CCDC no. **1498255**. The anisotropic displacement parameters are depicted at the 50% probability level. The hydrogen atoms are omitted for clarity.

5.5.2.2. Structures determined with Chandrajeet Mohapatra within the group of Herbert W. Roesky

Reference: Chandrajeet Mohapatra, Subrata Kundu, Alexander N. Paesch, Regine Herbst-Irmer, Dietmar Stalke, Diego M. Andrada, Gernot Frenking, and Herbert W. Roesky, *J. Am. Chem. Soc.* **2016**, *138*, 10429−10432, 10.1021/jacs.6b07361.

CCDC number(s): 1474405

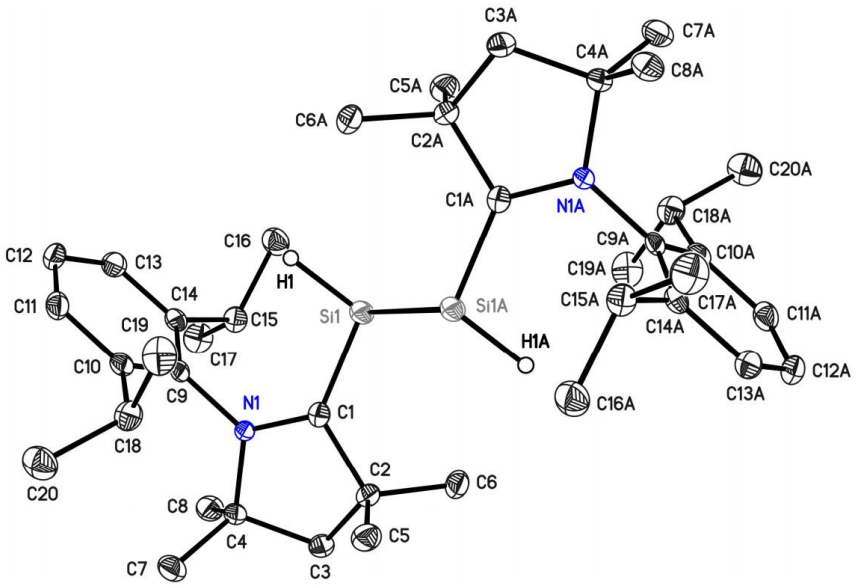

Figure 51. Asymmetric unit of CCDC no. **1474405**. The anisotropic displacement parameters are depicted at the 50% probability level. The hydrogen atoms are omitted for clarity.

5.5.2.3. Structures determined with Kartik Chandra Mondal within the group of Herbert W. Roesky

Reference: Jayasree Kumar, N. V. T. Sai Manoj Gorantla, Sudipta Roy, Alexander N. Paesch, Regine Herbst-Irmer, Dietmar Stalke, Chakkittakandiyil Anusha, Susmita De, Pattiyil Parameswaran, Herbert W. Roesky, and Kartik Chandra Mondal, *ChemistrySelect* **2018**, *3*, 8221–8228, 10.1002/slct.201801172.

CCDC number(s): 1429845

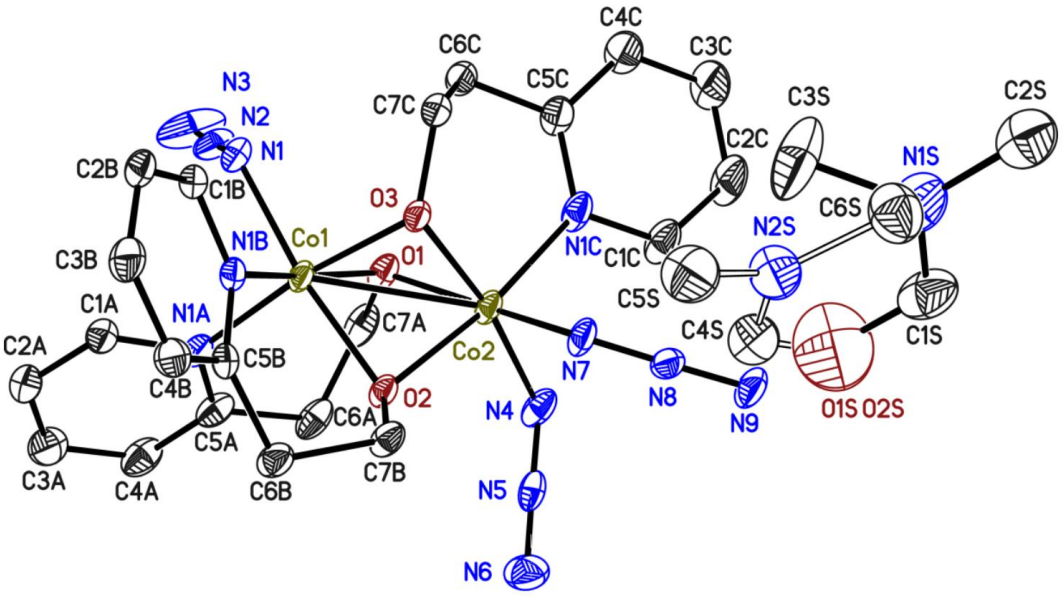

Figure 52. Asymmetric unit of CCDC no. **1429845**. The anisotropic displacement parameters are depicted at the 50% probability level. The hydrogen atoms are omitted for clarity.

5.5.2.4. Structures determined with Soumen Sinhababu within the group of Herbert W. Roesky

Reference: Soumen Sinhababu, Subrata Kundu, Alexander N. Paesch, Regine Herbst-Irmer, Dietmar Stalke, Israel Fernández, Gernot Frenking, A. Claudia Stückl, Brigitte Schwederski, Wolfgang Kaim, and Herbert W. Roesky, *Chem. Eur. J.* **2018**, *24*, *6*, 1264–1268, 10.1002/chem.201705773.

CCDC number(s): 1580421, 1588169

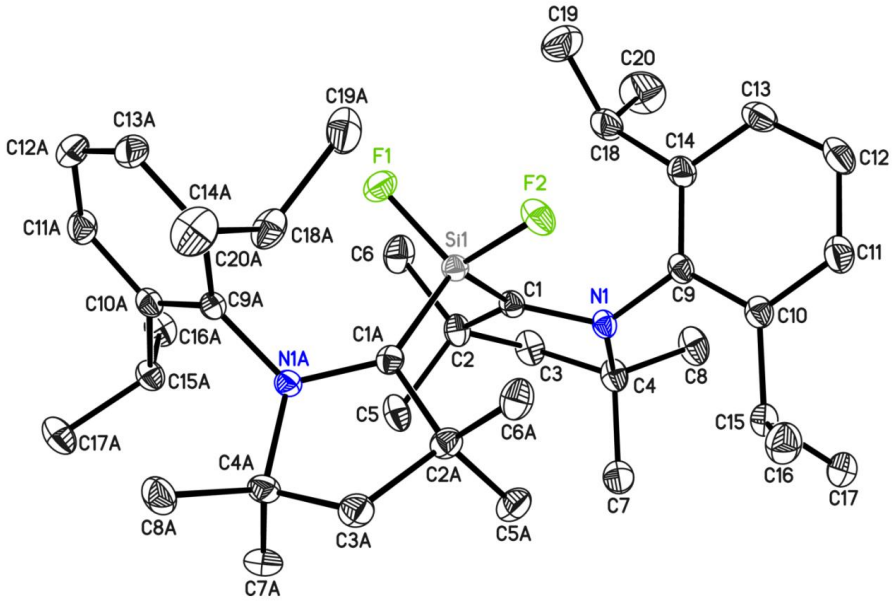

Figure 53. Asymmetric unit of CCDC no. **1580421**. The anisotropic displacement parameters are depicted at the 50% probability level. The hydrogen atoms are omitted for clarity.

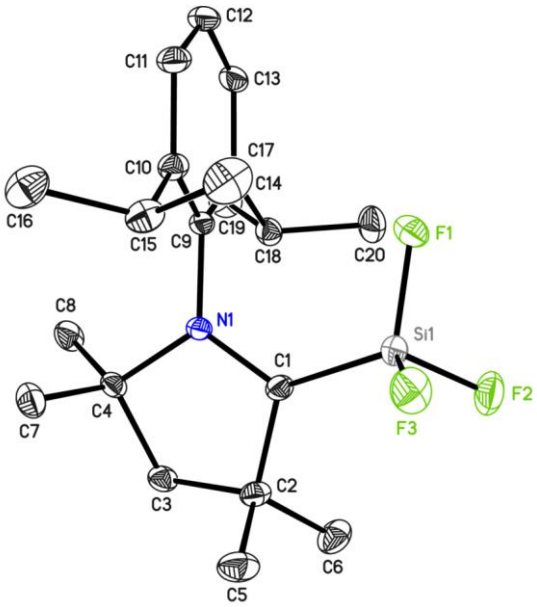

Figure 54. Asymmetric unit of CCDC no. **1588169**. The anisotropic displacement parameters are depicted at the 50% probability level. The hydrogen atoms are omitted for clarity.

Reference: Soumen Sinhababu, Subrata Kundu, Alexander N. Paesch, Regine Herbst-Irmer, Dietmar Stalke, and Herbert W. Roesky, *Eur. J. Inorg. Chem.* **2018**, *20*, 2237–2240, 10.1002/ejic.201701347.

CCDC number(s): 1580439, 1580440

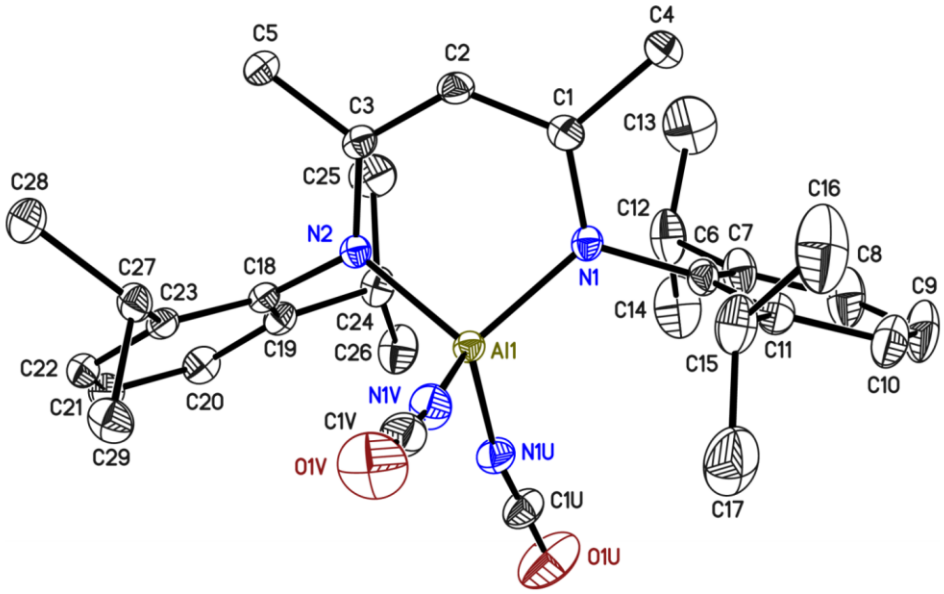

Figure 55. Asymmetric unit of CCDC no. **1580439**. The anisotropic displacement parameters are depicted at the 50% probability level. The hydrogen atoms are omitted for clarity.

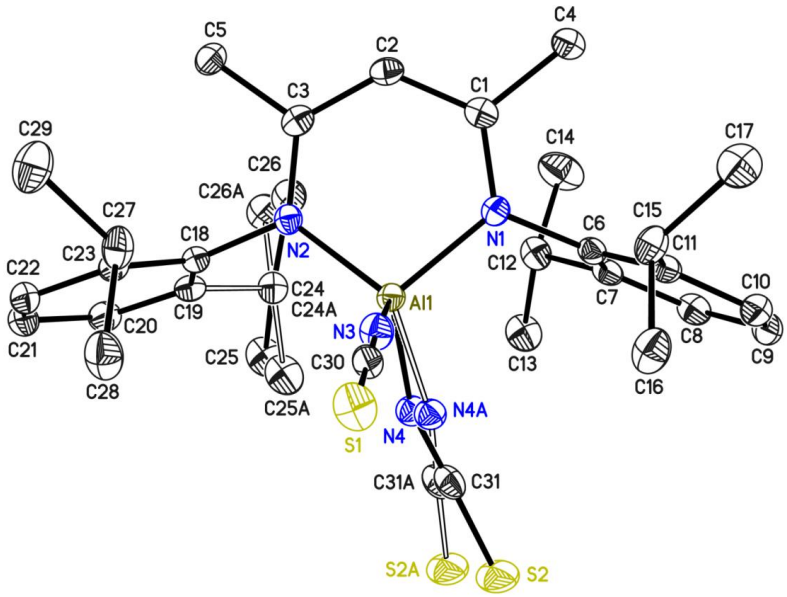

Figure 56. Asymmetric unit of CCDC no. **1580440**. The anisotropic displacement parameters are depicted at the 50% probability level. The hydrogen atoms are omitted for clarity.

Reference: Soumen Sinhababu, Subrata Kundu, Mujahuddin M. Siddiqui, Alexander N. Paesch, Regine Herbst-Irmer, Brigitte Schwederski, Pinaki Saha, Lili Zhao, Gernot Frenking, Wolfgang Kaim, Dietmar Stalke, and Herbert W Roesky, *Chem. Commun.* **2019**, 1359–7345, 10.1039/c9cc01448a.

CCDC number(s): 1894458, 1894459

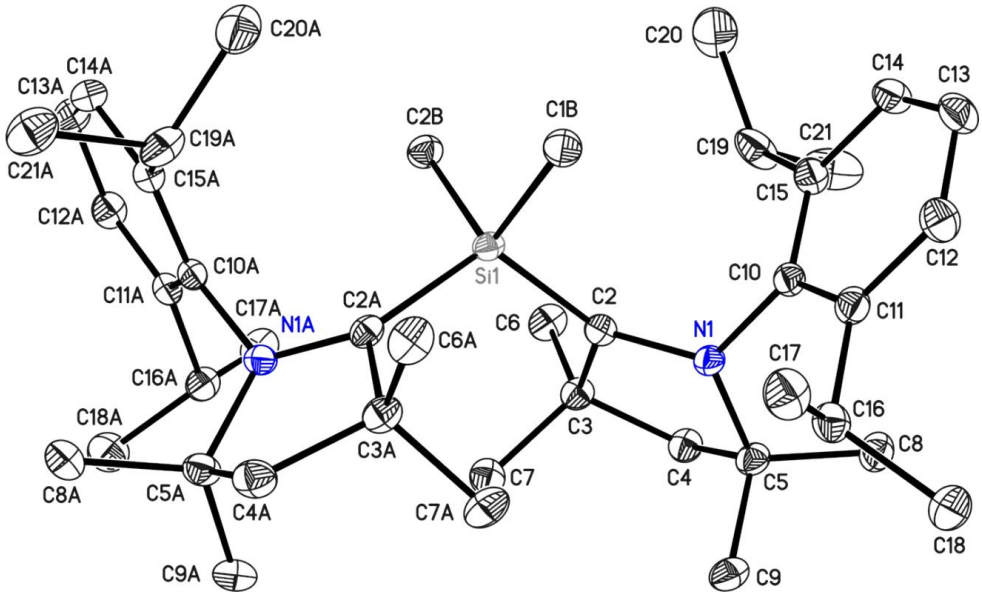

Figure 57. Asymmetric unit of CCDC no. **1894458**. The anisotropic displacement parameters are depicted at the 50% probability level. The hydrogen atoms are omitted for clarity.

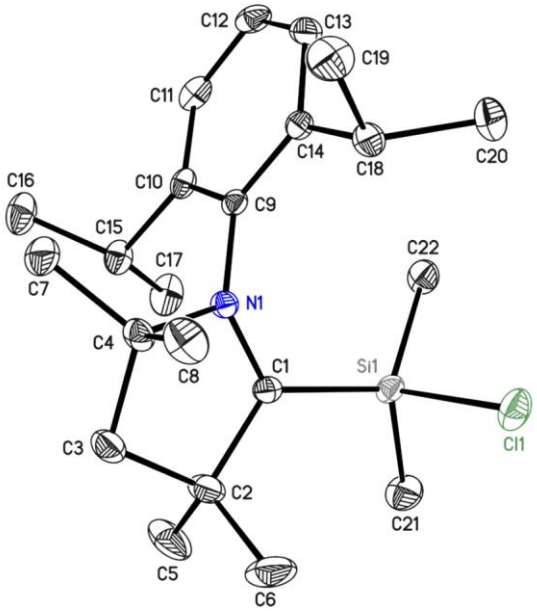

Figure 58. Asymmetric unit of CCDC no. **1894459**. The anisotropic displacement parameters are depicted at the 50% probability level. The hydrogen atoms are omitted for clarity.

6. References

[1] a) Z. Rappoport, Y. Apeloig, *The Chemistry of Organic Silicon Compounds*, John Wiley & Sons, Ltd, Chichester, UK, **1998**; b) V. Y. Lee, *Organosilicon Compounds*. *Theory and Experiment (Synthesis)*, Elsevier Science, San Diego, **2017**.

[2] B. Blom, M. Driess in *Structure and Bonding*, *v.156* (Ed.: D. Scheschkewitz), Springer International Publishing, Cham, **2014**, pp. 85–123.

[3] G. Schmid, E. Welz, *Angew. Chem. Int. Ed. Engl.* **1977**, *16*, 785.

[4] R. West, M. J. Fink, J. Michl, *Science* **1981**, *214*, 1343.

[5] P. Jutzi, U. Holtmann, D. Kanne, C. Krüger, R. Blom, R. Gleiter, I. Hyla-Kryspin, *Chem. Ber.* **1989**, *122*, 1629.

[6] A. J. Arduengo, R. L. Harlow, M. Kline, *J. Am. Chem. Soc.* **1991**, *113*, 361.

[7] M. Denk, R. Lennon, R. Hayashi, R. West, A. V. Belyakov, H. P. Verne, A. Haaland, M. Wagner, N. Metzler, *J. Am. Chem. Soc.* **1994**, *116*, 2691.

[8] Z. Benedek, T. Szilvási, *RSC Adv.* **2015**, *5*, 5077.

[9] B. Gehrhus, M. F. Lappert, J. Heinicke, R. Boese, D. Bläser, *J. Chem. Soc., Chem. Commun.* **1995**, *116*, 1931.

[10] J. Heinicke, A. Oprea, M. K. Kindermann, T. Karpati, L. Nyulászi, T. Veszprémi, *Chem. Eur. J.* **1998**, *4*, 541.

[11] M. Driess, S. Yao, M. Brym, C. van Wüllen, D. Lentz, *J. Am. Chem. Soc.* **2006**, *128*, 9628.

[12] L. Kong, J. Zhang, H. Song, C. Cui, *Dalton Trans.* **2009**, 5444.

[13] C.-W. So, H. W. Roesky, J. Magull, R. B. Oswald, *Angew. Chem., Int. Ed.* **2006**, *45*, 3948.

[14] S. S. Sen, H. W. Roesky, D. Stern, J. Henn, D. Stalke, *J. Am. Chem. Soc.* **2010**, *132*, 1123.

[15] D. Gallego, B. Blom, G. Tan, M. Driess in *Reference Module in Chemistry, Molecular Sciences and Chemical Engineering*, Elsevier, **2015**.

[16] C.-W. So, H. W. Roesky, P. M. Gurubasavaraj, R. B. Oswald, M. T. Gamer, P. G. Jones, S. Blaurock, *J. Am. Chem. Soc.* **2007**, *129*, 12049.

[17] S. S. Sen, J. Hey, M. Eckhardt, R. Herbst-Irmer, E. Maedl, R. A. Mata, H. W. Roesky, M. Scheer, D. Stalke, *Angew. Chem. Int. Ed. Engl.* **2011**, *50*, 12510.

[18] R. Azhakar, R. S. Ghadwal, H. W. Roesky, H. Wolf, D. Stalke, *Organometallics* **2012**, *31*, 4588.

[19] W. Wang, S. Inoue, S. Enthaler, M. Driess, *Angew. Chem. Int. Ed. Engl.* **2012**, *51*, 6167.

[20] K. Junold, J. A. Baus, C. Burschka, R. Tacke, *Angew. Chem. Int. Ed. Engl.* **2012**, *51*, 7020.

[21] K. Junold, M. Nutz, J. A. Baus, C. Burschka, C. Fonseca Guerra, F. M. Bickelhaupt, R. Tacke, *Chem. Eur. J.* **2014**, *20*, 9319.

[22] B. Blom, D. Gallego, M. Driess, *Inorganic Chemistry Frontiers* **2014**, *1*, 134.

[23] M. Kira, S. Ishida, T. Iwamoto, C. Kabuto, *J. Am. Chem. Soc.* **1999**, *121*, 9722.

[24] M. Asay, S. Inoue, M. Driess, *Angew. Chem. Int. Ed. Engl.* **2011**, *50*, 9589.

[25] R. S. Ghadwal, H. W. Roesky, S. Merkel, J. Henn, D. Stalke, *Angew. Chem., Int. Ed.* **2009**, *48*, 5683.

[26] A. C. Filippou, O. Chernov, G. Schnakenburg, *Angew. Chem.* **2009**, *121*, 5797.

[27] A. C. Filippou, O. Chernov, B. Blom, K. W. Stumpf, G. Schnakenburg, *Chemistry* **2010**, *16*, 2866.

[28] A. Sekiguchi, T. Tanaka, M. Ichinohe, K. Akiyama, S. Tero-Kubota, *J. Am. Chem. Soc.* **2003**, *125*, 4962.

[29] B. D. Rekken, T. M. Brown, J. C. Fettinger, H. M. Tuononen, P. P. Power, *J. Am. Chem. Soc.* **2012**, *134*, 6504.

[30] A. V. Protchenko, K. H. Birjkumar, D. Dange, A. D. Schwarz, D. Vidovic, C. Jones, N. Kaltsoyannis, P. Mountford, S. Aldridge, *J. Am. Chem. Soc.* **2012**, *134*, 6500.

[31] M. C. Holthausen, W. Koch, Y. Apeloig, *J. Am. Chem. Soc.* **1999**, *121*, 2623.

[32] a) B. Blom, M. Stoelzel, M. Driess, *Chem. Eur. J.* **2013**, *19*, 40; b) P. P. Power, *Nature* **2010**, *463*, 171.

[33] A. F. Holleman, N. Wiberg, E. Wiberg, *Lehrbuch der Anorganischen Chemie*, Walter de Gruyter, Berlin, New York, **2007**.

[34] M. Driess, H. Grützmacher, *Angew. Chem. Int. Ed. Engl.* **1996**, *35*, 828.

[35] a) D. Bourissou, O. Guerret, F. P. Gabbai, G. Bertrand, *Chem. Rev.* **2000**, *100*, 39; b) G. P. Moss, P. A. S. Smith, D. Tavernier, *Chemistry* **1995**, *67*, 1307.

[36] a) I. Shavitt, *Tetrahedron* **1985**, *41*, 1531; b) B. T. Luke, J. A. Pople, M. B. Krogh-Jespersen, Y. Apeloig, J. Chandrasekhar, P. v. R. Schleyer, *J. Am. Chem. Soc.* **1986**, *108*, 260; c) B. T. Luke, J. A. Pople, M. B. Krogh-Jespersen, Y. Apeloig, M. Karni, J. Chandrasekhar, P. v. R. Schleyer, *J. Am. Chem. Soc.* **1986**, *108*, 270.

[37] A. Sekiguchi, T. Tanaka, M. Ichinohe, K. Akiyama, P. P. Gaspar, *J. Am. Chem. Soc.* **2008**, *130*, 426.

[38] Y. Mizuhata, T. Sasamori, N. Tokitoh, *Chem. Rev.* **2009**, *109*, 3479.

[39] C. Boehme, G. Frenking, *Organometallics* **1998**, *17*, 5801.

[40] a) L. Alvarez-Rodriguez, J. A. Cabeza, P. Garcia-Alvarez, D. Polo, *ChemInform* **2015**, *46*, no-no; b) H. W. Roesky (Ed.) *Efficient methods for preparing silicon compounds*, Academic Press is an imprint of Elsevier, London, UK, **2016**; c) S. U. Ahmad, S. Inoue in *Efficient methods for preparing silicon compounds* (Ed.: H. W. Roesky), Academic Press is an imprint of Elsevier, London, UK, **2016**, pp. 27–72.

[41] a) P. V. Bharatam, R. Moudgil, D. Kaur, *Organometallics* **2002**, *21*, 3683; b) A. Pal, K. Vanka, *Chem. Commun.* **2014**, *50*, 8522; c) T. A. Schmedake, M. Haaf, B. J. Paradise, A. J. Millevolte, D. R. Powell, R. West, *J. Organomet. Chem.* **2001**, *636*, 17; d) B. Tumanskii, P. Pine, Y. Apeloig, N. J. Hill, R. West, *J. Am. Chem. Soc.* **2004**, *126*, 7786; e) D. Sheberla, B. Tumanskii, A. C. Tomasik, A. Mitra,

N. J. Hill, R. West, Y. Apeloig, *Chem. Sci.* **2010**, *1*, 234; f) T. Szilvási, T. Veszprémi, *Struct Chem* **2015**, *26*, 1335.

[42] M. Schmidt, B. Blom, T. Szilvási, R. Schomäcker, M. Driess, *Eur. J. Inorg. Chem.* **2017**, *2017*, 1284.

[43] Y.-P. Zhou, S. Raoufmoghaddam, T. Szilvási, M. Driess, *Angew. Chem. Int. Ed. Engl.* **2016**, *55*, 12868.

[44] A. Brück, D. Gallego, W. Wang, E. Irran, M. Driess, J. F. Hartwig, *Angew. Chem. Int. Ed. Engl.* **2012**, *51*, 11478.

[45] A. Poater, B. Cosenza, A. Correa, S. Giudice, F. Ragone, V. Scarano, L. Cavallo, *Eur. J. Inorg. Chem.* **2009**, 1759.

[46] C. A. Tolman, *Chem. Rev.* **1977**, *77*, 313.

[47] H. Clavier, S. P. Nolan, *Chem. Commun.* **2010**, *46*, 841.

[48] A. Meltzer, S. Inoue, C. Präsang, M. Driess, *J. Am. Chem. Soc.* **2010**, *132*, 3038.

[49] Y.-P. Zhou, M. Driess, *Angew. Chem. Int. Ed. Engl.* **2019**, *58*, 3715.

[50] T. Troadec, A. Prades, R. Rodriguez, R. Mirgalet, A. Baceiredo, N. Saffon-Merceron, V. Branchadell, T. Kato, *Inorg. Chem.* **2016**, *55*, 8234.

[51] R. Rodriguez, T. Troadec, T. Kato, N. Saffon-Merceron, J.-M. Sotiropoulos, A. Baceiredo, *Angew. Chem., Int. Ed.* **2012**, *51*, 7158.

[52] a) M. L. Crawley, B. M. Trost, *Applications of Transition Metal Catalysis in Drug Discovery and Development*, John Wiley & Sons, Inc, Hoboken, NJ, USA, **2012**; b) M. Beller, C. Bolm, *Transition Metals for Organic Synthesis*, WILEY-VCH Verlag GmbH, Weinheim, Germany, **2004**.

[53] M. Melaimi, M. Soleilhavoup, G. Bertrand, *Angew. Chem., Int. Ed.* **2010**, *49*, 8810.

[54] M. Scholl, T. M. Trnka, J. P. Morgan, R. H. Grubbs, *Tetrahedron Lett.* **1999**, *40*, 2247.

[55] J. Huang, H.-J. Schanz, E. D. Stevens, S. P. Nolan, *Organometallics* **1999**, *18*, 5375.

[56] R. H. Grubbs, *Angew. Chem. Int. Ed. Engl.* **2006**, *45*, 3760.

[57] J. K. Huang, E. D. Stevens, S. P. Nolan, J. L. Petersen, *J. Am. Chem. Soc.* **1999**, *121*, 2674.

[58] J. Huang, H.-J. Schanz, E. D. Stevens, S. P. Nolan, *Organometallics* **1999**, *18*, 2370.

[59] T. Sajoto, P. I. Djurovich, A. Tamayo, M. Yousufuddin, R. Bau, M. E. Thompson, R. J. Holmes, S. R. Forrest, *Inorg. Chem.* **2005**, *44*, 7992.

[60] D. M. Khramov, A. J. Boydston, C. W. Bielawski, *Angew. Chem. Int. Ed. Engl.* **2006**, *45*, 6186.

[61] C. Zybill, G. Müller, *Angew. Chem. Int. Ed. Engl.* **1987**, *26*, 669.

[62] S. D. Grumbine, T. D. Tilley, F. P. Arnold, A. L. Rheingold, *J. Am. Chem. Soc.* **1993**, *115*, 7884.

[63] S. D. Grumbine, T. D. Tilley, A. L. Rheingold, *J. Am. Chem. Soc.* **1993**, *115*, 358.

[64] S. K. Grumbine, T. D. Tilley, F. P. Arnold, A. L. Rheingold, *J. Am. Chem. Soc.* **1994**, *116*, 5495.

[65] a) M. C. Lipke, A. L. Liberman-Martin, T. D. Tilley, *J. Am. Chem. Soc.* **2016**, *138*, 9704; b) Y. Li, T. Liu, H. Liu, M.-Z. Tian, Y. Li, *Acc. Chem. Res.* **2014**, *47*, 1186; c) M. C. Lipke, T. D. Tilley, *J. Am.*

Chem. Soc. **2014**, *136*, 16387; d) S. K. Grumbine, G. P. Mitchell, D. A. Straus, T. D. Tilley, A. L. Rheingold, *Organometallics* **1998**, *17*, 5607; e) G. P. Mitchell, T. D. Tilley, *J. Am. Chem. Soc.* **1997**, *119*, 11236; f) D. A. Straus, T. D. Tilley, A. L. Rheingold, S. J. Geib, *J. Am. Chem. Soc.* **1987**, *109*, 5872.

[66] A. Fürstner, H. Krause, C. W. Lehmann, *Chem. Commun.* **2001**, *32*, 2372.

[67] B. Blom, S. Enthaler, S. Inoue, E. Irran, M. Driess, *J. Am. Chem. Soc.* **2013**, *135*, 6703.

[68] M. Stoelzel, C. Präsang, B. Blom, M. Driess, *Austr. J. Chem.* **2013**, *66*, 1163.

[69] M. Zhang, X. Liu, C. Shi, C. Ren, Y. Ding, H. W. Roesky, *Z. anorg. allg. Chem.* **2008**, *634*, 1755.

[70] a) J. Chatt, L. A. Duncanson, *J. Chem. Soc.* **1953**, 2939; b) J. Chatt, L. A. Duncanson, L. M. Venanzi, *J. Chem. Soc.* **1955**, 4456.

[71] D. Stalke, M. Wedler, F. T. Edelmann, *J. Organomet. Chem.* **1992**, *431*, C1-C5.

[72] R. A. Benkeser, *Acc. Chem. Res.* **1971**, *4*, 94.

[73] H. Cui, Y. Shao, X. Li, L. Kong, C. Cui, *Organometallics* **2009**, *28*, 5191.

[74] R. Azhakar, R. S. Ghadwal, H. W. Roesky, H. Wolf, D. Stalke, *Chem. Commun.* **2012**, *48*, 4561.

[75] S. S. Sen, S. Khan, P. P. Samuel, H. W. Roesky, *Chem. Sci.* **2012**, *3*, 659.

[76] W. Wang, S. Inoue, S. Yao, M. Driess, *J. Am. Chem. Soc.* **2010**, *132*, 15890.

[77] W. Wang, S. Inoue, E. Irran, M. Driess, *Angew. Chem.* **2012**, *124*, 3751.

[78] F. M. Mück, K. Junold, J. A. Baus, C. Burschka, R. Tacke, *Eur. J. Inorg. Chem.* **2013**, *2013*, 5821.

[79] R. Tacke, T. Ribbeck, *Dalton Trans.* **2017**, *46*, 13628.

[80] F. M. Mück, D. Kloss, J. A. Baus, C. Burschka, R. Tacke, *Chemistry* **2014**, *20*, 9620.

[81] J. A. Baus, F. M. Mück, H. Schneider, R. Tacke, *Chem. Eur. J.* **2017**, *23*, 296.

[82] a) A. Bader, E. Lindner, *Coord. Chem. Rev.* **1991**, *108*, 27; b) P. Braunstein, F. Naud, *Angew. Chem., Int. Ed.* **2001**, *40*, 680.

[83] R. G. Pearson, *J. Am. Chem. Soc.* **1963**, *85*, 3533.

[84] S. Pal, N. Kathewad, R. Pant, S. Khan, *Inorg. Chem.* **2015**, *54*, 10172.

[85] a) H. Schmidbaur, *Chem. Soc. Rev.* **1995**, *24*, 391; b) H. Schmidbaur, *Gold Bulletin* **1990**, *23*, 11; c) F. Scherbaum, A. Grohmann, G. Müller, H. Schmidbaur, *Angew. Chem. Int. Ed. Engl.* **1989**, *28*, 463; d) F. Scherbaum, A. Grohmann, B. Huber, C. Krüger, H. Schmidbaur, *Angew. Chem. Int. Ed. Engl.* **1988**, *27*, 1544; e) H. Schmidbaur, F. Scherbaum, B. Huber, G. Müller, *Angew. Chem. Int. Ed. Engl.* **1988**, *27*, 419.

[86] A. Pinto, N. Svahn, J. C. Lima, L. Rodríguez, *Dalton Trans.* **2017**, *46*, 11125.

[87] H. Schmidbaur, A. Schier, *Chem. Soc. Rev.* **2012**, *41*, 370.

[88] V. W.-W. Yam, E. C.-C. Cheng, *Chem. Soc. Rev.* **2008**, *37*, 1806.

[89] H. Schmidbaur, *Gold Bulletin* **2000**, *33*, 3.

[90] a) R. Narayanaswamy, M. A. Young, E. Parkhurst, M. Ouellette, M. E. Kerr, D. M. Ho, R. C. Elder, A. E. Bruce, M. R. M. Bruce, *Inorg. Chem.* **1993**, *32*, 2506; b) K. Dziwok, J. Lachmann, D. L. Wilkinson, G. Müller, H. Schmidbaur, *Chem Ber* **1990**, *123*, 423; c) H. Schmidbaur, K. Dziwok, A. Grohmann, G. Müller, *Chem Ber* **1989**, *122*, 893; d) J. Zank, A. Schier, H. Schmidbaur, *J. Chem. Soc., Dalton Trans.* **1998**, 323; e) D. E. Harwell, M. d. Mortimer, C. B. Knobler, F. A. L. Anet, M. F. Hawthorne, *J. Am. Chem. Soc.* **1996**, *118*, 2679; f) H. Schmidbaur, A. Kolb, P. Bissinger, *Inorg. Chem.* **1992**, *31*, 4370; g) H. Schmidbaur, W. Graf, G. Müller, *HCA* **1986**, *69*, 1748.

[91] a) P. Schwerdtfeger, A. E. Bruce, M. R. M. Bruce, *J. Am. Chem. Soc.* **1998**, *120*, 6587; b) N. Kaltsoyannis, *J. Chem. Soc., Dalton Trans.* **1997**, 1; c) P. Pyykkö, F. Mendizabal, *Chem. Eur. J.* **1997**, *3*, 1458; d) P. Pyykkö, N. Runeberg, F. Mendizabal, *Chem. Eur. J.* **1997**, *3*, 1451; e) P. Pyykkö, K. Angermaier, B. Assmann, H. Schmidbaur, *J. Chem. Soc., Chem. Commun.* **1995**, *23*, 1889; f) O. d. Haeberlen, H. Schmidbaur, N. Roesch, *J. Am. Chem. Soc.* **1994**, *116*, 8241.

[92] P. Pyykkö, *Chem. Rev.* **1997**, *97*, 597.

[93] B. Assadollahzadeh, P. Schwerdtfeger, *Chem Phys Lett* **2008**, *462*, 222.

[94] a) W. Lu, N. Zhu, C.-M. Che, *J. Am. Chem. Soc.* **2003**, *125*, 16081; b) R. L. White-Morris, M. M. Olmstead, A. L. Balch, O. Elbjeirami, M. A. Omary, *Inorg. Chem.* **2003**, *42*, 6741; c) D. Rios, D. M. Pham, J. C. Fettinger, M. M. Olmstead, A. L. Balch, *Inorg. Chem.* **2008**, *47*, 3442; d) T. K.-M. Lee, N. Zhu, V. W.-W. Yam, *J. Am. Chem. Soc.* **2010**, *132*, 17646; e) L. Rodríguez, M. Ferrer, R. Crehuet, J. Anglada, J. C. Lima, *Inorg. Chem.* **2012**, *51*, 7636; f) S. H. Lim, J. C. Schmitt, J. Shearer, J. Jia, M. M. Olmstead, J. C. Fettinger, A. L. Balch, *Inorg. Chem.* **2013**, *52*, 823; g) T. Zhang, M. Drouin, P. d. Harvey, *Inorg. Chem.* **1999**, *38*, 4928; h) J. C. Vickery, M. M. Olmstead, E. Y. Fung, A. L. Balch, *Angew. Chem., Int. Ed.* **1997**, *36*, 1179; i) H. Xiao, Y.-X. Weng, W.-T. Wong, T. C. W. Mak, C.-M. Che, *J. Chem. Soc., Dalton Trans.* **1997**, 221; j) Z. Assefa, B. G. McBurnett, R. J. Staples, J. P. Fackler, B. Assmann, K. Angermaier, H. Schmidbaur, *Inorg. Chem.* **1995**, *34*, 75; k) D. Li, C.-M. Che, S.-M. Peng, S.-T. Liu, Z.-Y. Zhou, T. C. W. Mak, *J. Chem. Soc., Dalton Trans.* **1993**, 189; l) V. W.-W. Yam, T.-F. Lai, C.-M. Che, *J. Chem. Soc., Dalton Trans.* **1990**, 3747.

[95] S.-W. Wen, M.-T. Lee, C. H. Chen, *J. Display Technol.* **2005**, *1*, 90.

[96] a) S. S. Pathaneni, G. R. Desiraju, *J. Chem. Soc., Dalton Trans.* **1993**, 319; b) M. H. Keefe, K. D. Benkstein, J. T. Hupp, *ChemInform* **2000**, *31*, no-no; c) V. W.-W. Yam, C.-L. Chan, C.-K. Li, K. M.-C. Wong, *Coord. Chem. Rev.* **2001**, *216-217*, 173; d) N. W. Mitzel, C. Lustig, R. J. F. Berger, N. Runeberg, *Angew. Chem., Int. Ed.* **2002**, *41*, 2519; e) C.-K. Li, X.-X. Lu, K. M.-C. Wong, C.-L. Chan, N. Zhu, V. W.-W. Yam, *Inorg. Chem.* **2004**, *43*, 7421; f) E. J. Fernández, J. M. López-de-Luzuriaga, M. Monge, M. E. Olmos, R. C. Puelles, A. Laguna, A. A. Mohamed, J. P. Fackler, *Inorg. Chem.* **2008**, *47*, 8069; g) P. Zaleski-Ejgierd, P. Pyykkö, *J. Phys. Chem. A* **2009**, *113*, 12380; h) A. Laguna, T. Lasanta, J. M. López-de-Luzuriaga, M. Monge, P. Naumov, M. E. Olmos, *J. Am. Chem. Soc.*

2010, *132*, 456; i) C. E. Strasser, V. J. Catalano, *J. Am. Chem. Soc.* **2010**, *132*, 10009; j) X. He, V. W.-W. Yam, *Coord. Chem. Rev.* **2011**, *255*, 2111.

[97] S. Khan, S. Pal, N. Kathewad, I. Purushothaman, S. De, P. Parameswaran, *Chem. Commun.* **2016**, *52*, 3880.

[98] A. Murso, D. Stalke, *Dalton Trans.* **2004**, 2563.

[99] a) H. Brunner, A. F. M. Mokhlesur Rahman, *Chemische Berichte* **1984**, *117*, 710; b) E. Drent, P. Arnoldy, P.H.M. Budzelaar, *J. Organomet. Chem.* **1993**, *455*, 247; c) G. R. Newkome, *Chem. Rev.* **1993**, *93*, 2067.

[100] H. Yang, M. Alvarez, N. Lugan, R. Mathieu, *J.Chem. Soc., Chem. Commun.* **1995**, 1721.

[101] a) K. Issleib, H. Oehme, D. Wienbeck, *J. Organomet. Chem.* **1974**, *76*, 345; b) A. N. PUDOVIK, G. V. ROMANOV, V. M. POZHIDAEV, *Chemischer Informationsdienst* **1978**, *9*, 2173.

[102] J. Andrieu, C. Baldoli, S. Maiorana, R. Poli, P. Richard, *Eur. J. Org. Chem.* **1999**, *1999*, 3095.

[103] J. Andrieu, J. Dietz, R. Poli, P. Richard, *New J. Chem.* **1999**, *23*, 581.

[104] a) K. Issleib, M. Lischewski, A. Zschunke, *Z. Chem.* **1974**, *14*, 243; b) K. Kellner, A. Tzschach, *Z. Chem.* **1984**, *24*, 365.

[105] P. H. M. Budzelaar, *J. Org. Chem.* **1998**, *63*, 1131.

[106] R. T. Boeré, V. Klassen, G. Wolmershäuser, *J. Chem. Soc., Dalton Trans.* **1998**, 4147.

[107] Z.-X. Wang, D.-Q. Wang, J.-M. Dou, *J. Organomet. Chem.* **2003**, *665*, 205.

[108] T. van Dijk, S. Burck, M. K. Rong, A. J. Rosenthal, M. Nieger, J. C. Slootweg, K. Lammertsma, *Angew. Chem. Int. Ed. Engl.* **2014**, *53*, 9068.

[109] S. C. Rathnayaka, S. V. Lindeman, N. P. Mankad, *Inorg. Chem.* **2018**, *57*, 9439.

[110] J. Andrieu, J.-M. Camus, J. Dietz, P. Richard, R. Poli, *Inorg. Chem.* **2001**, *40*, 1597.

[111] J. Barluenga, F. López, F. Palacios, *Synthesis* **1989**, *1989*, 298.

[112] a) T. Hayashi, M. Konishi, M. Fukushima, K. Kanehira, T. Hioki, M. Kumada, *J. Org. Chem.* **1983**, *48*, 2195; b) C. G. Arena, F. Nicolo, D. Drommi, G. Bruno, F. Faraone, *J. Chem. Soc., Chem. Commun.* **1994**, 2251.

[113] D. J. Peterson, *J. Organomet. Chem.* **1967**, *8*, 199.

[114] a) E. P. Kyba, *J. Am. Chem. Soc.* **1975**, *97*, 2554; b) E. P. Kyba, *J. Am. Chem. Soc.* **1976**, *98*, 4805.

[115] S. Díez-González, N. Marion, S. P. Nolan, *Chem. Rev.* **2009**, *109*, 3612.

[116] a) J. I. Urzúa, R. Contreras, C. O. Salas, R. A. Tapia, *RSC Adv.* **2016**, *6*, 82401; b) F. Lazreg, F. Nahra, C. S.J. Cazin, *Coord. Chem. Rev.* **2015**, *293-294*, 48.

[117] R. Heath, H. Muller-Bunz, M. Albrecht, *Chem. Commun.* **2015**, *51*, 8699.

[118] a) L. Biasiolo, A. Del Zotto, D. Zuccaccia, *Organometallics* **2015**, *34*, 1759; b) R. Yuan, Z. Lin, *ACS Catal.* **2015**, *5*, 2866.

[119] S. S. Gunatilleke, C. A. F. de Oliveira, J. A. McCammon, A. M. Barrios, *J Biol Inorg Chem* **2008**, *13*, 555.

[120] S. Khan, S. K. Ahirwar, S. Pal, N. Parvin, N. Kathewad, *Organometallics* **2015**, *34*, 5401.

[121] R. Azhakar, R. S. Ghadwal, H. W. Roesky, J. Hey, L. Krause, D. Stalke, *Dalton Trans.* **2013**, *42*, 10277.

[122] R. Azhakar, R. S. Ghadwal, H. W. Roesky, J. Hey, D. Stalke, *Chemistry – An Asian Journal* **2012**, *7*, 528.

[123] R. Azhakar, R. S. Ghadwal, H. W. Roesky, H. Wolf, D. Stalke, *J. Am. Chem. Soc.* **2012**, *134*, 2423.

[124] R. Azhakar, S. P. Sarish, H. W. Roesky, J. Hey, D. Stalke, *Inorg. Chem.* **2011**, *50*, 5039.

[125] B. Blom, M. Driess, D. Gallego, S. Inoue, *Chemistry* **2012**, *18*, 13355.

[126] S. Khoo, H.-X. Yeong, Y. Li, R. Ganguly, C.-W. So, *Inorg. Chem.* **2015**, *54*, 9968.

[127] G. Tan, B. Blom, D. Gallego, M. Driess, *Organometallics* **2014**, *33*, 363.

[128] G. Tavcar, S. S. Sen, R. Azhakar, A. Thorn, H. W. Roesky, *Inorg. Chem.* **2010**, *49*, 10199.

[129] D. Scheschkewitz (Ed.) *Structure and Bonding*, *v.156*, Springer International Publishing, Cham, **2014**.

[130] F. Chen, S.-W. Oh, R. E. Wasylishen, *Can. J. Chem.* **2009**, *87*, 1090.

[131] a) J. C. Dyason, P. C. Healy, L. M. Engelhardt, C. Pakawatchai, V. A. Patrick, C. L. Raston, A. H. White, *J. Chem. Soc., Dalton Trans.* **1985**, 831; b) A. Vega, J.-Y. Saillard, *Inorg. Chem.* **2004**, *43*, 4012; c) M. R. Churchill, K. L. Kalra, *Inorg. Chem.* **1974**, *13*, 1427.

[132] N. Parvin, S. Pal, J. Echeverría, S. Alvarez, S. Khan, *Chem. Sci.* **2018**, *118*, 5581.

[133] N. Parvin, S. Pal, S. Khan, S. Das, S. K. Pati, H. W. Roesky, *Inorg. Chem.* **2017**, *56*, 1706.

[134] L. Álvarez-Rodríguez, J. A. Cabeza, P. García-Álvarez, D. Polo, *Organometallics* **2015**, *34*, 5479.

[135] W.-P. Leung, C.-W. So, K.-H. Chong, K.-W. Kan, H.-S. Chan, T. C. W. Mak, *Organometallics* **2006**, *25*, 2851.

[136] S. Bachmann, R. Neufeld, M. Dzemski, D. Stalke, *Chem. Eur. J.* **2016**, *22*, 8462.

[137] R. Neufeld, D. Stalke, *Chem. Sci.* **2015**, *6*, 3354.

[138] A. S. Guram, R. A. Rennels, S. L. Buchwald, *Angew. Chem., Int. Ed.* **1995**, *34*, 1348.

[139] J. Louie, J. F. Hartwig, *Tetrahedron Lett* **1995**, *36*, 3609.

[140] A. S. Guram, S. L. Buchwald, *J. Am. Chem. Soc.* **1994**, *116*, 7901.

[141] F. Paul, J. Patt, J. F. Hartwig, *J. Am. Chem. Soc.* **1994**, *116*, 5969.

[142] D. M.T. Chan, K. L. Monaco, R.-P. Wang, M. P. Winters, *Tetrahedron Letters* **1998**, *39*, 2933.

[143] P. Y.S. Lam, C. G. Clark, S. Saubern, J. Adams, M. P. Winters, D. M.T. Chan, A. Combs, *Tetrahedron Letters* **1998**, *39*, 2941.

[144] D. A. Evans, J. L. Katz, T. R. West, *Tetrahedron Lett* **1998**, *39*, 2937.

[145] K.-S. Masters, T. R. M. Rauws, A. K. Yadav, W. A. Herrebout, B. van der Veken, B. U. W. Maes, *Chemistry* **2011**, *17*, 6315.

[146] A. Ito, H. Fujino, K. Ushiyama, E. Yamanaka, R. Yamasaki, I. Okamoto, *Tetrahedron Letters* **2016**, *57*, 4737.

[147] H. Horie, I. Koyama, T. Kurahashi, S. Matsubara, *Chem. Commun.* **2011**, *47*, 2658.

[148] T. HISANO, T. Matsuoko, K. TSUTSUMI, K. MURAOKA, M. ICHIKAWA, *Chem. Pharm. Bull.* **1981**, *29*, 3706.

[149] a) C. P. Kubiak, R. Eisenberg, *J. Am. Chem. Soc.* **1977**, *99*, 6129; b) M. M. Olmstead, H. Hope, L. S. Benner, A. L. Balch, *J. Am. Chem. Soc.* **1977**, *99*, 5502; c) N. S. Lewis, K. R. Mann, J. G. Gordon, H. B. Gray, *J. Am. Chem. Soc.* **1976**, *98*, 7461.

[150] H. Werner, M. Manger, M. Laubender, M. Teichert, D. Stalke, *J. Organomet. Chem.* **1998**, *569*, 189.

[151] a) T. Murahashi, H. Kurosawa, *Coord. Chem. Rev.* **2002**, *231*, 207; b) H. J. Barnett, A. F. Hill, *Chem. Commun.* **2019**, *55*, 1734; c) K. d. Wells, M. J. Ferguson, R. McDonald, M. Cowie, *Organometallics* **2008**, *27*, 691.

[152] W.-F. Fu, X. Gan, C.-M. Che, Q.-Y. Cao, Z.-Y. Zhou, N. N.-Y. Zhu, *Chemistry* **2004**, *10*, 2228.

[153] S. Maier, W. Hiller, J. Strähle, *Z. Naturforsch. B* **1988**, *43*, 1628.

[154] a) D. Braga, L. Maini, P. P. Mazzeo, B. Ventura, *Chemistry* **2010**, *16*, 1553; b) P. Pyykko, *Chem. Rev.* **1988**, *88*, 563; c) C. L. Collins, K. G. Dyall, H. F. Schaefer, *J. Chem. Phys.* **1995**, *102*, 2024; d) P. Pyykkö, *Angewandte Chemie (International ed. in English)* **2004**, *43*, 4412.

[155] A. A. D. Tulloch, A. A. Danopoulos, S. Kleinhenz, M. E. Light, M. B. Hursthouse, G. Eastham, *Organometallics* **2001**, *20*, 2027.

[156] a) H. L. Hermann, G. Boche, P. Schwerdtfeger, *Chem. Eur. J.* **2001**, *7*, 5333; b) A. M. Willcocks, T. P. Robinson, C. Roche, T. Pugh, S. P. Richards, A. J. Kingsley, J. P. Lowe, A. L. Johnson, *Inorg. Chem.* **2012**, *51*, 246.

[157] A. Heine, R. Herbst-Irmer, D. Stalke, *J. Chem. Soc., Chem. Commun.* **1993**, 1729.

[158] M. J. Sgro, W. E. Piers, P. E. Romero, *Dalton Trans.* **2015**, *44*, 3817.

[159] J. Beck, J. Strähle, *Angew. Chem. Int. Ed. Engl.* **1985**, *24*, 409.

[160] A. Heine, D. Stalke, *Angew. Chem. Int. Ed. Engl.* **1993**, *32*, 121.

[161] J. Plotzitzka, C. Kleeberg, *Inorg. Chem.* **2016**, *55*, 4813.

[162] S. Gu, J. Du, J. Huang, H. Xia, L. Yang, W. Xu, C. Lu, *Beilstein J. Org. Chem.* **2016**, *12*, 863.

[163] a) B. Liu, X. Ma, F. Wu, W. Chen, *Dalton Trans.* **2015**, *44*, 1836; b) V. J. Catalano, L. B. Munro, C. E. Strasser, A. F. Samin, *Inorg. Chem.* **2011**, *50*, 8465; c) C. Chen, H. Qiu, W. Chen, *J. Organomet. Chem.* **2012**, *696*, 4166.

[164] X. Qi, T. Zheng, J. Zhou, Y. Dong, X. Zuo, X. Li, H. Sun, O. Fuhr, D. Fenske, *Organometallics* **2019**.

[165] a) M.-P. Luecke, D. Porwal, A. Kostenko, Y.-P. Zhou, S. Yao, M. Keck, C. Limberg, M. Oestreich, M. Driess, *Dalton Trans.* **2017**, *46*, 16412; b) D. Gallego, S. Inoue, B. Blom, M. Driess, *Organometallics* **2014**, *33*, 6885.

[166] S. Schafer, R. Koppe, M. T. Gamer, P. W. Roesky, *Chem. Commun.* **2014**, *50*, 11401.

[167] J. M. Seco, M. J. González Garmendia, E. Pinilla, M. R. Torres, *Polyhedron* **2002**, *21*, 457.

[168] Y. Inagawa, S. Ishida, T. Iwamoto, *Chemistry Letters* **2014**, *43*, 1665.

[169] N. Parvin, R. Dasgupta, S. Pal, S. S. Sen, S. Khan, *Dalton Trans.* **2017**, *46*, 6528.

[170] J. M. Hayes, M. Viciano, E. Peris, G. Ujaque, A. Lledós, *Organometallics* **2007**, *26*, 6170.

[171] J. C. Garrison, W. J. Youngs, *Chemical reviews* **2005**, *105*, 3978.

[172] H. M. J. Wang, C. Y. L. Chen, I. J. B. Lin, *Organometallics* **1999**, *18*, 1216.

[173] a) I. J.B. Lin, C. S. Vasam, *Coord. Chem. Rev.* **2007**, *251*, 642; b) I. J. B. Lin, C. S. Vasam, *Comments on Inorganic Chemistry* **2004**, *25*, 75; c) P. L. Arnold, *Heteroatom Chem* **2002**, *13*, 534.

[174] D. Rottschäfer, C. J. Schürmann, J.-H. Lamm, A. N. Paesch, B. Neumann, R. S. Ghadwal, *Organometallics* **2016**, *35*, 3421.

[175] P. Jutzi, A. Möhrke, *Angew. Chem. Int. Ed. Engl.* **1990**, *29*, 893.

[176] A. Pintado-Alba, H. de La Riva, M. Nieuwhuyzen, D. Bautista, P. R. Raithby, H. A. Sparkes, S. J. Teat, J. M. López-de-Luzuriaga, M. C. Lagunas, *Dalton Trans.* **2004**, 3459.

[177] A. Deák, T. Megyes, G. Tárkányi, P. Király, L. Biczók, G. Pálinkás, P. J. Stang, *J. Am. Chem. Soc.* **2006**, *128*, 12668.

[178] a) C. Dash, M. M. Shaikh, R. J. Butcher, P. Ghosh, *Inorg. Chem.* **2010**, *49*, 4972; b) A. John, P. Ghosh, *Dalton Trans.* **2010**, *39*, 7183; c) M. K. Samantaray, K. Pang, M. M. Shaikh, P. Ghosh, *Inorg. Chem.* **2008**, *47*, 4153; d) M. V. Baker, P. J. Barnard, S. J. Berners-Price, S. K. Brayshaw, J. L. Hickey, B. W. Skelton, A. H. White, *J. Organomet. Chem.* **2005**, *690*, 5625; e) P. de Frémont, N. M. Scott, E. D. Stevens, S. P. Nolan, *Organometallics* **2005**, *24*, 2411.

[179] a) J. D. E. T. Wilton-Ely, A. Schier, N. W. Mitzel, H. Schmidbaur, *Inorg. Chem.* **2001**, *40*, 6266; b) M. Preisenberger, A. Schier, H. Schmidbaur, *J. Chem. Soc., Dalton Trans.* **1999**, 1645.

[180] A. S. K. Hashmi, G. J. Hutchings, *Angew. Chem. Int. Ed. Engl.* **2006**, *45*, 7896.

[181] a) J. Serra, T. Parella, X. Ribas, *Chem. Sci.* **2017**, *8*, 946; b) J. Serra, P. Font, E. D. Sosa Carrizo, S. Mallet-Ladeira, S. Massou, T. Parella, K. Miqueu, A. Amgoune, X. Ribas, D. Bourissou, *Chem. Sci.* **2018**, *9*, 3932.

[182] S. Enthaler, *ACS Catal.* **2013**, *3*, 150.

[183] A. J. Arduengo, H.V.R. Dias, F. Davidson, R. L. Harlow, *J. Organomet. Chem.* **1993**, *462*, 13.

[184] a) S. K. Bose, K. Fucke, L. Liu, P. G. Steel, T. B. Marder, *Angew. Chem. Int. Ed. Engl.* **2014**, *53*, 1799; b) P. Jochmann, D. W. Stephan, *Angew. Chem. Int. Ed. Engl.* **2013**, *52*, 9831; c) Y. Lee, B. Li, A. H. Hoveyda, *J. Am. Chem. Soc.* **2009**, *131*, 11625; d) T. R. Jensen, L. E. Breyfogle, M. A. Hillmyer, W. B. Tolman, *Chem. Commun.* **2004**, 2504.

[185] A. Rit, T. P. Spaniol, L. Maron, J. Okuda, *Angew. Chem. Int. Ed. Engl.* **2013**, *52*, 4664.

[186] S. Schäfer, R. Köppe, P. W. Roesky, *Chem. Eur. J.* **2016**, *22*, 7127.

[187] F. M. Mück, J. A. Baus, A. Ulmer, C. Burschka, R. Tacke, *Eur. J. Inorg. Chem.* **2016**, *2016*, 1660.

[188] S. Yadav, E. Sangtani, D. Dhawan, R. G. Gonnade, D. Ghosh, S. S. Sen, *Dalton Trans.* **2017**.

[189] a) S. P. Sarish, S. Nembenna, S. Nagendran, H. W. Roesky, *Acc. Chem. Res.* **2011**, *44*, 157; b) C. Ruspic, S. Harder **2007**, *46*, 10426.

[190] K. Junold, J. A. Baus, C. Burschka, C. Fonseca Guerra, F. M. Bickelhaupt, R. Tacke, *Chemistry (Weinheim an der Bergstrasse, Germany)* **2014**, *20*, 12411.

[191] K. Junold, J. A. Baus, C. Burschka, T. Vent-Schmidt, S. Riedel, R. Tacke, *Inorganic chemistry* **2013**, *52*, 11593.

[192] F. M. Mück, D. Kloß, J. A. Baus, C. Burschka, R. Bertermann, J. Poater, C. Fonseca Guerra, F. M. Bickelhaupt, R. Tacke, *Chemistry (Weinheim an der Bergstrasse, Germany)* **2015**, *21*, 14011.

[193] Y.-P. Zhou, M. Karni, S. Yao, Y. Apeloig, M. Driess, *Angew. Chem. Int. Ed. Engl.* **2016**, *55*, 15096.

[194] E. Gómez, V. Santes, V. de La Luz, N. Farfán, *J. Organomet. Chem.* **1999**, *590*, 237.

[195] E. Gómez, Z. Hernández, C. Alvarez-Toledano, R. A. Toscano, V. Santes, P. Sharma, *J. Organomet. Chem.* **2002**, *648*, 280.

[196] a) S. Wingerter, M. Pfeiffer, F. Baier, T. Stey, D. Stalke, *Z Anorg Allg Chem* **2000**, *626*, 1121; b) T. Stey, D. Stalke, *Z. Anorg. Allg. Chem.* **2005**, *631*, 2931; c) A. Murso, D. Stalke, *Eur. J. Inorg. Chem.* **2004**, *2004*, 4272; d) H. Gornitzka, C. Hemmert, G. Bertrand, M. Pfeiffer, D. Stalke, *Organometallics* **2000**, *19*, 112.

[197] F. Baier, Z. Fei, H. Gornitzka, A. Murso, S. Neufeld, M. Pfeiffer, I. Rüdenauer, A. Steiner, T. Stey, D. Stalke, *J. Organomet. Chem.* **2002**, *661*, 111.

[198] a) H. Bürger, W. Sawodny, U. Wannagat, *J. Organomet. Chem.* **1965**, *3*, 113; b) M. Steiner, H. Grützmacher, H. Prtizkow, L. Zsolnai, *Chem. Commun.* **1998**, 285.

[199] S. J. Birch, S. R. Boss, S. C. Cole, M. P. Coles, R. Haigh, P. B. Hitchcock, A. E. H. Wheatley, *Dalton Trans.* **2004**, 3568.

[200] A. Baishya, M. K. Barman, T. Peddarao, S. Nembenna, *J. Organomet. Chem.* **2014**, *769*, 112.

[201] J. B. Waters, J. M. Goicoechea, *Dalton Trans.* **2014**, *43*, 14239.

[202] R. E. Mulvey, *Organometallics* **2006**, *25*, 1060.

[203] S. E. Baillie, E. Hevia, A. R. Kennedy, R. E. Mulvey, *Organometallics* **2007**, *26*, 204.

[204] W. Clegg, G. C. Forbes, A. R. Kennedy, R. E. Mulvey, S. T. Liddle, *Chem. Commun.* **2003**, 406.

[205] X. Qi, H. Sun, X. Li, O. Fuhr, D. Fenske, *Dalton Trans.* **2018**, *47*, 2581.

[206] C. I. Someya, M. Haberberger, W. Wang, S. Enthaler, S. Inoue, *Chemistry Letters* **2013**, *42*, 286.

[207] R. Berg, B. F. Straub, *Beilstein J. Org. Chem.* **2013**, *9*, 2715.

[208] a) M. G. Finn, V. V. Fokin, *Chem. Soc. Rev.* **2010**, *39*, 1231; b) M. Meldal, C. W. Tornøe, *Chem. Rev.* **2008**, *108*, 2952.

[209] F. Himo, T. Lovell, R. Hilgraf, V. V. Rostovtsev, L. Noodleman, K. B. Sharpless, V. V. Fokin, *J. Am. Chem. Soc.* **2005**, *127*, 210.

[210] H. C. Kolb, M. G. Finn, K. B. Sharpless, *Angew. Chem.* **2001**, *113*, 2056.

[211] a) J. N. Brantley, K. M. Wiggins, C. W. Bielawski, *Science* **2011**, *333*, 1606; b) A. A. Dippold, T. M. Klapötke, *J. Am. Chem. Soc.* **2013**, *135*, 9931; c) C. He, J.'n. M. Shreeve, *Angew. Chem. Int. Ed. Engl.* **2015**, *54*, 6260; d) M. Juríček, P. H. J. Kouwer, A. E. Rowan, *Chem. Commun.* **2011**, *47*, 8740; e) B. Schulze, U. S. Schubert, *Chem. Soc. Rev.* **2014**, *43*, 2522; f) D. Wang, C. Deraedt, L. Salmon, C. Labrugère, L. Etienne, J. Ruiz, D. Astruc, *Chemistry* **2015**, *21*, 6501; g) C. Wang, D. Wang, S. Yu, T. Cornilleau, J. Ruiz, L. Salmon, D. Astruc, *ACS Catal.* **2016**, *6*, 5424.

[212] S. Holm, A. Siegle, C. Loos, F. Rominger, B. Straub, *Synthesis* **2010**, *2010*, 2278.

[213] a) M. Melaimi, A. M. Z. Slawin, G. Bertrand, C. S. J. Cazin, *Adv Synth Catal* **2015**, *357*, 3155; b) S. C. Sau, S. R. Roy, T. K. Sen, D. Mullangi, S. K. Mandal, *Adv. Synth. Catal.* **2013**, *355*, 2982; c) S. Díez-González, A. Correa, L. Cavallo, S. P. Nolan, *Chemistry* **2006**, *12*, 7558.

[214] S. Diez-Gonzalez, E. C. Escudero-Adan, J. Benet-Buchholz, E. D. Stevens, A. M. Z. Slawin, S. P. Nolan, *Dalton Trans.* **2010**, *39*, 7595.

[215] S. Díez-González, S. P. Nolan, *Angew. Chem. Int. Ed. Engl.* **2008**, *47*, 8881.

[216] a) R. Huisgen, *Angew. Chem. Int. Ed. Engl.* **1963**, *2*, 633; b) R. Huisgen, G. Szeimies, L. Möbius, *Chem Ber* **1967**, *100*, 2494; c) R. Huisgen, *Angew. Chem. Int. Ed. Engl.* **1968**, *7*, 321; d) S. Bräse, C. Gil, K. Knepper, V. Zimmermann, *Angew. Chem. Int. Ed. Engl.* **2005**, *44*, 5188; e) K. N. Houk, J. Gonzalez, Y. Li, *Acc. Chem. Res.* **1995**, *28*, 81; f) R. Huisgen, *J. Org. Chem.* **1968**, *33*, 2291; g) R. Huisgen, *J. Org. Chem.* **1976**, *41*, 403.

[217] V. V. Rostovtsev, L. G. Green, V. V. Fokin, K. B. Sharpless, *Angew. Chem., Int. Ed.* **2002**, *41*, 2596.

[218] C. W. Tornøe, C. Christensen, M. Meldal, *J. Org. Chem.* **2002**, *67*, 3057.

[219] A. Makarem, R. Berg, F. Rominger, B. F. Straub, *Angew. Chem. Int. Ed. Engl.* **2015**, *54*, 7431.

[220] V. O. Rodionov, V. V. Fokin, M. G. Finn, *Angew. Chem.* **2005**, *117*, 2250.

[221] B. T. Worrell, J. A. Malik, V. V. Fokin, *Science* **2013**, *340*, 457.

[222] A. L. Schöffler, A. Makarem, F. Rominger, B. F. Straub, *Beilstein J. Org. Chem.* **2016**, *12*, 1566.

[223] a) V. O. Rodionov, V. V. Fokin, M. G. Finn, *Angew. Chem. Int. Ed. Engl.* **2005**, *44*, 2210; b) M. Ahlquist, V. V. Fokin, *Organometallics* **2007**, *26*, 4389; c) B. F. Straub, *Chem. Commun.* **2007**, *75*, 3868; d) C. Nolte, P. Mayer, B. F. Straub, *Angew. Chem. Int. Ed. Engl.* **2007**, *46*, 2101.

[224] a) W. Schlenk, A. Thal, *Chem. Ber.* **1913**, *46*, 2840; b) T. T. Tidwell, *Angew. Chem., Int. Ed.* **2001**, *40*, 331; c) Georg-August-University, "Virtuelles Labor I", can be found under http://www.stalke.chemie.uni-goettingen.de/virtuelles_labor/advanced/13_de.html, **2014**.

[225] G. R. Fulmer, Alexander J. M. Miller, N. H. Sherden, H. E. Gottlieb, A. Nudelman, B. M. Stoltz, J. E. Bercaw, K. I. Goldberg, *Organometallics* **2010**, *29*, 2176.

[226] Georg-August-University, "Virtuelles Labor II", can be found under http://www.stalke.chemie.uni-goettingen.de/virtuelles_labor/nmr/de.html, **2014**.

[227] a) G. Bodenhausen, D. J. Ruben, *Chem. Phys. Lett.* **1980**, *69*, 185; b) A. Bax, M. F. Summers, *J. Am. Chem. Soc.* **1986**, *108*, 2093.

[228] A.-K. Kreyenschmidt, S. Bachmann, T. Niklas, D. Stalke, *ChemistrySelect* **2017**, *2*, 6957.

[229] A. Kreyenschmidt, S. Bachmann, D. Stalke, in preparation.

[230] S. Bachmann, B. Gernert, D. Stalke, *Chem. Commun.* **2016**, *52*, 12861.

[231] a) T. Kottke, D. Stalke, *J. Appl. Cryst.* **1993**, *26*, 615; b) T. Kottke, D. Stalke, *Angew. Chem., Int. Ed.* **1993**, *32*, 580; c) D. Stalke, *Chem. Soc. Rev.* **1998**, *27*, 171; d) Georg-August-University, "Virtuelles Labor III", can be found under http://www.stalke.chemie.uni-goettingen.de/virtuelleslabor/special/22de.html, **2014**.

[232] T. Kottke, R. J. Lagow, D. Stalke, *J. Appl. Cryst.* **1996**, *29*, 465.

[233] T. Schulz, K. Meindl, D. Leusser, D. Stern, J. Graf, C. Michaelsen, M. Ruf, G. M. Sheldrick, D. Stalke, *J. Appl. Cryst.* **2009**, *42*, 885.

[234] *APEX2 v2.2012.2-0*. *APEX2*, WI, USA, Madison, **2012**.

[235] *Bruker SAINT v8.30C*. *Bruker AXS Inst. Inc.*, WI, USA, Madison, **2013**.

[236] L. Krause, R. Herbst-Irmer, G. M. Sheldrick, D. Stalke, *J. Appl. Cryst.* **2015**, *48*, 3.

[237] G. M. Sheldrick, *TWINABS 2012/1*. *TWINABS 2012/1*, Göttingen, **2012**.

[238] L. Krause, R. Herbst-Irmer, D. Stalke, *J. Appl. Cryst.* **2015**, *48*, 1907.

[239] G. M. Sheldrick, *XPREP in SHELXTL 2014/2*, Göttingen, **2014**.

[240] G. Sheldrick, *Acta Cryst. A* **2008**, *64*, 112.

[241] C. B. Huebschle, G. M. Sheldrick, B. Dittrich, *J. Appl. Cryst.* **2011**, *44*, 1281.

[242] G. M. Sheldrick, *SHELXL in SHELXTL v2014/7*, WI, USA, Madison, **2014**.